

Université de Montréal

Mechanosensitive ATP Release in the Lungs

Par

Ju Jing Tan

Programme de sciences biomédicales, Faculté de médecine

Thèse présentée en vue de l'obtention du grade de *Philosophiæ doctor* (Ph. D.)

en sciences biomédicales, option générale

Décembre 2019

© Ju Jing Tan, 2019

Université de Montréal

Programme de sciences biomédicales, Faculté de médecine

Cette thèse intitulée

Mechanosensitive ATP Release in the Lungs

Présentée par

Ju Jing Tan

A été évaluée par un jury composé des personnes suivantes

Shao-Ling Zhang, Ph. D.

Présidente-rapporteuse

Ryszard Grygorczyk, Ph. D.

Directeur de recherche

Emmanuelle Brochiero, Ph. D.

Codirectrice

François Yu, Ph. D.

Membre du jury

Svetlana Komarova, Ph. D.

Examinatrice externe

Madhu Anand-Srivastava, Ph. D.

Représentante de la doyenne

Résumé

L'ATP est bien connue pour son rôle de transporteur d'énergie à l'intérieur des cellules, mais en dehors de la cellule, elle agit en tant que molécule de signalisation extracellulaire. En se liant aux récepteurs purinergiques, l'ATP extracellulaire amorce la signalisation purinergique afin de réguler certains processus physiologiques et pathophysiologiques. Dans les poumons, l'ATP stimule la sécrétion de surfactant et promeut la clairance mucociliaire. Compte tenu du rôle critique de l'ATP extracellulaire dans les poumons, il est important de comprendre le mécanisme du relargage d'ATP cellulaire — la première étape de la signalisation purinergique. Parce que les forces mécaniques constituent le déclencheur principal du relargage d'ATP, cette thèse a pour but d'investiguer le(s) mécanisme(s) physiologique(s) et les sources cellulaires d'un tel relargage d'ATP mécanosensible. Cet ouvrage est divisé en trois parties :

1) Pour étudier les caractéristiques spatiales et temporelles du relargage d'ATP, j'ai développé une technique d'imagerie hautement sensible basée sur la bioluminescence de la luciférine-luciférase couplée avec un système de lentilles à grand champ de vision (WFOV, *wide field of view*) optimisant l'apport de lumière. Pour évaluer notre approche d'imagerie, j'ai soumis des cellules A549, dérivées d'un adénocarcinome pulmonaire humain, à un étirement ou un choc hypotonique de 50% pour déclencher un relargage d'ATP. J'ai démontré que notre technique nous permet de quantifier précisément la quantité et le taux (ou l'efflux) d'ATP s'échappant des cellules. Le WFOV constitue un outil essentiel utilisé dans les études décrites dans cette thèse pour déterminer le mécanisme et la source cellulaire du relargage d'ATP dans l'alvéole.

2) Afin d'examiner le mécanisme physiologique du relargage d'ATP induit par l'étirement dans les cellulaires alvéolaires primaires, j'ai déterminé les contributions individuelles des cellules alvéolaires de type 1 (AT1) en comparaison des cellules alvéolaires de type 2 (AT2). Pour ce faire, des cellules AT2 fraîchement isolées de poumons de rats ont étéensemencées sur une chambre flexible en silicone et cultivées jusqu'à sept jours, ce qui permettait aux cellules AT2 de se transdifférencier progressivement en cellules semblables aux cellules AT1. Le ratio des cellules alvéolaires (AT2:AT1), étant de 4:1 au jour 3, est devenu 1:4 au jour 7. La quantité d'ATP

libérée diminuait avec le nombre décroissant de cellules AT2, les impliquant en tant que principale source pour le relargage d'ATP en réponse à un étirement. Alors que les modulateurs pharmacologiques des canaux d'ATP, carbenoxolone et probénécide, ne diminuaient pas la quantité d'ATP libérée, le BAPTA, un chélateur de calcium intracellulaire ($[Ca^{2+}]_i$), l'a significativement réduite. De même, ces trois modulateurs exercent des effets similaires sur les réponses calciques intracellulaires mesurées par le Fura-2, suggérant une connexion entre le relargage d'ATP et les niveaux de $[Ca^{2+}]_i$.

3) Pour explorer le rôle qu'ont les propriétés viscoélastiques de la membrane dans le relargage d'ATP mécanosensible, j'ai démontré qu'une déformation de 30% induisait un relargage d'ATP transitoire qui était accompagné d'une absorption d'iodure de propidium (PI, *propidium iodide*) chez des cellules AT2. Ceci est cohérent avec une rupture membranaire transitoire induite par une déformation, assez large pour le passage d'ATP et de PI. L'efflux d'ATP augmente aussi selon le taux de déformation, et la durée de déformation prolonge la demi-vie du relargage d'ATP. Donc, ces résultats fournissent des indices sur la manière dont l'étirement de la membrane viscoélastique peut mener au relargage d'ATP par un mécanisme alternatif impliquant une mécanoporation de la membrane cellulaire.

Dans l'ensemble, ces résultats démontrent que le relargage d'ATP ne se produit pas à travers les canaux conduisant l'ATP mais plutôt par une mécanoporation transitoire de la membrane. D'autres études sur les dommages membranaires sont nécessaires pour mieux comprendre sa contribution dans le relargage d'ATP mécanosensible et les signaux de $[Ca^{2+}]_i$. De telles études élucideront la signalisation purinergique dans les organes qui sont constamment exposés à des contraintes physiques. Ceci pourrait suggérer des cibles/approches thérapeutiques pour moduler les impacts négatifs d'un relargage d'ATP excessif observés lors de certaines conditions pathologiques, telles que les lésions pulmonaires induites par la ventilation mécanique.

Mots-clés : bioluminescence de la luciférine-luciférase, cellules alvéolaires, contrainte mécanique, imagerie d'ATP, lésions pulmonaires induites par la ventilation mécanique, mécanoporation, relargage d'ATP, signalisation purinergique, viscoélasticité membranaire.

Abstract

ATP is widely known to be an energy carrier within cells, but outside of the cell, it acts as an extracellular signaling molecule. Upon binding to purinergic receptors, extracellular ATP initiates the purinergic signaling to regulate certain physiological and pathophysiological processes. In the lungs, ATP stimulates surfactant secretion and promotes mucociliary clearance. Given the critical role of extracellular ATP in the lungs, it is important to understand the mechanism of cellular ATP release — the first step of purinergic signaling. Because mechanical forces constitute the primary trigger of ATP release, this thesis aims to investigate the physiological mechanism(s) and cellular sources of such mechanosensitive ATP release. This work is divided into three parts:

1) To study the spatial and temporal characteristics of ATP release, I developed a highly sensitive imaging technique based on luciferin-luciferase bioluminescence coupled with a custom-designed lens system, which combined a wide field of view (WFOV) and high light-gathering power. To evaluate our imaging approach, I subjected A549 cells, derived from human lung adenocarcinoma, to stretch or 50% hypotonic shock to trigger ATP release. I demonstrated that our technique allows us to precisely quantify the amount and the rate (or efflux) of ATP escaping from cells. The WFOV constitutes an essential tool used in the studies described in this thesis to determine the mechanism and cellular source of ATP release in the alveolus.

2) To examine the physiological mechanism of stretch-induced ATP release in primary alveolar cells, I determined the individual contributions of alveolar type 1 (AT1) in comparison with alveolar type 2 (AT2) cells. To this end, freshly isolated AT2 cells from rat lungs were seeded on a flexible silicone chamber and were cultured for up to seven days, which allowed AT2 cells to progressively transdifferentiate into AT1-like cells. The ratio of alveolar cells (AT2:AT1), being 4:1 on day 3, became 1:4 on day 7. The quantity of released ATP decreased with the decreasing numbers of AT2 cells, implicating them as the main source of ATP release in response to stretch. While pharmacological ATP channel modulators, carbenoxolone and probenecid, did not diminish the amount of ATP release, BAPTA, an intracellular calcium ($[Ca^{2+}]_i$) chelator,

significantly reduced it. Likewise, these three modulators had similar effects on intracellular calcium responses measured by Fura-2, suggesting a connection between ATP release and $[Ca^{2+}]_i$ levels.

3) To explore the role of membrane viscoelastic properties in mechanosensitive ATP release, I demonstrated that a 30% strain induced transient ATP release that was accompanied by uptake of propidium iodide (PI) in AT2 cells. This is consistent with a strain-induced transient membrane rupture, big enough for the passage of ATP and PI. ATP efflux also increases with strain rate, and hold time prolongs the half-life of ATP release. Thus, these results provide clues on how stretching of the viscoelastic membrane may lead to ATP release via an alternate mechanism involving transient mechanoporation of the cell membrane.

Overall, these findings demonstrate that stretch-induced ATP release does not occur through ATP-conducting channels but rather a transient membrane mechanoporation. Further studies on membrane injury induced by strain are needed to better understand its contribution to mechanosensitive ATP release and $[Ca^{2+}]_i$ signaling. Such studies will elucidate purinergic signaling in organs that are constantly exposed to physical stresses. This could suggest novel therapeutic targets/approach to modulate the negative impacts of excessive ATP release observed under certain pathological conditions, such as ventilator-induced lung injury.

Keywords: alveolar cells, ATP imaging, ATP release, luciferin-luciferase bioluminescence, mechanical stress, mechanoporation, membrane viscoelasticity, purinergic signaling, ventilation-induced lung injury.

Table of Content

Résumé.....	5
Abstract.....	7
Table of Content.....	9
List of Tables.....	15
List of Figures.....	17
List of Acronyms and Abbreviations.....	19
Acknowledgments.....	25
Chapter 1 – Introduction.....	29
1.1 The Lungs.....	29
1.1.2 Airway Anatomy.....	29
1.2 Alveolar Cells.....	32
1.2.1 Alveolar Type 1 (AT1) Cells.....	32
1.2.2 Alveolar Type 2 (AT2) Cells.....	33
1.3 Lung Injury and Mechanical Ventilation (MV).....	34
1.3.1 Acute Respiratory Distress Syndrome (ARDS) and Acute Lung Injury (ALI).....	35
1.3.2 Ventilator-Induced Lung Injury (VILI).....	37
1.4 Purinergic Signaling.....	38
1.4.1 Adenosine Triphosphate (ATP).....	38
1.4.2 Purinergic Receptors.....	40
1.4.3 Conversion and Metabolism of Extracellular ATP.....	42
1.5 Extracellular Nucleotides in the Lungs.....	44
1.5.1 Surfactant Secretion.....	44

1.5.2 Fluid Secretion.....	44
1.5.3 Mucociliary Clearance (MCC).....	46
1.5.4 Danger-Associated Molecular Pattern (DAMP)	47
1.6 Candidate Pathways for ATP Release.....	48
1.6.1 ATP Release via Lytic Pathway	49
1.6.2 Non-Lytic Mechanisms: Conductive Pathways	49
1.6.3 Non-Lytic Mechanisms: Exocytotic Pathways.....	50
1.7 Mechanically Induced ATP Release	51
Chapter 2 – Hypothesis & Objectives.....	53
2.1 Our Previous Studies	53
2.2 Hypothesis.....	56
2.3 Objectives	56
Chapter 3 – Article #1.....	57
3.1 Preamble	57
3.2 Article #1	59
3.2.1 Contribution	59
3.3 Wide field of view quantitative imaging of cellular ATP release	60
3.3.1 Abstract	61
3.3.2 Introduction.....	62
3.3.3 Materials and Methods	64
3.3.4 Results	70
3.3.5 Discussion	76
3.3.6 Grants.....	77
3.3.7 Disclosures.....	77

3.3.8 Author Contributions	78
3.3.9 References.....	78
3.3.10 Figures and Captions	81
Chapter 4 – Article #2.....	97
4.1 Preamble	97
4.2 Article #2	98
4.2.1 Contribution	98
4.3 Type 2 secretory cells are primary source of ATP release in mechanically stretched lung alveolar cells	99
4.3.1 Abstract	100
4.3.2 Introduction.....	101
4.3.3 Methods	103
4.3.4 Results	107
4.3.5 Discussion	110
4.3.6 Acknowledgments.....	114
4.3.7 Grants	114
4.3.8 Disclosures.....	114
4.3.9 Author Contributions	115
4.3.10 References.....	115
4.3.11 Figures and Captions	120
Chapter 5 – Article #3.....	133
5.1 Preamble	133
5.2 Article #3	134
5.2.1 Contribution	134

5.3 Cellular ATP efflux through transient membrane rupture formed by mechanical stretch in alveolar epithelial cells	135
5.3.1 Abstract	136
5.3.2 Introduction.....	137
5.3.3 Material and Methods	138
5.3.4 Results	140
5.3.5 Discussion	141
5.3.6 Acknowledgments.....	143
5.3.7 Grants	143
5.3.8 Disclosures.....	143
5.3.9 References.....	143
5.3.10 Figures and Captions	145
Chapter 6 – Discussion	151
6.1 Article #1	151
6.1.1 Limitations.....	152
6.2 Article #2	153
6.2.1 Limitations.....	155
6.3 Article #3	156
6.3.1 Limitations.....	157
6.4 Proposed Mechanism of Mechanosensitive ATP Release in the Lungs.....	158
Chapter 7 – Conclusion & Perspectives	161
7.1 Conclusion	161
7.1.1 Summary of Original Contributions	161
7.2 Perspectives	162

References.....	165
Appendices	181
Appendix A	181
Appendix B	214
Appendix C	229
Appendix D	240

List of Tables

Table 1. –	Agonists and Signaling Properties of Purinergic Receptors	42
------------	---	----

List of Figures

Figure 1. –	Subdivision of Human Lung Airways	30
Figure 2. –	Ion Transport in AT1 and AT2 Cells	33
Figure 3. –	Molecular Structure of Adenine Nucleotides	39
Figure 4. –	Characteristics of Purinergic Receptors	40
Figure 5. –	Breakdown of Extracellular ATP and Binding of Ligands to Purinergic Receptors ..	43
Figure 6. –	Purinergic Regulation of Ion Transport in the ASL.....	46
Figure 7. –	Light-Emitting ATP-Dependent Reaction of Luciferin and Luciferase.....	58
Figure 8. –	Figure 1 of Article #1	81
Figure 9. –	Figure 2 of Article #1	83
Figure 10. –	Figure 3 of Article #1.....	85
Figure 11. –	Figure 4 of Article #1.....	87
Figure 12. –	Figure 5 (Panels A, B and C) of Article #1	89
Figure 13. –	Figure 5 (Panels D and E) of Article #1	90
Figure 14. –	Figure 6 of Article #1.....	92
Figure 15. –	Figure 7 of Article #1.....	94
Figure 16. –	Figure 1 of Article #2.....	120
Figure 17. –	Figure 2 of Article #2.....	122
Figure 18. –	Figure 3 of Article #2.....	124
Figure 19. –	Figure 4 of Article #2.....	126
Figure 20. –	Figure 5 of Article #2.....	128
Figure 21. –	Figure 6 of Article #2.....	130
Figure 22. –	Figure 1 of Article #3.....	145
Figure 23. –	Figure 2 of Article #3.....	147
Figure 24. –	Figure 3 of Article #3.....	149

List of Acronyms and Abbreviations

[Ca²⁺]_i: Intracellular calcium

ABC: Adenosine triphosphate-binding cassette

AC: Adenylyl cyclase

ADA: Adenosine deaminase

ADP: Adenosine diphosphate

AECC: American-European Consensus Conference

AFC: Alveolar fluid clearance

ALI: Acute lung injury

AM: Acetoxymethyl ester

AMP: Adenosine monophosphate

AQP5: Aquaporin-5

ARDS: Acute respiratory distress syndrome

ASL: Airway surface liquid

AT1: Alveolar type 1

AT2: Alveolar type 2

ATP: Adenosine triphosphate

ATPDase: ATP diphosphohydrolase

BALF: Bronchoalveolar lavage fluid

BAPTA: 1,2-bis(*o*-aminophenoxy)ethane-*N,N,N',N'*-tetraacetic acid

CaCC: Ca²⁺-activated Cl⁻ channel

cAMP: Cyclic adenosine monophosphate

CBX: Carbenoxolone

CCSP: Club cell secretory proteins

CFTR: Cystic fibrosis transmembrane conductance regulator

CHO: Chinese hamster ovary

DAG: Diacylglycerol

DAMP: Danger-associated molecular pattern

DCPIB: 4-(2-butyl-6,7-dichloro-2-cyclopentyl-1-oxo-3*H*-inden-5-yl)-2-oxobutanoic acid

E-5'-N: Ecto-5'-nucleotidase

E-NPP: Ecto-nucleotide pyrophosphatase/phosphodiesterase

E-NTDPase: Ecto-nucleoside triphosphate diphosphohydrolase

EMCCD: Electron multiplying charge-coupled device

ENaC: Epithelial sodium channel

ER: Endoplasmic reticulum

ERK1/2: Extracellular signal-regulated kinases 1 and 2

EthBr: Ethidium bromide

EthD-1: Ethidium homodimer-1

FiO₂: Fraction of inspired oxygen

HPLC: High-performance liquid chromatography

ICU: Intensive care unit

IL: Interleukin

IP₃: Inositol 1,4,5-triphosphate

JNK1/2/3: c-Jun N-terminal kinases 1, 2 and 3

LB: Lamellar bodies

LL: Luciferin-luciferase

MAPK: Mitogen-activated protein kinase

MCC: Mucociliary clearance

MV: Mechanical ventilation

Na⁺/K⁺-ATPase: Sodium-potassium adenosine triphosphatase (Na⁺/K⁺ pump)

NEM: *N*-ethylmaleimide

NPPB: 5-nitro-2-(3-phenylpropyl-amino) benzoic acid

PaO₂: Arterial oxygen partial pressure

PCL: Periciliary liquid

PEEP: Positive end-expiratory pressure

PI: Propidium iodide

PIP2: Phosphatidylinositol 4,5-bisphosphate

PKA: Protein kinase A

PKC: Protein kinase C

PLC: Phospholipase C

pme-LUC: Plasma membrane luciferase

PRO: Probenecid

ROI: Region of interest

ROS: Reactive oxygen species

RTK: Receptor tyrosine kinase

t_{1/2}: Half-life

TBI: Traumatic brain injury

TG: Thapsigargin

TIRF: Total internal reflection fluorescence

TLC: Total lung capacity

TNF: Tumor necrosis factor

TRP: Transient receptor potential

TRPV4: Transient receptor potential vanilloid 4

VILI: Ventilator-induced lung injury

VNUT: Vesicular nucleotide transporter

WFOV: Wide field of view

To my Family

Acknowledgments

I would first like to thank all of the jury members for taking the time to evaluate my doctoral thesis. Your constructive comments and valuable insights made my work better.

To my supervisor, Dr. Ryszard Grygorczyk: I sincerely thank you for having given me the opportunity to be your Ph. D. student. I initially felt that this project was perfectly suited for me, and since the beginning, you have taught me a lot and have fostered in me many skills relevant to research. I cannot thank you enough for letting me grow under your guidance. You gave me freedom and autonomy to conduct my research, and you were always there for me to keep me focused on achieving my goals. I greatly appreciate your presence and your infinite patience in helping me to succeed throughout my studies and to become a better researcher. I am blessed, honoured and privileged to have you as my supervisor and to be part of your lab.

I also thank all of the past and present members of the lab. It was a real pleasure to be and to work with you all. To Dr. Francis Boudreault: I thank you for your help and constant supervision on my work. I am always amazed and impressed by the depth of your knowledge and insight. Your support, mentorship and assistance throughout my studies were very valuable to me and contributed greatly to my success as well. To Olga, now Dr. Ponomarchuk: I thank you for being beside me through these years. Together, we faced head on the challenges and overcame them to earn a Ph. D. degree. Your wisdom brought so many solutions to my problems. To Mariusz Grygorczyk: I thank you for having trained me when I first arrived in the lab. You instilled in me many skills, which helped me to complete my work and experiments.

I extend my thanks to my co-supervisor, Dr. Emmanuelle Brochiero: I thank you for exposing me to your work and giving me your valuable input into my project. Your expertise helped me a lot to learn more and to refine my research. I also find myself very fortunate to be alongside all of the members of your lab. To those cooperating with me, Anik Privé, Nguyen Thu Ngan Trinh, Jasmine Chebli, Damien Adam, Méliissa Aubin Vega, Caroline Landry, Mays Merjaneh and, saving the best for last, Laura Sognigbé: We shared not only our common work area but also many great laughs. I thank you for the amazing moments that we spent together.

Had people told me before I started my doctoral studies that I would win a prestigious award to go to Japan, I would tell them that they're crazy, but actually, it did happen. To Dr. Kishio Furuya: I thank you for receiving me in your lab and for seeking the best for me during my stay in Japan. To Dr. Masahiro Sokabe and everybody in the Mechanobiology Lab: I thank you all for making me feel welcome and for helping me to have a great time in Nagoya. I would also like to thank the Nakahama Family, my host family in Yokohama, as well as my friends whom I met during my fellowship for the great time. Finally, I express my gratitude to Mitacs, the Embassy of Canada to Japan and the Japan Society for the Promotion of Science (JSPS) for granting me this once-in-a-lifetime opportunity to conduct research and have an incredible experience in Japan.

To all my colleagues and labmates, many of whom have become my friends, from Hôtel-Dieu to the new CRCHUM, especially on the 8th floor, particularly Abel Oppong, Aida Kasaei Roodsari, Anindya Ghosh, Chao-Sheng (Willie) Lo, Denis Yip, Estelle Rolande Simo Cheyou, Henry Nchienzia, Jennifer Lu, Kadidia Diallo, Marcos Fernando Ocaña Sánchez, Michel Desjarlais, Min-Chun (Matthew) Liao, Rafael Ochoa-Sanchez, Sarah Maximos, Shiao-Ying (Nicole) Chang, Shuiling (Susie) Zhao, Sophie-Annabelle Barratteau, Valérie Bergeron, Valérie Clermont, Vanessa Truong, Viktoria Youreva, Xinping (Jane) Zhao, Yat Hei (Henry) Leung, Yessoufou Aliou, Yixuan (Steven) Shi, Yves Mugabo, Zulaykho Shamansurova: It was a real pleasure and joy working with you all. You all made my everyday life at work more than enjoyable through these years. I cannot express my gratitude enough to you all for your friendship. Thank you all for being there for me by lending me a hand or an ear, and even looking out for me. I will forever keep fond memories of our time together at and around the CRCHUM. With all the fun and countless laughter we had, it would not have been such a wonderful experience without you guys.

I had the privilege to be involved in my academic community. To Dr. Marc Prentki and Alix Zutter: I thank you for welcoming me to the Montreal Diabetes Research Center (MDRC) even though my work was not related to diabetes. You allowed me to broaden my horizons and to actively participate in your scientific activities. I am also grateful to have collaborated with my colleagues at the MDRC. To Dr. Pierrette Gaudreau and Joanne Auclair: It was a pleasure working with you when I presided over the student committee, and I thank you for your help. To Dr. Patrick James and Dr. Daniel Borcard: I thank you for trusting me to be your TA for BIO 2041.

To all of my friends outside the CRCHUM, whom I have met during the different stages of my life, especially my childhood friends (Martin Dubé and Maxime Lauzon), Les 3 amigos (Alanna Yazi Yu and Tuong-Vi (Tina) Ton), my IB friends or Le Club de JJ (Cynthia Benoit-Labrèche, David Mark, Isaac Nzaramba, Lisa Traversy, Martin-Pierre Boisvert, Stéphanie Wong and Vanessa Patrice), James Martin and Horia Nicolae Roman: Although I spent most of my time working towards this degree, your presence, near or far, has always been appreciated during these years. Seeing you guys always cheers me up. I value our friendship and your endless encouragements, which motivated me to excel in my work and overcome adversity. Thank you to you all for believing in me and seeing in me what I should believe in regarding myself.

Finally, I would not be here if it weren't for my Family. From the bottom of my heart, I thank my parents: Words are not enough to express all my love and gratitude for everything that you have done for us. I hope that this Ph. D. is a testament to your sacrifice and hard work, as well as to all your love and care that you put into raising us. Thank you for always being there for us and going beyond the extra mile to create the best conditions for us to live. To my siblings: While I am far from being perfect myself, I strive to be the best brother as I can be for you all. To me, you are all simply the best, and you all inspire me to surpass myself. I have always looked up to you all, and I will forever admire each one of you. I thank you all for being there for me by still looking out for me and by always taking care of me in your own way.

Of course, I will never forget the generous funding agencies for granting me numerous awards and prizes throughout my doctoral studies so that I have extra financial support during these years, as well as the means to attend international conferences. Thank you.

P.S. To the many other people who have played an integral part of my life, from past mentors and supervisors to current colleagues and friends: I am deeply indebted to you all for your kindness and help, which contributed to my personal and professional development, through your advice, encouragement and support. Without you all, I would not be the person who I am now, nor would I be where I am today, so I personally thank all of you for being, as Maya Angelou would say, rainbows in my clouds. You were indeed in your own way a blessing to me.

Chapter 1 – Introduction

1.1 The Lungs

The human body requires oxygen (O₂) for its cells to produce adenosine triphosphate (ATP) as a source of energy. Through cellular respiration, a cell can produce up to 29–32 molecules of ATP from a single molecule of glucose by glycolysis, the Krebs cycle and oxidative phosphorylation (1, 2). In return, the cell's many metabolic processes produce carbon dioxide (CO₂), which needs to be expelled. Hence, the respiratory system ensures the adequate gas exchange to acquire O₂ from the air and to eliminate CO₂ from the blood (3, 4). Both left and right lungs are within the thoracic cage, where the main muscles enable volume changes to facilitate inspiration and expiration of air. In average, a human adult at rest inhales up to 12,000 liters of air per day (5, 6). The adult lungs hold approximately 2,400 kilometres (1,500 miles) of airways and 300–500 million alveoli, providing an extremely large surface area for gas exchange that is estimated to be between 70 m² and 145 m² (7, 8).

1.1.2 Airway Anatomy

Respiration ensures the in-and-out movement of air through the airways to ultimately bring it to the distal part of the lung, an area adjacent to the pulmonary capillaries, thus favourable for gas exchange (8). The airways are composed of a single branching tube, which begins at the nasal and oral cavities, followed by the pharynx, the larynx and the trachea. As seen in Figure 1, the trachea is where the first division takes place. Each division occurs in a dichotomous fashion (i.e., it is divided into two), essentially creating a tree-like network. As the respiratory tract successively divides itself, it becomes more and more narrow (smaller diameter), and its histological composition changes (4). In function of how many divisions (i.e., generation) does the tube endure, we can distinguish different sections of the airways.

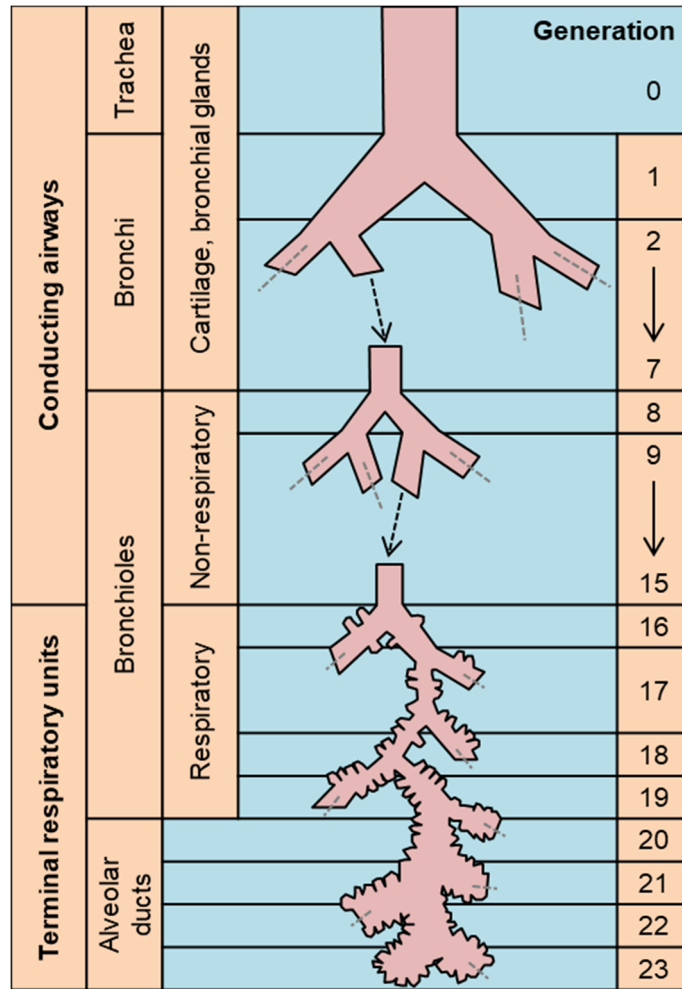


Figure 1. – Subdivision of Human Lung Airways

(Figure adapted from Hammer *et al.* (9))

The airway is mainly organized in two zones: a conductive (or condition) zone and a respiratory zone. The former's function is to clean, moisten and transport the air towards the distal part of the lung (10). The airways are regularly exposed to various environments and dangerous pathogenic agents. It is estimated that over 100 billion particles, chemicals and pathogens are inhaled on a daily basis (6, 11). Hence, the airway epithelium forms a protective barrier as it is covered by a layer of airway surface liquid (ASL), made of a mucus layer over a periciliary liquid (PCL) layer (10). In the conductive zone, the epithelium is pseudostratified,

where the airways are lined with epithelial cells, composed mainly of ciliated, goblet and basal cells (10).

Ciliated cells have motile cilia, which create a coordinated movement to propel the mucus towards the throat, as well as ion channels, which control water flow across the epithelium by modulating ion transport, notably through sodium (Na^+) reabsorption and chloride (Cl^-) secretion, to regulate the PCL for optimal mucociliary clearance (MCC) (12). Goblet cells produce and secrete mucus, which lubricates the apical surface, moistens air and traps particles, as well as absorbs harmful gas (e.g., ozone (O_3)) (10). Basal cells maintain the homeostasis of the epithelium by repairing it after injury or by renewing the tissue as they can also act as resident stem cells (10).

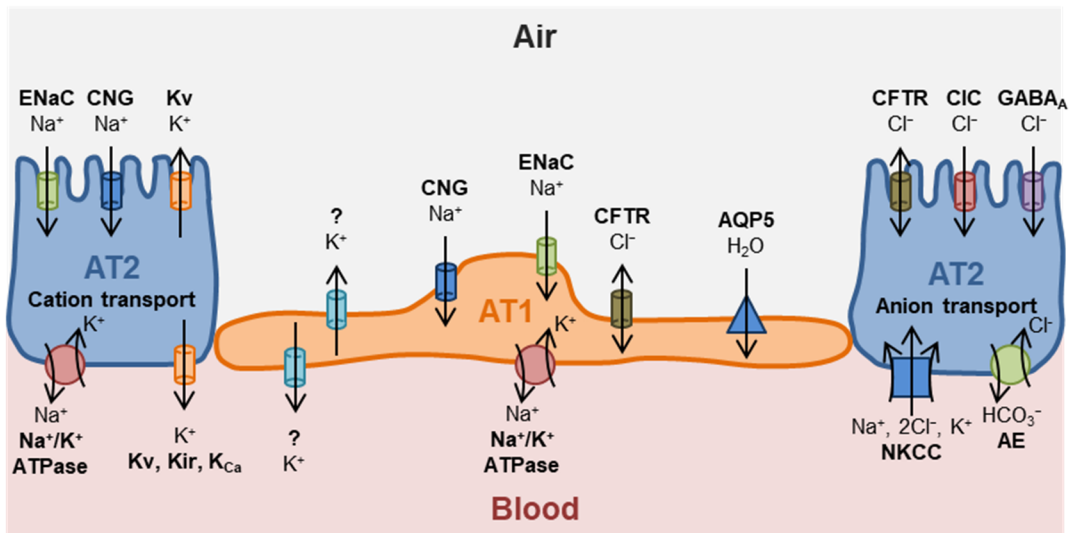
The conductive zone slowly transitions into the respiratory zone, which is the area where gas exchange between the air and the blood occurs, or where blood becomes oxygenated (8). This portion of the lung includes the respiratory bronchioles, alveolar ducts, alveolar sacs and alveoli (8). The three main cell types described above gradually decrease in number towards the distal airways as we find more non-ciliated cells called club cells (formerly known as Clara cells). These are dome-shaped cells, which secrete club cell secretory proteins (CCSP), mucins and antimicrobial peptides (10). Club cells act as progenitor cells to repopulate ciliated cells. The epithelium becomes thinner and changes from a cuboidal shape to a simple squamous in alveolar ducts and sacs (10).

An alveolar sac is composed of many alveoli. These structures cover 99% of the lung surface area and are in close proximity (0.1–0.2 μm) to endothelial capillaries (13). Its thin walls and large surface area facilitate gas exchange between the inspired air and the capillaries (8, 14). In addition to ensuring an efficient exchange of gases, the close distance between the alveolar epithelium and the vascular endothelium forms a tight barrier, which prevents liquid and proteins from the vascular and interstitial spaces from entering the alveolar airspace: an alveolus is relatively dry (13). The alveolar epithelium is lined with two specialized cells: alveolar type 1 (AT1) and alveolar type 2 cells (AT2) (10, 15).

1.2 Alveolar Cells

1.2.1 Alveolar Type 1 (AT1) Cells

AT1 cells are squamous, flat and thin, with a thickness of 0.1–0.2 μm covering a large surface (50 μm in diameter) (8, 16, 17). It is thought that because of their morphology, AT1 cells solely enable efficient gas diffusion across the alveolar wall and the capillary endothelium, given their low resistance for diffusion, the minimal thickness and the large surface area (3, 13, 18). This maximizes gas exchange between the alveolar airspace and pulmonary capillaries (19). However, because it is better for the alveolar space to remain relatively dry for optimal gas exchange, alveolar cells are also involved in fluid transport (20). Fluid movement across the alveolar epithelium is achieved by active salt transport, which creates an osmotic gradient favourable for water absorption (13). As depicted in Figure 2, AT1 cells notably express, on the apical side, aquaporin-5 (AQP5), a water channel, and sodium channels, particularly epithelial sodium channel (ENaC), to draw water into the cell (13, 20). Intracellular Na^+ is actively transported out of the cell, in exchange for extracellular potassium (K^+), through the basolateral membrane by sodium-potassium adenosine triphosphatase (Na^+/K^+ -ATPase), also known as sodium–potassium pump (20). Ridge *et al.* demonstrated the $\alpha 2$ isoform of Na^+/K^+ -ATPases is present in AT1 cells, and it is preferentially upregulated by adrenergic agonist isoproterenol, which can increase reabsorption of alveolar fluid in the lung (20). The resulting K^+ ions pumped into the cell are then recycled by potassium channels expressed at the basolateral side to maintain intracellular K^+ and membrane potential homeostasis (21). When injured or damaged, AT1 cells shed off or are removed from the epithelial surface, which exposes the basement membrane (18). Since they are terminally differentiated, AT1 cells are unable to restore the naked areas of the epithelium (22). However, Jain *et al.* showed that AT1 cells may possess some form of plasticity, being able to become AT2 cells (16). This is also supported by Yang *et al.*, who demonstrated that AT1 cells have both structural and signaling roles in alveolar maturation and can exit their terminally differentiated non-proliferative state (23).



↑, ↓, ↕: Direction of ion movement across the cell membrane; ?: Unknown K^+ channel;
AE: Anion exchanger; **AQP5**: Aquaporin 5; **CFTR**: Cystic fibrosis transmembrane
 conductance regulator; **CIC**: Voltage-sensitive Cl^- channels; **CNG**: Cyclic-nucleotide-
 gated channel; **ENaC**: Epithelial Na^+ channel; **GABA_A**: γ -aminobutyric acid type A Cl^- -
 channel; **K_{Ca}**: Calcium-activated potassium channel; **Kir**: Inward rectifying K^+ channel;
Kv: Voltage-gated potassium channel; **Na⁺/K⁺-ATPase**: Sodium/potassium ATPase;
NKCC: Sodium/potassium two chloride cotransporter

Figure 2. – Ion Transport in AT1 and AT2 Cells

(Figure adapted from Hollenhorst *et al.* (12))

1.2.2 Alveolar Type 2 (AT2) Cells

AT2 cells are usually located on the edges or corners of the alveolus, lying isolated amongst AT1 cells, and they are cuboidal in shape, roughly $9\ \mu\text{m}$ in diameter (17, 19). While AT1 cells were thought to be unable to divide, AT2 cells are progenitor cells for airway regeneration to renew damaged alveolar cells (8, 16, 18). Barkauskas *et al.* demonstrated that AT2 cells may display stem cell abilities to become AT1 cells (24). Nevertheless, the principal role of AT2 cells is the production and secretion of pulmonary surfactant, a lipoprotein, which covers the alveolar wall in order to reduce surface tension for easy expansion of the alveolus (8). Furthermore, these cells contain microvilli, as well as lamellar bodies (LB), which are surfactant-producing organelles in their cytoplasm, measuring between $0.2\ \mu\text{m}$ and $2\ \mu\text{m}$ in diameter (16, 17, 25). LB fuse with the apical plasma membrane to secrete pulmonary surfactant into the alveolar space

(26). Similarly to AT1 cells, AT2 cells are equally involved in the transport of Na^+ (and Cl^-) for active transport of fluid from the apical to the basolateral side, to remove liquid from the alveolar space (13). As depicted in Figure 2, AT2 cells have a variety of channels involved in ion transport, including Na^+ and Cl^- transport pathways to maintain liquid homeostasis on the alveolar surface (12). Na^+ uptake occurs through apical amiloride-sensitive ENaCs and gets pumped out by basolateral ouabain-sensitive Na^+/K^+ -ATPases in exchange of K^+ , which later exits through potassium channels (15, 21). Cl^- transport mainly occurs through the cystic fibrosis transmembrane conductance regulator (CFTR), which plays an important role in the secretion of water (15, 27). Therefore, alveolar cells can absorb and secrete liquid to maintain the liquid layer over them, crucial for efficient gas exchange, surfactant homeostasis, as well as defence against inhaled toxins and pathogens (15, 28). Being the first in line to defend the alveolus against microbial infection, AT2 cells also secrete a multitude of mediators, including pro-inflammatory cytokines (chemoattractants) and mitogenic growth factors, to recruit immune cells and activate macrophages (29, 30).

Even though there is more than twice the number of AT2 cells in the alveolus than AT1 cells, roughly 95% of the alveolar surface area is covered by AT1 cells and 5% by AT2 cells (15, 18, 19). Both alveolar cell types, being close together, may share a role in mechanosensing by propagating intracellular calcium ($[\text{Ca}^{2+}]_i$) signals (31). Between them, cytosolic calcium ions (Ca^{2+}) may be transmitted directly through gap junctions, as well as indirectly via secretion of ATP and paracrine stimulation of purinergic receptors, when they are mechanically stimulated (32).

1.3 Lung Injury and Mechanical Ventilation (MV)

The lung epithelium may be injured in presence of infections, inflammation or physical trauma (33). In such instances, the repair mechanism of lung injury primarily involves the host defence and tissue repair. On one hand, there is an acute inflammatory response, where various cells (e.g., fibroblasts, endothelial and epithelial cells) respond by releasing a number of chemokines, as well as pro- and anti-inflammatory cytokines, to resolve the inflammation (33, 34). For instance, lung epithelial cells produce and release a host of mediators, such as reactive

oxygen species (ROS), cytokines (interleukin (IL)-1 β , tumor necrosis factor (TNF)- α , granulocyte/macrophage colony-stimulating factor), and platelet-activating factor for inflammatory cells recruitment at the site of inflammation (35). Moreover, alveolar macrophages release cytokines (IL-1 β and TNF- α) to attract immune cells, namely neutrophils and leukocytes (33, 36). On the other hand, progenitor cells will migrate over surfaces having no cells in an attempt to rebuild the epithelium by proliferating and differentiating their phenotypes (29). It also seems that the repair mechanism is halted when mechanical stretch is applied to the wounded area (33). If the damage persisted, the epithelium's integrity would be altered, and fibroblasts would be activated, ultimately promoting fibrosis. Uncontrolled inflammation in the lung may lead to inflammatory diseases, such as those described in the following section.

1.3.1 Acute Respiratory Distress Syndrome (ARDS) and Acute Lung Injury (ALI)

In 1967, Ashbaugh *et al.* provided the initial description of acute respiratory distress syndrome (ARDS), but it was only until 1994 that the American-European Consensus Conference (AECC) defined ARDS (37-39). ARDS is characterized by damage to the alveolar epithelial and vascular endothelial barriers, hyperinflammatory response and pulmonary edema, all of which impair gas exchange, resulting in hypoxemia and hypercapnia (40, 41). Based on the degree of hypoxemia, designated by the quotient of arterial oxygen partial pressure (PaO₂) by the fraction of inspired oxygen (FiO₂), also known as the Horowitz index, the AECC defined ARDS with a PaO₂/FiO₂ ratio \leq 200 mmHg (38, 42). In addition, the AECC Definition introduced acute lung injury (ALI), a less severe form of ARDS, when PaO₂/FiO₂ \leq 300 mmHg (38, 42). However, in 2012, the latest ARDS definition, the Berlin Definition, defined ARDS with a PaO₂/FiO₂ less than 300 mmHg with a positive end-expiratory pressure (PEEP) of at least 5 cmH₂O, in addition to other clinical criteria (39). The Berlin Definition also removed the term ALI used previously by the AECC Definition and proposed to categorize the severity of ARDS according to the Horowitz index: mild (200 mmHg < PaO₂/FiO₂ \leq 300 mmHg), moderate (100 mmHg < PaO₂/FiO₂ \leq 200 mmHg), and severe (PaO₂/FiO₂ \leq 100 mmHg) (39).

Indeed, ARDS is an acute inflammatory lung injury and is associated with increased pulmonary vascular permeability, increased lung weight and loss of aerated lung tissue characterized by acute respiratory failure (43, 44). ARDS is a result of many major insults or severe traumas to the lungs, whether directly (e.g., pneumonia, aspiration of gastric contents, lung contusion, near drowning) or indirectly (e.g., sepsis, acute pancreatitis, non-thoracic trauma, transfusion of blood products) (40, 42). The most common pulmonary and extrapulmonary causes are pneumonia and sepsis, respectively (40).

These injurious stimuli damage or destroy the alveolar epithelial cell and pulmonary microvascular endothelial cell (43). When the alveolar-capillary barrier is disrupted (e.g., due to vascular inflammation), microvessels in this barrier become more permeable, which allows a protein-rich fluid to flow into the alveolar airspace (42, 45, 46). This common clinical problem may persist due to the impairment of the active Na^+ and water transports, which are responsible for reabsorbing fluid, as hydrostatic and protein osmotic pressures no longer favour fluid reabsorption (13, 46, 47). Pulmonary edema fluid within the alveoli contributes to the pathogenesis of ARDS (47). As an inflammatory condition, this even facilitates the infiltration and excessive recruitment of neutrophils into the lung, from the increased levels of inflammatory proteins (cytokines and chemokines), which can be detrimental for lung function (43, 48). Wounded and repaired cells also activate stress response genes and alter protein expressions, releasing pro-inflammatory mediators and promoting fibrosis, which all exacerbate the injury (49).

In 50 countries, ARDS represented 10.4% of total admissions to the intensive care unit (ICU) and 23.4% of all patients in the ICU requiring mechanical ventilation (MV), representing 0.42 cases per ICU bed over 4 weeks (44). Unfortunately, this respiratory disease is associated with high mortality rates, averaging 34.9%, 40.3% and 46.1% for patients with mild, moderate and severe ARDS, respectively (44). ARDS is therefore a life-threatening impairment of pulmonary gas exchange, causing hypoxemia, hypercapnia and respiratory acidosis. Hypoxia is caused by an inefficient support of the respiratory system or the oxygen delivery system (cardiac output, hemoglobin level) (41). To manage ARDS, patients resort to MV as a rescue measure to deliver O_2 to the blood through a lower tidal volume and a higher PEEP (44). While

MV supports and manages patients, who are unable to breathe properly on their own, this treatment can, at times, do more harm than good (50).

1.3.2 Ventilator-Induced Lung Injury (VILI)

Mechanical ventilators constitute a life-support device, which provides full or partial respiratory assistance to patients with inadequate breathing in the ICU (51). Though life-saving, MV may introduce additional pulmonary complications, which increases morbidity and mortality (29, 51, 52). In mechanically ventilated patients with respiratory failure, notably due to ARDS, the already impaired lungs are exposed to excessive stretch, which often worsens the damage at the cellular level and causes fibrosis, collectively referred to as ventilator-induced lung injury (VILI) (52, 53).

Fortunately, there are current ventilation strategies, whose aim is to prevent and minimize VILI (41, 51, 54). On one hand, applying low tidal volumes (6 mL/kg) limits alveolar overdistension (54). On the other hand, using high PEEP levels (≥ 5 cmH₂O), with recruitment maneuvers, reinflates collapsed lung regions (atelectasis) and reduces inhomogeneous ventilation, thereby preventing lung injury from atelectrauma (impact of stress and strain maldistribution) (54). Other procedures, specifically placing the patient in the prone position and administering neuromuscular blocking agents, may complement these preventive strategies (41, 54). Santos *et al.* also demonstrated that a low degree of mechanical power (i.e., the energy transfer from the ventilator to the lungs over time) minimizes VILI in rats having ARDS (55).

In extreme conditions, such as positive pressure MV or during severe bronchoconstriction, cells in the lung are compressed and/or stretched exceeding normal values, leading to pathological outcomes, namely alveolar rupture and barotrauma (54, 56, 57). Ventilator-induced lung overdistension, as a result of high large tidal volumes, disrupts the alveolar epithelium, increasing its permeability, aggravating alveolar edema and producing an inflammatory lesion reminiscent of diffuse alveolar damage (54, 56, 58). MV affects AT2 cell differentiation, hindering these cells to replenish the damaged alveolar epithelium (50). Cell death due to such deformations could give rise to the development of VILI (50). Nevertheless,

inflating with small lung volumes may even give rise to atelectraumatic lung injury because of the increased lung inhomogeneity caused by the presence of collapsed alveoli. (54). Whether the distending force is large or moderate, mediators are released to recruit neutrophils in the lung, which promotes fibrosis (54).

In the rat model, injurious ventilation strategies induce early-response genes, particularly *c-fos*, and promote inflammation through the release of cytokines, such as TNF- α (36, 58). Vlahakis *et al.* demonstrated that 30% mechanical stretch induces cytokine (IL-8) release in human lung adenocarcinoma A549 cells, which leads to alveolitis, a condition associated with VILI (58, 59). IL-8 is a chemoattractant and activator of neutrophils, and it can initiate inflammatory responses associated with lung diseases (59). In rat models of VILI, ATP levels in the bronchoalveolar lavage fluid (BALF) were significantly increased by high pressure MV (52). Rich *et al.*, using mechanically ventilated rats at low and high pressure (15 cmH₂O and 40 cmH₂O, respectively) for 30 minutes, observed that the BALF contained higher levels of ATP from rats ventilated at high pressure than low pressure (60). The increased levels of extracellular ATP also seemed to be associated with alveolar edema, which may suggest a role of extracellular ATP in the development of VILI (60).

1.4 Purinergic Signaling

1.4.1 Adenosine Triphosphate (ATP)

As shown in Figure 3, ATP is a nucleotide and consists of a nitrogenous base (purine, adenine), a sugar molecule (ribose) and a chain of three ionized phosphates (61). Considered to be the universal energy currency, ATP provides energy for a variety of intracellular biological reactions in all mammalian life, making it a source of energy, vital for the cell's survival (62, 63). When the bond between two phosphate groups is hydrolyzed, energy is released (7.3 kcal/mol) (64, 65). As a result, ATP is converted into adenosine diphosphate (ADP), a nucleotide with two phosphate groups. Similarly, losing another phosphate group through a second hydrolysis turns ADP into adenosine monophosphate (AMP).

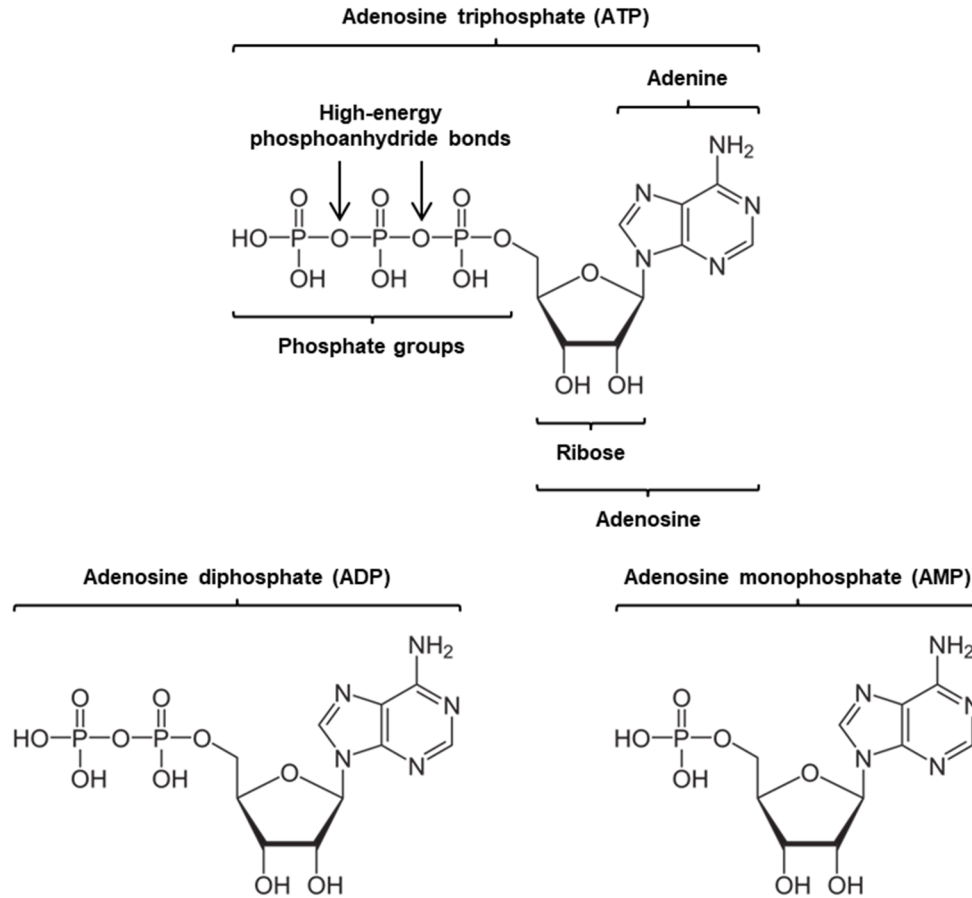


Figure 3. – Molecular Structure of Adenine Nucleotides

(Figure adapted from Zimmerman *et al.* (61))

ATP is produced through cytosolic glycolysis, whose end products enter the Krebs cycle and undergo oxidative phosphorylation in the electron transport chain to produce more molecules of ATP in the mitochondrion (62, 66). Within a cell, the concentration of ATP ranges from 3 mM to 10 mM, which is considerably higher than its values outside the cell (66-68). ATP can also be stored within vesicles, reaching up to 100 mM (66). Under resting conditions, the estimated concentration of extracellular ATP is in the low nM range (69).

In fact, through a mechanism, which is still debated (see 1.6 *Candidate Pathways for ATP Release*), ATP can exit the cell in small amounts, with an estimated ATP efflux at around 20–200 fmol/min (62, 68). Once out of the cell, ATP functions as an extracellular signaling molecule, where extracellular local ATP concentration may be in the μM up to $<1 \text{ mM}$ range during signaling (68). Because it is a weak acid ($\text{pK}_a = 6.9$), it exists as an anionic form under physiological conditions (66). Being water soluble, this large hydrophilic molecule can freely diffuse in the extracellular environment due to its negatively charged phosphate residues (62, 70). Upon binding on specific cell-surface purinergic receptors, ATP activates and initiates the purinergic signaling.

1.4.2 Purinergic Receptors

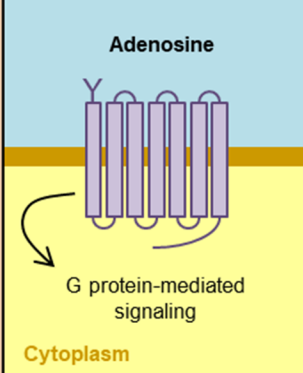
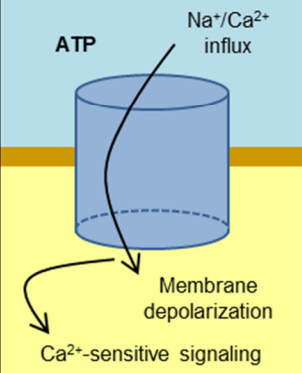
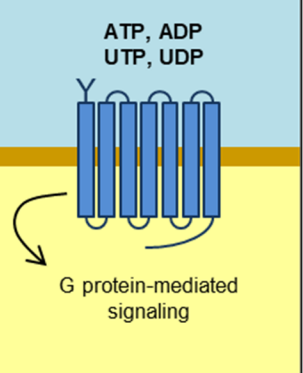
Purinergic Receptors			
Family	Adenosine or P1 receptors	P2 receptors	
Subfamily		P2X	P2Y
Receptor subtypes	A_1, A_{2A}, A_{2B}, A_3	$P2X_1, P2X_2, P2X_3, P2X_4, P2X_5, P2X_6, P2X_7$	$P2Y_1, P2Y_2, P2Y_4, P2Y_6, P2Y_{11}, P2Y_{12}, P2Y_{13}, P2Y_{14}$
Structure	G protein-coupled receptors	Ligand-gated ion channels	G protein-coupled receptors
Ligands	<p>Adenosine</p>  <p>G protein-mediated signaling</p> <p>Cytoplasm</p>	<p>ATP</p>  <p>$\text{Na}^+/\text{Ca}^{2+}$ influx</p> <p>Membrane depolarization</p> <p>Ca^{2+}-sensitive signaling</p>	<p>ATP, ADP, UTP, UDP</p>  <p>G protein-mediated signaling</p>

Figure 4. – Characteristics of Purinergic Receptors

(Figure adapted from Rajagopal *et al.* (71))

Purinergic receptors are located on the cell surface of most, if not all, cells. They are classified into two main families, P1 and P2 receptors, with the latter having two subfamilies, P2X and P2Y, as seen in Figure 4, which also provides the receptor's subtypes, structure and ligands. Regarding the lungs, these receptors are expressed in airway smooth muscles, as well as in airway epithelial cells, including alveolar cells (67, 72, 73). More precisely, while all P1 receptors are expressed in the lung epithelium, only P2X₄, P2X₅, P2Y₁, P2Y₂, P2Y₄, P2Y₆ and P2Y₁₁ receptors are present (74-77).

P1 receptors are G protein-coupled receptors, whose ligand is exclusively adenosine, an end product of ATP hydrolysis. There are four subtypes attributed to P1 receptors: A₁, A_{2A}, A_{2B}, A₃ (71). A_{2A} and A_{2B} receptors couple with G_s protein, which activates adenylyl cyclase (AC), an enzyme that uses ATP as a substrate in order to produce cyclic AMP (cAMP). cAMP serves as a second messenger, which activates protein kinase A (PKA) (56). On the contrary, A₁ and A₃ receptors couple with G_i protein, which instead inhibits AC and reduces cAMP production, so PKA is not activated.

Nucleotides bind to P2 receptors, which are further subdivided into two subgroups: P2X and P2Y receptors. On one hand, P2X receptors are ligand-gated ion channel receptors, whose sole agonist is ATP (72). There are seven subtypes: from P2X₁ to P2X₇. On the other hand, similarly to P1 receptors, P2Y receptors are metabotropic and include eight subtypes: P2Y₁, P2Y₂, P2Y₄, P2Y₆, P2Y₁₁, P2Y₁₂, P2Y₁₃ and P2Y₁₄ (56, 71). P2Y₁, P2Y₂, P2Y₄ and P2Y₆ receptors couple with G_q protein, which stimulates phospholipase C (PLC) (β isotype) to cleave phosphatidylinositol 4,5-bisphosphate (PIP₂) into diacylglycerol (DAG) and inositol 1,4,5-triphosphate (IP₃). Binding of IP₃ to IP₃ receptors on the endoplasmic reticulum (ER) activates the IP₃-gated calcium channels. This releases Ca²⁺ into the cytoplasm, thereby increasing [Ca²⁺]_i, which, together with DAG, activates protein kinase C (PKC) (56). P2Y₁₁ receptors couple with G_s proteins, whereas P2Y₁₂, P2Y₁₃ and P2Y₁₄ receptors couple with G_i proteins. Unlike its ion channel counterpart, P2Y receptors can bind not only ATP but also ADP, UDP and UTP (71). However, each subtype binds a specific agonist. For example, P2Y₁ receptors bind ADP, while P2Y₂ receptors bind ATP and UTP (72). Table 1 summarizes the agonists and signaling properties of purinergic receptors (72).

Table 1. – Agonists and Signaling Properties of Purinergic Receptors

(Table adapted from Lazarowski (72))

	Agonist	Signaling Properties
Adenosine receptors		
A ₁ , A ₃	Adenosine	G _i → ↓AC/↓cAMP
A _{2A} , A _{2B}	Adenosine	G _s → ↑AC/↑cAMP
P2X receptors		
P2X ₁ to P2X ₇	ATP	ATP-gated cation channel
P2Y receptors		
P2Y ₁	ADP	G _q /PLCβ → Ca ²⁺ /PKC
P2Y ₂	ATP, UTP	G _q /PLCβ → Ca ²⁺ /PKC
P2Y ₄	UTP	G _q /PLCβ → Ca ²⁺ /PKC
P2Y ₆	UDP	G _q /PLCβ → Ca ²⁺ /PKC
P2Y ₁₁	ATP	G _q /PLCβ → Ca ²⁺ /PKC G _s → ↑AC/↑cAMP
P2Y ₁₂ , P2Y ₁₃	ADP	G _i → ↓AC/↓cAMP
P2Y ₁₄	UDP-glucose	G _i → ↓AC/↓cAMP

↑: Activation; ↓: Inhibition; **AC**: Adenylyl cyclase; **cAMP**: Cyclic AMP

PLCβ: Phospholipase C (β isotype); **PKC**: Protein kinase C

1.4.3 Conversion and Metabolism of Extracellular ATP

Once out of the cell, ATP can bind to ligand-gated P2X receptors and metabotropic P2Y receptors (66, 78). However, its concentration quickly declines as extracellular ATP is also degraded by enzymes bound to the plasma membrane and by soluble secreted nucleotidases present in the ASL, which further expands the diversity of the purinergic signaling (66, 78-80). Ecto-nucleoside triphosphate diphosphohydrolase (E-NTDPase) enzymes can hydrolyze bonds between phosphate groups in ATP and ADP, converting ATP to ADP, and ADP to AMP. E-NTDPase enzymes include ecto-ATPase, ATP diphosphohydrolase (ATPDase), apyrase (or CD39) and nucleoside diphosphatase (78, 81). Direct conversion of ATP into AMP can also be achieved

by ecto-nucleotide pyrophosphatase/phosphodiesterase (E-NPP) (82). Ecto-5'-nucleotidase (E-5'-N) (or CD73) breaks down AMP into adenosine (67, 78). Finally, alkaline phosphatases, such as adenosine deaminase, can catalyze the deamination of adenosine, which inactivates the nucleoside so that it can re-enter the cell via nucleoside transporters due to a favourable concentration gradient (63, 67, 78, 81). Within the cell, enzymes adenylate kinase, nucleoside diphosphate kinase and ATP synthase regenerate adenosine to ATP (78). These enzymes can be co-expressed on the cell surface to achieve the same results (78). Therefore, ATP that is released can stimulate both P1 and P2 families of purinergic receptors due to its conversion/hydrolysis into ADP, AMP and adenosine. Figure 5 illustrates the breakdown of extracellular ATP to adenosine, as well as the binding of ATP and its metabolites to their respective purinergic receptors.

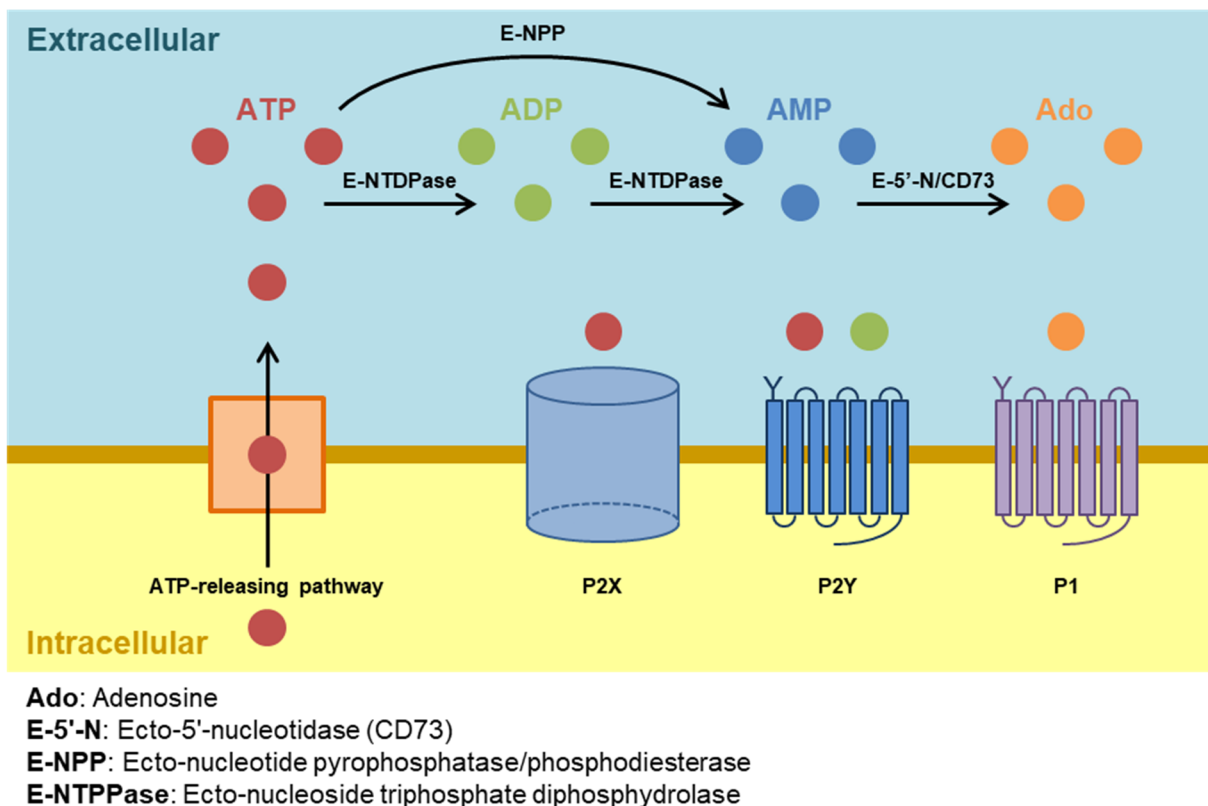


Figure 5. – Breakdown of Extracellular ATP and Binding of Ligands to Purinergic Receptors

(Figure adapted from Velasquez *et al.* (83))

It should be noted that ATP is typically not released alone from stimulated cells but rather co-released with its metabolites (ADP, AMP, adenosine), as well as other nucleotides (UTP and UDP) as demonstrated by Tatur *et al.* in hypotonic shock-stimulated A549 cells (84). Interestingly, the ratios of released ADP:ATP and UDP:UTP were both markedly higher than those within the cytoplasm, suggesting that a nucleotide diphosphate-rich compartment (e.g., a secretory pathway) may contribute to nucleotide release, consistent with a regulated exocytotic release mechanism (84).

1.5 Extracellular Nucleotides in the Lungs

Extracellular nucleotides are found on the surface of the respiratory epithelium (85). Through a paracrine and/or autocrine fashion, ATP and its metabolites bind to purinergic receptors, whose activation initiates the purinergic signaling cascade, capable of regulating a host of functions in the lungs (86). Generally, the activation of P2 and P1 receptors often transduces opposite effects (63). These lung functions include, amongst others, secretion of surfactant and fluid, cell proliferation, stem cell homing, pain sensation, neutrophil chemotaxis and MCC (87).

1.5.1 Surfactant Secretion

ATP is a potent secretagogue that stimulates surfactant secretion by AT2 cells (31, 88). Pulmonary surfactant is made of lipids and surfactant proteins, which is stored in LB within AT2 cells (26, 31). Upon binding to P2Y₂ receptors, ATP has been found to stimulate the fusion of LB to the plasma membrane, promoting surfactant secretion into the extracellular environment (26, 31). Activation of the P2Y₂ receptor increases $[Ca^{2+}]_i$ via IP₃ pathway, which triggers the fusion of secretory vesicles with the cell membrane, hence enhancing the release of their content (31, 69).

1.5.2 Fluid Secretion

By activating purinergic receptors, ATP and other nucleotides present in the ASL are important modulators of ion transport, which regulates mucus hydration and MCC through the modulation of Na⁺ absorption and Cl⁻ secretion across the apical surface of the airway

epithelium (56, 85, 89). Binding of ATP to P2Y₂ receptors stimulates Cl⁻ secretion and inhibits Na⁺ absorption by ENaC, which hydrates the ASL (56, 75, 88). As shown in Figure 6, Cl⁻ secretion can be achieved by the Ca²⁺-activated Cl⁻ channel (CaCC), from the increase of [Ca²⁺]_i upon the activation of P2X₄, P2Y₂ and P2Y₆ receptors by ATP (only P2Y₂ receptor is shown) (75). In fact, the concentration of extracellular ATP proportionally alters the rates of ion absorption and secretion regarding ASL hydration and MCC (46, 90). However, excessive ATP desensitizes receptors, which ceases fluid secretion, and prevents airways flooding (90).

Regarding the alveolar space, Bove *et al.* demonstrated that the ion and liquid homeostasis in human AT2 cell monolayers differs from that in airway epithelial cells (15). In AT2 cells, Na⁺ absorption is mediated by ENaC, which is positively regulated by cAMP and not inhibited by CFTR activation, and Cl⁻ is secreted only by CFTR, with no contribution of CaCC (15). As for purinergic signaling, it seemed that only the activation of P2X₄ and P2Y₄ receptors is involved in ion transport, despite also the presence of P2Y₂ and P2Y₆ receptors in AT2 cells (15).

In addition to ATP, adenosine is even involved in the hydration of the ASL by purinergic signaling, which regulates ion transport and fluid clearance through the increase of Cl⁻ secretion and inhibition of Na⁺ absorption (90, 91). It should be noted, however, that the earlier hypothesis that CFTR directly inhibits ENaC via direct protein-protein interactions or via signaling molecules, has been refuted by several studies, which demonstrated that apparent ENaC inhibition results from altered Na⁺ electrical driving force following stimulation of CFTR-mediated Cl⁻ transport (92). Figure 6 also shows that binding of adenosine to A_{2B} receptors promotes Cl⁻ secretion via activation of CFTR and a reduction of Na⁺ absorption through ENaC (56, 75, 93). In the alveolus, activation of A₁ receptors creates a Cl⁻ efflux through CFTR, which counterbalances active Na⁺ absorption, required for the homeostasis of the alveolar lining fluid (46). Factor *et al.* demonstrated that in rat AT2 cells, physiological doses ($\geq 1 \mu\text{M}$) of adenosine decrease alveolar fluid clearance (AFC) via A₁ receptors, but at low doses ($\leq 10 \text{ nM}$), AFC is increased via A_{2A} and/or A₃ receptors (46).

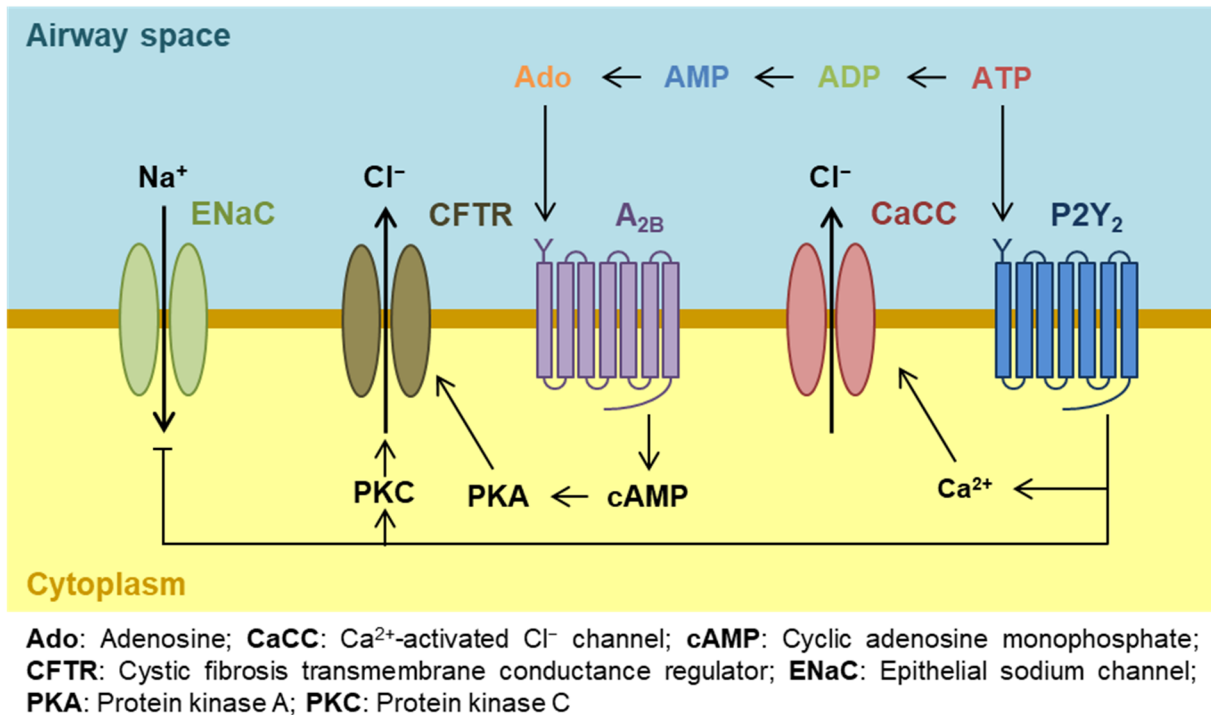


Figure 6. – Purinergic Regulation of Ion Transport in the ASL

(Figure adapted from Lazarowski *et al.* (75))

1.5.3 Mucociliary Clearance (MCC)

Many cellular functions in the airways are related to regulating MCC, which is the primary innate defence mechanism that helps to protect the lungs from inhaled noxious and infectious materials (68, 94). This involves production and secretion of mucus to trap foreign particles and pathogens on airway surfaces (52). Subsequent clearing of mucus from the airway is achieved by the movement of cilia in the PCL, which is controlled by ion and liquid transport in the airways (90, 94). All three components of the MCC system (mucus secretion, fluid secretion, and cilia beating) are under purinergic control (73). ATP in the ASL controls MCC functions via the activation of airway epithelial purinergic receptors (89). By binding to P2Y₂ (and to an extent P2Y₆) receptors, ATP regulates ciliary beat frequency in airway epithelial cells, a process involving [Ca²⁺]_i (75, 88). Hansen *et al.* showed that ATP application propagates Ca²⁺ wave and increases the ciliary beat frequency in epithelial cells from the tracheal mucosa of New Zealand

White Rabbits (95). In the absence of $[Ca^{2+}]_i$, ciliary beating can be stimulated by activation of A_{2B} receptors by adenosine, as well as downstream via cAMP and PKA (75).

1.5.4 Danger-Associated Molecular Pattern (DAMP)

Given its high concentration under pathophysiological conditions, ATP can even act as a danger signal or danger-associated molecular pattern (DAMP) (52, 96). DAMPs are endogenous molecules and fragments of damaged cells that are recognized by host pattern recognition receptors as danger signals to evoke immune and inflammatory responses (96, 97).

During injury, ATP is released from damaged cells and, as a DAMP, may initiate a detrimental uncontrolled response. It has been shown that this nucleotide triggers the synthesis and release of IL-1 β , a potent pro-inflammatory cytokine during infection or injury (98, 99). Kouzaki *et al.* demonstrated that activation of the non-selective cation channel P2X₇ and P2Y₂ receptors, with the latter leading to Ca²⁺ mobilization from intracellular stores, are involved in the release of stored cytokine IL-33 (97). Because purinergic receptors are as well expressed in immunocompetent cells (e.g., neutrophils and macrophages), excessive ATP in the ASL contributes to airway inflammation (89). In fact, there is a higher amount of ATP released into the airway during inflammatory processes, which may act as a mediator, thus aggravating inflammation (88).

During ARDS, levels of extracellular nucleotides are also high (42). Shah *et al.* demonstrated that in their mice model of ALI/ARDS, extracellular ATP may trigger late phase neutrophil recruitment, and its attenuation reduces vascular leakage and neutrophil recruitment (48). Other experimental studies showing elevated levels of pulmonary ATP following exposure to lung injury indicate that activation of P2 receptors, such as P2Y₆ or P2X₇ receptors, results in enhanced inflammation and vascular leakage (63). ATP increases pulmonary edema, acting as an inflammatory mediator, which regulates the permeability of the pulmonary microvasculature, commonly observed in the pathophysiology of VILI (52). Therefore, extracellular ATP is considered to participate in the pathophysiology of pulmonary diseases as a DAMP.

Activation of P1 receptors by adenosine leads to pro- or anti-inflammatory effects (42, 81). When the level of adenosine is elevated during ARDS, P1 receptors activation promotes anti-inflammatory and tissue protective mechanisms. Here, its binding initially stops cytokine production, decreases inflammatory cell infiltration and preserves vascular barrier function (42, 81). On the contrary, when the activation of these P1 receptors is sustained, it rather has pro-inflammatory effects, where cytokine production is increased and infiltration of inflammatory cells is observed (81).

Such responses contribute to the pathogenesis of ARDS and VILI, due to the overdistension of the lungs, and may provoke apoptosis and inflammation in the alveoli (52, 96). Recurring damage to the epithelium, destruction of alveolar cells and persistent inflammation may all trigger pulmonary fibrosis. Fibrotic patients have elevated ATP content in their BALF compared to that of control individuals (98).

Nevertheless, responses from cellular damage signals generating inflammation, namely ATP, ultimately promote wound healing (96). Interestingly, alveolar inflammation, caused by lung overdistension, as observed in VILI, may be the first stage leading to wound healing (58). Belete *et al.* demonstrated that in rat primary AT1 cells, binding of ATP (nM range), released in response to injurious strains, to P2Y₂ receptors promotes wound repair in the alveoli (49).

1.6 Candidate Pathways for ATP Release

Since extracellular ATP evokes various important biological responses in the lungs, understanding how ATP is released constitutes an important physiological question (72). The origin of extracellular nucleotides in the lungs and their mechanisms of release still remains unclear (87). In response to various stimuli, especially those of mechanical nature, ATP release usually occurs via two pathways: one involving cell lysis and another involving non-lytic mechanisms (97). Regarding the latter ones, release of nucleotides may occur through secretory pathways and plasma membrane channels or transporters in secretory or non-excitatory cells (94). However, the exact mechanism of stretch-induced ATP release in the lungs remains unclear.

1.6.1 ATP Release via Lytic Pathway

During injury or inflammation, massive cell death may occur, where cells are lysed (62). With apoptosis and necrosis being the two forms of cell death, ATP comes from injured cells, macrophages or lymphocytes at the inflammation sites (100). When the membrane is damaged, the cell's content is released, including ATP (66). While cell death may play important physiological roles in the release of ATP, as exemplified by ATP release from red blood cells, cells can also release this nucleotide without involving cell lysis (52, 62, 101).

1.6.2 Non-Lytic Mechanisms: Conductive Pathways

As most ATP exists in an anionic form at physiological pH, an anion channel can electrogenically let through anionic ATP, thereby serving as a conductive pathway for ATP release (62). The difference in concentration between extracellular ATP (nM range) and intracellular ATP (mM range) makes an outwardly electrochemical potential gradient (10^{10} for ATP^{4-} and 10^8 for MgATP^{2-}) when the intracellular potential is -60 mV, which might allow any conductive pore large enough to accommodate ATP molecules to secrete this nucleotide (62, 66). Since ATP cannot be transported across lipid bilayers by simple diffusion, some channels or transporters (carriers or pumps) may be involved in its transport. The main candidates include ATP-binding cassette (ABC) transporters, gap junction hemichannels and anion channels, such as CFTR and maxi-anion channels (62, 68).

Upon binding of ATP to nucleotide-binding domains of an ABC transporter, the latter undergoes a series of conformational changes, which will allow the active transport (either uptake or extrusion) of various hydrophobic and hydrophilic solutes, particularly ATP (62).

The CFTR protein forms a cAMP-activated chloride channel, an anion channel, which was proposed to be involved in ATP release (62, 66). However, subsequent studies with luminometry and a variety of electrophysiological techniques (patch-clamp and planar lipid bilayer) could not detect CFTR-mediated or CFTR-regulated efflux of ATP (102, 103).

A hemichannel (connexon) is formed with six connexins, and is open towards the extracellular environment (68). If a connexon docks with another one of a neighbouring cell, it forms a gap junction channel between both of them (68, 104). Gap junctions are a subset of membrane channels that allow diffusion of ions and small molecules between the interiors of coupled cells. Left alone, the opening of hemichannels, while short-lasting, is non-selective and big enough for ATP to go through, but this also requires removal of extracellular Ca^{2+} , making this process a questionable mechanism under physiological conditions (62, 104, 105).

Pannexins, orthologs of innexins, are also candidates for ATP release (98, 106). Contrary to innexins and connexins, pannexins do not form a functional gap junction but rather a pannexon or pannexin hemichannel, a channel with an outward gradient for ATP, which shows a homology to gap junction-forming invertebrate innexins (98, 107). Co-expressed with P2Y receptors, this channel opens in response to extracellular ATP that signals via $[\text{Ca}^{2+}]_i$ (68). Nevertheless, ATP conduction by pannexins remains uncertain as there are no single channel recordings of ATP^- currents in the literature that would directly prove conductive ATP release, and the exact mechanism of channel activation and selectivity for ATP over small cations still remains unclear (108, 109) (see *Appendix A* for reference 109).

While activation of P2X_7 receptors allows the influx of Ca^{2+} , it can also convert itself to form a non-selective transmembrane pore or a gated channel to relatively large molecules (<900 Da), such as ATP (507.181 Da) (26, 68, 98, 104).

1.6.3 Non-Lytic Mechanisms: Exocytotic Pathways

Exocytosis involves the release of content stored in secretory granules or vesicles into the extracellular space (62, 104). Vesicular exocytosis is dependent on $[\text{Ca}^{2+}]_i$ to trigger the vesicular release pathway (66, 68). The presence of SLC17A9, a vesicular nucleotide transporter (VNUT), is a key feature that supports vesicular ATP release because it allows ATP to be stored in vesicles (110). Hence, ATP may be secreted by fusion of ATP-containing vesicles with the cell membrane (52, 111). Furthermore, airway goblet cells release ATP through exocytosis, which is regulated by VNUT (110). Mucin granules are an additional source of nucleotide release in Calu-

3 cells, a model of airway epithelial goblet cells, given that VNUT is present in mucin granules as well (112).

1.7 Mechanically Induced ATP Release

The lungs form a mechanically dynamic organ, whose cells are constantly subjected to many different types of physical forces as a result of its function to move air in and out of the lungs (113, 114). During normal breathing/respiratory cycle, airflow along the surface of the airway epithelium produces shear stress, as well as other tensile and compressive forces (113, 114). Lung expansion and relaxation during breathing movements exert deformation to lung cells through stretch or strain (115). During normal tidal breathing, the alveolus undergoes volume fluctuations that have been estimated to cause 4% linear distension of the basement membrane (14). At total lung capacity (TLC), the surface area of the basement membrane of alveolar cells has been shown to increase by 15–35% (116). Passage of air also generates shear stress and stretches the walls of the airways. The intensity of these complex physical forces varies during breathing, coughing and vascular perfusion (88). These mechanical stimuli travel to the alveolar epithelium, where they regulate certain lung functions (e.g., AT2 cell differentiation) dependent on the changes in mechanical stresses, such as airflow, stretching and pressure (56, 115, 117).

Sensing and subsequent conversion of mechanical stimuli into biological signals are ensured by a variety of mechanosensors, including stretch-sensitive ion channels, integrin-cytoskeletal interactions, nuclear-cytoskeletal interactions and ROS generators (115). First, many ion channels, namely stretch-activated channels and transient receptor potential (TRP) channels, in addition to cell surface receptors, particularly receptor tyrosine kinase (RTK), act as mechanoreceptors (56, 118). Then, following detection, transduction of physical forces may involve cytoskeleton reorganization. For example, stretch-activated channels, which are coupled with the cytoskeleton, will open in response to mechanical stresses, allowing a cation influx to initiate downstream signaling pathways (56). Indeed, there are many mechanically induced intermediate signaling events, including second messengers, change of phosphorylation status of proteins, amplification through enzymatic cascades and transmission via a network of

signaling molecules (56). More importantly, mitogen-activated protein kinases (MAPK) are known to be activated when cells are mechanically stretched (118). Boudreault *et al.* illustrated that tonic stretch triggers extracellular signal-regulated kinases 1 and 2 (ERK1/2), c-Jun N-terminal kinases 1, 2 and 3 (JNK1/2/3, also known as stress activated protein kinases), as well as p38 MAPK pathways in human lung fibroblasts (118). In addition, Correa-Meyer *et al.* demonstrated that cyclic stretch activates the ERK1/2 MAPK pathway in rat primary alveolar epithelial cells (119). Activation of TRP channels, most notably the Ca²⁺-permeable cation channel TRP vanilloid 4 (TRPV4), evokes an increase in [Ca²⁺]_i in response to mechanical stress (120). Furthermore, Seminario-Vidal *et al.* reported that along with [Ca²⁺]_i signaling, TRPV4 channels and rho signaling constitute important elements for the transduction of hypotonic stress (stretch/strain), which induces ATP release in A549 cells (121).

For airway and alveolar epithelial cells, these physical forces often translated into release of nucleotides as mechanical stimulation induces ATP release, the first step of the purinergic signaling cascade (56, 87). Airway epithelial cells normally release ATP and other nucleotides in response to cell swelling, shear and compressive stress, and other physiological stimuli, via conductive and vesicular pathways (67, 89). In fact, airway epithelial cells respond to direct mechanical stresses by modulating the rate of ATP release (90). In the alveolus, tidal breathing may generate enough mechanical stresses to release nucleotides into the alveolar space from human AT2 cells (15). Moreover, Belete *et al.* showed that in response to strain, rat AT1 cells release ATP proportionally to the extent of stretch (49).

Nevertheless, how cells can sense physical forces and convert these mechanical signals into biochemical ones for intracellular signal transduction leading to ATP release is still unknown (53, 56).

Chapter 2 – Hypothesis & Objectives

2.1 Our Previous Studies

It has been established that ATP release is mechanosensitive or occurs through a mechanosensitive reaction (103).

Boudreault *et al.* demonstrated that hypotonic shock, a surrogate for mechanical stretch capable of stretching or unfolding the cell membrane, triggers ATP release, which is not from stretch-activated channel, in A549 cells and NIH 3T3 mouse embryonic fibroblasts (122). Gadolinium (Gd^{3+}), an inhibitor of these channels, hindered the luciferin-luciferase (LL)-reaction rather than ATP efflux (122). When chelated, prior to assessment of ATP content by LL-luminometry, Gd^{3+} was found to enhance rather than inhibit cellular ATP release induced by hypotonic shock (122). Therefore, stretch-activated channels are not involved in hypotonicity-induced ATP release, as suggested by several earlier studies (122, 123).

In A549, human bronchial epithelial 16HBE14o⁻ and NIH 3T3 cell lines, Boudreault *et al.* also observed that ATP release induced by cell swelling is tightly dependent on $[Ca^{2+}]_i$ elevations (124). $[Ca^{2+}]_i$ -dependent exocytosis is a major mechanism for ATP release, which might be activated in response to the deformation of the plasma membrane (124).

Hypotonic shock makes water enter the cell, which increases the volume and surface area of the cell during swelling (125). In A549, 16HBE14o⁻, Chinese hamster ovary (CHO) and NIH 3T3 cells, Groulx *et al.* demonstrated that cells have large membrane reserves, which allow them to increase their surface area by 3.6 ± 0.2 fold and volume by 10.7 ± 1.5 fold (125). Large membrane reserves provide a simple mechanism to maintain membrane tension below lytic level during mechanical perturbations (125).

Tatur *et al.* showed that 50% hypotonic shock in A549 cells increases $[Ca^{2+}]_i$, whose source is not from extracellular environment but rather from intracellular stores (i.e., ER), which are thapsigargin (TG)-sensitive (126). Initially, released ATP binds to P2Y2 receptors, which

mobilizes Ca^{2+} from the ER stores via IP₃ pathway (126). Blocking these TG-sensitive stores reduced by 70% ATP release triggered by cell swelling (126).

Tatur *et al.* also examined adenosine and uridine nucleotide concentrations via high-performance liquid chromatography (HPLC) analysis (84). After the onset of 50% hypotonic shock, amounts of ATP, ADP, UTP and UDP in the perfusates increased significantly and peaked at approximately 2.5 min after stimulation (84). Nucleotide release was almost completely abolished from cells loaded with the $[\text{Ca}^{2+}]_i$ chelator, which suggests that nucleotide release occurs via vesicular means (84).

Ramsingh *et al.* then demonstrated that ATP release is mechanosensitive as it is induced by the tension forces at the air-liquid interface, in addition to stretch and shear stress from the airflow acting on the lung epithelium (127). By using air bubbles over a cell monolayer or by tilting the cell culture dish to expose cells to air, they created tension forces at the air-liquid interface, causing mechanical deformation. Such stimulation of human bronchial epithelial 16HBE14o⁻ and alveolar A549 cells resulted in ATP release, which did not involve cell lysis (i.e., no ethidium bromide (EthBr) uptake) (127). The release of ATP was $[\text{Ca}^{2+}]_i$ -dependent and reduced by 1,2-bis(*o*-aminophenoxy)ethane-*N,N,N',N'*-tetraacetic acid (BAPTA)-acetoxymethyl ester (AM), a chelator for $[\text{Ca}^{2+}]_i$, by 40–90% and 100% by *N*-ethylmaleimide (NEM) (127). Therefore, this study showed that cell deformation at the air-liquid interface causes increase in $[\text{Ca}^{2+}]_i$ and Ca^{2+} -dependent ATP release (127).

Akopova *et al.* demonstrated that in A549 cells, ATP release occurs through $[\text{Ca}^{2+}]_i$ -regulated vesicular exocytosis (87). Total internal reflection fluorescence (TIRF) microscopy showed that A549 cells contain ATP-loaded vesicle (stained with fluorescent markers of intracellular ATP storage sites quinacrine or Bodipy-ATP), which fused with the plasma membrane and released their ATP content upon stimulation by hypotonic shock (87). The use of brefeldin A and monensin (both inhibiting vesicular transport), as well as nocodazole and cytochalasin D (both disrupting the cytoskeleton) decreased ATP release (87).

With real-time LL bioluminescence imaging coupled with simultaneous infrared tissue imaging, Grygorczyk *et al.* studied stretch-induced ATP release in A549 cells, using the method detailed by Furuya *et al.* (128, 129). This approach allowed them to see 1-s uniaxial stretch induced ATP release ($>10 \mu\text{M}$ local concentration), which diffused around $150 \mu\text{m}$ from the initial releasing site/cell (128). Carbenoxolone (CBX, putative ATP channels blocker) and 5-nitro-2-(3-phenylpropyl-amino) benzoic acid (NPPB, a potent Cl^- channel blocker) did not affect ATP release, but it was inhibited by NEM and bafilomycin (two vesicle inhibitors) (128). $[\text{Ca}^{2+}]_i$ probe Fluo-8 displayed two types of stretch-induced responses: 1) initial $[\text{Ca}^{2+}]_i$ rise in the actively responding cells, followed by 2) Ca^{2+} wave propagation through neighbouring cells (128). They concluded that stretch-induced ATP release occurs via exocytosis of ATP-containing vesicles and that 10% stretch is sufficient to elicit such response (128).

Recently, with the same approach, Furuya *et al.* simulated an edematous lung by filling rat *ex vivo* lungs with a culture medium containing LL (129, 130) (see *Appendix B* for reference 130). We inflated the lungs with positive (intra-alveolar) pressure, and we observed that, during inflation, ATP release only occurs at the terminal sites of the lungs, where the alveolar sites are located (130). These responses ended when the alveoli were deflated. This study showed that inflation induces ATP release in the lungs and that the ATP-releasing sites occur at the alveolar level (130).

Overall, stretching the plasma membrane of lung cells has been proven to induce release of intracellular nucleotides, notably ATP, and an increase in $[\text{Ca}^{2+}]_i$ with no indication of cell lysis or death. These findings suggest that the membrane has the capacity to stretch, allowing ATP to be released through a $[\text{Ca}^{2+}]_i$ -dependent pathway (perhaps through exocytosis). However, because the exact mechanism of mechanosensitive ATP release in the lungs is still not fully understood, I posed the following questions: What is the exact relationship between ATP release kinetics and stretch stimulus parameters, such as extent, rate and duration? What are the cellular sources of ATP release in the alveoli (i.e., contribution of AT1 vs. AT2 cells)? Are there other non-lytic pathways of ATP release alternative to vesicular exocytosis or ATP channels?

2.2 Hypothesis

Based on the presented information and our previous findings, I considered stretch as an important mechanical stimulus in lung physiology and pathophysiology. I hypothesized that when the lungs inflate, stretching of alveolar cells at a certain rate and beyond a certain threshold causes them to release ATP into the lung airspaces. In alveolar cells, one known pathway for stretch-induced ATP release depends on Ca^{2+} liberation from intracellular stores, leading to Ca^{2+} -dependent exocytosis of ATP-loaded vesicles. However, alternate pathways may co-exist, involving transient mechanoporation of the rapidly stretched plasma membrane. Should the cell membrane display viscoelastic properties under physiological strain, I would expect to observe a stretch-induced ATP efflux dependent on strain rate, as well as a stress relaxation, where constant strain decreases the rate of ATP release.

2.3 Objectives

Therefore, my general objective was to study the effect of stretch on ATP release in the lungs. The specific goals in this thesis were:

- 1) To develop a method, which will accurately quantify the amount of ATP released, using a real-time imaging approach. This will provide the means to characterize the kinetics of ATP release.
- 2) To characterize stretch-induced ATP release in primary alveolar cells, to investigate its physiological mechanisms/pathways, as well as to determine the contribution of AT2/AT1 cells in this process. This may suggest the cellular source of ATP release in the alveolus.
- 3) To explore if and how viscoelastic properties of the alveolar cell membrane are influencing stretch-induced ATP release. To this end, I examined the relationship between ATP efflux and strain rate, as well as ATP efflux and strain duration. This may suggest an alternate pathway for the release of ATP.

Chapter 3 – Article #1

3.1 Preamble

In order to identify the pathways of ATP release, an accurate technique for ATP measurement is required.

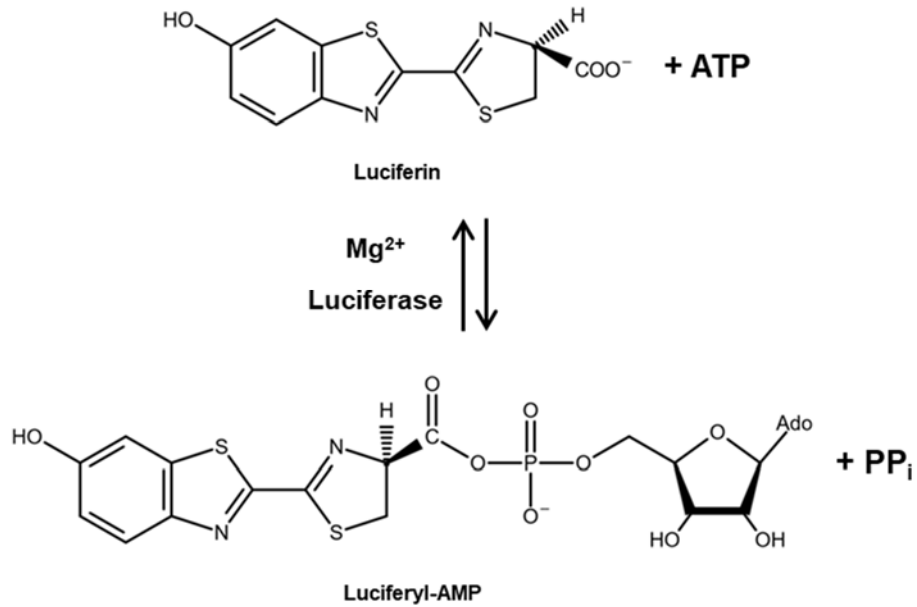
According to a meta-analysis conducted by Mikolajewicz *et al.*, more than 90% (255/278) of studies measured ATP with the LL bioluminescence assay (131). Other techniques include: HPLC, hexokinase-based enzymatic assays, surface-bound luciferase probes (plasma membrane luciferase (pme-LUC)), microelectrodes and cell-based biosensors (122, 131, 132).

The bioluminescence assay is based on light production from ATP-dependent enzymatic reaction that utilizes consumable substrate luciferin and the enzyme luciferase from firefly (66). Intensity of emitted light is proportional to the concentration of ATP. Luciferase converts the chemical energy into light by using luciferin, ATP and O₂ in a two-step process, as shown in Figure 7 via the luciferyl-AMP intermediate (133).

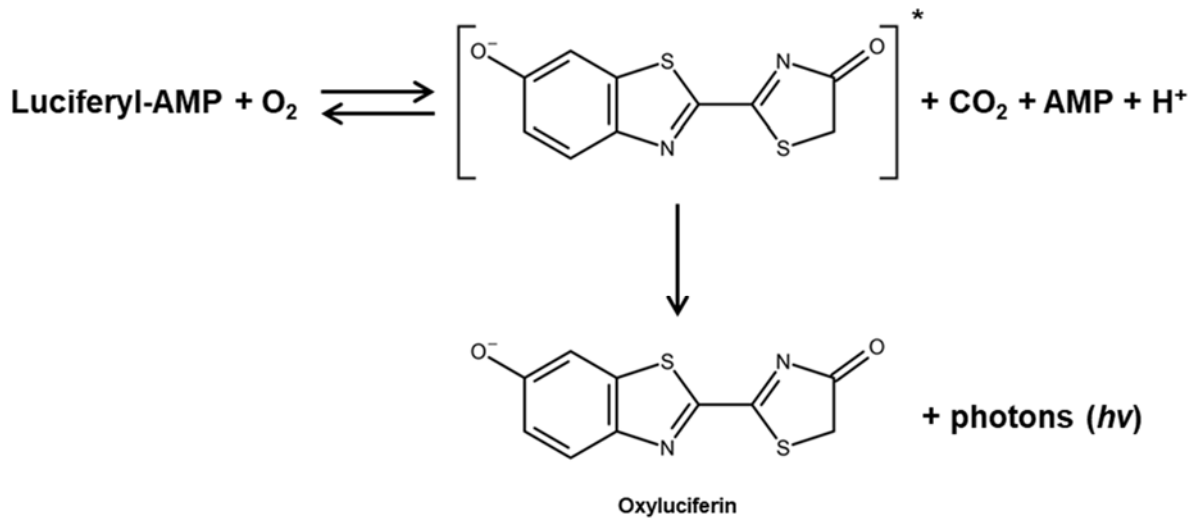
First, luciferase catalyzes the reaction to form an enzyme-bound luciferyl adenylate intermediate, typically bound to AMP. Secondly, in the presence of O₂, the luciferyl adenylate is oxidized, producing AMP, CO₂ and oxyluciferin. The latter is in an electronically excited state, where the transition from this state to the ground state emits photons ($h\nu$), detectable at 561 nm (peak intensity) (66, 134).

Therefore, LL is used to measure ATP, as it is simple, highly sensitive, fast and specific to ATP (66, 135). Because it is an enzymatic reaction, the production of light depends on numerous factors, including ionic strength, pH, temperature and the concentration of divalent cations (122).

1) First reaction:



2) Second reaction:



Ado: Adenosine; **AMP:** Adenosine monophosphate; **ATP:** Adenosine triphosphate;
PP_i: Inorganic pyrophosphate

Figure 7. – Light-Emitting ATP-Dependent Reaction of Luciferin and Luciferase

(Figure adapted from Nakatsu *et al.* (133))

With the LL-based approach, the presence of light indicates that there is ATP present in the environment containing LL. Experiments usually involve taking the bulk fluid and reading the faint bioluminescent signal through a luminometer. The strengths of this assay are that no endogenous ATP is present in the medium containing the LL reagent, nanomolar quantities of ATP can be measured, and adherent and viable cells growing on collagen-coated substrates can be studied (136). Despite this, measuring ATP-dependent LL bioluminescence through a luminometer fails to provide spatial-temporal information regarding ATP release sites and diffusion kinetics. Hence, we can overcome these issues by imaging extracellular ATP over cells with an EMCCD camera, which may provide additional information on the kinetics and spatial distribution of ATP release (52, 129).

Because this approach still needs an accurate quantification method, we developed in Article #1 a novel method that accurately quantitates the amount of extracellular ATP and maps its spatial distribution over time.

3.2 Article #1

Title: Wide field of view quantitative imaging of cellular ATP release

Authors: Ju Jing Tan, Olga Ponomarchuk, Ryszard Grygorczyk, Francis Boudreault

Status: Published in *American Journal of Physiology-Cell Physiology (Methods in Cell Physiology)* (137) (see *Appendix C* for reference 137)

3.2.1 Contribution

Under the supervision of Dr. Ryszard Grygorczyk and Dr. Francis Boudreault, I participated in the experimental design, and I conducted the majority of the experiments presented in this article (Figures 1 to 6), while Dr. Olga Ponomarchuk performed the experiments of Figure 7 regarding hypotonic shock. Dr. Francis Boudreault and Dr. Ryszard Grygorczyk drafted the manuscript. I also analyzed the data, prepared the figures and participated in the drafting of the manuscript.

3.3 Wide field of view quantitative imaging of cellular ATP release

Ju Jing Tan,^{1,2} Olga Ponomarchuk,¹ Ryszard Grygorczyk,^{1,2} and Francis Boudreault¹

¹Centre de Recherche du Centre Hospitalier de l'Université de Montréal, Montreal, Quebec, Canada; and ²Department of Medicine, Université de Montréal, Montreal, Quebec, Canada

Submitted 21 March 2019; accepted in final form 17 June 2019

Running Title: Wide field of view ATP imaging

Address for reprint requests and other correspondence:

F. Boudreault

Centre de recherche du CHUM

900, rue Saint-Denis, Pavillon R

Montréal, QC H2X 0A9

Canada

(e-mail: )

3.3.1 Abstract

Tan JJ, Ponomarchuk O, Grygorczyk R, Boudreault F. Wide field of view quantitative imaging of cellular ATP release. *Am J Physiol Cell Physiol* 317: C566–C575, 2019. First published June 19, 2019; doi:10.1152/ajpcell.00096.2019.—Although several mechanical stressors promote ATP secretion from eukaryotic cells, few mechanosensitive pathways for ATP release have been precisely characterized and none have been clearly identified. To facilitate progress, we report here a wide field of view ($\sim 20 \times 20$ mm sample area) imaging technique paired with a quantitative image analysis to accurately map the dynamics of ATP release from a cell population. The approach has been tested on A549 cells stretched at high initial strain rate ($2\text{--}5\text{ s}^{-1}$) or swelled by hypotonic shock. The amount of ATP secreted in response to a series of five graded stretch pulses (5–37% linear deformation, 1-s duration at 25°C) changed nonmonotonically with respect to strain amplitude and was inhomogeneous across the cell monolayer. In a typical experiment, extracellular ATP density averaged 250 fmol/mm^2 , but the area of detectable signal covered only $\sim 40\%$ of the cells. In some areas, ATP accumulation peaked around 900 fmol/mm^2 , which corresponded to an estimated concentration of $4.5\text{ }\mu\text{M}$. The total amount of ATP released from the combined stretch pulses reached $384 \pm 224\text{ pmol/million cells}$ ($n = 4$). Compared with stretch, hypotonic shock (50%, 30°C) elicited a more homogeneous ATP secretion from the entire cell population but at a lower yield totaling $28 \pm 12\text{ pmol/million cells}$ ($n = 4$). The quantitative extracellular ATP mapping of several thousand cells at once, with this wide field of view imaging system, will help identify ATP release pathways by providing unique insights on the dynamics and inhomogeneities of the cellular ATP secretion that are otherwise difficult to assess within the smaller field of view of a microscope.

Keywords: ATP release; bioluminescence; imaging; mechanical stress

3.3.2 Introduction

Extracellular adenosine 5'-triphosphate was recognized as a signaling molecule several decades ago, and many of its target purinergic receptors of the P2X₁₋₇ and P2Y_{1,2,4,6,11-14} families have since been sequenced and pharmacologically characterized (3). Yet several aspects regarding the modes of signaling of this nucleotide remain perplexing. In particular, while mechanical deformations of all kinds have been found to stimulate ATP release, no mechanosensitive pathways permitting ATP secretion have been unambiguously characterized as of today (9, 10, 18). There are currently two major acknowledged modes of cellular ATP release: lytic and nonlytic. Cell lysis resulting from plasma membrane rupture allowing the free passage of cytosolic ATP can be induced by physical or chemical stressors; the damages can be transient or lead to cell death (16). The nonlytic mode of ATP release is generally divided into conductive (ionic channels) and nonconductive pathways, with the latter further splitting up into regulated and nonregulated exocytosis (9).

Regardless of the stimulus under investigation, an accurate measurement technique for ATP is necessary to identify the transmembrane pathways used by this nucleotide. The most widely used technique to detect and quantify ATP is the luciferase-luciferin (LL) assay, a photon-producing enzymatic reaction whose light intensity serves as an indicator of ATP content in the solution. An alternative to the soluble luciferase is the pmELUC cell expression system, featuring a plasma membrane-bound and extracellular-facing luciferase enzyme. It is a versatile tool suitable for *in vitro* as well as *in vivo* applications (12). However, in most cell-based experimental assays, the quantity of released ATP is tiny, and either soluble or membrane-bound luciferase approaches yield a very faint bioluminescent signal that is barely detectable with a conventional microscopy imaging system. Therefore, the standard procedure to quantify cellular ATP release generally involves collecting bulk extracellular solution for subsequent offline determination of ATP content using a luminometer or a plate reader. Although such approaches constitute a highly sensitive biochemical assay for ATP detection, it cannot provide information on the spatial kinetics of ATP release, a prerequisite to fully characterize and solve the identity of ATP release pathways.

To accurately map cellular ATP release, it is essential to combine a microscopy setup that has a strong light-gathering power with a very sensitive light detection apparatus. Currently available digital cameras with maximal light sensitivity, such as an electron-multiplying charge-coupled device (EMCCD), although well suited for low-light applications in fluorescence microscopy, are not yet adequate for such extremely low bioluminescent signals. A simple technique to circumvent this weak source of luminescence is to capture light for longer periods of time (8, 11). With this approach, however, the advantages of an imaging system mostly vanish as the spatial kinetics of ATP efflux (light emission) is lost. Image intensifier has been used with success for ATP imaging (6, 17), but it is an expensive and not widely available solution.

The brightness of an image acquired with a microscope increases with the objective's numerical aperture (NA) but decreases with the lateral magnification (M) (*Eq. 1*). Since in general the NA of microscope objectives changes in proportion to their magnification, very little brightness can be gained by choosing an objective with the highest NA available. Besides, in most modern microscopes, the need to fit complex optical components within the main optical path results in longer lens-to-lens distance and thereby substantial loss of peripheral and off-axis image-forming rays.

$$\text{Image brightness} \propto \left(\frac{\text{NA}}{\text{M}}\right)^2 \quad (1)$$

Thus, to boost the light intensity signal, we chose a macroscopic imaging approach similar to the one described by Feranchak et al. (5), but instead of a 1:1 object-to-image magnification, we chose a threefold reduction (M = 0.33) with an objective lens of NA = 0.15. Based on *Eq. 1*, the theoretical increase in brightness from those optical parameters alone compared with, for example, a $\times 5/0.25$ objective is $[(0.15/0.33)/(0.25/5)]^2 = 83$ -fold. The true increase in captured luminescence with our imaging system can surpass this ratio, however, due to its shorter optical path compared with nowadays microscopes. While this higher light-gathering power came at the cost of reducing the image resolution, our imaging system with its wide field of view (FOV) that spans the whole of our experimental chambers ($\sim 20 \times 20$ mm), coupled with our approach to map and quantify over time the distribution and rate of secreted

ATP in our experimental chambers, provided new insights on the overall nature and dynamics of the cellular ATP secretion otherwise difficult to assess with standard microscopes and their small FOV.

3.3.3 Materials and Methods

Cells. Human lung carcinoma A549 cells were grown on cell culture dishes (Cellstar; Greiner Bio-One, Frickenhausen, Germany) in HyClone High Glucose Dulbecco's modified Eagle's medium (GE Healthcare Life Sciences, HyClone Laboratories, Logan, UT) supplemented with 10% fetal bovine serum, 2 mM L-glutamine, 50 U/mL penicillin-G, and 50 µg/mL streptomycin sulfate (antibiotics were only included in media of cells grown for hypo experiments) at 37°C and 5% CO₂. For stretch experiments, trypsinized A549 cells were seeded at ~700 cells/mm² (~25,000 cells/36 mm²) with culture media on a bottom-stretchable chamber (see below) and kept at 37°C and 5% CO₂ until the time of the experiment. For hypotonic shock, A549 cells after trypsinization were seeded with culture media on 15-mm-diameter glass coverslips and used after they reached 90% confluence (~400–500 cells/mm²; 24–72 h after plating). All added media constituents were from Gibco/ThermoFisher Scientific (Burlington, ON, Canada).

Stretch experiments. Stretch chambers were made with a Sylgard 184 silicone elastomer base and curing agent (Dow Corning, Midland, MI) as described previously (6, 7). The elastomer base and curing agent were poured into the stretch chamber's mold and then baked for 1 h at 60°C. To facilitate the attachment of cells onto silicone, the 2-mm-wide stretchable groove was coated with 20% collagen type 1 from rat tail diluted in distilled H₂O (Sigma-Aldrich, St. Louis, MO). During all stretch experiments, cells were bathed in 200 µL of Gibco's phenol red-free DMEM (Invitrogen Canada, Burlington, ON, Canada) containing the ATP detection reagents prepared as follows: one vial of ATP assay mix-lyophilized powder (Sigma-Aldrich) was reconstituted with 5 mL of sterile double-distilled water and isotonicly adjusted with 5× physiological solution (LL). For ATP imaging, 100 µL of the isotonicly adjusted LL was added to 100 µL of Gibco's phenol red-free DMEM (LL-DMEM).

The stretch chamber mounted on the stage of our custom-designed ATP imaging system (see below) was clamped to the STREX NS-600W Cell Stretching System (STREX, Osaka, Japan). The stretching apparatus applied a horizontal stretch onto the silicone chamber for 1 s. All stretch experiments consisted of five consecutive stretch pulses of increasing amplitude at 5-min intervals. Effective applied strains, along the main axis of load application, were measured on images acquired after the experiments with a repetition of the stretch sequence.

Hypotonic challenge. A549 cells on glass coverslips were placed in a glass-bottomed (25-mm diameter coverslip no. 1) chamber (RC-40LP; Warner Instruments, Hamden, CT), bathed in LL-DMEM solution (500 μ L), and warmed at 30°C with a DH-35 Culture Dish Heater (Warner) wired to a TC-324B Automatic Heater Controller (Warner) until hypotonic challenge. To keep the ATP detection reaction reagents at prehypotonic levels, the added hypotonic LL solution (hypoLL) contained the same level of LL reagent as LL-DMEM (for details see Stretch experiments). The luciferase reaction is well known for its sensitivity to ionic content, however (1). For instance, if the ionic concentration of an isotonic medium is lowered by 50%, it will result in approximate doubling of the luciferase reaction speed. As a result, before converting the pixel values into ATP (see ATP calibration and quantification), we divided by 2 the rate of light units (LU) per second. In addition, to keep divalent cation concentration constant during the course of the experiments, the hypoLL also contained (in mM) 1 MgCl₂ and 1 CaCl₂ (Fisher Scientific, Pittsburgh, PA). ATP release was stimulated by adding 500 μ L of hypoLL solution to the chamber (~50% hypo final).

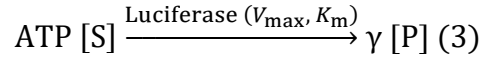
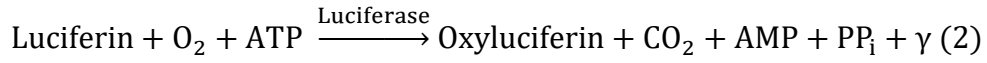
ATP release imaging. We chose an inverted configuration for the imaging system, with the EMCCD camera Evolve 512 (Photometrics, Tucson, AZ) placed underneath the experimental stage (see Fig. 1A). To position the stretch or hypotonic shock chamber, we used a standard manual mechanical XY translational stage. Focus was provided by moving vertically the camera positioned on a pinion-and-rack system. We selected a parallel path (sometimes referred to as infinity space) in our optical design, but instead of a distance between the two main lenses in excess of 200 mm, as typically used in infinity-corrected microscopes, we shortened it to 40 mm. This shorter distance means that more of the off-axis peripheral rays are captured, hence resulting in enhanced brightness. For the objective, we chose a standard bi-convex lens with f_{obj}

= 75 mm ($D_{\text{obj}} = 25$ mm, $NA = 0.15$), and we fixed to the EMCCD camera a standard c-mount convex-type camera lens with $f_{\text{cam}} = 25$ mm ($D_{\text{cam}} = 20$ mm) that resulted in $\times 0.33$ ($f_{\text{cam}}/f_{\text{obj}}$) magnification (3-fold reduction). It should be noted that this particular optical configuration with large-diameter lenses and magnification at or below $\times 1$ is similar to macrophotography. Given the size of the camera chip per the manufacturer's specifications of 6.7×6.7 mm (512×512 , $13 \mu\text{m}$ pixel size), the resulting FOV was $\sim 20 \times 20$ mm. With such a wide FOV, large diameter lenses are essential to minimize optical aberrations. Our imaging system is not entirely devoid of optical aberrations, however. In particular, coma aberrations from intense punctual light sources, e.g., from isolated cells suddenly ruptured by lysis, have been observed at the periphery of the field of view during hypotonic assay. Those image distortions are minor and not expected to diminish appreciably the exactness of the ATP quantification but will be addressed in the future.

To further amplify the signal, we set the on-chip camera binning at 2×2 , achieving a final resolution of $\sim 78 \mu\text{m}/\text{pixel}$. Control of the EMCCD and data acquisition were done via AxioVision software (AxioVs40 V 4.8.2.0; Carl Zeiss MicroImaging, Jena, Germany). Images were acquired at 0.5-Hz frequency and 1-s exposure time for stretch and for hypo at 0.2 Hz and 5-s exposure and gain settings at the lowest readout speed at 5 MHz. Stacks of 900 images were captured and stored for offline analyses with Metamorph (Meta Series Software 7.7.9; Molecular Devices, Downingtown, PA) or ImageJ open-source software (15).

To acquire brightfield images of the stretch or hypotonic chamber (Fig. 1B), we installed an external variable illumination source (incandescent bulb, 15 W, T6/collector lens $f_{\text{coll}} = 25$ mm, $D_{\text{coll}} = 40$ mm) in-line with a standard condenser ($f_{\text{cond}} = 60$ mm, $D_{\text{cond}} = 40$ mm, $NA = 0.3$). We also placed a diaphragm in the parallel optical path for additional light intensity control and fine-tuning for the brightfield-acquired images. Finally, to minimize light background, the entire imaging system was installed inside an opaque box and was accessible through a front door panel.

ATP calibration and quantification. Extracellular luminescence, in contrast to intracellular fluorescence, is not enclosed within the boundary of cellular membranes; the spatial distribution of the light-emitting reaction is governed by time-dependent diffusion processes and is dispersed throughout the fluid covering the cells. Since the light intensity captured in the image is proportional not only to $[ATP]_o$ but also to the depth (in the object space) of the in situ generated luminescence, an ATP calibration technique independent of the dimensions of the light-generating reaction is required. This is achieved by calibrating the rate of light generation with respect to the quantity of ATP_o molecules rather than its local concentration.



Although ATP is only a cofactor in the LL reaction and light (γ) a by-product of it (see chemical reaction 2, PP_i : inorganic pyrophosphate), when using this reaction for ATP determination with $[\text{luciferin}] \gg [ATP]$, we can posit ATP as the sole reactant and light as the main product as described in the simplified chemical reaction 3 (the rate of production of oxyluciferin can be directly inferred from the rate of light generation). By using the Michaelis-Menten equation $\Delta[P]/\Delta t = (V_{max} \times [S]) / (K_m + [S])$ and assuming $K_m \sim 200 \mu\text{M}$ (4) $> [S] = [ATP]$, we obtain this simplified relation: $(\Delta\gamma/\Delta t)/V = (V_{max}/K_m) \times [ATP]$ (V : volume of reaction), where the rate of photon production ($\Delta\gamma/\Delta t$) per unit of volume is linearly proportional to the concentration of ATP. Multiplying both sides of the equation by V yields the volume-independent relationship: $\Delta\gamma/\Delta t = (V_{max}/K_m) \times ATP$, which directly relates the rate of photon emission to the quantity of ATP molecules. We rearranged this equation and combined the enzymatic reaction constants and other parameters pertaining to the specifics of our imaging system into a single calibration factor (see Eq. 4). An example of parameters intrinsically included in this factor is the numerical aperture. The imaging system collects only a fraction of all the photons generated by the reaction. The capture ratio of those photons is determined by the NA, but it remains constant for the entire FOV and is unaffected by the signal intensity. In Eq. 4, the rate of photon generation ($\Delta\gamma/\Delta t$) is replaced by the pixel intensity value [identified as light unit (LU)] divided by the exposure time (Δt) of the image. The quantity of ATP_o for a region

of interest (ROI) in the recorded image covering the whole chamber or a subarea within and containing n pixels can then be obtained from the sum of individual pixel values divided by exposure time and multiplied by the calibration factor:

$$\text{ATP}_{\text{ROI}} \text{ (moles)} = \text{calibration_factor} \left(\frac{\text{moles} \cdot \text{s}}{\text{LU}} \right) \times \frac{1}{\Delta t \text{ (s)}} \sum_{i=1}^{n \text{ pixels}} \text{pixel_value}_i \text{ (LU)} \quad (4)$$

To determine the value of the calibration factor, we first recorded the light intensity generated by known concentrations of ATP (5 nM to 50 μ M, in 10-fold increments) within the stretch chamber for three volumes (18, 36, and 54 μ L) of solution. The volumes were chosen to achieve heights of liquid of 1, 1.5, and 2 mm. Those height increments serve to validate that a large proportion of the luminescence is captured longitudinally along the optical axis of our imaging system, a property dependent on optical characteristics such as the depth of field. This validation requires that while keeping the ATP concentration unchanged, a step increase in solution height will augment the light signal in proportion. The ATP-Mg₂ dissolved in DMEM was pre-mixed 1:1 with LL-DMEM (2 \times) and then immediately transferred within the stretch chamber and images acquired as described above (see *ATP release imaging*) during 1 min. The slowly declining rate of LU per second (minus background level) for the whole chamber was then averaged over the first 10 s. We reported the results for the three series of volume (corresponding height) and [ATP] in Fig. 2A and the calculated quantity of ATP for the 15 combinations of volume and [ATP] in Fig. 2B.

Note that while there are three possible rates of light generation (1 for each height) for a given [ATP] (Fig. 2A), only a unique value exists for a given quantity of ATP (Fig. 2B). Note also how the ATP-light signal relationship on Fig. 2B displays a strong linear proportionality over several orders of magnitude of ATP molecule content. Another important observation from those calibration measurements is the additive property of the relationship, whereby the rate of light generation from a 2-mm layer of a given concentration of ATP is approximately twice the value of a 1-mm layer at the same concentration (light signal at 2 mm/1 mm = 1.9 \pm 0.22). Thus, the 2-mm layer can otherwise be regarded as two stacked layers of 1 mm each. We believe this additive property to remain valid even with two hypothetically immiscible layers containing

different ATP concentrations. We further reason that it can be extended to a gradient of ATP concentration, whereby a series of layers of infinitesimal height can be integrated over the entire depth to obtain the quantity of ATP molecules. In short, the rate of light production is a direct measure of the current quantity of ATP molecules independent of the spatial distribution of ATP. The calibration factor calculated from the average of individual ratio of ATP (moles) over light signal (LU/s) for each data point ($n = 15$) in Fig. 2B is $5 \pm 2.6 \times 10^{-18}$ moles \cdot s $^{-1}$ \cdot LU $^{-1}$ (mean \pm SD). In other words, 1 LU/s corresponds approximately to 5 amol or 3×10^6 molecules of ATP. Although the calibration factor is not influenced by the height of the reaction (Fig. 2C), there is a small deviation from linearity with respect of [ATP] (Fig. 2C). As a result, using the average of the calibration factor ratio comes with the caveat that as the light signal gets bigger, ATP underestimation grows. Even though this small deviation from linearity is not believed to significantly impact the accuracy of the measurements, a complete 3D modeling of diffusion processes and enzymatic kinetics could be implemented to minimize the anticipated underestimation and further improve ATP quantification.

Based on our pseudo-first-order reaction assumption, we have calculated the half-life of the calibration signal decay at two submicromolar concentration for the three volumes of solution and obtained: $t_{1/2} = 6.6 \pm 0.2$ min, $R^2 > 0.90$ at $0.05 \mu\text{M}$ ($n = 3$) and $t_{1/2} = 6.8 \pm 0.2$ min, $R^2 > 0.95$ at $0.5 \mu\text{M}$ ($n = 3$). The magnitude of this parameter indicates that the detectable luminescence takes considerable time to decay. At higher ATP concentration ($>5 \mu\text{M}$), however, the measured half-life from our calibration assay shortens: $t_{1/2} = 5.6 \pm 0.1$ min, $R^2 > 0.95$ at $5 \mu\text{M}$ ($n = 3$) and $t_{1/2} = 4.2 \pm 0.9$ min, $R^2 > 0.99$ at $50 \mu\text{M}$ ($n = 3$). The reason for this deviation is well known and is a consequence of the typical “flash kinetics” of the LL reaction at elevated reactant concentration that had been explained mainly by the generation of the autoinhibitory product dehydroluciferyl-adenylate (L-AMP) (14). In the context of experimental stretching of cells this is not a concern, since L-AMP diffuses away from the main sites of reaction and has a negligible impact on the speed of the reaction. To demonstrate this, we simulated the ATP efflux originating from several cells as a large punctual source by injecting (PLI-100A Picoliter Microinjector; Warner) a small volume of ATP solution ($<10 \mu\text{L}$) at high concentrations ($100 \mu\text{M}$) in a RC-40LP glass-bottomed cell-free chamber filled with LL solution (~ 1 mL) and measured the

half-life from the signal coming from the initially small but bright source and then continuously expanding but fading luminescence to obtain $t_{1/2} = 7.6 \pm 1.0$ min, $R^2 > 0.90$ ($n = 3$). Thus, even though we used a high level of ATP concentration (100 μM), there was no diminution in half-life compared with our calibration assay at submicromolar values of 0.05 μM and 0.5 μM (unpaired t -test, two-tailed, $P = 0.24$ and $P = 0.29$, respectively).

The image noise distribution of the EMCCD camera at baseline (dark current; no illumination) was Gaussian (Kolmogorov-Smirnov test: $P = 0.134$ H_0 : distribution is normal), and its standard deviation (σ_{noise}) tended toward 5 LU/pixel (e.g., for 1-s exposure this yields a rate of 5 LU/s/pixel equivalent to 25 amol ATP/pixel). At pixel level per 1-s exposure image, we suppose that this reading noise limits ATP detection to $3\sigma_{\text{noise}} = 75$ amol or 0.075 fmol (per pixel). Note that the signal noise from the LL reaction may exceed this value.

The individual LU values per pixel for the 1-s acquisition time for stretch (or 5 s for hypo) were converted into ATP, with the calibration factor and linear fitting on ImageJ. The total amount of detectable extracellular ATP (ATP_o) within the chamber or a smaller specific ROI can be calculated and monitored over the entire course of the experiment. The quantity of secreted ATP for each stretch impulse is calculated by subtracting the prestretch ATP_o level from the stretch-generated peak value. The rate of ATP release, expressed in fmol/s or pmol/s, is the first derivative of ATP_o within any ROI over time. Color-coded images reporting ATP_o density in fmol/mm^2 (1 pixel image = 6×10^{-3} mm^2) with respect to the surface substrate or rate of ATP release density in $(\text{fmol}/\text{s})/\text{mm}^2$ were generated with ImageJ.

3.3.4 Results

Cell stretch and amount of ATP secretion. To test the sensitivity and resolution of our wide FOV quantitative ATP imaging approach, we first uniaxially stretched silicone substrate-adherent A549 cells. Application of a stretch pulse at high initial speed (2–5 s^{-1}) is known to result in rapid ATP secretion (7) and, as such, is well suited to assess the temporal resolution of our imaging system. All five graded stepped pulses, applied every five minutes, generated a detectable and quantifiable signal.

The ATP_o density images pre- and poststretch of a typical experiment are presented in Fig. 3A. Local increases in extracellular ATP can be detected as early as 5% strain, but ATP_o level rose mostly near the edge of the chamber, perhaps as a result of localized stress concentration. Some isolated areas reached an ATP density of ~180 fmol/mm² (Fig. 3A, *top right*), although their contribution to the overall ATP secretion level was minimal (Fig. 3B). Whereas the detectable signal from the following pulse (9%) was more widespread, it remained concentrated mostly in the middle region of the stretched area, with a range covering (~14 mm² or 40% of the stretchable groove) and a maximal ATP_o density of ~250 fmol/mm². The 5-min interval between stretch pulses is too short for the complete breakdown of ATP_o by ectoATPases and LL reaction below the theoretical detection level of 12.5 fmol ATP/mm² (0.075 fmol/pixel ÷ 6 × 10⁻³ mm²/pixel). In consequence, ATP signal remnants from the previous stretch were still present before application of the 21% extension load, but the addition of newly released ATP can be measured by subtracting pre- from poststretch level (Fig. 3C). The 21% deformation created a markedly inhomogeneous distribution of extracellular ATP, with two distinct regions where ATP_o density triples to >750 fmol/mm² (Fig. 3A). While ATP_o density continued to rise with the subsequent 27 and 37% strain, it was due mostly to additional ATP release in the vicinity of already existing high accumulation ATP, not as a result of higher ATP efflux. The stretch-induced ATP response was not monotonic. The 21% strain produced the highest response with ~7 pmol of secreted ATP for the whole chamber, a magnitude more than twice the previous stretches, and declined thereafter for the subsequent loads. This threshold level at 21% strain had been identified for all four independent chambers tested and is comparable with that occurring during lung inflation. It has been estimated that at total lung capacity inflation, the distension of alveolar space measured from fixed rat lungs reaches a maximum of ~37% surface strain (19), which corresponds to 17% linear strain, assuming an equibiaxial field of deformation.

For autocrine/paracrine purinergic studies with ATP as an effector, it is essential to estimate the concentration of extracellular ATP. We can derive an average value for [ATP]_o in the vicinity of the cell monolayer from the map of ATP_o density level and the estimated extent of the LL reaction. The upper limit of the LL reaction (emitting a detectable signal) is not known, but assuming the reaction initially grows into a hemispherical shape, it should correspond to the

lateral diffusion radius of small isolated ATP sources on the acquired images. The height of the reaction was varying and was not uniformly distributed throughout the chamber, but we found that a 200- μm limit was a good approximation for the experiment shown in Fig. 3A. We reported the average $[\text{ATP}]_o$ on the alternate calibration bar for this estimated reaction height (h_r). Since the concentration is derived from ATP_o accumulation in the chamber, the largest area with the highest $[\text{ATP}]_o$ at 4.5 μM for this experiment was seen after the last stretch (37% strain) took place. The $[\text{ATP}]_o$ in vicinity of the cell surface ought to be higher, however, due to the existence of a gradient of ATP_o concentration near the cell surface and upward.

While a complete 3D modeling will be required to fully characterize the vertical distribution of ATP in the medium, we attempted nonetheless at estimating the $[\text{ATP}]_o$ near the cell surface by hypothesizing a linear distribution of ATP_o . Our rationale is based on the ATP breakdown activity of endogenous cell-attached ecto-ATPases coupled with the consumption from LL reaction being proportional to the concentration of ATP. We expect those processes to lessen the concentration gradient and thereby “linearize” the vertical distribution of ATP. We assumed the $[\text{ATP}]_o$ upward and away from the monolayer surface to be low: $[\text{ATP}]_{\text{away}} \sim 1 \text{ nM}$. The formula for the $[\text{ATP}]_o$ near the monolayer at the location of highest $[\text{ATP}]_o$ can be expressed as: $[\text{ATP}]_{\text{average}} = ([\text{ATP}]_{\text{near}} - [\text{ATP}]_{\text{away}})/2 = 4.5 \mu\text{M}$. Solving for the unknown gives $[\text{ATP}]_{\text{near}} = 9 \mu\text{M}$.

Cell stretch and rate of ATP secretion. While the amount of secreted ATP and ATP_o density map reveal the extent of the bulk release of ATP per chamber and per normalized surface as well as the nature of the inhomogeneous secretion pattern, the true dynamics of ATP secretion are best revealed with the time derivative of the ATP accumulation response. The highly transient nature of ATP secretion by stretch is depicted in Fig. 4 and can be seen for all five incremental loads. As opposed to the accumulated ATP, the rate of release already went back to prestretch level before the subsequent stretch as depicted on the color-coded images (Fig. 4A). But similarly to the amount of ATP secreted, a threshold was also crossed at 21% strain (Fig. 4B) with a peak rate of 1.2 pmol/s. Whether a small lingering ATP efflux persisted poststretch and/or that ATP-induced ATP release took place between load pulses could not be resolved. This ATP efflux, if it existed, ought to have been small since it failed to override the

feeble but continuous degradation of ATP from LL reaction and ecto-ATPases, as shown on Fig. 4B, with the return to pre-stretch baseline level in less than ~1 min for all applied deformations.

In addition, half-life analysis of the decay signal past the culminating ATP accumulation suggested that very little, if any, additional ATP had been released. The average half-life from all interpulse decay signals from the four stretch chambers we analyzed in this report was $t_{1/2} = 9.3 \pm 2.2$ min, $R^2 > 0.90$ ($n = 20$). This average half-life value is slightly higher than the ones from our cell-free experiments ($t_{1/2} \sim 7$ min) described in MATERIALS AND METHODS. If additional ATP had been released after the stretch pulse, it would have supplemented the level of ATP and accordingly increased the half-life to a value higher than the one we measured in the absence of cells. The amplitude of this increase, however, is extremely small. For instance, in Fig. 3B, the half-life from the decaying signal following the 21% deformation load was $t_{1/2} = 9.8$ min. In the same graph at ~16 min, corresponding to ~4 min past the 21% strain peak of cumulated ATP and just before the next incoming stretch, there was a total of ~7.4 pmol in the chamber. Had the half-life been 7 min instead of the measured 9.8 min, the remaining ATP would have been 6.7 pmol (-0.7 pmol) and the difference in rate of ATP release during this period would have amounted to only +0.003 pmol/s, a tiny value when compared with reported efflux at Fig. 4B. Thus, the luminescent signal between stretch pulses is almost entirely remnants from the previous stretch and a consequence of the slow degradation of ATP but unlikely a result of substantial ATP secretion.

Regional analysis of ATP secretion. The ability to monitor extracellular ATP fluctuation, not only for the whole chamber but also for any region of interest (ROI), is another interesting feature of our integrative ATP quantification technique. The total production rate of photons in any region in the chamber, represented by the sum of LU in this region on the image, corresponds to the quantity of ATP_o present in this location from the surface of cells and above. To illustrate this, we tracked the variation in ATP_o content for five different ROIs of 0.4 mm² from another stretch assay (Fig. 5). The quantity of ATP detected in the extracellular medium in response to stretching this chamber and the ATP efflux (Figs. 5, B–C) was less than that described in Fig. 3 and had a different distribution (Fig. 5A) but presented the same strain threshold. The cumulated ATP_o for all five regions and their corresponding efflux is shown in Fig.

5, *D* and *E*. As expected, the values are much lower than the whole chamber (see Fig. 5*B*), with <10 fmol per pulse stretches for most ROIs, with the exception of ROI no. 3 reaching ~40 fmol at 21% strain pulse. While the ATP efflux kinetics of the individual regions ROI no. 3–5 located near or within the main response area (see Fig. 5*A*) resembled, albeit at lower magnitude, the ones observed for the whole chamber, the isolated regions (ROI nos. 1 and 2) presented a contrasting response with near-maximal ATP response at lower strain values (5 and 9%).

Mean normalized ATP secretion. Figure 6*A* summarizes the stretch-induced ATP accumulation in extracellular medium over time for four independent experiments. The nearly continuous accumulation of ATP in the extracellular medium masks the very dynamic response of A549 cells under mechanical stretch. The ATP secretion activity occurred immediately after the onset of stretch and dissipated in <5 s. The average amount of secreted ATP after each pulse and the peak efflux during the burst of ATP release are reported on Fig. 6, *B* and *C*. Maximal responses were observed at 21% deformation, with ATP release reaching 184 ± 81 pmol/million cells (or 184 ± 81 amol/cell) and ATP efflux climbing to 26 ± 16 (pmol/s)/million cells (or 26 ± 16 (amol/s)/cell).

Given that an adherent A549 cell has a volume of ~5–10 pL (2), and assuming the cytosolic fraction occupies the whole cell, with an estimated cytosolic ATP concentration of 1–5 mM, the total cytosolic ATP content would reach 5–50 fmol/ cell. Thus, in response to a 21% strain, ~0.4–4% of cytosolic ATP content has been expelled extracellularly. Our imaging system clearly showed that not all cells were responsive, however, and that higher values for a single stretch can be anticipated in high release areas. For example, in the experiment shown in Fig. 3*A* at 21% deformation, the level of ATP attained 280 pmol/million cells (280 amol/cell) for the whole chamber, but the density map revealed a peak region reaching ~900 fmol/mm² from a prestretch value of ~200 fmol/mm². With a relative ATP density gain of ~700 fmol/mm² and the seeding cell density of 700 cells/mm² (see MATERIALS AND METHODS), we computed ~1 fmol/cell or 2–20% of total cytosolic ATP content in this high-release zone from a single stretch. The rate of ATP release also showed considerable spatial heterogeneity. On Fig. 4*A*, for instance, the same region presented the highest ATP efflux, reaching ~270 (fmol/s)/mm² and normalizing this rate with cell density yields ~386 (amol/s)/cell.

Hypotonic shock and ATP secretion. A sudden decrease in medium tonicity is another well-studied stimulus known to provoke ATP secretion (2). We tested A549 cells, which were seeded on glass coverslips and mounted on the stand of our real-time imaging system, for swelling-induced extracellular ATP elevation. To prevent cells from being acutely exposed to the remotely controlled addition of hypotonic solution, a small piece of the coverslip underneath the tip of the fluid dispenser was removed before testing, and hypotonic solution was added slowly (~3–5 s) to minimize mechanical perturbation while achieving a steady mixing.

Compared with stretch experiments, the secretion dynamics progressed at a slower pace and was more homogeneous. In the experiment shown in Fig. 7A, the distribution of secreted ATP was evenly spread over the cell population during the initial phase of the response ($t < 15$ min; Fig. 7B) within 10 min after the addition of hypotonic fluid and ~3 min after the rise of detectable ATP above background level (Fig. 7B). Afterward, a hot spot of ATP release gradually expanded near the edge of the coverslip. The ATP_o density, ranging between 20 and 30 fmol/mm² for most of the coverslip during the rising phase of the response (Fig. 7A), climbed in excess of 100 fmol/mm² in this hot spot region but remained far from the density level observed during stretch loads (see Fig. 3A and 5A). This heterogeneous luminescence intensity, markedly distinct at $t = 37.5$ min (Fig. 7A), is likely a consequence of spatial differences in ATP efflux arising from regional variation in cell density. This may not be the sole explanation, however, since the heterogeneity of ATP accumulation was augmented even further after ATP secretion had ceased ($t > 37.5$ min). This nonhomogeneous spatial distribution in bioluminescence appears related in part to the chemistry of the ongoing enzymatic reaction with the spatial segregation and establishment of gradients of either reagents or ATP throughout the volume of the reaction rather than exclusively linked to cellular ATP efflux, although this cannot be answered firmly unless a more detailed three-dimensional diffusion analysis and enzymatic kinetics of the reaction is undertaken.

Contrary to stretch, the hypotonically induced secretion lasted several minutes after the initiation of cell swelling (Fig. 7B). This sluggish response has been observed on three other independently tested coverslips. In a previous report from our laboratory, using an offline analysis and a perfusion chamber, the measured swelling-induced ATP efflux peaked around 1.5

min after the medium tonicity was lowered and reached a mean rate of $5 \pm 1.1 \text{ pmol}\cdot\text{s}^{-1}\cdot\text{million cells}^{-1}$ ($n = 9$) or $5 \pm 1.1 \text{ amol}\cdot\text{s}^{-1}\cdot\text{cell}^{-1}$ (2), but here, the efflux halted at 0.03 ± 0.01 (pmol/s)/million cells or 30 ± 10 (zmol/s)/cell and at a much later time: ~ 15 min on average after medium dilution ($n = 4$). While this lower ATP secretion is mostly a consequence of diminished release, a prolonged but feeble ATP efflux tends toward underestimation. Indeed, when the ATP efflux is strong, it largely exceeds the ATP breakdown from the LL reaction and ectoATPases, but a weak ATP efflux struggles to accumulate ATP_o in the chamber against that constant degradation. Several reasons, in addition to the ATP breakdown activity of the ecto-ATPases and LL reaction, could explain those differences. The first and foremost is the lack of perfusion resulting in a slower change in bulk medium tonicity, a critical factor determining the rate of cell swelling (13). Other factors include the lower experimental temperature, 30°C instead of 37°C in (2), and the absence of tonic fluid shear mixing the cell boundary layer in the present configuration. In addition to efflux, the total hypo-induced ATP release ($n = 4$) was similarly smaller at 28 ± 12 pmol/million cells (Fig. 7C) when compared with the former study from our lab (2) with $1,002 \pm 154$ pmol/million A549 cells ($n = 9$). Notice that the total amount of ATP secreted from the sum of the five stretch pulses reached 384 ± 224 pmol/million A549 cells (Fig. 7C).

3.3.5 Discussion

The real-time ATP imaging technique described herein produces images with superior brightness when compared with a standard microscope, thanks to its threefold object-to-image reduction. It also expands considerably the field of view to encompass the whole of typical experimental chambers used for ATP release investigation and permits to exclusively visualize the heterogeneous nature of mechanosensitive ATP release from a cell monolayer. It is also a compact free-standing imaging system easy to enclose in a light-tight box for bench-top assays and a less expensive solution than other microscopy-based techniques. Other advantages of macroscopic imaging include a very long working distance (~ 70 mm with the lenses described in this study) to accommodate a variety of experimental chambers and the option to change the magnification level with additional lenses.

A large proportion of earlier ATP release studies had reported dimensionless LU in lieu of quantity of ATP, making it difficult to compare the cellular responses between independent studies and further impeding the progress in search of the nature and identities of ATP release pathways. The quantification of ATP from recorded images as detailed in the present report will help eliminate this difficulty and facilitate interstudies comparisons. In addition, our ability to identify areas of higher rate of ATP secretion and accumulation despite the limited resolution of our imaging system enabled us to estimate peak ATP secretion at the cellular level, an important characteristic to help identify the mechanisms of ATP release. Furthermore, by estimating the extent of ATP diffusion, we could produce a fair approximation of the local concentration of ATP in the vicinity of the cell, an essential measure for purinergic signaling studies. Finally, we are also looking forward to improving the ATP mapping accuracy by estimating the ATP distribution in the extracellular fluid using a 3D model incorporating enzymatic kinetics and diffusion processes.

In conclusion, our macroscopic wide FOV quantitative ATP imaging approach, despite its lower imaging resolution when compared with that of a microscope, has nonetheless a very high level of ATP_o mapping resolution and quantification. Further, by revealing the big picture, this novel approach will enrich our understanding of the inhomogeneities and subtle dynamics of mechanically triggered ATP secretion from a cell monolayer.

3.3.6 Grants

This study was supported by Canadian Institutes of Health Research (MOP64364) and Natural Sciences and Engineering Research Council of Canada (R. Grygorczyk).

3.3.7 Disclosures

No conflicts of interest, financial or otherwise, are declared by the authors.

3.3.8 Author Contributions

J.J.T., O.P., R.G., and F.B. conceived and designed research; J.J.T. and O.P. performed experiments; J.J.T., O.P., and F.B. analyzed data; J.J.T., O.P., R.G., and F.B. interpreted results of experiments; J.J.T. prepared figures; J.J.T., R.G., and F.B. drafted manuscript; J.J.T., O.P., R.G., and F.B. edited and revised manuscript; J.J.T., O.P., R.G., and F.B. approved final version of manuscript.

3.3.9 References

1. **Boudreault F, Grygorczyk R.** Cell swelling-induced ATP release and gadolinium-sensitive channels. *Am J Physiol Cell Physiol* 282: C219–C226, 2002. doi:10.1152/ajpcell.00317.2001.
2. **Boudreault F, Grygorczyk R.** Cell swelling-induced ATP release is tightly dependent on intracellular calcium elevations. *J Physiol* 561: 499–513, 2004. doi:10.1113/jphysiol.2004.072306.
3. **Burnstock G.** Purine and pyrimidine receptors. *Cell Mol Life Sci* 64: 1471–1483, 2007. doi:10.1007/s00018-007-6497-0..
4. **DeLuca M, McElroy WD.** Two kinetically distinguishable ATP sites in firefly luciferase. *Biochem Biophys Res Commun* 123: 764–770, 1984. doi:10.1016/0006-291X(84)90295-X.
5. **Feranchak AP, Lewis MA, Kresge C, Sathe M, Bugde A, Luby-Phelps K, Antich PP, Fitz JG.** Initiation of purinergic signaling by exocytosis of ATP-containing vesicles in liver epithelium. *J Biol Chem* 285: 8138–8147, 2010. doi:10.1074/jbc.M109.065482.
6. **Furuya K, Sokabe M, Grygorczyk R.** Real-time luminescence imaging of cellular ATP release. *Methods* 66: 330–344, 2014. doi:10.1016/j.ymeth.2013.08.007.
7. **Grygorczyk R, Furuya K, Sokabe M.** Imaging and characterization of stretch-induced ATP release from alveolar A549 cells. *J Physiol* 591: 1195–1215, 2013. doi:10.1113/jphysiol.2012.244145.
8. **Koizumi S, Fujishita K, Inoue K, Shigemoto-Mogami Y, Tsuda M, Inoue K.** Ca²⁺ waves in keratinocytes are transmitted to sensory neurons: the involvement of extracellular ATP and P2Y2 receptor activation. *Biochem J* 380: 329–338, 2004. doi:10.1042/bj20031089.
9. **Lazarowski ER.** Vesicular and conductive mechanisms of nucleotide release. *Purinergic Signal* 8: 359–373, 2012. doi:10.1007/s11302-012-9304-9.

10. **Lohman AW, Billaud M, Isakson BE.** Mechanisms of ATP release and signalling in the blood vessel wall. *Cardiovasc Res* 95: 269–280, 2012. doi:10.1093/cvr/cvs187.
11. **Mochizuki T, Sokabe T, Araki I, Fujishita K, Shibasaki K, Uchida K, Naruse K, Koizumi S, Takeda M, Tominaga M.** The TRPV4 cation channel mediates stretch-evoked Ca²⁺ influx and ATP release in primary urothelial cell cultures. *J Biol Chem* 284: 21257–21264, 2009. doi:10.1074/jbc.M109.020206.
12. **Pellegatti P, Falzoni S, Pinton P, Rizzuto R, Di Virgilio F.** A novel recombinant plasma membrane-targeted luciferase reveals a new pathway for ATP secretion. *Mol Biol Cell* 16: 3659–3665, 2005. doi:10.1091/mbc.e05-03-0222.
13. **Ponomarchuk O, Boudreault F, Orlov SN, Grygorczyk R.** Calcium is not required for triggering volume restoration in hypotonically challenged A549 epithelial cells. *Pflugers Arch* 468: 2075–2085, 2016. doi:10.1007/s00424-016-1896-4.
14. **Ribeiro C, Esteves da Silva JC.** Kinetics of inhibition of firefly luciferase by oxyluciferin and dehydroluciferyl-adenylate. *Photochem Photobiol Sci* 7: 1085–1090, 2008. doi:10.1039/b809935a.
15. **Schindelin J, Arganda-Carreras I, Frise E, Kaynig V, Longair M, Pietzsch T, Preibisch S, Rueden C, Saalfeld S, Schmid B, Tinevez JY, White DJ, Hartenstein V, Eliceiri K, Tomancak P, Cardona A.** Fiji: an open-source platform for biological-image analysis. *Nat Methods* 9: 676–682, 2012. doi:10.1038/nmeth.2019.
16. **Skotak M, Wang F, Chandra N.** An in vitro injury model for SH-SY5Y neuroblastoma cells: effect of strain and strain rate. *J Neurosci Methods* 205: 159–168, 2012. doi:10.1016/j.jneumeth.2012.01.001.
17. **Takada H, Yonekawa J, Matsumoto M, Furuya K, Sokabe M.** Hyperforin/HP-β-cyclodextrin enhances mechanosensitive Ca²⁺ signaling in HaCaT keratinocytes and in atopic skin ex vivo which accelerates wound healing. *BioMed Res Int* 2017: 1–9, 2017. doi:10.1155/2017/8701801.
18. **Taruno A.** ATP release channels. *Int J Mol Sci* 19: 808, 2018. doi:10.3390/ijms19030808.

19. **Tschumperlin DJ, Margulies SS.** Equibiaxial deformation-induced injury of alveolar epithelial cells in vitro. *Am J Physiol Lung Cell Mol Physiol* 275: L1173–L1183, 1998. doi:10.1152/ajplung.1998.275.6.L1173.

3.3.10 Figures and Captions

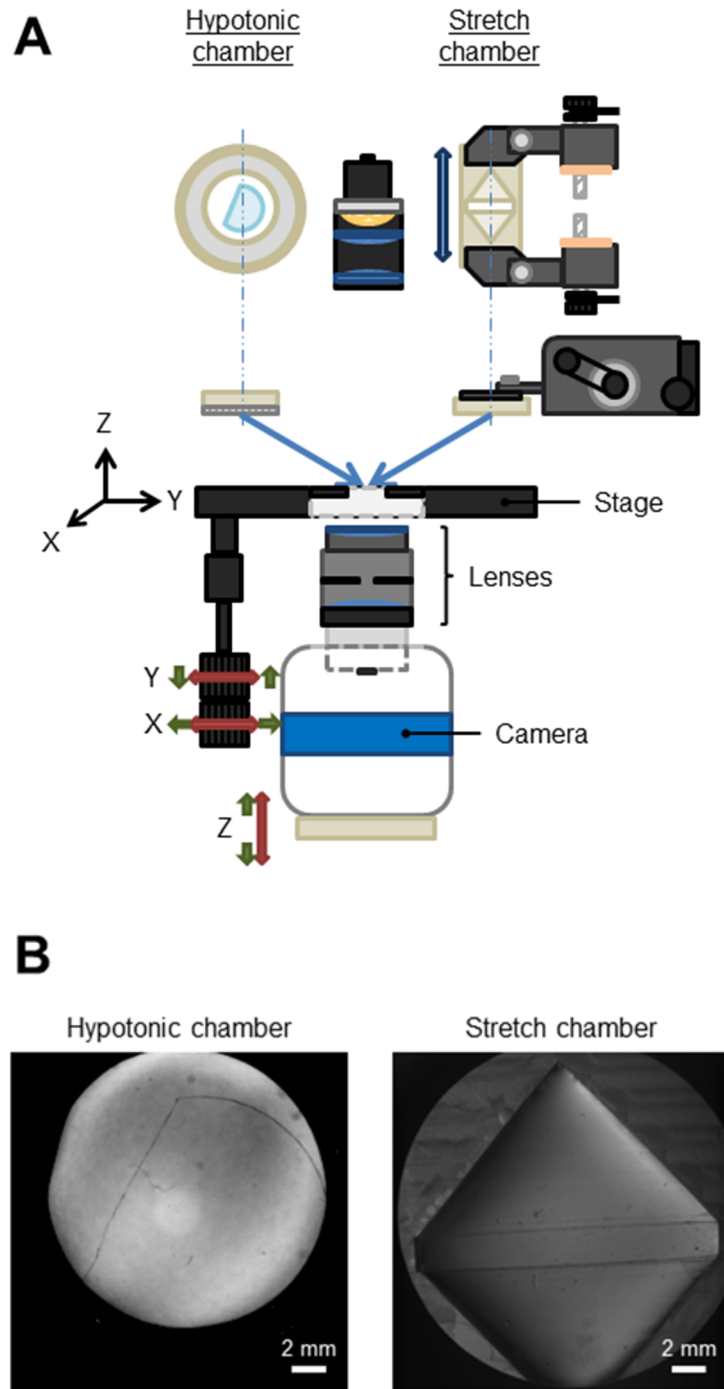


Figure 1

Figure 8. – Figure 1 of Article #1

Fig. 1. Experimental setup for imaging ATP release from cultured cells. *A*: a Photometrics Evolve 512 electron-multiplying charge-coupled device (EMCCD) camera is mounted on a pinion-and-rack device for z-axis focus and installed under a translational (*x-y*-axis) mechanical stage. A pair of lenses with a 3:1 object-to-image ratio and a working distance of ~70 mm are attached on the camera. Cells are seeded onto either a 2 × 18 mm collagen-coated groove of a flexible silicon chamber for stretch experiments or a 15-mm-diameter glass coverslip for hypotonic shock challenge. During the experiments, cells are covered with DMEM containing LL reagent. The stretch chamber is attached to a stretching apparatus fixed on the movable stage. The hypotonic chamber is fixed directly on the stage and kept warm with an incubator (not shown). An incandescent lamp installed above the stage and centered in the system's optical axis is turned on only during pre- and postexperiment brightfield image acquisition. *B*: the coverslip placed in hypotonic chamber and the rectangular stretchable groove area can be visualized in brightfield acquisition mode.

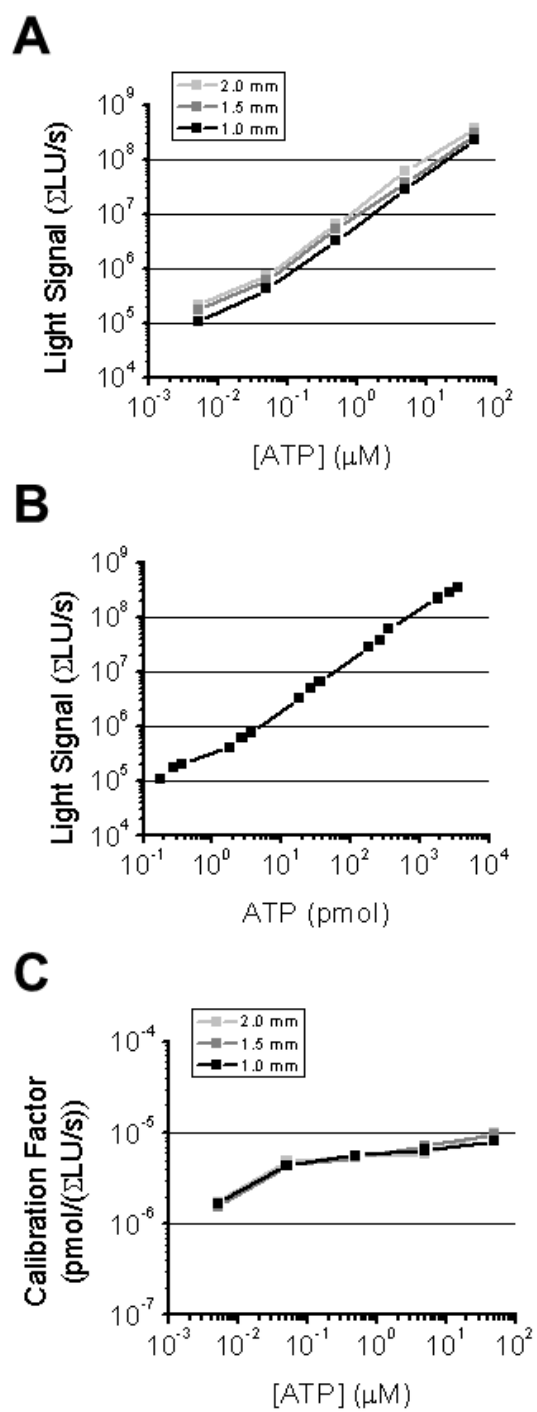


Figure 2

Figure 9. – Figure 2 of Article #1

Fig. 2. Calibration factor determination. *A*: light signal in Σ LU/s (background corrected) against a series of [ATP] for 3 different heights of solution within the stretchable groove. Note that for a given Σ LU/s value, the [ATP] is undetermined without knowing the height of the reaction. Also, for a given [ATP], the light signal increases proportionally with the height of the reaction: with 1 mm signal as reference, the increases in light signal for all [ATP] are 1.5 ± 0.15 (1.5:1 mm) and 1.9 ± 0.22 (2:1 mm). *B*: light signal (Σ LU/s) against total ATP. In contrast to *A*, there is only one corresponding quantity of ATP for a given light signal value. *C*: calibration factor varies slightly with [ATP]. The average of the measured calibration factor was used to calibrate all ATP experiments (stretch and hypo). LU, light unit.

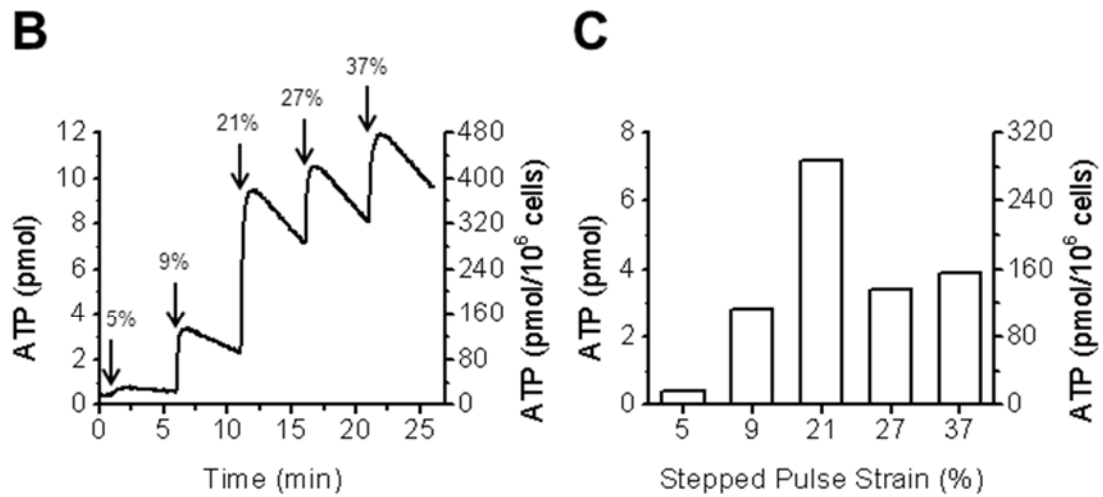
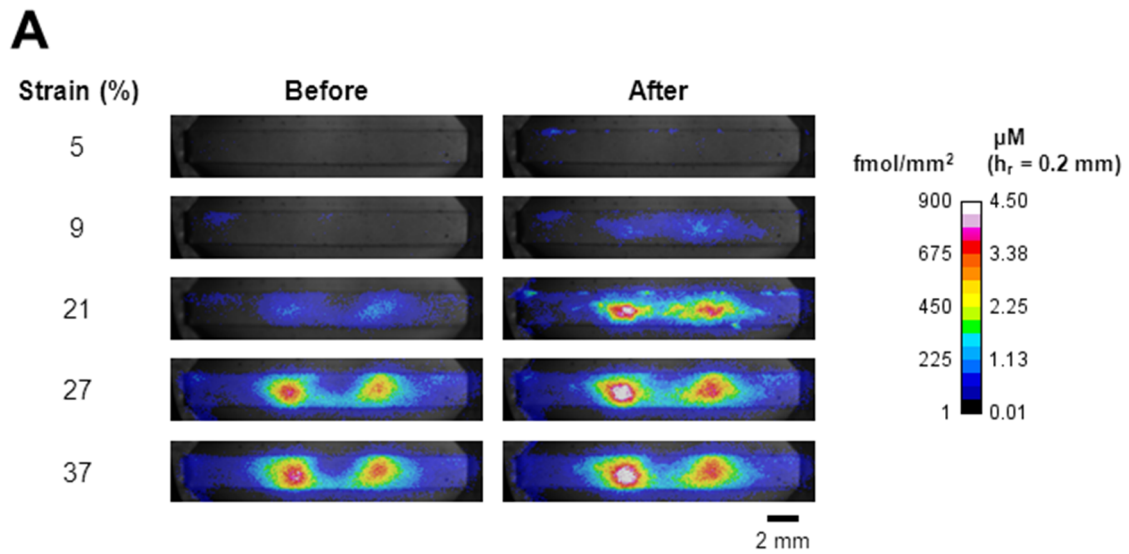


Figure 3

Figure 10. – Figure 3 of Article #1

Fig. 3. Quantitative imaging of extracellular ATP for an entire stretchable area (*sample no. 1*). *A*: overlay color-coded images of ATP density or average $[ATP]_o$ (reaction height, h_r , = 200 μm) over transmitted light (static) image of the stretch chamber (gray) with A549 cells ($\sim 25,000$). Images have been cropped to show only the stretchable groove. ATP release is shown in response to a sequence of 5 uniaxial 1-s duration stretch pulses of increasing amplitude (from 5 to 37% strain) given at 5-min intervals (25°C). Extracellular ATP density recorded seconds before (*left*) and after stretch (*right*). Note that with the stimulation protocol used in this experiment, the ATP-dependent luminescence in those images does not fully return to the background level between the consecutive stretches. *B*: the quantity of released ATP (in pmol) in function of time during the experiment illustrated in *A*. The timing of stretch stimuli is indicated by arrows. *C*: bar graph indicating ATP released (pmol) at each given stretch. The quantity of ATP secreted by cells was calculated from *B* by subtracting prestretch from after stretch peak value.

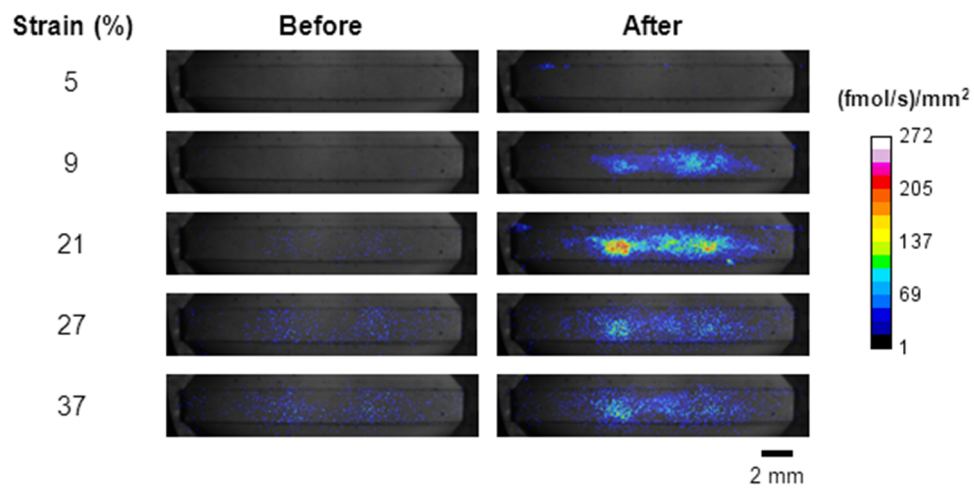
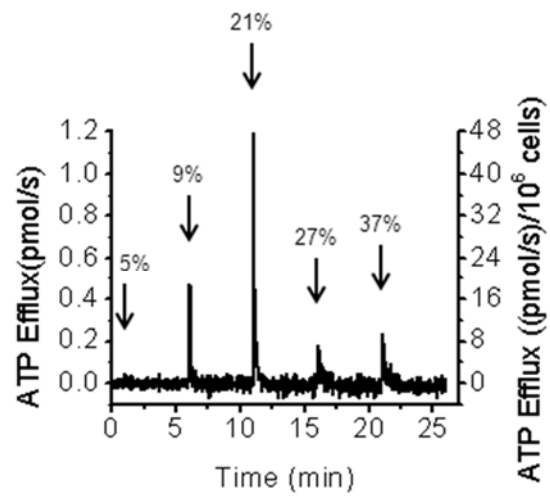
A**B****Figure 4**

Figure 11. – Figure 4 of Article #1

Fig. 4. Quantitative imaging of ATP efflux for whole stretchable groove (*sample no. 1*). *A*: overlay images of time derivative of total ATP signal (described in Fig. 3) over brightfield image of the A549 cell-adherent stretchable groove. *Left* and *right* columns show density efflux of ATP recorded seconds before and after stretch, respectively. Note that, as opposed to the prestretch images in Fig. 3A, the rate of ATP-dependent luminescence in those images returns to near background levels before the following stretch. *B*: ATP efflux in function of time during the experiments illustrated in A. The timing of stretch stimuli is indicated by arrows.

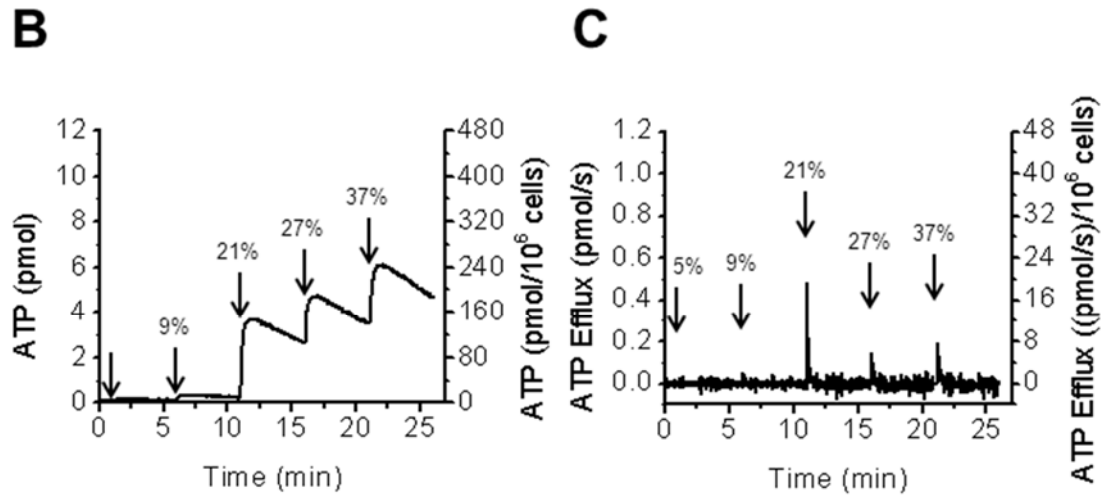
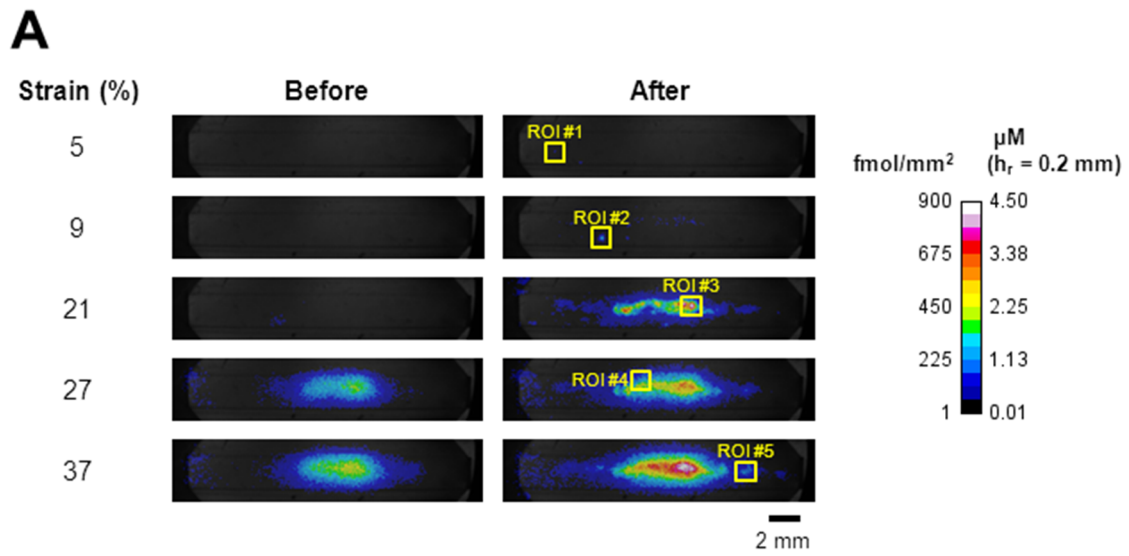
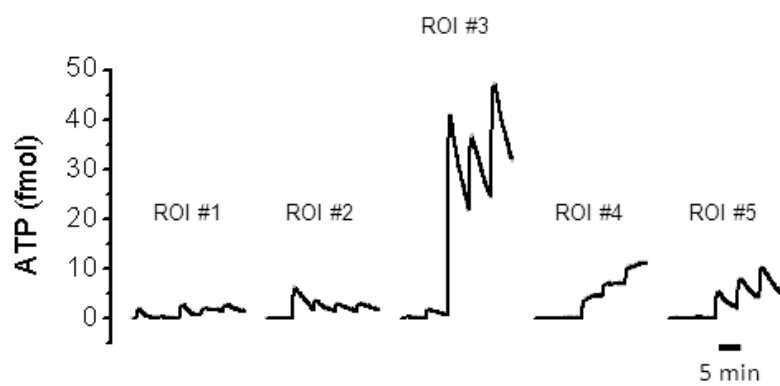


Figure 5

Figure 12. – Figure 5 (Panels A, B and C) of Article #1

D



E

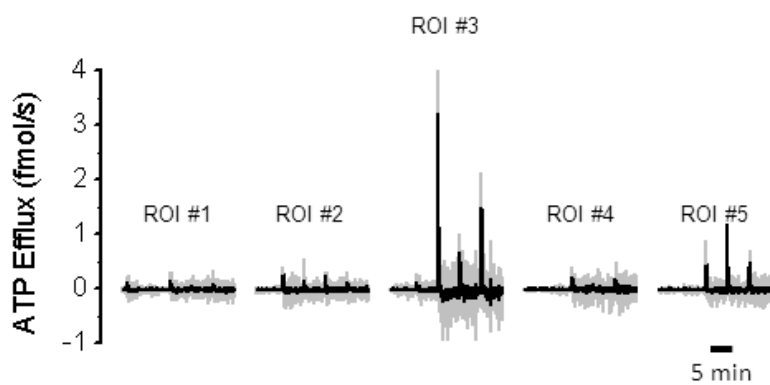


Figure 5

Figure 13. – Figure 5 (Panels D and E) of Article #1

Fig. 5. Quantitative imaging of regional ATP release by stretch (*sample no. 2*). *A*: ATP density and average $[ATP]_o$ (reaction height, h_r , = 200 μm) overlaid on transmitted light image of the stretch chamber are shown in response to a sequence of 5 uniaxial 1-s duration stretch pulses of increasing amplitude (from 5 to 37% strain) given at 5-min intervals at 25°C. Extracellular ATP density images for each pulse recorded immediately before or after stretch are shown. Note that similarly to the experiment presented in Fig. 3A, the major ATP secretion activity is localized in the middle portion of the stretchable zone. *B*: quantity of released ATP (in pmol) by A549 cells in function of time for the whole chamber. Stretch stimuli occurrences are indicated by arrows. *C*: ATP efflux in function of time for the whole chamber derived from *B*. *D*: ATP accumulation response from the 5 regions outlined in *A*. For clarity, the positions of the regions of interest (ROI) are shown on a single image, but analysis was performed over the complete experimental time course. *E*: rate of ATP release for the 5 regions indicated in *A*. Data were smoothed with a running average ($n = 5$) before the derivative calculation to reduce the signal noise from the luciferase-luciferin reaction and better highlight the peak values. Gray area is $\pm\text{SD}$.

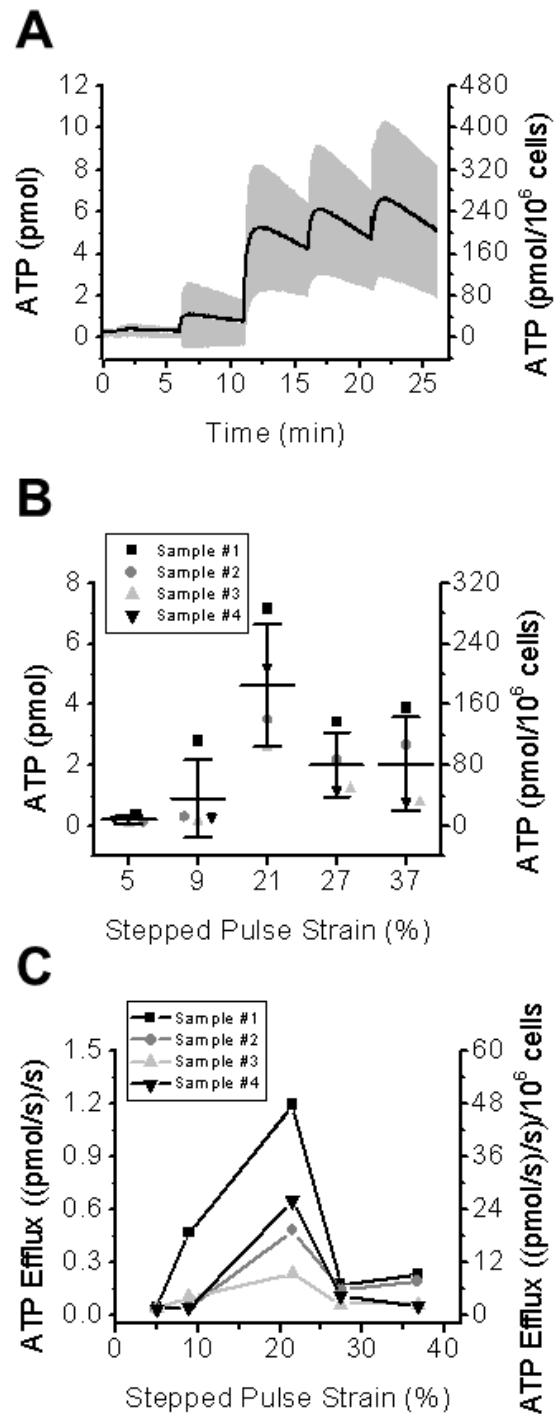


Figure 6

Figure 14. – Figure 6 of Article #1

Fig. 6. Summary of accumulated ATP release per chamber/pulse and rate per pulse. ATP secretion and max efflux per pulse of increasing strain are not monotonic. *A*: average total ATP secreted per chamber and normalized per million cells in response to pulse stretch of increasing strain ($n = 4$ chambers). Gray area is \pm SD. *B*: ATP secreted per pulse. *C*: maximal ATP efflux per pulse of increasing strain. Data come from the same set of experiments analyzed in *A*. Note the similar pattern of response for total ATP secreted (in *B*) and ATP efflux per pulse. Mean \pm SD (strain): 1.7 ± 0.2 (5%), 6.7 ± 8.2 (9%), 25.6 ± 16.2 (21%), 5.0 ± 1.9 (27%), and 5.4 ± 3.6 (37%) $\text{pmol}\cdot\text{s}^{-1}\cdot\text{million of cells}^{-1}$ ($n = 4$).

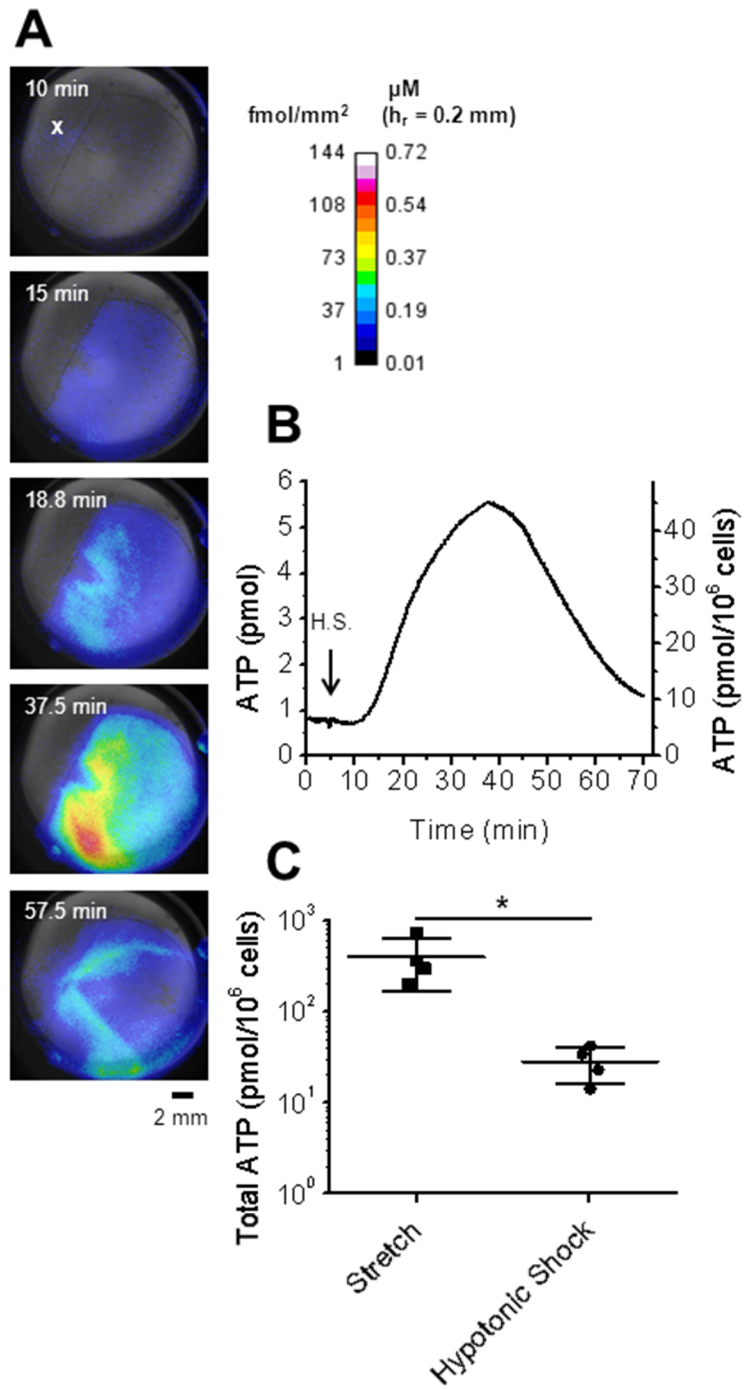


Figure 7

Figure 15. – Figure 7 of Article #1

Fig. 7. Quantitative imaging of ATP efflux induced by hypotonic shock. A549 cell swelling results in initially more homogeneous ATP secretion but slower efflux than stretch. *A*: color-coded images of ATP density or average $[ATP]_o$ (reaction height, h_r , = 200 μm) overlaid on brightfield-acquired (static) image of the hypotonic chamber (gray) are shown in response to an acute diminution of extracellular fluid tonicity (50%) at 30°C. HypoLL solution was added at a location marked with an X at $t = 5$ min. Note that the addition of the hypotonic solution to the medium containing protein-rich LL solution created 2 air bubbles located at the periphery of the chamber wall. They did not interfere with the reaction but reflected some of the luminescence, and were especially visible at $t = 37.5$ min. *B*: cumulated ATP in the chamber over time has been calculated similarly as stretch experiments and is presented for the whole experiment until luminescence level went back to initial level. The detectable ATP efflux lasted for several minutes and ceased ~ 33 min after the onset of hypotonic shock. *C*: total ATP secretion from stretch load (sum of all 5 consecutive stretch pulses; $n = 4$) and hypotonic challenge per million of A549 cells ($n = 4$). Secretion levels were different ($*P < 0.05$) by Mann-Whitney test (R, version 3.4.1 Open-source software <http://www.R-project.org/>).

Chapter 4 – Article #2

4.1 Preamble

To further the knowledge on stretch-induced ATP release in lung alveolar cells, we used the approach devised in Article #1 and conducted similar experiments with rat primary alveolar cells (137).

Previously, we used human lung carcinoma A549 cell line, which shares similar properties to that of AT2 cells (128). For example, they contain LB and are able to synthesize surfactant (25). However, because immortalized cells do not fully recapitulate the biology of primary AT2 cells, we used a primary cell culture to depict a more accurate representation of what is happening in the lungs (138). Recently, Furuya *et al.* showed that inflation induces ATP release in the *ex vivo* lung and that this release solely occurred at the alveolar level (130). However, the specific alveolar cell type responsible for ATP release is still unknown.

While there are only two types of alveolar cells (AT1 and AT2 cells), current data regarding the sources of intra-alveolar ATP release induced by mechanical stimuli are conflicting. Patel *et al.* demonstrated that AT1 cells released fourfold more ATP than AT2 cells in response to 21% stretch (31). However, studies conducted by Isakson *et al.* demonstrated that only AT2 cells release ATP (32, 139).

For this study, we obtained both cell types of the alveolus by culturing freshly isolated rat AT2 cells (a mixture of approximately 85% of AT2 cells and 15% AT1 cells) and maintaining them in culture for up to seven days in order to obtain variable proportions of AT2 and AT1 cells. It has been shown that after several days on a collagen matrix, AT2 cells lose specific cell markers and gain AT1-like phenotypes (32). We then investigated stretch-induced ATP release in cell cultures containing both cell types, and aimed to determine the contribution of AT1 and AT2 cells, as well as the mechanisms involved in such release.

4.2 Article #2

Title: Type 2 secretory cells are primary source of ATP release in mechanically stretched lung alveolar cells

Authors: Ju Jing Tan, Francis Boudreault, Damien Adam, Emmanuelle Brochiero, Ryszard Grygorczyk

Status: Published in *American Journal of Physiology-Lung Cellular and Molecular Physiology* (140) (see *Appendix D* for reference 140)

4.2.1 Contribution

Under the supervision of Dr. Francis Boudreault and Dr. Ryszard Grygorczyk, I participated in the experimental design. I conducted the majority of the experiments presented in this article (Figures 1 to 6). Dr. Damien Adam assisted and performed part of the experiments and analysis of the immunofluorescence staining (panels C to E of Figure 1). Dr. Emmanuelle Brochiero's laboratory provided rat epithelial alveolar cells and protocols for primary culture. Dr. Emmanuelle Brochiero also provided advice for the experimental design and contributed to drafting of the manuscript. I also analyzed the data and prepared the final figures for the manuscript. Dr. Ryszard Grygorczyk and I drafted the manuscript.

4.3 Type 2 secretory cells are primary source of ATP release in mechanically stretched lung alveolar cells

Ju Jing Tan,^{1,2} Francis Boudreault,¹ Damien Adam,^{1,2} Emmanuelle Brochiero,^{1,2} and Ryszard Grygorczyk^{1,2}

¹Centre de recherche du Centre hospitalier de l'Université de Montréal, Montreal, Quebec, Canada; and ²Department of Medicine, Université de Montréal, Montréal, Québec, Canada, Montreal, Quebec, Canada

Submitted 8 August 2019; accepted in final form 3 October 2019

Running Head: ATP release in alveolar cells

Address for reprint requests and other correspondence:

R. Grygorczyk

Centre de recherche du CHUM

900, rue Saint-Denis, Pavillon R

Montréal, QC H2X 0A9

Canada

(e-mail: ryszard.grygorczyk@umontreal.ca)

4.3.1 Abstract

Tan JJ, Boudreault F, Adam D, Brochiero E, Grygorczyk R. Type 2 secretory cells are primary source of ATP release in mechanically stretched lung alveolar cells. *Am J Physiol Lung Cell Mol Physiol* 318: L49–L58, 2020. First published October 9, 2019; doi:10.1152/ajplung.00321.2019.— Extracellular ATP and its metabolites are potent paracrine modulators of lung alveolar cell function, including surfactant secretion and fluid transport, but the sources and mechanism of intra-alveolar ATP release remain unclear. To determine the contribution of gas-exchanging alveolar type 1 (AT1) and surfactant-secreting type 2 (AT2) cells to stretch-induced ATP release, we used quantitative real-time luminescence ATP imaging and rat primary alveolar cells cultured on silicon substrate for 2–7 days. When cultured on solid support, primary AT2 cells progressively transdifferentiated into AT1-like cells with ~20% of cells showing AT1 phenotype by day 2–3 (AT2:AT1 \approx 4:1), while on day 7, the AT2:AT1 cell ratio was reversed with up to 80% of the cells displaying characteristics of AT1 cells. Stretch (1 s, 5–35%) induced ATP release from AT2/AT1 cell cultures, and it was highest on days 2 and 3 but declined in older cultures. ATP release tightly correlated with the number of remaining AT2 cells in culture, consistent with ~10-fold lower ATP release by AT1 than AT2 cells. ATP release was unaffected by inhibitors of putative ATP channels carbenoxolone and probenecid but was significantly diminished in cells loaded with calcium chelator BAPTA. These pharmacological modulators had similar effects on stretch-induced intracellular Ca²⁺ responses measured by Fura2 fluorescence. The study revealed that AT2 cells are the primary source of stretch-induced ATP release in heterocellular AT2/AT1 cell cultures, suggesting similar contribution in intact alveoli. Our results support a role for calcium-regulated mechanism but not ATP-conducting channels in ATP release by alveolar epithelial cells.

Keywords: lung ATP release; mechanosensitivity; purinergic signaling

4.3.2 Introduction

The mammalian lung alveolar epithelium comprises two main cell types, gas-exchanging squamous alveolar type 1 (AT1) and cuboidal surfactant-secreting alveolar type 2 (AT2) cells. AT2 cells synthesize and secrete surfactants, regulate depth of alveolar lining fluid, initiate the innate immune response, and act as progenitors for AT1 and AT2 cells during natural regeneration and epithelial repair after injury (7, 26). Even though in human alveolus the number of AT2 cells is higher than AT1 cells, the thin and large surface area of AT1 cells covers >95% of the alveolus surface. Pulmonary epithelial cells are constantly subjected to physical forces as a result of the cyclic breathing, coughing, and sneezing. These forces include air flow shear stress in the airways, cell stretch during alveoli inflation, and cell distortion by tension forces at the air-liquid interface in the alveoli and airways. Under clinically relevant pathological conditions, such as lung edema and mechanical ventilation, considerable fluid shear stress may also occur. Moreover, edematous lungs show inhomogeneous inflation in which some air-filled alveoli adjacent to the liquid-filled ones are subjected to significant overdistensions during breathing (29), which may lead to ventilator-induced lung injury (VILI). It is characterized by mechanical rupture of pulmonary structures, inflammation, and edema and constitutes a major clinical complication in ventilated patients in the intensive care unit (8, 43).

Mechanical forces, particularly stretch, play important roles in regulating lung function, development, alveolar cell differentiation and regeneration after injury (12, 33, 36). This requires translation of mechanical stimuli into biochemical signals, which often involves stress-sensitive release of ATP and activation of purinergic signaling events (19, 24, 32). Extracellular ATP and other nucleotides can bind to nucleotide-specific cell-surface purinergic receptors, which are categorized into ionotropic P2X₁₋₇ receptors and G-protein-coupled P2Y_{1,2,4,6,11,12,13,14} receptors. The potential of extracellular nucleotide signaling is further diversified by the presence of nucleotidases, which sequentially hydrolyze ATP to ADP, AMP, and finally adenosine (45). Adenosine in turn may activate another family of G-protein-coupled receptors consisting of A₁, A_{2A}, A_{2B}, and A₃ subtypes (38). In the lungs, purinergic receptors are expressed on epithelial cells lining the lung surfaces, including AT2/AT1 cells, and often many receptor subtypes may be present on the same cell (4, 23). Purinergic signaling regulates surfactant release and all three

components of the mucociliary clearance system: cilia beat frequency, fluid, and mucus secretion (6, 37). It also plays an important role in a number of lung diseases and associated clinical complications, including asthma, chronic obstructive pulmonary disease, acute respiratory distress syndrome, and VILI (6, 20). In experimental animal models, considerable amounts of ATP and other purines were found in the alveolar space of mechanically ventilated rat lungs as detected in vivo in bronchoalveolar lavage fluids (10, 35, 44). Excessively high levels of extracellular ATP act as a danger-associated signal and contribute to the pathogenesis of VILI by triggering the release of multiple proinflammatory mediators, lung inflammation, edema, and tissue damage (20). Given the critical responses that extracellular nucleotides can evoke in the lungs under physiological and pathophysiological conditions, it is of importance to understand the mechanism of cellular ATP release: the first step of purinergic signaling cascade. Besides cell injury-induced release, several pathways have been implicated in nonlytic release of ATP, including channels and/or Ca^{2+} -regulated exocytosis of ATP-loaded vesicles, but the exact mechanisms are still debated (17, 25, 31).

Release of cellular nucleotides is stress sensitive, as demonstrated by several groups (19, 24). Physical forces, such as mechanical stretch, cell deformation by tension forces at the air-liquid interface, and hypotonic shock induce increases in intracellular calcium levels ($[\text{Ca}^{2+}]_i$) and $[\text{Ca}^{2+}]_i$ -dependent release of ATP out of the cell (3, 40, 41). In carcinoma A549 cell line, a model of human alveolar cells, single stretch stimulus of more than 10% was sufficient to induce $[\text{Ca}^{2+}]_i$ -dependent ATP release with local ATP concentrations exceeding 10 μM (18). A recent real-time bioluminescence ATP imaging study with ex vivo rat lungs provided the first direct evidence that inflation induces ATP release in lung airspaces. The functional units where ATP release occurred consisted of alveolar sacs or their clusters (15). However, the contribution of AT1/AT2 cells lining the alveoli could not be determined in these experiments. Ex vivo confocal microscopy study has determined that the bulk of the alveolar distension during lung expansion occurs in AT1 and not AT2 cells (28), suggesting that AT1 cells act as a mechanosensor where transient intracellular Ca^{2+} signaling is initiated during lung inflation (2). However, conflicting data exist regarding the sources of intra-alveolar ATP release. In vitro studies with rat primary alveolar cells by Isakson et al. (21, 22) indicate that AT2 cells act as the primary source of

extracellular ATP, while a study by Patel et al. (27) suggested that AT1 cells release significantly more ATP than AT2 cells and thus have a principal role in paracrine stimulation of surfactant secretion by AT2 cells. These early studies used bulk luminometry for ATP determinations, which lack spatial information on ATP release sites and have limited sensitivity and temporal resolution. These limitations could be overcome with the use of recently established real-time, high-sensitivity ATP release imaging technique (14) or a simplified low-cost version of that system based on wide-field-of-view (WFOV) imaging (39). Therefore, the objective of this study was to address the question of cellular source and mechanism of ATP release in mechanically distended AT2 and AT1 cell cultures using a quantitative WFOV ATP imaging approach. Clarifying release mechanisms and sources of intra-alveolar ATP is important for better understanding intercellular communication that coordinates alveoli responses to mechanical stimuli under physiological and pathological conditions, such as mechanical ventilation.

4.3.3 Methods

Cell culture. Primary alveolar epithelial cells were isolated from lungs of adult male Sprague-Dawley rats (175–200 g, Charles River Laboratories, Senneville, QC, Canada), according to a well-established protocol as previously described (5, 16). In brief, the lungs were first washed to remove red blood cells and most of the alveolar macrophages before digestion with elastase (Worthington, Lakewood, NJ). They were then minced, and the resulting suspension was filtered. A differential adherence technique (9, 16) was then used to discard the remaining macrophages bound on IgG and to purify alveolar epithelial cells. The freshly isolated alveolar cells were seeded onto custom-designed silicon chambers in MEM (Thermo Fisher Scientific Ltd., Saint-Laurent, QC, Canada) containing 10% fetal bovine serum (FBS, Wisent, Saint-Bruno, QC, Canada), 0.08 mg/L gentamicin, Septra (3 µg/mL trimethoprim + 17 µg/mL sulfamethoxazole, Glaxo Smith Kline Biologicals, Laval, QC, Canada), 0.2% NaHCO₃ (Sigma-Aldrich, Oakville, ON, Canada), 10 mM HEPES, and 2 mM L-glutamine (Thermo Fisher Scientific Ltd.). After seeding, alveolar cells were cultured for up to 7 days in MEM-FBS medium without Septra. All procedures pertaining to the use of animals were approved by the Comité Institutionnel de protection des animaux of the Centre de recherche du Centre hospitalier de l'Université de Montréal in compliance with guidelines of the Canadian Council of Animal Care.

Alkaline phosphatase histochemical staining. High alkaline phosphatase (AP) activity of AT2 cells is particularly useful to discriminate between AT2 and AT1 cells. AP staining was performed in cultures of freshly isolated alveolar cells seeded on silicone chambers or on 35 × 10 mm Petri dishes (Sarstedt Inc., Montreal, QC, Canada). On day 2, 3, 4, and 7 after seeding, cells were fixed, stained with 0.05% Fast Blue BB, and counterstained with 0.1% neutral red solution, as described in Ref. 42. Blue staining identified cells with high alkaline phosphatase activity present in AT2 cells, whereas those that counterstained in red only were AT1 cells (5, 11).

Immunofluorescence staining. For immunofluorescence staining, alveolar cells were seeded on an 8-well Laboratory-Tek (Nunc, Thermo Fisher Scientific, Rochester, NY). At 3 or 7 days after seeding, cells were fixed with 4% paraformaldehyde, permeabilized with Triton 0.1%, blocked, and then incubated overnight (4°C) with primary antibodies, anti-pro-surfactant protein C (1:100, EMD Millipore Corporation, Billerica, MA) or anti-aquaporin 5 (1:100, Alomone Laboratories Ltd., Jerusalem, Israel). After blocking, a secondary antibody [donkey anti-rabbit IgG conjugated with Alexa Fluor 633 (1:200, Life Technologies, Thermo Fisher Scientific, Rockford, IL)] was then applied for 1 h at room temperature. Following a wash with PBS, a 4',6-diamidino-2-phenylindole, dihydrochloride (DAPI, 1:1,000, Life Technologies, Thermo Fisher Scientific, Burlington, ON, Canada) was added for 15 min and then washed (3×) with PBS. Slides were mounted with Prolong Gold (Invitrogen, Thermo Fisher Scientific) and preserved in darkness at 4°C. Pictures were taken with a fluorescence microscope (Olympus, BY53; magnification ×20 or ×40) and images were analyzed with Icy software (Institut Pasteur, France). For analysis, typically 800 cells/condition/experiment were used, $n = 8$ from 4 different cell preparations (animals).

Stretch chamber and stretching device. Stretch chambers were made with Sylgard 184 silicone (Dow Corning Corporation, Midland, MI) as described previously (14, 18). Briefly, silicone elastomer base and curing agent mixture were poured into a mold and baked for 1 h at 60°C. The mold-made flexible silicone block constituted our stretch chamber with a 2-mm wide groove in the center where cells could be seeded. To facilitate attachment of cells to the silicone surface, the groove was coated with 20% collagen type 1 (Sigma) diluted in H₂O. For

experiments, the chamber was attached to a stretching device (STREX, Cell Stretching System STB-150-W, B-Bridge International, Inc., Cupertino, CA) mounted on a stage above our custom-designed ATP imaging system (39). The stretching apparatus applied a horizontal distension onto the silicon chamber. In a typical experiment, five consecutive stretches of 1-s duration were applied at 5-min intervals with increasing nominal amplitudes. The real stretch amplitudes reported in the figures were measured after each experiment using the acquired images of the stretch chamber.

Real-time, wide-field-of-view bioluminescence ATP imaging. We used a WFOV luminescence ATP imaging as described in Ref. 39. Briefly, this approach uses a low-power objective ($\times 0.33$) mounted directly on an electron multiplying charge-coupled device (EMCCD) camera allowing a real-time two-dimensional (2D) visualization and quantification of ATP contained in the entire stretch chamber following its release from cells. During image analysis, the individual light unit values per pixel for the 1-s acquisition time were converted into ATP quantity with the calibration factor and linear fitting using ImageJ. The total amount of detectable extracellular ATP (ATP_o) within the chamber could be calculated and monitored over the entire course of the experiment. The quantity of secreted ATP for each stretch pulse was calculated by subtracting the prestretch ATP_o level from the stretch-generated peak value. The rate of ATP release, expressed in fmol/s or pmol/s, is the first time derivative of ATP_o . Color-coded images reporting ATP_o density in fmol/mm² (one pixel image = 6×10^{-3} mm²) with respect to the substrate surface or rate of ATP release density in (fmol/s)/mm² were generated with ImageJ. On some images estimates of ATP_o concentration (in μ M) is given as an average value along the z-axis assuming 200 μ m height of a liquid layer above the cells where ATP-dependent LL reaction generates luminescence signal (39).

For imaging of cellular ATP release, stock of LL solution was prepared as follows. One vial of LL (Sigma-Aldrich Corporation, St. Louis, MO) was reconstituted with 5 mL of sterile double-distilled water and isotonicly adjusted with 5 \times physiological solution. One milliliter aliquots of the stock solution were stored in a freezer and used within 1 mo. Once thawed, the LL aliquot was used only during the day of experimentation, and its activity was checked using ATP standard TD 20/20 luminometer (Turner BioSystems, Sunnyvale, CA). Before the ATP imaging

experiment, cells in the stretch chamber were covered with 200 μL solution mixture containing 100 μL of LL stock solution and 100 μL of Gibco's phenol red-free Dulbecco's modified Eagle's medium (DMEM, Invitrogen Canada Inc., Burlington, ON, Canada). Following stretch stimulation, luminescence produced by ATP-dependent LL reaction was captured by the EMCCD camera Evolve 512 (Photometrics, Tucson, AZ) in our custom-designed wide field of view system. Control of the EMCCD and data acquisition were done via AxioVision software (AxioVs40 V 4.8.2.0, Carl Zeiss MicroImaging GmbH, Jena, Germany). Images were acquired at 0.5 Hz frequency with 1-s exposure time, with gain settings at the lowest, readout speed at 5 MHz, and 2×2 binning. Stacks of 900 images were captured and stored for offline analyses with Metamorph (Meta Series Software 7.7.9, Molecular Devices, Downingtown, PA) or ImageJ open-source software.

Intracellular calcium measurements. Calcium imaging experiments were performed as described in Ref. 30. Briefly, AT2 cells were loaded with a ratiometric fluorescent probe Fura2-AM (10 μM , Molecular Probes, Thermo Fisher Scientific) in MEM + FBS cell culture medium for 1 h (37°C, 5% CO_2). Cells were then washed in MEM + FBS, and the medium was changed to phenol-free DMEM. During the experiment, cells were exposed to alternate (100 ms) 340/380 nm illumination from a high-pressure mercury short arc lamp (100 W/2, Osram GmbH, Augsburg, Germany) via interference filters (Chroma Technology, Brattleboro, VT) mounted on a filter wheel (Sutter Lambda 10-C, Sutter Instrument, Novato, CA). Fluorescence images were recorded at 1- to 3-s intervals with a MicroMAX digital camera (Princeton Instruments Inc., Trenton, NJ) and stored for later analysis. As a positive control for Ca^{2+} detection, 30 μL of 100 μM ATP was applied to the cells (13 μM final concentration) at the end of each experiment. Changes of $[\text{Ca}^{2+}]_i$ are shown as Fura2 fluorescence F_{340}/F_{380} ratio normalized to initial baseline level

Pharmacological modulators of ATP release and Ca^{2+} signaling. To study the physiological mechanisms for ATP release, ATP and Ca^{2+} imaging experiments were carried out in the presence of 100 μM carbenoxolone (CBX) or 2.5 mM probenecid (PRO) from Sigma-Aldrich, Inc. (St. Louis, MO) in phenol-free DMEM. To study the role of $[\text{Ca}^{2+}]_i$, AT2 cells were pretreated with 25 μM BAPTA (Life Technologies, Burlington, ON, Canada) and reconstituted in DMSO (Sigma-

Aldrich Canada Co., Oakville, ON, Canada) in MEM + FBS. Controls were also pretreated with MEM + FBS with the same amount of DMSO but without BAPTA.

Statistics. Results are expressed as mean \pm SD. Statistical analyses were performed with R (3.6.0) to compare averages of samples between their conditions. When comparing the average between two groups, an *F* test was first performed to determine whether the variance of both groups was equal to perform the adequate *t* test. For smaller samples ($n = 3-4$), Wilcoxon–Mann–Whitney and Kruskal–Wallis *H* tests were performed to compare with the average of two or more groups, respectively. Pearson product-moment correlation was used for evaluating linear association between two variables. Differences between groups were considered to be significant at $P < 0.05$.

4.3.4 Results

Phenotypic changes of cultured rat primary alveolar epithelial cells. Freshly isolated rat primary alveolar cells were grown on collagen-coated silicon stretch chambers for up to 7 days. AT2 phenotype was identified by alkaline phosphatase staining (blue color, Fig. 1A). AT2 was highest on day 2, but it was gradually lost on days 3–7 when cells progressively acquired AT1-like phenotype, indicated by red counterstain. Figure 1B shows the relative number of AT2 and AT1-like cells on different days in culture as determined by alkaline phosphatase staining. It demonstrates that on days 2 and 3, ~80% of cells still showed AT2 phenotype, corresponding to AT2/AT1 ratio of 4:1, while on day 7, the ratio was reversed to 1:4, with ~80% of cells showing AT1-like phenotype. Gradual transdifferentiation of cultured AT2 to AT1-like cells was further supported by time-dependent reduction of specific immunostaining with pro-surfactant protein C (pro-SPC, marker of AT2 cells) and increased expression of aquaporin-5 (characteristic of AT1 cells) on day 7 compared with day 3 in culture (Fig. 1, C and D, respectively). Quantitative analysis of cell immunostaining (Fig. 1E) demonstrated high consistency with AP staining presented in Fig. 1B. Subsequently, we examined stretch-induced ATP release in such heterocellular 2- to 7-day-old cultures of different AT2 and AT1 cell content.

Stretch-induced ATP release is diminished in cell cultures of low AT2 cell content. Using a quantitative WFOV luminescence imaging approach, we first compared stretch-induced ATP release in 3- and 7-day-old alveolar cell cultures containing predominantly (~80%) AT2 or AT1-like cells, respectively. To quantitate ATP release, luminescence images were converted to two-dimensional (2D) ATP density maps (in fmol/mm²), or expressed as concentration (in μM, as described in METHODS). Figure 2A shows an example of an ATP density map (see pseudocolor scale) of a 3-day-old cell culture containing predominantly AT2 cells (AT2:AT1 ratio of 4:1) before the stretch stimulation and at the peak of response to 1-s stretches of 5–35% applied at 5-min intervals. Small ATP release that was localized to a limited number of release sites was seen for low stretches of 5% and 9% but increased significantly for stronger stretches, with a maximum response observed at 20% stretch. It involved the release from almost all cells in the stretch chamber, reaching, in some areas, up to 900 fmol/mm², corresponding to local ATP concentration of ~4.5 μM. Figure 2B presents similar ATP density maps for 7-day-old alveolar cell culture and shows that ATP release responses were significantly diminished in these cells. Only at the highest stretch of 35% was significant ATP release of 300–400 fmol/mm² observed. The graph in Fig. 2C compares the full time course of ATP released in the entire chamber containing 3-day or 7-day-old cell cultures induced by a sequence of stretches (5–35%) delivered at 5-min intervals. For 3-day-old cells, it peaked at 20% stretch and was significantly higher (>6-fold at the peak) when compared with the peak release in 7-day-old cells observed at 35% stretch. Figure 2D compares cumulative ATP released in response to all delivered stretches during the experiment and demonstrates an average of ~3-fold higher release in 3-day-old cells compared with 7-day-old cell cultures.

Next, we analyzed the rate of ATP release. Figure 3A illustrates an example of 2D maps of ATP release rate (ATP efflux, in fmol·mm⁻²·s⁻¹) at the peak of response after five consecutive stretches of 5% to 35%. It was calculated from a sequence of ATP density maps such as those illustrated in Fig. 2A. Low stretches of 5–10% produced small but detectable ATP efflux. The peak response was observed at 20% stretch with the efflux of ATP reaching ~450 fmol/mm²/s in some spots. The graph on the *right* shows the full time course of ATP release rate averaged for the entire area of the stretch chamber. Note the very short duration (spikes) of ATP release

following stretch stimulation and the absence of the release between the stretches. The *insets* show the spikes of ATP efflux at expanded time scale during 20% stretch (at 11 min) and 35% stretch (at 21 min), demonstrating their duration of <5 s and their peaks of ~5 pmol/s and ~1 pmol/s, respectively. By contrast, 7-day-old cell cultures showed no response or very low responses for stretches of up to 28%, and only at the highest stretch of 35% was considerable ATP efflux (reaching 200 fmol/mm²/s) observed, as shown in 2D maps in Fig. 3B. The corresponding full time course of ATP efflux in the entire chamber is shown on the right, with the spike of ATP release of ~1 pmol/s in response to 35% extension (at 21 min). Figure 3C compares the average rate of ATP release ($n = 5$) in response to stretches of increasing amplitude for 3-day-old and 7-day-old cell cultures with AT2:AT1 of 4:1 and AT2:AT1 of 1:4, respectively. It shows that, in AT2-rich cell cultures, ATP efflux peaked at ~20% stretch but declined for stronger stretches of >25%, while in AT1-rich cultures, significant efflux was observed only at the maximal stretches of 28–35%. The data demonstrated that in cultures containing predominantly AT2 cells the maximal rate of ATP release was observed at lower stretches, and it was ~5-fold higher when compared with older cell cultures containing mostly AT1 cells.

The relative contribution of AT2 and AT1 cells to ATP release was quantified by comparing total ATP release with relative AT2 cell content remaining on each day of culture from 2 to 7 days (Fig. 4). The stretch-induced release of ATP was found to be the highest in early cell cultures (days 2 and 3) but declined progressively for older cultures, showing a tight correlation between decreasing ATP release and the number of remaining AT2 cells (Pearson's correlation coefficient $r = 0.94$, $P = 0.0053$). The data strongly suggest that AT2 cells are the major contributors of stretch-induced ATP release.

Effects of ATP release modulators. To determine the mechanism of stretch-induced ATP release in 3-day-old alveolar epithelial cells, we tested the effects of two commonly used inhibitors of putative ATP channels, carbenoxolone (CBX) and probenecid (PRO). Figure 5A shows the time course of ATP release induced by 9% and 20% stretch under control conditions and in the presence of CBX or PRO. Although the time course of release was not affected, CBX showed a tendency to reduce the peak ATP release and total released ATP (Fig. 5A), but the

effects remained not statistically significant. Interestingly, PRO produced a noticeable increase of the peak and total ATP release, but the effect was not statistically significant either. Thus, the results do not support involvement of putative ATP channels, such as pannexin 1, in stretch-induced ATP release in alveolar cells.

To explore the possible involvement of intracellular Ca^{2+} signaling in ATP release via regulated exocytosis of ATP-containing vesicles (1, 40), cells were loaded with BAPTA-AM to chelate free intracellular Ca^{2+} . Figure 5B shows significant (~40%) inhibition of the peak of stretch-induced ATP release and total released ATP in BAPTA-loaded cells. Data demonstrate the importance of intracellular Ca^{2+} signaling in regulating stretch-induced ATP release. Therefore, we subsequently explored stretch-induced intracellular Ca^{2+} responses in more detail in AT2/AT1 cells using Fura2 fluorescence microscopy.

Stretch-induced intracellular Ca^{2+} responses in AT2 cells. Fig. 6A shows pseudocolor images of Fura2 F_{340}/F_{380} fluorescence ratio in 3-day-old AT2 cell culture subjected to stretch stimulation. At lower stretches (~5%) rapid $[\text{Ca}^{2+}]_i$ responses were observed in very few single cells. The number of responding cells increased with rising stretch amplitude and involved mostly clusters of adjacent cells. Interestingly, CBX inhibited and PRO stimulated stretch-induced $[\text{Ca}^{2+}]_i$ responses, which were almost completely abolished in BAPTA-loaded cells (Fig. 6B). These effects on $[\text{Ca}^{2+}]_i$ are similar to those observed for ATP release, suggesting that the light inhibition of ATP release by CBX and stimulation by PRO may be an indirect result of their effects on $[\text{Ca}^{2+}]_i$ signaling rather than on ATP conductive pathway.

4.3.5 Discussion

The goal of this study was to investigate the cellular source (AT2 vs. AT1 cells) and the mechanism of stretch-induced ATP release in primary AT2 and AT1 cell cultures of rat lungs. We found that AT2 cells, when grown in a 2D culture on collagen-coated silicon stretch chambers, transdifferentiate over time into AT1 cells. This agrees with previous reports where cells were cultured on various substrates, including fibronectin-coated silicon and glass coverslips, or tissue culture treated plastic (21, 22). Using such heterocellular AT2 and AT1 cultures on different days after cell seeding, we have 1) characterized the quantity and rate of stretch-induced ATP release

and 2) determined the relationship between the release and AT2/AT1 cell ratio that varied approximately from 4:1 to 1:4.

ATP release kinetics and quantity. Data of ATP release rate demonstrated that 1-s stretch induced very transient efflux of cellular ATP immediately after the onset of stretch that dissipated in less than 5–10 s. Such kinetics were similar in AT2-rich (day 2 and 3) and AT1-rich (day 7) cell cultures. It was also comparable with the responses observed in our earlier study with A549 cells, a model of human AT2 cells, in which ATP release was examined with the same WFOV approach and the duration of the release was also found to be <10 s (39). The 2–3-day-old cell cultures were significantly more susceptible to stretch stimulation, responding at 5–10% distension and reaching maximum response at 20%, while 7-day old cells were essentially nonresponsive to lower deformations and released noticeable ATP only at the highest strain of 35%. In that respect, the 2- to 3-day-old rat primary AT2 cells appear to be comparable with A549 cells, which showed a similar threshold for ATP release responses of ~10% strain (18).

Transient release resulted in accumulation of significant amounts of extracellular ATP_o that persisted for 5- to 15-min before returning to the prestretch level due to its relatively slow consumption by LL reaction and breakdown by ectoATPases, as discussed before (39). From the data of Fig. 2D, we have determined that the average amount of secreted ATP was 0.72 ± 0.14 fmol/cell and 0.24 ± 0.15 fmol/cell on day 3 and 7, respectively. For comparison, in A549 cells the cumulative ATP released in response to a similar sequence of 5 stretches of increasing amplitude was 0.18 ± 0.08 fmol/cell (39), i.e., comparable with 7-day-old alveolar cell cultures. Importantly, with an estimated cytosolic ATP concentration of 1–5 mM, it could be calculated that for a single stretch of 20%, the total quantity of released ATP in 3-day-old alveolar cells was 0.47 fmol/cell, which represents only ~0.9–9% of cytosolic ATP content. In A549 cells, in response to a 21% strain, ~0.4–4% of cytosolic ATP content has been expelled extracellularly (39).

Based on the total amounts of released ATP in a typical experiment, such as those illustrated in Fig. 2 (5 sequential stretches of 5–35%), and the relative AT2 to AT1 cell content on day 3 and day 7, one can estimate relative contribution of AT2 and AT1 cells to the release. We found that, on average, AT2 cells release at least 11-fold more ATP than AT1 cells, i.e., ~880 pmol versus 80 pmol per 10^6 cells, respectively. This estimate is based on the assumption that the phenotype-specific capability of releasing ATP by AT2 and AT1 cells does not change with cell number/density and days in culture. This model also does not consider the effect of cell-to-cell communication that could modulate/synchronize cellular Ca^{2+} and ATP responses (see below). However, with the precise determinations of ATP release and cell number, this model does not exclude the possibility that AT1 cells do not secrete ATP at all and AT2 cells are the sole contributors. At the present, we have no direct proof that in 7-day-old cell cultures only the remaining AT2 cells are contributors to ATP release. It would require identifying individual ATP-releasing cells, which is technically challenging with the current version of WFOV approach due to limited spatial resolution (39).

Our findings that AT2 cells are the major contributor to ATP release differs from that reported by Patel et al. (27). They found that at lower stretches (21% change in surface area = 10% linear), AT1 cells released 5 times more ATP than AT2 cells, but at higher distension of 30% area change (14% linear), the release was similar in both cell types. The cause of this discrepancy is not clear but could be due to several important methodological differences between the two studies. Patel et al. used continuous stretch for 10 min, and all experiments were conducted in the presence of 100 μM ARL-67156 to inhibit ATP degradation by ecto-ATPases and improve detection of released ATP. Moreover, ATP was evaluated at one time point after the stretch by sampling the cell media that represented bulk ATP concentration with no information on its temporal and spatial distribution. Therefore, it is difficult to compare their data with that obtained using recently improved technology for quantitative ATP measurements in which cellular ATP efflux was investigated in 2D in real time, and cells were stimulated by physiologically more relevant 1-s stretching in the absence of ecto-ATPase inhibitors. Results of this study are consistent with Isakson et al. (21, 22), who found that in heterocellular AT2/AT1 cultures, stimulation of single AT2 cells with micropipette touching generated intracellular Ca^{2+}

signals that propagated to neighboring cells via two routes, one involving gap junctions and the other via the release of ATP. The latter was inhibited by degradation of extracellular ATP with apyrase. Conversely, when single AT1 cells were mechanically stimulated, propagation of Ca^{2+} signals was inhibited only by gap junction blockers but not by apyrase, suggesting that only AT2 cells are capable of ATP release

It is interesting to note that AT2 cells, as primary releasers of ATP, also show high alkaline phosphatase activity, an ecto-ATPase and marker of AT2 cells. Coexpression of high ecto-ATPase activity at the ATP release sites may have functional significance, serving to terminate/diverge the ATP-mediated purinergic signaling.

Mechanism of ATP release. Failure of ATP channel inhibitors to significantly affect stretch-induced ATP release in AT2 cells indicates that the release mechanism does not involve pannexin/connexin channels (34). By contrast, significant reduction of the release in BAPTA-loaded cells is consistent with $[\text{Ca}_2^+]_i$ -dependent mechanisms, such as exocytosis of ATP-containing vesicles. It has been shown previously that ATP is stored in intracellular vesicles in A549 cells (1) and in lamellar bodies of AT2 cells (13). Moreover, exocytotic release of ATP has been directly demonstrated by total internal reflection fluorescence microscopy in A549 alveolar cells (1), making it a plausible mechanism also contributing to the release in primary AT2 cells. On the other hand, residual ~50% ATP release in BAPTA-loaded cells could represent a Ca^{2+} -independent nonexocytotic mechanism of the release. The nature of such pathway is currently under investigation.

Some differences in stretch-induced ATP release between A549 and AT2 cells can be noted. In A549 cells, ATP is released mostly from isolated cells with no evidence for coordinated release from adjacent cells (18). This contrasts with our recent study with rat primary AT2 cells, in which, using luminescence microscopy of higher spatial resolution compared with the WFOV approach used herein, we have found that the release occurs from clusters of cells producing dense clouds of released ATP for stronger stimuli (17). Such ability of AT2 cells to coordinately release ATP from cell clusters likely involves cell-to-cell communication and synchronization of the release by intracellular Ca^{2+} signals via gap junctions. This notion is consistent with stretch-

induced Ca^{2+} responses observed in clusters of adjacent cells in our Fura2 experiments and in the study of Isakson et al. (21, 22).

Conclusion. In summary, our results demonstrate that AT2 cells are major, perhaps sole, contributors to mechanosensitive ATP release in primary cultures of rat AT2/AT1 cells and strongly suggest that they may have a similar role in intact alveoli in vivo. Because the bulk of the alveolar distension during lung expansion occurs in AT1 cells (28), they may act as principal mechanosensors in which transient increase of $[\text{Ca}^{2+}]_i$ occurs during lung inflation, initiating a Ca^{2+} signal that is communicated via gap junction to adjacent AT1 and AT2 cells (2). Although both cell types have the capability to generate Ca^{2+} signals in response to stretch, the Ca^{2+} -regulated release of ATP occurs primarily from the secretory AT2 cells. By paracrine stimulation of purinergic receptors on neighboring cells, it contributes to $[\text{Ca}^{2+}]_i$ wave propagation and triggering purinergic signaling-regulated responses such as surfactant secretion. Further studies should aim to employ whole lung ATP imaging (15) combined with fluorescence cell imaging and molecular biology approaches to elucidate the role of ATP release and specific purinergic receptors in alveoli functions under physiological and pathological conditions. Better understanding of alveolar ATP release pathways and sources will facilitate translation to new therapies and optimization of ventilation strategies to improve survival of critically ill patients.

4.3.6 Acknowledgments

We give special thanks to members of E. Brochiero's laboratory (Anik Privé, Jasmine Chebli, Mélissa Aubin Vega, and Caroline Landry) for the isolation and primary culture of alveolar cells.

4.3.7 Grants

This work was supported by Canadian Institutes of Health Research Grants MOP64364 (to R. Grygorczyk) and PJT15340 (to E. Brochiero) and the Natural Sciences and Engineering Research Council of Canada Grant RGPIN-2016-04378 (to E. Brochiero).

4.3.8 Disclosures

No conflicts of interest, financial or otherwise, are declared by the authors.

4.3.9 Author Contributions

F.B. and R.G. conceived and designed research; J.J.T., D.A., and F.B. performed experiments; J.J.T., F.B., D.A., and R.G. analyzed data; J.J.T., F.B., D.A., E.B., and R.G. interpreted results of experiments; J.J.T., D.A., and F.B. prepared figures; J.J.T., E.B., and R.G. drafted manuscript; J.J.T., F.B., D.A., E.B., and R.G. edited and revised manuscript; J.J.T., F.B., D.A., E.B., and R.G. approved final version of manuscript.

4.3.10 References

1. **Akopova I, Tatur S, Grygorczyk M, Luchowski R, Gryczynski I, Gryczynski Z, Borejdo J, Grygorczyk R.** Imaging exocytosis of ATP-containing vesicles with TIRF microscopy in lung epithelial A549 cells. *Purinergic Signal* 8: 59–70, 2012. doi:10.1007/s11302-011-9259-2.
2. **Ashino Y, Ying X, Dobbs LG, Bhattacharya J.** $[Ca^{2+}]_i$ oscillations regulate type II cell exocytosis in the pulmonary alveolus. *Am J Physiol Lung Cell Mol Physiol* 279: L5–L13, 2000. doi:10.1152/ajplung.2000.279.1.L5.
3. **Boudreault F, Grygorczyk R.** Cell swelling-induced ATP release is tightly dependent on intracellular calcium elevations. *J Physiol* 561: 499–513, 2004. doi:10.1113/jphysiol.2004.072306.
4. **Bove PF, Grubb BR, Okada SF, Ribeiro CM, Rogers TD, Randell SH, O’Neal WK, Boucher RC.** Human alveolar type II cells secrete and absorb liquid in response to local nucleotide signaling. *J Biol Chem* 285: 34939–34949, 2010. doi:10.1074/jbc.M110.162933.
5. **Brochiero E, Dagenais A, Privé A, Berthiaume Y, Grygorczyk R.** Evidence of a functional CFTR Cl^- channel in adult alveolar epithelial cells. *Am J Physiol Lung Cell Mol Physiol* 287: L382–L392, 2004. doi:10.1152/ajplung.00320.2002.
6. **Burnstock G, Brouns I, Adriaensen D, Timmermans JP.** Purinergic signaling in the airways. *Pharmacol Rev* 64: 834–868, 2012. doi:10.1124/pr.111.005389.
7. **Castranova V, Rabovsky J, Tucker JH, Miles PR.** The alveolar type II epithelial cell: a multifunctional pneumocyte. *Toxicol Appl Pharmacol* 93: 472–483, 1988. doi:10.1016/0041-008X(88)90051-8.

8. **Cereda M, Emami K, Xin Y, Kadlecsek S, Kuzma NN, Mongkolwisetwara P, Profka H, Pickup S, Ishii M, Kavanagh BP, Deutschman CS, Rizi RR.** Imaging the interaction of atelectasis and overdistension in surfactant-depleted lungs. *Crit Care Med* 41: 527–535, 2013. doi:10.1097/CCM.0b013e31826ab1f2.
9. **Dobbs LG, Gonzalez R, Williams MC.** An improved method for isolating type II cells in high yield and purity. *Am Rev Respir Dis* 134: 141–145, 1986. doi:10.1164/arrd.1986.134.1.141.
10. **Douillet CD, Robinson WP III, Milano PM, Boucher RC, Rich PB.** Nucleotides induce IL-6 release from human airway epithelia via P2Y2 and p38 MAPK-dependent pathways. *Am J Physiol Lung Cell Mol Physiol* 291: L734–L746, 2006. doi:10.1152/ajplung.00389.2005.
11. **Edelson JD, Shannon JM, Mason RJ.** Alkaline phosphatase: a marker of alveolar type II cell differentiation. *Am Rev Respir Dis* 138: 1268–1275, 1988. doi:10.1164/ajrccm/138.5.1268.
12. **Edwards YS.** Stretch stimulation: its effects on alveolar type II cell function in the lung. *Comp Biochem Physiol A Mol Integr Physiol* 129: 245–260, 2001. doi:10.1016/S1095-6433(01)00321-X.
13. **Fois G, Winkelmann VE, Bareis L, Staudenmaier L, Hecht E, Ziller C, Ehinger K, Schymeinsky J, Kranz C, Frick M.** ATP is stored in lamellar bodies to activate vesicular P2X4 in an autocrine fashion upon exocytosis. *J Gen Physiol* 150: 277–291, 2018. doi:10.1085/jgp.201711870.
14. **Furuya K, Sokabe M, Grygorczyk R.** Real-time luminescence imaging of cellular ATP release. *Methods* 66: 330–344, 2014. doi:10.1016/j.ymeth.2013.08.007.
15. **Furuya K, Tan JJ, Boudreault F, Sokabe M, Berthiaume Y, Grygorczyk R.** Real-time imaging of inflation-induced ATP release in the ex vivo rat lung. *Am J Physiol Lung Cell Mol Physiol* 311: L956–L969, 2016. doi:10.1152/ajplung.00425.2015.
16. **Girault A, Chebli J, Privé A, Trinh NT, Maillé E, Grygorczyk R, Brochiero E.** Complementary roles of KCa3.1 channels and β 1-integrin during alveolar epithelial repair. *Respir Res* 16: 100, 2015. doi:10.1186/s12931-015-0263-x.
17. **Grygorczyk R, Boudreault F, Tan JJ, Ponomarchuk O, Sokabe M, Furuya K.** Mechanosensitive ATP release in the lungs: new insights from real-time luminescence imaging studies. *Curr Top Membr* 83: 45–76, 2019. doi:10.1016/bs.ctm.2019.02.001.

18. **Grygorczyk R, Furuya K, Sokabe M.** Imaging and characterization of stretch-induced ATP release from alveolar A549 cells. *J Physiol* 591: 1195–1215, 2013. doi:10.1113/jphysiol.2012.244145.
19. **Grygorczyk R, Hanrahan JW.** CFTR-independent ATP release from epithelial cells triggered by mechanical stimuli. *Am J Physiol* 272: C1058–C1066, 1997. doi:10.1152/ajpcell.1997.272.3.C1058.
20. **Hasan D, Blankman P, Nieman GF.** Purinergic signalling links mechanical breath profile and alveolar mechanics with the pro-inflammatory innate immune response causing ventilation-induced lung injury. *Purinergic Signal* 13: 363–386, 2017. doi:10.1007/s11302-017-9564-5.
21. **Isakson BE, Evans WH, Boitano S.** Intercellular Ca²⁺ signaling in alveolar epithelial cells through gap junctions and by extracellular ATP. *Am J Physiol Lung Cell Mol Physiol* 280: L221–L228, 2001. doi:10.1152/ajplung.2001.280.2.L221.
22. **Isakson BE, Seedorf GJ, Lubman RL, Evans WH, Boitano S.** Cell-cell communication in heterocellular cultures of alveolar epithelial cells. *Am J Respir Cell Mol Biol* 29: 552–561, 2003. doi:10.1165/rcmb.2002-0281OC.
23. **Lazarowski ER, Boucher RC.** Purinergic receptors in airway epithelia. *Curr Opin Pharmacol* 9: 262–267, 2009. doi:10.1016/j.coph.2009.02.004.
24. **Lazarowski ER, Homolya L, Boucher RC, Harden TK.** Direct demonstration of mechanically induced release of cellular UTP and its implication for uridine nucleotide receptor activation. *J Biol Chem* 272: 24348–24354, 1997. doi:10.1074/jbc.272.39.24348.
25. **Lazarowski ER, Sesma JI, Seminario-Vidal L, Kreda SM.** Molecular mechanisms of purine and pyrimidine nucleotide release. *Adv Pharmacol* 61: 221–261, 2011. doi:10.1016/B978-0-12-385526-8.00008-4.
26. **Olajuyin AM, Zhang X, Ji HL.** Alveolar type 2 progenitor cells for lung injury repair. *Cell Death Discov* 5: 63, 2019. doi:10.1038/s41420-019-0147-9.
27. **Patel AS, Reigada D, Mitchell CH, Bates SR, Margulies SS, Koval M.** Paracrine stimulation of surfactant secretion by extracellular ATP in response to mechanical deformation. *Am J Physiol Lung Cell Mol Physiol* 289: L489–L496, 2005. doi:10.1152/ajplung.00074.2005.

28. **Perlman CE, Bhattacharya J.** Alveolar expansion imaged by optical sectioning microscopy. *J Appl Physiol* (1985) 103: 1037–1044, 2007. doi:10.1152/jappphysiol.00160.2007.
29. **Perlman CE, Lederer DJ, Bhattacharya J.** Micromechanics of alveolar edema. *Am J Respir Cell Mol Biol* 44: 34–39, 2011. doi:10.1165/rcmb.2009-0005OC.
30. **Ponomarchuk O, Boudreault F, Orlov SN, Grygorczyk R.** Calcium is not required for triggering volume restoration in hypotonically challenged A549 epithelial cells. *Pflugers Arch* 468: 2075–2085, 2016. doi:10.1007/s00424-016-1896-4.
31. **Praetorius HA, Leipziger J.** ATP release from non-excitabile cells. *Purinergic Signal* 5: 433–446, 2009. doi:10.1007/s11302-009-9146-2.
32. **Ramsingh R, Grygorczyk A, Solecki A, Cherkaoui LS, Berthiaume Y, Grygorczyk R.** Cell deformation at the air-liquid interface induces Ca²⁺-dependent ATP release from lung epithelial cells. *Am J Physiol Lung Cell Mol Physiol* 300: L587–L595, 2011. doi:10.1152/ajplung.00345.2010.
33. **Rannels DE.** Role of physical forces in compensatory growth of the lung. *Am J Physiol Lung Cell Mol Physiol* 257: L179–L189, 1989. doi:10.1152/ajplung.1989.257.4.L179.
34. **Ransford GA, Fregien N, Qiu F, Dahl G, Conner GE, Salathe M.** Pannexin 1 contributes to ATP release in airway epithelia. *Am J Respir Cell Mol Biol* 41: 525–534, 2009. doi:10.1165/rcmb.2008-0367OC.
35. **Rich PB, Douillet CD, Mahler SA, Husain SA, Boucher RC.** Adenosine triphosphate is released during injurious mechanical ventilation and contributes to lung edema. *J Trauma* 55: 290–297, 2003. doi:10.1097/01.TA.0000078882.11919.AF.
36. **Sanchez-Esteban J, Cicchiello LA, Wang Y, Tsai SW, Williams LK, Torday JS, Rubin LP.** Mechanical stretch promotes alveolar epithelial type II cell differentiation. *J Appl Physiol* (1985) 91: 589–595, 2001. doi:10.1152/jappl.2001.91.2.589.
37. **Schmid A, Clunes LA, Salathe M, Verdugo P, Dietl P, Davis CW, Tarran R.** Nucleotide-mediated airway clearance. *Subcell Biochem* 55: 95–138, 2011. doi:10.1007/978-94-007-1217-1_5.
38. **Sheth S, Brito R, Mukherjea D, Rybak LP, Ramkumar V.** Adenosine receptors: expression, function and regulation. *Int J Mol Sci* 15: 2024–2052, 2014. doi:10.3390/ijms15022024.

39. **Tan JJ, Ponomarchuk O, Grygorczyk R, Boudreault F.** Wide field of view quantitative imaging of cellular ATP release. *Am J Physiol Cell Physiol* 317: C566–C575, 2019. doi:10.1152/ajpcell.00096.2019.
40. **Tatur S, Groulx N, Orlov SN, Grygorczyk R.** Ca²⁺-dependent ATP release from A549 cells involves synergistic autocrine stimulation by coreleased uridine nucleotides. *J Physiol* 584: 419–435, 2007. doi:10.1113/jphysiol.2007.133314.
41. **Tatur S, Kreda S, Lazarowski E, Grygorczyk R.** Calcium-dependent release of adenosine and uridine nucleotides from A549 cells. *Purinergic Signal* 4: 139–146, 2008. doi:10.1007/s11302-007-9059-x.
42. **Trinh NT, Privé A, Kheir L, Bourret JC, Hijazi T, Amraei MG, Noël J, Brochiero E.** Involvement of K_{ATP} and KvLQT1 K⁺ channels in EGF-stimulated alveolar epithelial cell repair processes. *Am J Physiol Lung Cell Mol Physiol* 293: L870–L882, 2007. doi:10.1152/ajplung.00362.2006.
43. **Uhlig U, Uhlig S.** Ventilation-induced lung injury. *Compr Physiol* 1: 635–661, 2011. doi:10.1002/cphy.c100004.
44. **Verbrugge SJ, de Jong JW, Keijzer E, Vazquez de Anda G, Lachmann B.** Purine in bronchoalveolar lavage fluid as a marker of ventilation-induced lung injury. *Crit Care Med* 27: 779–783, 1999. doi:10.1097/00003246-199904000-00035.
45. **Yegutkin GG.** Nucleotide- and nucleoside-converting ectoenzymes: Important modulators of purinergic signalling cascade. *Biochim Biophys Acta* 1783: 673–694, 2008. doi:10.1016/j.bbamcr.2008.01.024.

4.3.11 Figures and Captions

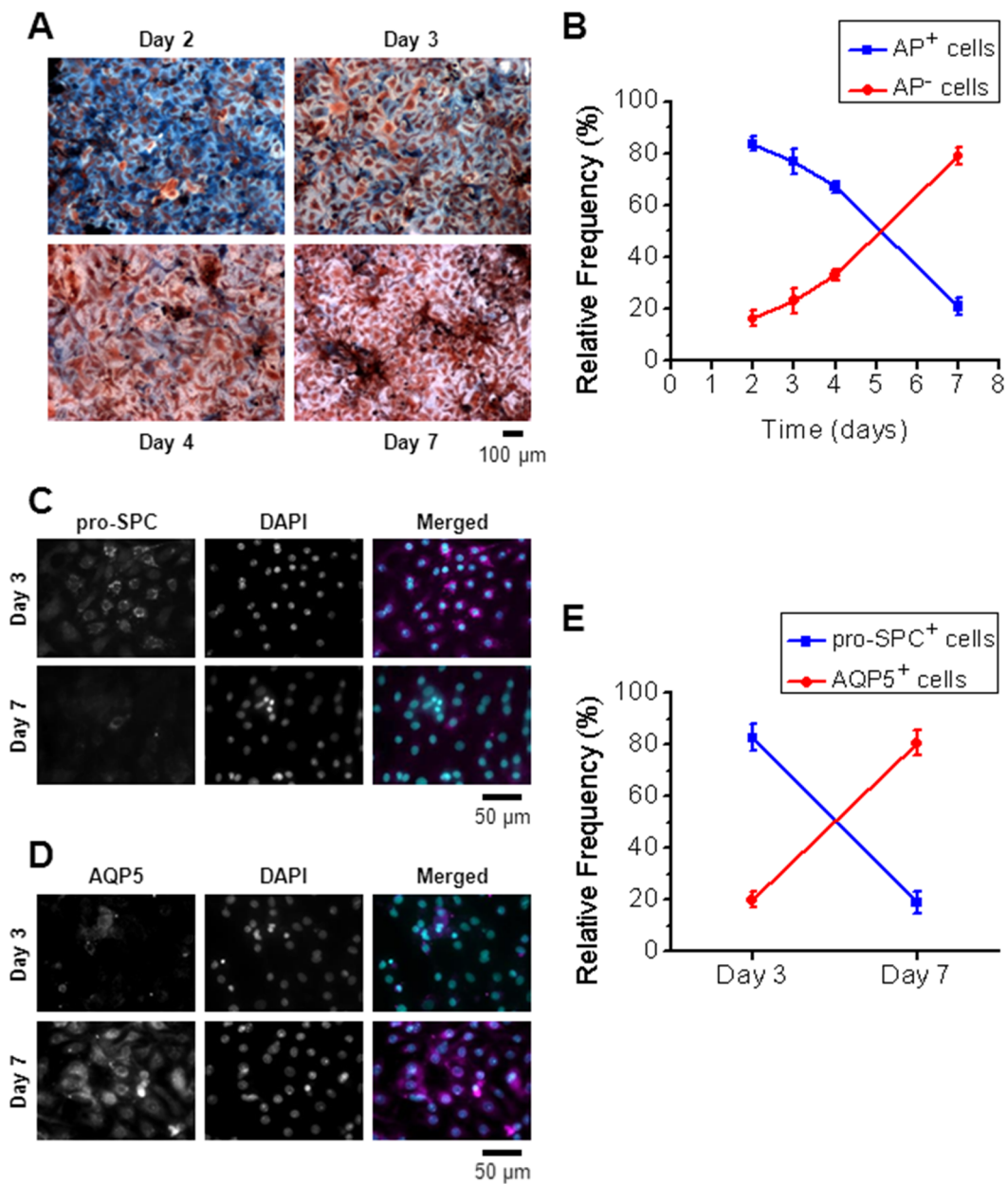


Figure 1

Figure 16. – Figure 1 of Article #2

Fig. 1. Phenotypic changes of rat primary alveolar epithelial cells in culture. *A*: changes in alkaline phosphatase (AP) staining of alveolar type 2 (AT2) and alveolar type 1 (AT1) cell cultures grown on flexible silicone stretch chambers as a function of time (days 2–7). Blue staining indicates AP activity, which is characteristic of AT2 cells, while those counterstained in red only correspond to AT1 cells. Images are representative of three independent cell preparations. *B*: relative number (in %) of AT2 and AT1 cells (blue and red lines, respectively) as a function of time in culture. Data are mean \pm SD of three independent experiments. For analysis, cells with AP activity (AP⁺, blue/red) and without AP activity (AP⁻, red only), corresponding to AT2 or AT1-like phenotypes, respectively, were manually counted. Note a time-dependent gradual loss of AT2 phenotype and increase of AT1-like phenotype. The pictures were taken with $\times 20$ phase-contrast objective and the Eclipse TE200 (Nikon) microscope equipped with an AxioCam ICc 1 (Zeiss) camera. *C* and *D*: immunostaining of 3- and 7-day-old alveolar epithelial cell cultures with anti-pro-surfactant protein C (pro-SPC) (marker of AT2 cells) or anti-aquaporin (AQP)-5 (marker of AT1 cells) and secondary antibody conjugated to Alexa Fluor 633 (magenta on merged images). Nuclei were then counterstained with DAPI (cyan on merged images). Images are representative of eight independent experiments from four different cell preparations (four animals). *E*: quantification of the number of pro-SPC (pro-SPC⁺, blue line) and AQP5 (AQP5⁺, red line) positive cells in 3- and 7-day-old alveolar epithelial cell cultures, presented as percentage of total cells (DAPI staining); $n = 8$.

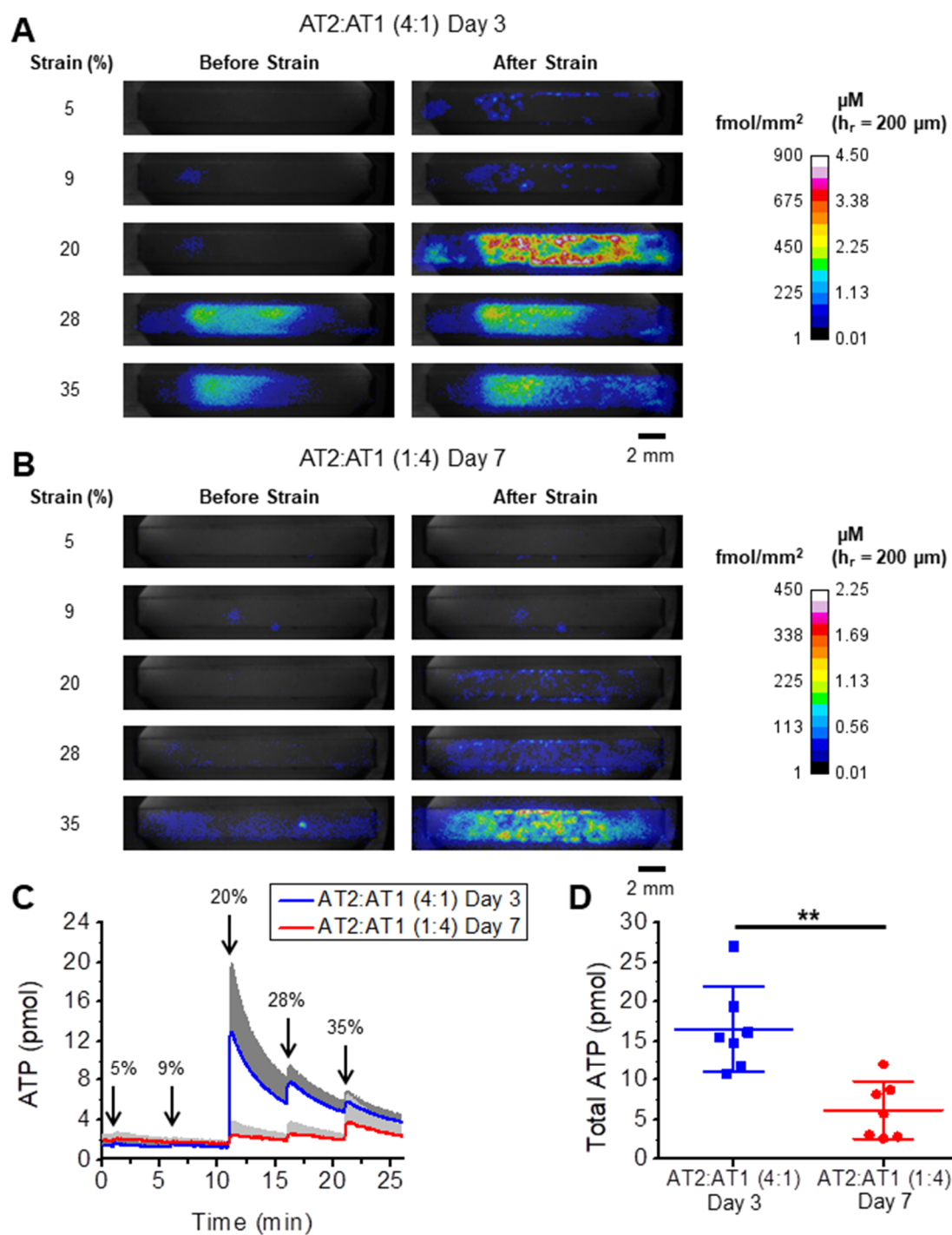


Figure 2

Figure 17. – Figure 2 of Article #2

Fig. 2. Quantification of stretch-induced ATP release in alveolar type 2 (AT2) and alveolar type 1 (AT1) cell cultures. *A*: example images of two-dimensional (2D) ATP density map (fmol/mm²; see pseudocolor scale) in 3-day-old cell culture containing predominantly AT2 cells (AT2:AT1 ratio of 4:1) at the peak of response to a sequence of 1-s stretches of 5–35% applied at 5-min intervals. *Left* and *right* columns show ATP density map before and after stretch stimulus, respectively. Residual ATP released by preceding stretches is clearly visible on images in the Before Strain column, particularly after the 20% and 28% stretch. Estimated ATP concentrations (in μM) are also indicated on the pseudocolor scale bar that represents the average value for the 200- μm -high reaction layer (h_r) of fluid covering the cells (see METHODS). *B*: example images of 2D ATP density map in 7-day-old cell culture containing predominantly AT1 cells (AT2:AT1 ratio of 1:4) at the peak of response to a sequence of stretches described in *A*. Note different pseudocolor scale and significantly lower ATP release responses compared with those shown in *A*. *C*: the graph shows a full time course of ATP released from cells in the entire chamber in response to a sequence of five 1-s stretches of increasing amplitude (see labels on each trace) as described in *A*. The blue and red traces represent mean \pm SD (gray shadow, $n = 7$) for 3- and 7-day-old cell cultures, respectively. For clarity only positive direction of SD is shown. *D*: cumulative ATP released in response to a sequence of stretches (5–35%) for 3- and 7-day-old cell cultures in the experiment shown in *C*. The quantity of secreted ATP for each stretch pulse is calculated by subtracting the prestretch extracellular ATP (ATP_o) level from the stretch-generated peak value (see METHODS). Data are shown as a scatterplot with mean \pm SD for seven independent experiments. Student's *t* test shows a statistical difference between both groups ($P < 0.05$). The 3-day-old cultures (AT2:AT1 ratio of 4:1) release almost three times more ATP than 7-day-old cultures (AT2:AT1 ratio of 1:4). **** $P < 0.01$.**

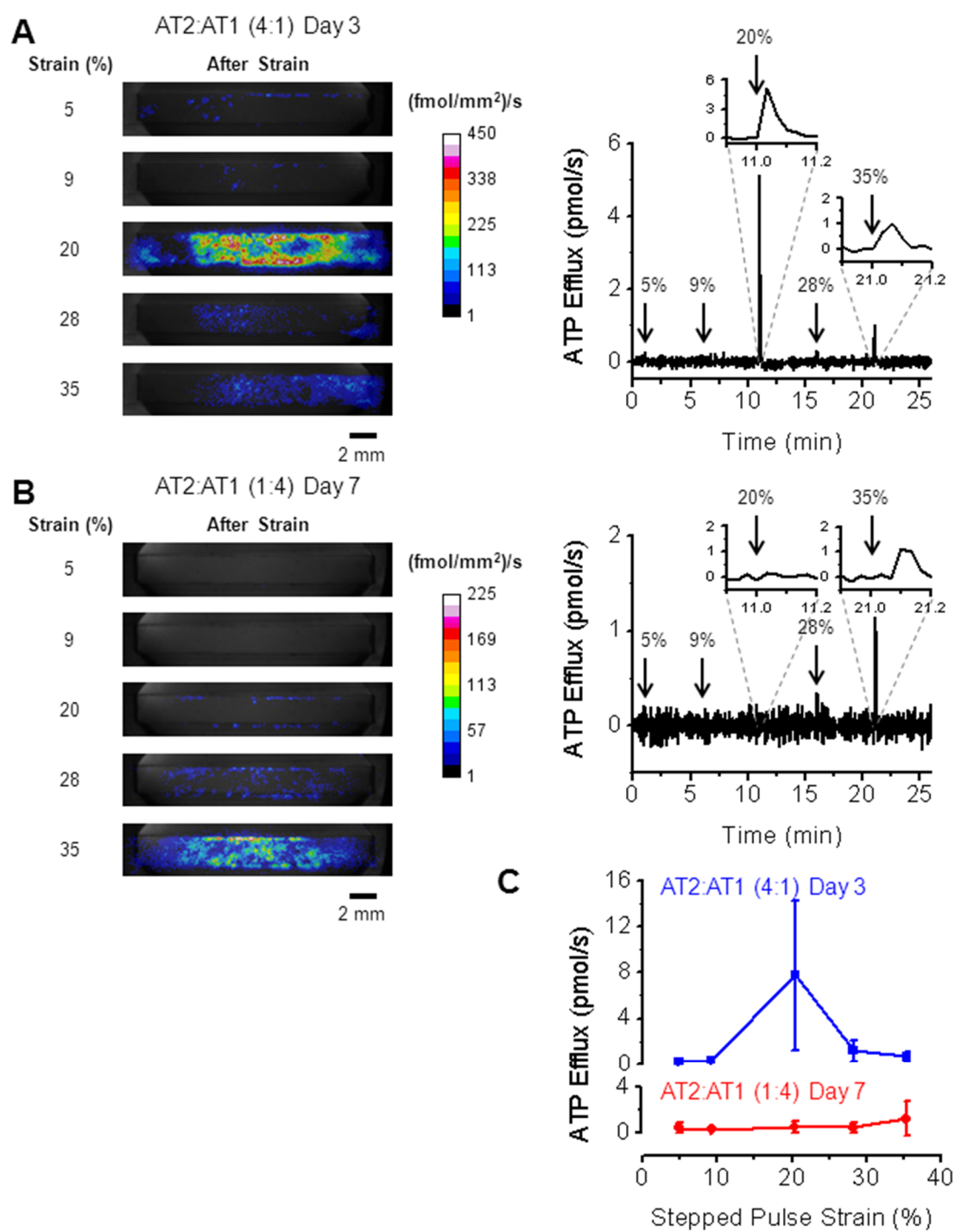


Figure 3

Figure 18. – Figure 3 of Article #2

Fig. 3. Quantification of the rate of ATP release. *A*: examples of two-dimensional (2D) maps of ATP release rate (in fmol/mm²/s) at the peak response in 3-day-old cell culture induced by a sequence of 1-s stretches of 5–35% applied at 5-min intervals in an experiment similar to that shown in Fig. 2A. The highest rate of ATP release was observed at 20% stretch. The graph on the *right* shows the time course of ATP release rate averaged for the entire area of the stretch chamber. Note very short duration (<5–10 s) of ATP release following stretch stimulation. The *insets* show spikes of ATP efflux at expanded time scale during 20% stretch (at 11 min) and 35% stretch (at 21 min). *B*: example of 2D maps of ATP release rate (fmol/mm²/s) at the peak response in 7-day-old cells induced by a sequence of stretches in an experiment similar to that shown in *A*. Only at the highest stretch of 35% was significant ATP efflux observed. The graph on the *right* shows the time course of ATP efflux averaged for the entire area of the stretch chamber. The *insets* show the time course of ATP efflux at expanded time scale during 20% stretch (at 11 min) and 35% stretch (at 21 min). *C*: comparison of the peak of ATP efflux (rate of ATP) release for stepped pulse stretches of increasing amplitude in 3- and 7-day-old cell cultures (blue and red traces, respectively). Data are mean ± SD of seven independent experiments. AT1, alveolar type 1; AT2, alveolar type 2.

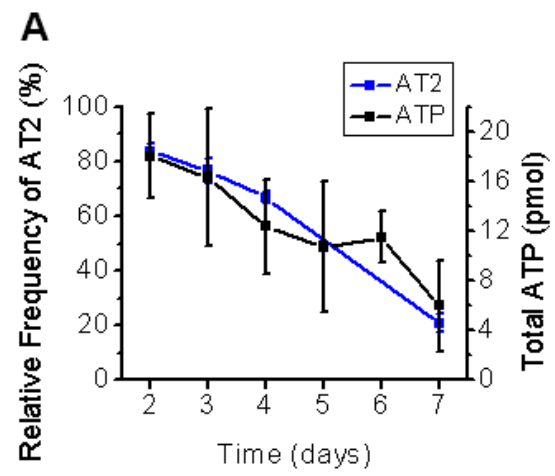


Figure 4

Figure 19. – Figure 4 of Article #2

Fig. 4. Stretch-induced ATP release closely correlates with alveolar type 2 (AT2) cell content in AT2 and alveolar type 1 (AT1) cell cultures. ATP release (pmol, black line, scale on the *right*) in alveolar cells decreases with the time in culture (from day 2 to 7). Total cumulative ATP release after sequence of stretches was calculated as described in Fig. 2D. Data are mean \pm SD of $n = 3-7$ independent experiments. The graph is superimposed on AT2 cell content data of Fig. 1B (blue line) to directly compare with relative AT2 cell content (in %, *left* scale). Note a close correlation between the decreasing ATP release and number of remaining AT2 cells. Statistical analysis (Pearson's product-moment correlation) reveals a strong correlation between ATP release and AT2 cell number (correlation coefficient $r = 0.94$, $P = 0.0053$).

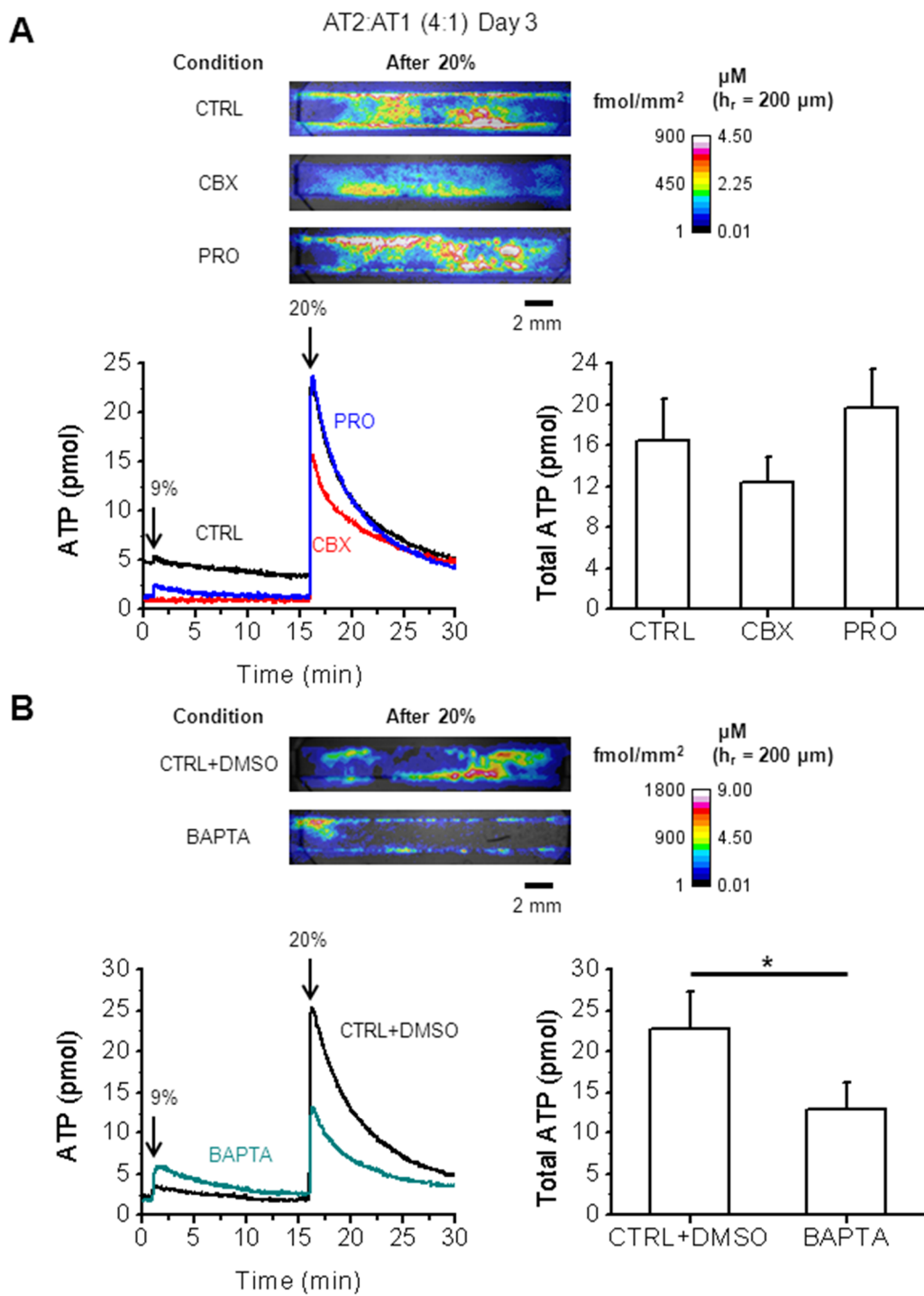


Figure 5

Figure 20. – Figure 5 of Article #2

Fig. 5. Effect of ATP release modulators. *A*: time course of ATP release in response to two stretches (9% and 20%) in 3-day-old cultures of control alveolar type 2 (AT2) cells (CTRL, representative of $n = 3$), and cells treated with 100 μ M carbenoxolone (CBX) or 2.5 mM probenecid (PRO, $n = 3$). ATP imaging and stretch stimulations were performed with inhibitors included in the LL + DMEM covering the cells. Images above show representative ATP density maps (fmol/mm²; see pseudocolor scale) at the peak response to 20% stretch for the three conditions (CTRL, CBX and PRO). Bar graph on the right shows the corresponding total quantity of secreted ATP (mean \pm SD, $n = 3$) for each condition. There was no significant difference between all three groups [CTRL (16.4 \pm 4.1 pmol), CBX (12.3 \pm 2.6 pmol), and PRO (19.7 \pm 3.6 pmol), $P = 0.11$]. *B*: effect of Ca²⁺ chelator BAPTA on ATP release in 3-day-old cultures of AT2 cells. Time course of ATP release (pmol) in response to two stretches (9% and 20%) in control AT2 cells treated with vehicle (DMSO, 30 min) and in cells loaded with 25 μ M BAPTA-AM for 30 min (representative of $n = 3$). Prior to ATP imaging, cells in the stretch chamber were washed with PBS solution and bathed in DMEM containing isotonic LL. Images above show examples of ATP density maps (fmol/mm²; see pseudocolor scale) at the peak response to 20% stretch for the two conditions (CTRL and BAPTA). Estimated ATP concentration (in μ M) is also indicated on the pseudocolor scale bar. Bar graph on the right shows total ATP released (mean \pm SD) during the entire experiment. Cells loaded with BAPTA showed statistically significant reduction of ATP release (12.9 \pm 3.3 pmol) compared with the controls (22.7 \pm 4.7 pmol), $*P < 0.05$.

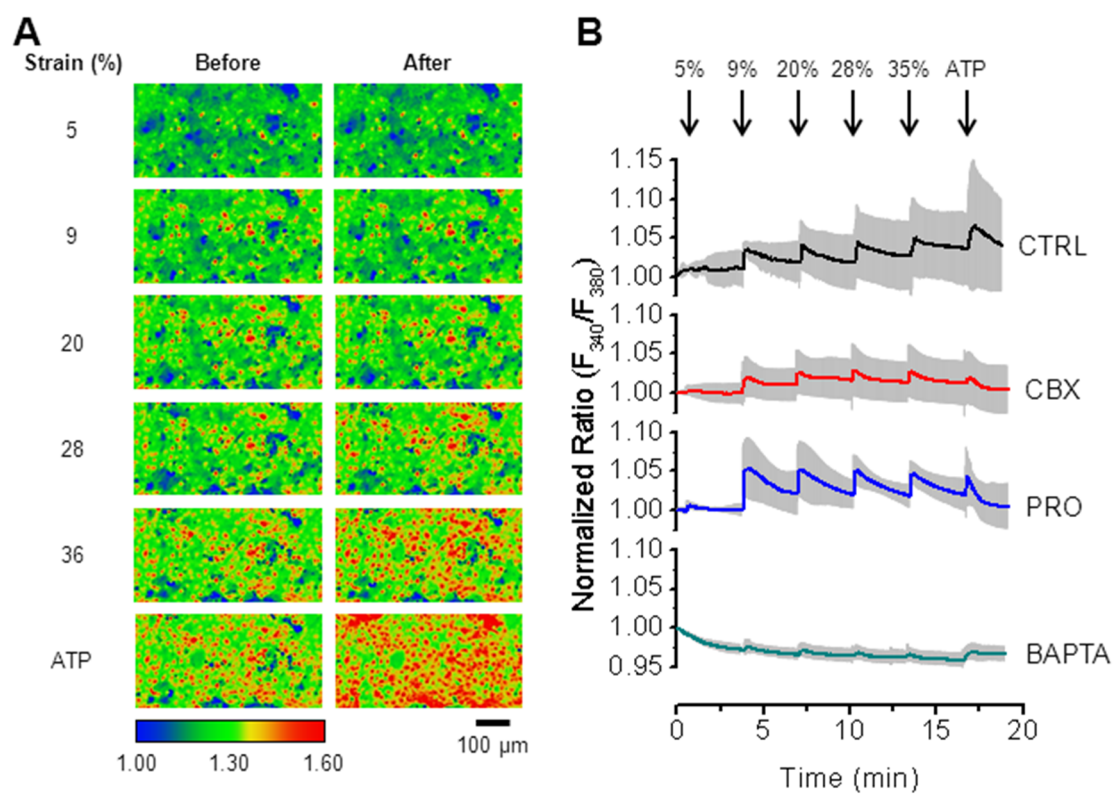


Figure 6

Figure 21. – Figure 6 of Article #2

Fig. 6. Stretch-induced intracellular Ca^{2+} responses in alveolar type 2 (AT2) cells. *A*: examples of a typical stretch-induced $[\text{Ca}^{2+}]_i$ responses in control (CTRL) 3-day-old AT2 cell cultures. *Left* and *right* columns display example images of Fura2 fluorescence ratio (F_{340}/F_{380}) in cells before and after stretch, respectively. Pseudocolor scale bar was normalized to initial F_{340}/F_{380} baseline value. Color turning from blue or green to yellow or red indicates increase in $[\text{Ca}^{2+}]_i$. Note the increased number of responding cells for stronger stretches. ATP (13 μM final concentration) was added at the end of each experiment and served as a positive control. Images are representative of four independent experiments. *B*: time course of $[\text{Ca}^{2+}]_i$ responses evoked by a sequence of five stretches of increasing amplitude (5–35%) given at 5-min intervals (arrows) in control cells and cells treated with carbenoxolone (CBX), probenecid (PRO), or BAPTA. Traces represent mean \pm SD from four experiments. Note that CBX inhibited and PRO stimulated stretch-induced $[\text{Ca}^{2+}]_i$ responses in AT2 cells, while BAPTA reduced the baseline level of $[\text{Ca}^{2+}]_i$ and almost completely abolished the responses to stretch stimulation.

Chapter 5 – Article #3

5.1 Preamble

In Article #2, we demonstrated that alveolar cells secrete more ATP in response to stretch at day 3 than at day 7 and that this mechanism does not involve ATP channels but rather is $[Ca^{2+}]_i$ -dependent, which may be consistent with regulated vesicular exocytosis (140).

Changes in phenotype in rat primary AT2 cells over time were also observed by Tschumperlin *et al.* (141). To evaluate cell viability in response to stretch, they employed a live/dead assay, where calcein-AM is used to label live or healthy cells and ethidium homodimer-1 (EthD-1) to label dead cells (or at least as an indicator of membrane rupture). They noticed that following a stretch, younger cell cultures (day 1) have a higher uptake of EthD-1 than older ones (day 5) (141). This difference in uptake of EthD-1 may suggest that cells are much more vulnerable to deformation within the days after seeding, and they become less prone to such mechanical forces over time (141).

In another study, Skotak *et al.* also used this assay to evaluate the viability of neuroblastoma SH-SH5Y cells in response to stretch (142). Following a strain, an uptake of EthD-1 was also observed, but most cells were labelled positive for both calcein and EthD-1, which indicates that they remain viable but with a compromised (injured) membrane (142). Moreover, at a fixed strain (50%), the number of injured cells did not differ for various strain rates (142). While these cells sustained injury from a strain of 42% or 50%, the cell membrane recovers after two hours (142). Hence, cell stretch may affect the cell membrane's integrity/permeability without necessarily causing cell death.

In light of this information, we hypothesized that transient ruptures in the membrane may constitute an alternate physiological pathway for stretch-induced ATP release. Because A549 cells responded to stretch in a viscoelastic manner, ATP release in alveolar epithelial cells could occur through membrane ruptures, whose formation would be determined by membrane

viscoelasticity (116). Therefore, we aimed to explore the influence of the plasma membrane's viscoelastic properties on stretch-induced ATP release.

5.2 Article #3

Title: Cellular ATP efflux through transient membrane rupture formed by mechanical stretch in alveolar epithelial cells

Authors: Ju Jing Tan, Francis Boudreault, Ryszard Grygorczyk

Status: In preparation

5.2.1 Contribution

Under the supervision of Dr. Francis Boudreault and Dr. Ryszard Grygorczyk, I participated in the experimental design and in drafting the manuscript. I conducted the experiments presented in this article (Figures 1, 2 and 3). I also analyzed the data and prepared the final figures for the manuscript.

5.3 Cellular ATP efflux through transient membrane rupture formed by mechanical stretch in alveolar epithelial cells

Ju Jing Tan,^{1,2} Francis Boudreault,¹ and Ryszard Grygorczyk^{1,2}

¹Centre de Recherche du Centre Hospitalier de l'Université de Montréal, Montreal, Quebec, Canada; and ²Department of Medicine, Université de Montréal, Montreal, Quebec, Canada

Address for correspondence:

R. Grygorczyk

Centre de recherche du CHUM

900, rue Saint-Denis, Pavillon R

Montréal, QC H2X 0A9

Canada

(e-mail: ryszard.grygorczyk@umontreal.ca)

5.3.1 Abstract

High levels of extracellular ATP were reported in injurious mechanical ventilation (MV). ATP and its metabolites were shown to be involved in the pathogenesis of ventilator-induced lung injury (VILI). Although ATP-conducting channels and exocytosis are frequently proposed mechanisms for stretch-induced ATP release, it could also involve transient membrane injury or ruptures, whose formation would be determined by membrane viscoelastic properties. To explore such alternate mechanisms, we performed quantitative real-time ATP imaging using bioluminescence microscopy of rat primary alveolar cells cultured on silicon substrate. When cells were subjected to a 30% strain of 1 s in the presence of propidium iodide (PI), we found that cells releasing ATP also displayed PI staining, indicating a transient change of the cell membrane permeability. To establish if ATP release depends on the cell membrane viscoelasticity, cells were subjected to a 30% strain at different rates with a hold time of 60 s. We found that ATP efflux showed a quasi-sigmoidal response curve, doubling for a five-fold increase in strain rate from 0.2 %/s to 1 %/s, while it increased 25-times for the 1–5%/s range. Furthermore, when cells were stretched at 30% strain with a fixed rate of 25 %/s and a hold time of 60 s or 1 s, the longer hold time produced longer half-life of ATP release relaxation. Our results are consistent with the view that stretch induces transient ruptures of viscoelastic plasma membrane, enabling ATP release and uptake of PI during strain. Subsequent membrane repair processes may allow cells to survive without cell lysis.

Keywords: lung ATP release; mechanoporation; mechanosensitivity; purinergic signaling; membrane viscoelasticity

5.3.2 Introduction

Patients with acute respiratory distress syndrome (ARDS) are often managed with mechanical ventilation (MV) in order to maintain adequate gas exchange (1). Although life-saving, MV may at times worsen lung injury, despite preventive rescue measures, due to alveolar overdistension and inhomogeneous ventilation (2). These mechanical insults lead to atelectrauma and barotrauma, exacerbating pulmonary edema and inflammation, collectively referred to as ventilator-induced lung injury (VILI) (2). Rich *et al.* previously observed in rats that there is a noticeable level of adenosine triphosphate (ATP) in bronchoalveolar lavage fluid, which became significantly higher under VILI-inducing conditions (3).

While commonly associated with its energy-providing role within the cell, ATP, once out of the cell, can bind to specific cell-surface purinergic receptors: ATP-gated ion channels P2X and metabotropic P2Y receptors (4). In presence of ecto-nucleotidases, extracellular ATP is degraded into adenosine, which binds to G protein-coupled P1 receptors (4, 5). Activation of purinergic receptors plays an important role in modulating various alveolar functions, and adenosine has been reported to display beneficial properties, which may help to resolve pulmonary edema and inflammation (6-8).

Cell stretch is an important mechanical stimulus, which provokes release of intracellular ATP into the alveolar space (9). Even though ATP-permeable channels and exocytosis are frequently proposed as the candidate mechanisms for mechanosensitive ATP release, the exact pathway for stretch-induced ATP release in the alveolus remains to be determined. We previously demonstrated that inhibitors for these pathways did not diminish stretch-induced ATP secretion in rat alveolar cells (10, 11). Therefore, an alternative option needs to be considered.

Tschumperlin *et al.* evaluated cell viability in response to stretch using a live/dead assay in rat primary alveolar cells (12). They noticed that stretch promotes uptake of cell-impermeant viability indicator ethidium homodimer-1 (EthD-1), a process likely dependent on the cell's vulnerability to deformation (12). Similarly, Skotak *et al.* also illustrated that neuroblastoma SH-SH5Y cells may be labeled with both cell-permeant fluorescent probe calcein and EthD-1 after

stretch, which hints a possible stretch-induced perturbations in the cell membrane that is transient (13). Trepap *et al.* also demonstrated that the cell membrane of human alveolar epithelial A549 cells display viscoelastic properties in response to stretch (14). Therefore, if ATP release occurred through transient breaks in the plasma membrane, this response should be determined by membrane viscoelasticity. Taken together, the present study aims to explore the role of viscoelastic properties of the plasma membrane in forming a transient pathway for stretch-induced ATP release in alveolar cells.

5.3.3 Material and Methods

Cell culture. Alveolar cells were freshly isolated from lungs of adult male Sprague-Dawley rats (Charles River Laboratories, Senneville, QC, Canada), as previously described in Tan *et al.* (11). In brief, after lung harvesting, blood was removed by perfusion. The minced pieces of the lungs were then filtered and purified to isolate alveolar cells, yielding a mixture of roughly 85% alveolar type 2 (AT2) cells and 15% alveolar type 1 (AT1) cells. Alveolar cells were seeded onto a 2 mm-wide groove of a flexible silicone chamber (see below in Stretch), covered in MEM culture medium (Thermo Fisher Scientific Ltd., Saint-Laurent, QC, Canada), supplemented with 10% fetal bovine serum (FBS, Wisent, Saint-Bruno, QC, Canada) and Septra (3 µg/mL trimethoprim + 17 µg/mL sulfamethoxazole, Glaxo Smith Kline Biologicals, Laval, QC, Canada). Rat primary alveolar cells culture were incubated at 37°C and 5% CO₂ up to 7 days, and the culture medium was replaced with Septra-free MEM-FBS medium every two days. The protocols regarding the use of animals were approved by the Comité Institutionnel de protection des animaux of the Centre de recherche du Centre hospitalier de l'Université de Montréal in conformity with the Canadian Council of Animal Care guidelines.

Stretch. Flexible silicon chambers were made with Sylgard® 184 silicone elastomer base and curing agent (Dow Corning Corporation, Midland, MI) as described in (9, 11, 15). The mixture containing both components was poured into a mould and was baked for 1 hour at 60°C. The stretch chamber has a 2 × 18 mm stretchable groove, which was coated with 20% collagen type 1 from rat tail diluted in distilled H₂O (Sigma-Aldrich Corporation, St. Louis, MO) to promote cell adhesion. During the experiment, 7-day-old cells were bathed in 100 µL Gibco's

phenol red-free DMEM (Invitrogen Canada Inc., Burlington, ON) with 100 μ L isotonicly-adjusted luciferin-luciferase (LL) (Sigma-Aldrich Canada Co., Oakville, ON) containing 1 μ g/mL of cell membrane-impermeant propidium iodide (PI, Sigma-Aldrich (not sure where)).

The stretch chamber was attached to the STREX NS-600W Cell Stretching System STREX, Cell Stretching System STB-150-W, B-Bridge International, Inc., Cupertino, CA), which was mounted over our custom-designed wide field of view (WFOV) ATP imaging system, as shown in (15). The rate of horizontal stretch was controlled by a step-motor device at different rates. All experiments applied a 30% stretch, which was maintained for 1 or 60 s. The strain rate to achieve 30% magnitude and to return back to 0% was 0.2%/s, 1%/s, 5%/s or 25%/s.

Real-time wide-field-of-view ATP Imaging. ATP imaging technique and calibration have been detailed in Tan *et al.* (15). In short, extracellular ATP was detected through the light-emitting reaction with LL. The light signals were captured by a highly sensitive electron multiplying charge-coupled device (EMCCD) camera Evolve 512 (Photometrics, Tucson, AZ) via AxioVision software (AxioVs40 V 4.8.2.0; Carl Zeiss MicroImaging, Jena, Germany). Two-dimensional images were acquired with an on-chip camera 2x2 binning, at a frequency of 0.5 Hz and an exposure time of 1 s. Offline analysis of images were performed with ImageJ open-source software.

Epifluorescence Microscopy. Pre- and post-stretch images of the PI dye were taken through an inverted microscope (Axio Observer Z1, Zeiss) equipped with a charge-coupled device (CCD) camera (CoolSNAP EZ, Photometrics). Emission wavelength of 470 nm was via a Colibri light-emitting diode (LED) light source (Zeiss). 80 images (512 \times 512 pixels, magnification 5 \times) were taken and stitched together to show the entire 2 \times 18 mm groove with ImageJ.

Statistics. Results are expressed as mean \pm SD. Comparison of two averages was done with appropriate Student *t* test following an F test for homoscedasticity evaluation. The differences between two groups were considered significant with $P < 0.05$. Statistical analyses were performed with R (version 3.6.0).

5.3.4 Results

Stretch-induced ATP release is co-localized with PI uptake in AT2 cell cultures. **Fig. 1A** shows the stitching of 80 bright-field images (512×512 pixels, magnification $5\times$), which reveals the entire stretch chamber's flexible groove (2×18 mm) covered by cells. Similarly, **Fig. 1B** and **1C** display the stitched images of PI-positive cells before and after a 30% strain application, respectively. In **Fig 1C**, we noticed a remarkable uptake of PI by the cells throughout the groove. During strain, we captured images of ATP-dependent LL bioluminescence through wide-field-of-view (WFOV) ATP imaging. **Fig. 1D** shows the peak rate of ATP release induced by a 1-s strain of 30% (see pseudocolor scale). **Fig. 1E** depicts an example region of interest (ROI, square) from Fig. 1A to 1D to highlight one of many co-localizations of ATP release and PI uptake after stretch. Another ROI (dotted circle) shows similar tendencies. Do take notice that areas with no PI uptake tightly correspond to those presenting little or no ATP release despite presence of cells in these regions. Overall, these images demonstrate that a strain of 30% induced both ATP release and PI uptake in these cell cultures. These results suggest that stretch alters the permeability of the cell membrane, which may cause transient membrane ruptures, big enough for ATP and PI to pass through during the stretch.

The role of the viscoelastic membrane properties in stretch-induced ATP release. First, we looked at the effect of strain rate on ATP efflux. We tested here 4 different strain rates, with each increasing by 5-fold of the other: 0.2 %/s, 1 %/s, 5 %/s and 25 %/s. **Fig 2A** shows the time-course of the applied strain for each strain rate. For a given rate, strain increases linearly until it reaches 30%, then is held at 30% for 60 s before returning to 0%. Using our quantitative ATP imaging method, we calculated ATP efflux induced by such stretch protocol in 7-day-old cultures of alveolar cells. In **Fig. 2B**, we can notice that the rate of ATP release is highly dependent on strain rate. We found that ATP efflux doubles for a five-fold increase in strain rate, except for the 1 to 5 %/s range, where the cells released 25 times more ATP. This quasi-sigmoidal response curve for ATP release is consistent with expected behaviour of the viscoelastic membrane, where due to limited membrane fluidity, faster stretching is more likely to rupture the membrane than the slow stretching.

Secondly, we explored the influence of strain duration on ATP efflux. With a fixed rate of 25%/s, cells were subjected to a 30% strain for 60 or 1 s, shown at the bottom of **Fig. 3A and 3B**, respectively. At the top of **Fig. 3A and 3B**, we can see the time-course of ATP efflux, which was normalized to its peak value. Visually, the curves already exhibit signs of stress relaxation, i.e., after reaching a peak, ATP efflux rapidly decays: for 60-s strain duration, it decays completely before the strain is released. For each curve, we calculated the half-life ($t_{1/2}$) of the decay of the rate of ATP release. In **Fig. C**, we compared the values of $t_{1/2}$ of strain-induced ATP (in s) between a 60-s ($n = 4$) and a 1-s ($n = 5$) strain of 30%. Student *t*-test shows a statistical difference between both groups ($P < 0.05$). Therefore, longer strain duration prolongs the $t_{1/2}$ of ATP efflux, which may indicate that the plasma membrane requires more time to return (relax) to its initial state during long-lasting stretches.

Taken together, **Fig. 2 and 3** demonstrate that the cell membrane's viscoelastic properties directly and significantly influence stretch-induced ATP release.

5.3.5 Discussion

Co-localization of ATP-releasing cells and PI-positive cells. Our results in Figure 1 show that 30% strain triggers ATP release and PI uptake in alveolar cells. Interestingly, we observed a strong spatial and temporal correlation between extracellular ATP and PI uptake, which suggests a potential conductive pathway for ATP secretion. Because ATP-permeable channels cannot allow such a high rate of ATP release per cell, a process involving membrane rupture may prove to be sound. Indeed, uptake of PI had to occur only in wounded cells, whose ruptures at the cell membrane appear to be transient due to short duration of ATP efflux.

Our preliminary study on inflation-induced ATP release in rat *ex vivo* lungs also supports this observation, where ATP-releasing alveolar cells also showed an uptake of ethidium bromide (EthBr), indicating compromised membrane integrity (10). In addition, Riquelme *et al.* showed that electrical stimulation (200-ms pulses of 40 V at 0.3 Hz for 30 min) of rat skeletal muscle fibers evoke uptake of EthBr, as well as ATP release (16). Even though the authors attributed ATP release to pannexin channels, a reversible change in cell membrane's permeability due to

electrical stimulation may be a result of electroporation, through which ATP can be released (16, 17).

Viscoelastic ATP release. Given how cell stretch disrupts the plasma membrane, one could expect that ATP release occurring through transient ruptures in the cell plasma membrane would be directly affected by its viscoelastic properties (14). First, Figure 2 illustrates the sensitivity of ATP efflux to strain rate: the faster the strain rate is applied, the higher ATP efflux is. Secondly, Figure 3 shows the effect of strain hold time on the rate of ATP release. Both 60-s and 1-s hold times exhibited a rapid decline in ATP efflux, but the $t_{1/2}$ of ATP decay was significantly higher for longer hold time. This shows that ATP release is influenced by the relaxation of the plasma membrane. Therefore, mechanosensitive ATP release displayed dependence to strain rate and relaxation response, both hallmarks of viscoelasticity.

Forsyth *et al.* studied ATP release in human red blood cells in function of the cell's ability to deform according to the level of cholesterol of its plasma membrane (18). As the red blood cell is a viscoelastic body, the authors subjected these cells to shear stress through a narrow passage, which elongated them. They observed that red blood cells, having less cholesterol in their plasma membrane, are prone to deformation, facilitating ATP release (18). They also used simvastatin, which increased the cell's ability to deform, and noted ATP release despite high levels of cholesterol (18). While the authors attributed ATP release to volume-regulated anion current channels, it seemed more likely that ATP release occurred in response to the mechanical deformation of the membrane, via transient ruptures.

In summary, this study examined mechanosensitive ATP release in rat primary alveolar cells. On one hand, we have co-localized ATP-release and PI uptake in cells subjected to stretch. On the other hand, stretch-induced ATP release displayed dependence on strain rate and the strain duration, both consistent with viscoelastic properties. These findings suggest an alternative mechanism for stretch-induced ATP release, which involves a non-lytic transient membrane rupture. Extracellular ATP induced by MV may be used as a biomarker to detect early signs of injury in mechanically ventilated lungs. This knowledge may help to optimize MV

settings to control ATP release, and subsequent Ado formation, in order to minimize or prevent VILI.

5.3.6 Acknowledgments

We would like to thank Anik Privé and Mélissa Aubin Vega from Dr. Emmanuelle Brochiero's laboratory for preparing primary rat alveolar cells for our experiments.

5.3.7 Grants

This work was supported by Canadian Institutes of Health Research Grants PJT166157 (to R. Grygorczyk).

5.3.8 Disclosures

No conflicts of interest, financial or otherwise, are declared by the authors.

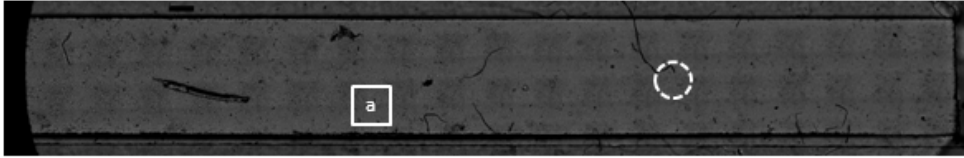
5.3.9 References

1. Pham T, Brochard LJ, Slutsky AS, editors. Mechanical ventilation: state of the art. Mayo Clinic Proceedings; 2017: Elsevier.
2. Slutsky AS, Ranieri VM. Ventilator-induced lung injury. *N Engl J Med.* 2013;369(22):2126-36.
3. Rich PB, Douillet CD, Mahler SA, Husain SA, Boucher RC. Adenosine triphosphate is released during injurious mechanical ventilation and contributes to lung edema. *Journal of Trauma and Acute Care Surgery.* 2003;55(2):290-7.
4. Rajagopal S, Ponnusamy M. Metabotropic GPCRs: TGR5 and P2Y Receptors in Health and Diseases: Springer; 2018.
5. Yegutkin GG. Nucleotide- and nucleoside-converting ectoenzymes: Important modulators of purinergic signalling cascade. *Biochim Biophys Acta.* 2008;1783(5):673-94.
6. Cronstein BN, Naime D, Ostad E. The antiinflammatory mechanism of methotrexate. Increased adenosine release at inflamed sites diminishes leukocyte accumulation in an in vivo model of inflammation. *The Journal of clinical investigation.* 1993;92(6):2675-82.
7. Reutershan J, Vollmer I, Stark S, Wagner R, Ngamsri K-C, Eltzschig HK. Adenosine and inflammation: CD39 and CD73 are critical mediators in LPS-induced PMN trafficking into the lungs. *The FASEB Journal.* 2009;23(2):473-82.

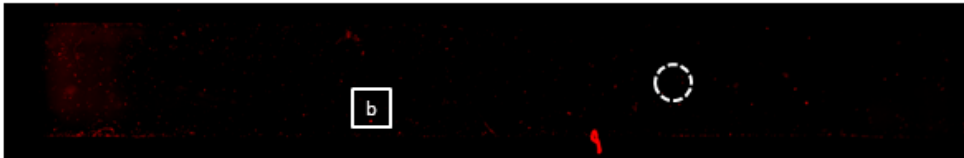
8. Eckle T, Koeppen M, Eltzschig HK. Role of extracellular adenosine in acute lung injury. *Physiology (Bethesda)*. 2009;24(5):298-306.
9. Grygorczyk R, Furuya K, Sokabe M. Imaging and characterization of stretch-induced ATP release from alveolar A549 cells. *J Physiol*. 2013;591(5):1195-215.
10. Tan J, Furuya K, Boudreault F, Brochiero E, Grygorczyk R. Mechanisms of Inflation-Induced ATP Release in Ex Vivo Rat Lungs: A Bioluminescence Imaging Study. D108 MECHANISM OF LUNG INJURY: American Thoracic Society; 2019. p. A7245-A.
11. Tan JJ, Boudreault F, Adam D, Brochiero E, Grygorczyk R. Type 2 secretory cells are primary source of ATP release in mechanically stretched lung alveolar cells. *Am J Physiol Lung Cell Mol Physiol*. 2020;318(1):L49-L58.
12. Tschumperlin DJ, Margulies SS. Equibiaxial deformation-induced injury of alveolar epithelial cells in vitro. *Am J Physiol*. 1998;275(6):L1173-83.
13. Skotak M, Wang F, Chandra N. An in vitro injury model for SH-SY5Y neuroblastoma cells: effect of strain and strain rate. *J Neurosci Methods*. 2012;205(1):159-68.
14. Trepas X, Grabulosa M, Puig F, Maksym GN, Navajas D, Farre R. Viscoelasticity of human alveolar epithelial cells subjected to stretch. *Am J Physiol Lung Cell Mol Physiol*. 2004;287(5):L1025-34.
15. Tan JJ, Ponomarchuk O, Grygorczyk R, Boudreault F. Wide field of view quantitative imaging of cellular ATP release. *Am J Physiol Cell Physiol*. 2019;317(3):C566-C75.
16. Riquelme MA, Cea LA, Vega JL, Boric MP, Monyer H, Bennett MV, et al. The ATP required for potentiation of skeletal muscle contraction is released via pannexin hemichannels. *Neuropharmacology*. 2013;75:594-603.
17. Granot Y, Rubinsky B. Mass Transfer Model for Drug Delivery in Tissue Cells with Reversible Electroporation. *Int J Heat Mass Transf*. 2008;51(23-24):5610-6.
18. Forsyth AM, Braunmuller S, Wan J, Franke T, Stone HA. The effects of membrane cholesterol and simvastatin on red blood cell deformability and ATP release. *Microvasc Res*. 2012;83(3):347-51.

5.3.10 Figures and Captions

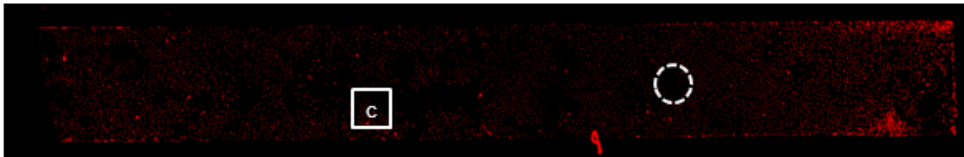
A Bright-field image



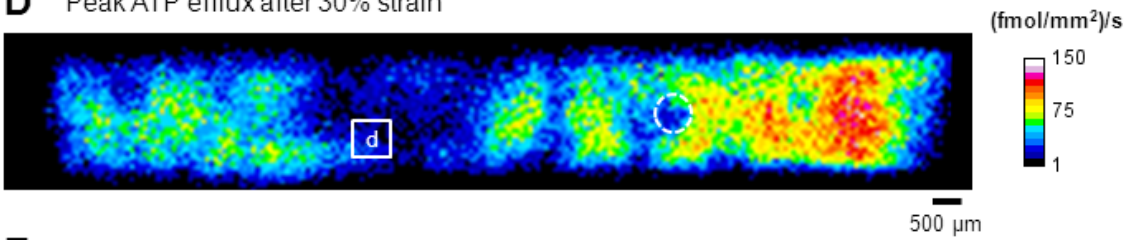
B PI staining before 30% strain



C PI staining after 30% strain



D Peak ATP efflux after 30% strain



E

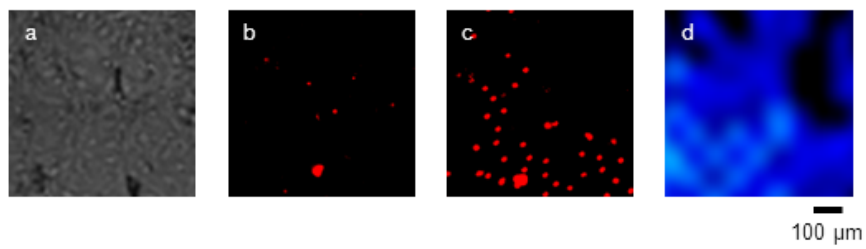


Figure 1

Figure 22. – Figure 1 of Article #3

Fig. 1. ATP release is co-localized with PI uptake in rat primary alveolar cells.

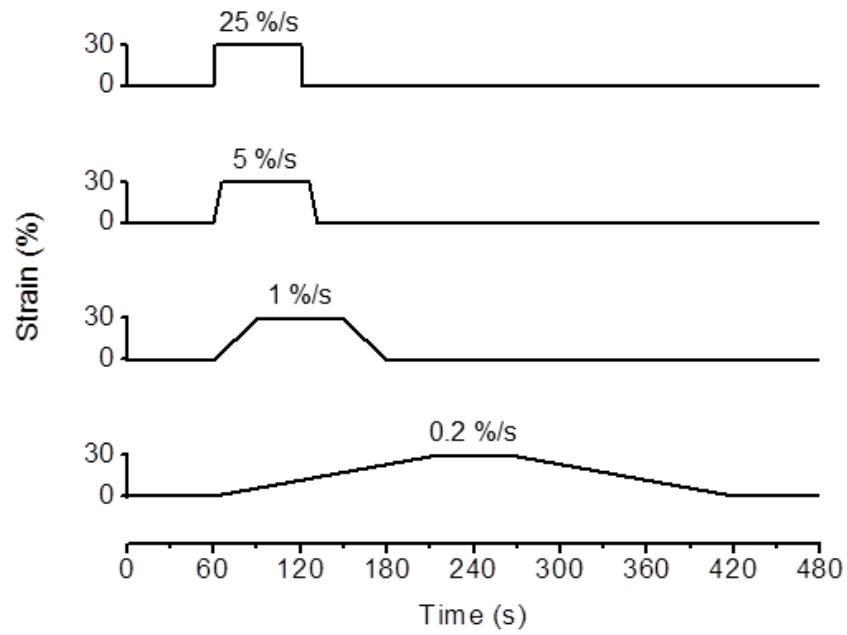
A. Bright-field images of the entire flexible silicone groove (2 × 18 mm) onto which rat primary AT2 cells were seeded. 80 images (512 × 512 pixels, magnification 5×) were stitched together to show the entire chamber.

B. PI fluorescence images of 7-day-old alveolar cells that were bathed in DMEM medium containing LL and propidium iodide (PI) (1 µg/mL) before a 1-s strain of 30%. 80 fluorescence images were stitched to show the entire chamber as in *A*.

C. PI fluorescence images of AT2 cells after 1-s strain of 30%, the same cells as in *B*.

D. ATP-dependent LL bioluminescence was captured via WFOV ATP imaging. Calibration bar represents the rate of ATP release ((fmol/mm²)/s). Squares represent one ROI, which are zoomed in *E.*, with letters corresponding to placement. Dotted circles represent another ROI, which displays lack of ATP release and PI uptake. In regions where ATP release was detected, it co-localized with cells showing PI uptake by cells.

A



B

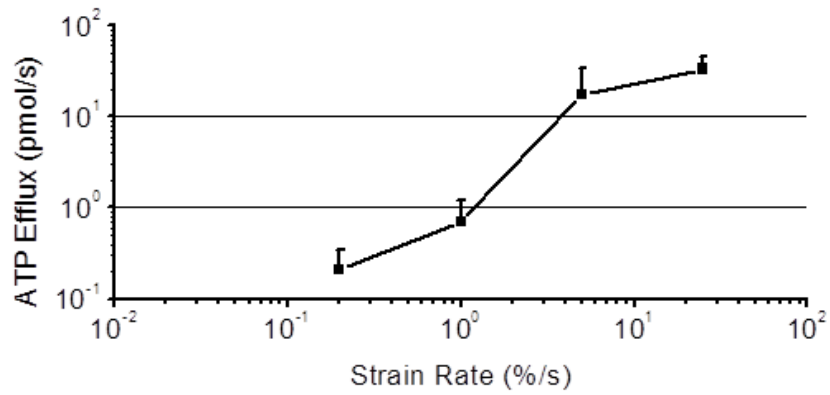


Figure 2

Figure 23. – Figure 2 of Article #3

Fig. 2. Effect of strain rate on ATP efflux in rat primary AT2 cells at day 7.

A. Time-course of 30% strain achieved at different rates. Four strain rates were tested, increasing at a 5-fold increment: 0.2 %/s, 1 %/s, 5 %/s and 25 %/s. All stretches begin at $t = 60$ s to reach a magnitude of 30% and is maintained for 60 s before returning to 0%. Do take notice of variable time required to reach the desired amplitude for different applied strain rates.

B. Graph showing ATP efflux (pmol/s) in function of the strain rate (%/s) in log scale. Data are expressed as mean (\pm SD, only positive are shown) from 3-5 experiments. These results demonstrate that the alveolar cells yield a higher rate of ATP release when the strain rate is faster, as expected for membrane rupture due to limited fluidity of the viscoelastic membrane.

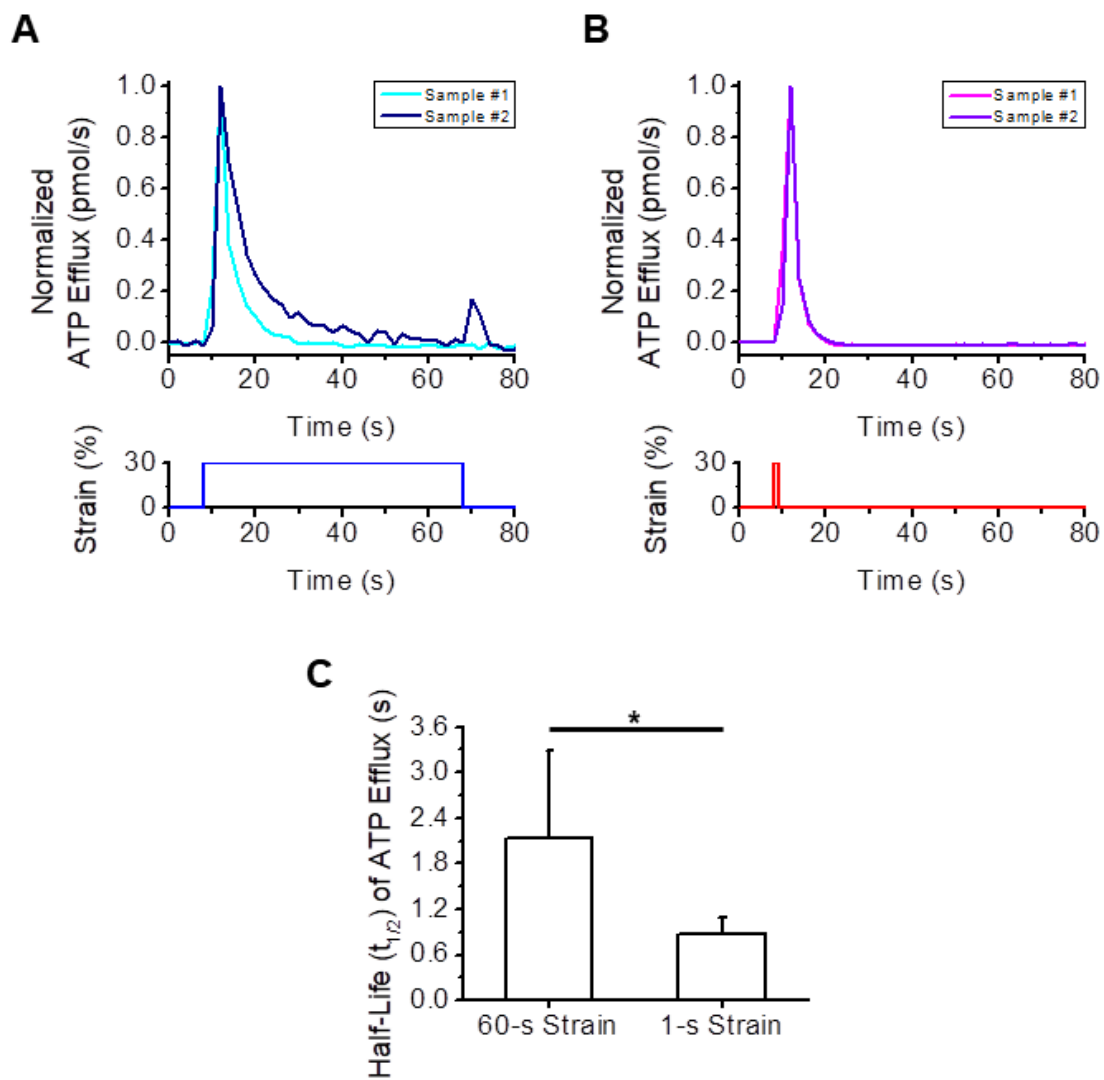


Figure 3

Figure 24. – Figure 3 of Article #3

Fig. 3. Effect of duration of strain on the rate of ATP release in rat primary alveolar cells.

(*Top*) Two representative traces of ATP efflux induced by a strain of 30%, which was maintained for (**A.**, blue) 60 s or (**B.**, red) 1 s. Curves were normalized to peak values from 4 and 5 experiments, respectively. From these curves, half-life ($t_{1/2}$) values were calculated.

(*Below*) Graph showing the time-course of stretch. 30% stretch was applied at $t=8$ s at a rate of 25%/s and lasted for (**A.**, blue) 60 s or (**B.**, red) 1 s.

C. Comparison of half-life ($t_{1/2}$) values of strain-induced ATP efflux (in s) between a 60-s ($n = 4$) and a 1-s ($n = 5$) strain of 30%. Student t -test shows statistical difference between both groups ($P < 0.05$). Therefore, the time for which stretch-induced ATP release to occur through the plasma membrane lasts longer with an increasing hold time of the strain.

Chapter 6 – Discussion

This thesis examined the effect of stretch on ATP release in the lung alveolar cells. We hypothesized that stretching of alveolar epithelial cells causes them to release ATP into the alveolar space by several mechanisms, including a previously unrecognized mechanism that arises from the viscoelastic properties of the cell membrane. In order to determine the involvement of different mechanisms/pathways to stretch-induced ATP release and the contributions of AT1 vs. AT2 cells in the alveolus, my doctoral research is divided into three articles:

6.1 Article #1

First, in order to study ATP release with real-time luminescence ATP imaging, we need to establish a standard method, which will reliably and accurately quantify ATP. We based our approach on real-time imaging of ATP release through a microscope equipped with a highly-sensitive EMCCD camera (129). Instead of using a microscope, we devised a custom-designed lens system, combining a wide field of view (WFOV) with a high light-gathering power, through which a faint ATP-dependent LL bioluminescence is directly captured by an EMCCD camera. This is critically important because LL luminescence is of very low intensity, typically more than 10^4 -fold lower compared to that in fluorescence imaging. To induce ATP release in A549 cells, we subjected them to a range of 1-s stretch (strain) or 50% hypotonic shock. With our approach, we were able to quantify the amount of released ATP (in the fmol range), to estimate the concentration of extracellular ATP, as well as to calculate ATP efflux. By comparing both mechanical ATP-releasing triggers, we showed that A549 cells release more ATP in response to stretch than to 50% hypotonic shock.

This innovative method constitutes an important tool that will help us to map and precisely characterize the dynamics of ATP-dependent LL bioluminescence (i.e., extracellular ATP) in real time. By drawing accurate metrics regarding the spatio-temporal kinetics of ATP release, in terms of amount and rate of ATP release, we are now able to gather valuable

information that can help us to determine the mechanistic pathway for ATP release. In addition, our method will offer a standard approach to quantitate ATP imaging, facilitating the comparison of ATP quantities (in moles) between studies, instead of arbitrary light units. Furthermore, viewing ATP release through a WFOV provides the bigger picture of all ATP release, and its heterogeneous nature, over the cell monolayer, rather than focusing on a small fraction of it. We can notably visualize the diffusion of ATP release from the original sites to study purinergic signaling, whose estimated extent allows us to produce a fair approximation of the local concentration of released ATP. While the WFOV approach lacks in image resolution compared to a standard microscope, it gains in greater capacity to detect and to record fainter light signals, which offers high levels of ATP mapping resolution and quantification.

6.1.1 Limitations

Although highly sensitive, our method is limited to capturing the intensity of the light emission produced by the LL reaction with ATP that is detectable by our system. However, adequate settings of the camera (e.g., exposure time and binning) were optimized to detect the faintest signals while avoiding saturation of peak intensities. We also use an exposure time of 1 s, which makes our EMCCD camera produce an image every 2 s. This frequency of image acquisition might not be high enough in some cases, hence a source of aliasing, which may introduce distortions and undervalue the original signal, especially within the moments after stretch.

Regarding the study of purinergic signaling, our method is only sensitive to detect extracellular ATP molecules because the reaction of LL is specific to ATP and not to other nucleotides (e.g., UTP) and its own by-products (i.e., ADP, adenosine) (66, 135). Therefore, this approach is limited to investigating the contribution of ATP in purinergic signaling and is highly relevant for studies pertaining to ATP release.

6.2 Article #2

Secondly, we used our quantitative WFOV ATP imaging approach to investigate the mechanism of stretch-induced ATP release in rat primary alveolar cells and to determine the contribution of AT2 vs. AT1 cells in this process. In summary, we seeded freshly isolated rat primary AT2 cells from rats on a flexible silicone chamber and maintained them in culture for up to seven days. This allows AT2 cells to acquire phenotypes of AT1-like cells, which is consistent with the findings of Patel *et al.* and Tschumperlin *et al.* (31, 141). We determined that the co-culture of alveolar cells at days 3 and 7 after seeding are composed of AT2:AT1 ratio of 4:1 and 1:4, respectively. Stretching the alveolar cell cultures on day 3 released threefold more ATP than on day 7. On day 3, a significant surge of extracellular ATP occurred when cells were subjected to a 20% strain, a magnitude of stretch corresponding to TLC, which might constitute a threshold to trigger ATP release. Likewise, in our previous study using A549 cells, we also observed that the highest occurrence of ATP release was in response to a 21% strain (137). Moreover, we demonstrated a tight correlation between the amount of ATP released and the proportion of AT2 cells in culture, which indicates that AT2 cells are the main contributor of stretched-induced ATP release in the alveolus, rather than AT1 cells.

As mentioned previously in Chapter 4, our findings contradict those of Patel *et al.*, which demonstrated that in response to stretch, AT1 cells released fourfold more ATP than AT2 cells (31). However, our results support those of Isakson *et al.*, who used apyrase, which catalyzes the hydrolysis of ATP, to avert $[Ca^{2+}]_i$ elevations from activation of purinergic receptors (139, 143). They found that apyrase inhibits intracellular Ca^{2+} signaling originating from AT2 cells but not from AT1 cells (139). In other words, AT2 cells displayed the capability of releasing ATP rather than AT1 cells.

We conducted our experiments on alveolar cells three days after seeding since they released important quantities of ATP at lower strains. To determine the physiological mechanism of stretch-induced ATP release, these cells were stretched in presence of putative ATP channels inhibitors, CBX and probenecid (PRO), which both did not considerably affect ATP release. However, cells loaded with BAPTA released ~43% less ATP compared to the controls.

The effect of these inhibitors produced similar responses in $[Ca^{2+}]_i$ variations, which highlights the importance of $[Ca^{2+}]_i$ in stretch-induced ATP release in rat primary AT2 cells.

Ransford *et al.* showed that in human airway epithelial cells, 10 μ M CBX and 1 mM PRO are sufficient to inhibit by 60% the amount of ATP released induced by hypotonic shock (68). Even though we used the same inhibitors but at a higher concentration (100 μ M CBX and 2.5 mM PRO), no significant decline in ATP release was observed by our quantitative method. Takahara *et al.* also observed that 100 μ M CBX did not inhibit stretch-induced ATP release in human airway smooth muscle cells (88). Hence, our results suggest that ATP release in AT2 cells does not occur, at least, through pannexins and connexins, as opposed to other findings in the airway epithelium, such as Ransford *et al.*, and as reported by Velasquez *et al.* (68, 83). Besides, there is still lack of direct proof regarding ATP conductance through pannexin channels, and its activation pathways remain unspecified/elusive in this context (108, 109).

In this study, these inhibitors do, however, seem to exert the similar effects on $[Ca^{2+}]_i$ fluctuations and ATP release, which suggests its indirect impact on stretch-induced ATP release, as we hypothesized. Since vesicular mechanism depends on an increase of $[Ca^{2+}]_i$, regulated vesicular exocytosis is a good candidate for the pathway for ATP release (68). Moreover, Takahara *et al.* demonstrated that stretch-induced ATP release is significantly decreased by inhibitors pertaining to vesicular exocytosis (88). In our previous findings in A549 cells, Akopova *et al.* revealed the presence of vesicles filled with ATP, whose fluorescent label was lost after the fusion of the vesicles with the plasma membrane following a hypotonic challenge (87). Fois *et al.* showed that AT2 cells isolated from Sprague-Dawley rats have ATP stored in LB, where VNUT is responsible for filling LB with ATP (69). Therefore, stretch-induced ATP release from AT2 cells may involve a $[Ca^{2+}]_i$ -dependent mechanism, which may be consistent with exocytosis.

In our other recent *ex vivo* study, we simultaneously imaged in real time ATP release by bioluminescence and cell/tissue by infrared in rat *ex vivo* lungs, as we quantified inflation-induced ATP release with our method (129, 137, 144). Again, as the lungs inflated, ATP release solely occurred in the alveoli. In presence of inhibitors for conductive pathways (100 μ M CBX, 100 μ M PRO, 20 μ M 4-(2-butyl-6,7-dichloro-2-cyclopentyl-1-oxo-3*H*-inden-5-yl)-2-oxobutanoic

acid (DCPIB), 20 μ M CFTR(inh)-172 or 100 μ M NPPB) or exocytosis (10 μ M clodronate), we observed no significant decrease in ATP release compared to controls (144). In addition, we observed that levels of $[Ca^{2+}]_i$ increase following lung inflation, similarly to our previous observations (128, 130, 144). These findings give clues on stretch-induced ATP release in the alveolus and are consistent with those presented in our present *in vitro* study (140). Our results suggest that stretching of alveolar cells causes them to release ATP through a pathway, which may imply $[Ca^{2+}]_i$ but does not involve ATP-conducting channels and exocytosis.

6.2.1 Limitations

Our rat primary AT2 cell model has time constraints as they acquire AT1-like features over time after seeding (32). Because we also noticed that the amount of stretch-induced ATP release decreased over time, we were able to correlate these findings with the number of AT2 cells present in culture to show that AT2 cells are the main source for ATP in the alveolus. However, Tschumperlin *et al.* worked on AT2 cells to determine the cell's vulnerability to deformation (141). Even though their cells also altered with time, their results suggest that these morphological and phenotypic changes in culture affected the vulnerability of alveolar epithelial cells to deformation, where AT2 cells were more prone to cell damage at Day 1 than at Day 5 (141). Hence, our alveolar cells on day 3 might be more vulnerable to stretch than on day 7, which might explain the higher occurrence of ATP release on day 3. To determine whether or not the cell's vulnerability is in question regarding ATP release, we will need to repeat our experiments with isolated rat AT1 cells or A549 cells, which are a model for AT2 cells, because both primary AT1 and A549 cells should not change in phenotype with time (25). Likewise, the murine lung epithelial cell line MLE-15 may also be another potential candidate since these cells continue to preserve many functional characteristics of AT2 cells after numerous passages (145). In this manner, we could compare the amount of released ATP on days 3 and 7 to determine if the cell's vulnerability to stretch is a factor in ATP release and not just from a difference in phenotypes. Furthermore, this *in vitro* study lacks the use of inhibitors regarding exocytosis, such as bafilomycin, which inhibits uptake of ATP in the vesicle, and clodronate, in order to confirm or rule out the possible mechanism of stretch-induced ATP release occurring through $[Ca^{2+}]_i$ -dependent vesicular exocytosis.

6.3 Article #3

Thirdly, as the exact mechanism of stretch-induced ATP release remains unclear, we aimed to find an alternative pathway for ATP release by exploring if and how the alveolar cell membrane's viscoelastic properties are involved in this process.

We chose to work with rat primary alveolar cell cultures seven days after seeding to avoid the cell's potential vulnerability to mechanical deformation in younger cell cultures (141). Bathed in DMEM containing LL and PI, 7-day-old alveolar cell cultures were subjected to a 1-s strain of 30%. Following this physical stress, there was, indeed, ATP release, as well as PI uptake. Surprisingly, PI-positive cells were co-localized with ATP release. Hence, stretching may provoke a transient increase in the cell membrane permeability to allow PI uptake and ATP release. Interestingly, in our recent *ex vivo* study, we also observed that in regions where ATP release occurs, uptake of EthBr was detected (144). This indicates once more that stretching of the plasma membrane creates pathways, perhaps through transient membrane ruptures, which are large enough for ATP and EthBr to pass through (144). Similarly, Riquelme *et al.* observed that electrical stimulation of rat skeletal muscle fibers induced an uptake of EthBr, in addition to ATP release (146). Despite the authors claiming that ATP release was through pannexin channels, we believe that changes in the permeability of the cell membrane by electrical stimulation may allow ATP to be released via reversible electroporation (146, 147). Although EthBr, EthD-1 and PI are classical indicators of cell death, their uptake may simply show signs of membrane damage as the cell membrane may sustain injury from an excessive strain (142).

Because stretch affects the cell membrane, we aimed to establish if its viscoelastic properties come into play with ATP release. To show this, we examined the relationship between ATP efflux and strain rate, as well as ATP efflux and strain duration. We first demonstrated that ATP efflux rises with increasing strain rate, and then showed ATP efflux relaxation under a prolonged strain, both being key features of viscoelasticity. Since ATP efflux is short-lasting, the tiny breaks in the plasma membrane due to cell deformation are transient, but it takes longer for them to close or reseal themselves when the applied strain persists, as observed with the prolonged half-life ($t_{1/2}$) of ATP release relaxation. Do note that because

there is no noticeable relaxation of the flexible stretch chamber during strain, the cell's viscoelastic behaviour is largely independent from that of the silicone substrate.

In their work, Forsyth *et al.* observed that human red blood cells, which are viscoelastic, released ATP when their plasma membrane is elongated by shear stress (148). Although the authors considered volume-regulated anion channels as the pathway for this ATP release, breaks in the membrane may occur for ATP release due to the deformation of the cell, but cell-impermeant markers were unfortunately not used to assess its uptake (148). Besides, the inhibitor of these channels, DCPIB, did not decrease ATP release in our *ex vivo* experiment (144).

Our results are consistent with findings in neurons, where strain rate alters the membrane's permeability. In their *in vitro* model for traumatic brain injury (TBI, discussed in 6.4 *Proposed Mechanism of Mechanosensitive ATP Release in the Lungs*), Geddes *et al.* seeded primary culture of rat neurons on a silicon substrate, which are subjected to an equibiaxial and uniform strain field (149). They demonstrated that exposing neurons to stretch may lead to a transient plasma membrane permeability increase as neurons immediately begin to uptake a host of fluorescent molecules (carboxyfluorescein (380 Da) and calcein (620 Da)) and dextrans of various molecular masses (10,000 to 150,000 Da), which depends on strain rate and magnitude (149). This shows that the cell membrane becomes permeable to large molecules during stretch, but the duration of permeability following the mechanical stimulus declines as the size of the molecule increases (149). In other words, the pore formation is transient, and it reseals itself moments after stretch. With the molecular mass of ATP being 507.181 Da, we estimated its molecular radius to be roughly 0.613 nm or at most 0.700 nm (149, 150). Therefore, the ATP is small enough to be released from the cell through transient membrane ruptures during stretch.

6.3.1 Limitations

Our experiments were done in the absence of calcein-AM, so we were unable to confirm the viability of injured cells. In fact, we previously attempted to simultaneously image extracellular ATP, $[Ca^{2+}]_i$ and EthBr in rat *ex vivo* lungs to correlate ATP release with transient membrane rupture. However, the LL present in the medium was also excited at 490–495 nm

(the range of our $[Ca^{2+}]_i$ indicator Fluo-8, the same for calcein), so we studied ATP release and PI uptake alone. It was also difficult to produce high-resolution images for ATP imaging due to our WFOV method. A higher image resolution for ATP release is desired to better correlate ATP-releasing cells with PI-positive ones. ATP imaging through a microscope may improve resolution for co-localization, but light signal capture will be diminished. Finally, because the cytoskeleton has been shown to be involved in the viscoelastic plasma membrane, tracking these internal structures may provide additional information to assess viscoelasticity in response to stretch, which will complement the findings regarding the pathway for ATP release (116).

6.4 Proposed Mechanism of Mechanosensitive ATP Release in the Lungs

Together, the three studies led to a better understanding of stretch-induced ATP release in rat primary alveolar cells. Because inhibitors of ATP conducting channels and vesicular exocytosis do not significantly diminish stretch-induced ATP release in our *in vitro* and *ex vivo* models, respectively, another non-lytic or at least non-lethal pathway needs to be considered (140, 144). We later co-localized ATP release with PI uptake, which exhibited signs of transient membrane rupture. Cell membrane also displays viscoelastic properties, which are involved in ATP release induced by strain. Therefore, we should explore the possibility of an alternative non-lytic conductive pathway resulting from a transient break in the plasma membrane, which allows the free passage of cytosolic ATP into the extracellular space.

As previously described, MV may contribute to injuring lung cells by excessively straining the plasma membrane (151, 152). Lung injury is associated with elevated levels of extracellular ATP, which, as a DAMP, contributes to the pathogenesis of VILI (42, 52, 96). Again, Groulx *et al.* demonstrated that the plasma membrane can slowly undergo large deformation through hypotonic shock and is able to adopt a shape, whose surface-to-volume ratio is below lytic tension (125). It seems that beyond a certain threshold, most cell membranes in response to high mechanical stresses might break or be wounded, but the cell can repair or reseal the holes within seconds, either through lateral flow of the lipid bilayer for tiny holes or through a $[Ca^{2+}]_i$ -dependent trafficking response for larger ruptures; otherwise, cell lysis would occur (152-154).

Of course, airway and alveolar epithelial (and endothelial) cells are prone to these cytopathological changes and, during this temporary state, may leak their cytosolic content (e.g., ATP) (155, 156). Despite their injury, the majority of the wounded cells do survive and repair these deformation-induced wounds/insults at a single-cell level (155, 156). Triggered by an influx of Ca^{2+} , this process, termed single-cell wound healing or plasma membrane repair/resealing, allows the cell to cease further loss of material (156-158).

Similarly to lung cells, cardiac myocytes are routinely subjected to mechanical forces from regular heart beats. The motion of the membrane forms small pores (<10 nm), in response to mechanical stimuli, but the hole is patched due to membrane fusion induced through exocytosis, endocytosis and contraction of actomyosin, all of which involve $[\text{Ca}^{2+}]_i$ signaling (156).

The formation of holes in the plasma membrane as a result of mechanical perturbation shares similarities to what occurs in diffuse TBI, where mechanical loads to the head transduce stress and strain to the brain, causing damage and injury to neuronal cells (159, 160). Here, these physical insults (stretch, compression, torsion or shear) physically breach the neuronal cell membrane and induce mechanical poration of the membrane (14, 159, 160). This membrane damage, or mechanoporation, allows non-specific flux of ions and other molecules into and out of the cell, and may ultimately lead to cell death, but the cell may reseal and recover once the physical perturbation ends (159, 160). Indeed, these changes affecting the cell membrane's permeability may trigger the abnormal release of large molecules, particularly ATP (149).

Furthermore, there are electroporation-based methods, which physically create transient pores at the cell membrane to deliver drugs or macromolecule probes, by using a combination of micro-bubbles, sonication or laser (161-164). These devices can be seen to mimic naturally occurring events in the body, where mechanical stresses cause the cell membrane to deform and to rupture, for which cells are inherently able to survive (165).

While the term mechanoporation per se is not used to describe similar phenomena in the lungs, Gajic *et al.* demonstrated that in rat lungs, a high tidal volume injures cells at the subpleural alveoli, as wounded cells are labelled with PI (155). A decrease in PI-positive cells

after the removal of injurious ventilation indicates that most injured cells were able to reseal, which they also observed in A549 cells (155). This process of plasma membrane wound resealing in the rat lungs is impaired by hypercapnia (166). Kawai *et al.* showed that in A549 cells, the wounded plasma membrane is promoted by transglutaminase 2, an enzyme catalyzing Ca^{2+} -dependent cross-linking between proteins, to reseal following a mechanical damage (167). Moreover, Godin *et al.* demonstrated that primary rat AT1 cells, sustaining a relatively large wound, induced by micropuncture, to the cell membrane, have an 80% probability to self-repair within 11 s to 39 s (168). Furthermore, Seminario-Vidal *et al.* noted that cell swelling induces ATP release and PI uptake in A549 cells, but the authors attributed these processes to pannexin channels (121). These temporarily formed wounds or pores at the plasma membrane could provide the means of allowing ATP to exit the cell, but further studies are required to clarify the actual mechanisms involved (154).

A model of ATP release is proposed by Mikolajewicz *et al.*, where mechanical stimulation induces ATP release and Ca^{2+} wave propagation in osteoblasts (169). This ATP release is not through vesicular exocytosis, despite the presence of ATP-containing vesicles (169). However, they proposed a model in which mechanically stimulated ATP release is related to membrane injury, whose process involves PKC-regulated vesicular exocytosis for membrane resealing (169). This cell membrane injury is non-lethal and adapted to mechanical forces (169).

Together with our findings, stretch-induced ATP release in primary rat alveolar cells may occur via a process similar to mechanoporation. Moreover, higher ATP release took place within the few days after seeding of alveolar cells might be due to their elevated susceptibility to mechanical forces as mentioned by Tschumperlin *et al.* (141). Stretching of AT2 cells beyond a certain threshold (~20% strain) induces transient injury or damage to the cell membrane for entry of the fluorescent marker for cell death (e.g., EthBr, EthD-1 and PI) and exit of intracellular ATP, which ceases as a result of membrane relaxation (141, 142). Our observed variations of $[\text{Ca}^{2+}]_i$ in response to strain might be an indicator for mechanoporation as elevation of $[\text{Ca}^{2+}]_i$ is required for cell membrane repair (142, 149, 153). Nevertheless, more studies are required to fully characterize this transient conductive pathway for stretch-induced ATP release, which involves non-lethal perturbations of the cell membrane, as well as its viscoelastic properties.

Chapter 7 – Conclusion & Perspectives

7.1 Conclusion

The work presented in my thesis aimed to study the effect of stretch on ATP release in the lungs. To this end, I presented the results of my research in three articles, which contributed to the identification of physiological mechanisms underlying mechanosensitive ATP release in alveolar cells.

7.1.1 Summary of Original Contributions

I developed a WFOV method, which enables the quantification of total extracellular ATP and its efflux based on images of ATP-dependent LL bioluminescence recorded in real time. This constitutes itself a significant progress regarding ATP measurements through imaging. By reliably and accurately calculating extracellular ATP and the kinetics of its diffusion, we can now draw valuable information to determine its release mechanism. Moreover, this tool may provide a standard method for researchers to compare their own ATP measurements to others'.

I demonstrated that in the rat alveolus, AT2 cells are a main source of ATP release induced by stretch. I also showed that this process depends on $[Ca^{2+}]_i$ and that it does not involve ATP-conductive channels. By observing a considerable surge of ATP release in response to a 1-s strain of 20% in AT2 cells, I was able to estimate a strain threshold for a collective ATP release by the cell culture.

To my knowledge, my work is the first to co-localize stretch-induced ATP release and PI uptake in rat primary alveolar cells. I have obtained compelling evidence to support ATP release through transient formation of pores during stretch, and I have shown that this transient process critically depends on the cell membrane's viscoelastic properties. This might lead the way towards establishing this novel non-lethal pathway as an important, previously not recognized, mechanism for ATP release induced by mechanical stretch in the lungs.

7.2 Perspectives

It is with humility that I wish that my thesis may inspire future experimental designs in order to determine the exact mechanism of ATP release in the lungs.

First, with more and more evidence supporting stretch-induced ATP release through mechanoporation, we need to pursue our *in vitro* study on the viscoelastic properties of the cell membrane in AT2 cells. Most notably, it would be interesting to conduct these experiments with a fluorescent probe for intracellular Ca^{2+} , as a cell viability measure, to evaluate the extent of membrane damage, as well as the cell's vulnerability to physical forces. Given the importance of stretch-induced $[\text{Ca}^{2+}]_i$ elevations, the impact of strain rate and hold time on $[\text{Ca}^{2+}]_i$ needs to be addressed. Plasma membrane and cytoskeleton markers (e.g., HTII-280 (for apical membrane of human AT2 cells) and Lifeact (for filamentous actin (F-actin) in eukaryotic cells), respectively) may also provide additional measurements to assess changes in these structures' organization in response to different strain rates (170, 171). A better understanding of the viscoelasticity of the cellular membrane will help to conceive a model that will accurately depict stretch-induced ATP release in the alveolus.

Secondly, we should apply our *in vitro* model in *ex vivo* rat lungs and study inflation-induced ATP release at the alveolar level at higher magnification (144). As this approach requires the filling of the alveoli with LL-containing solution, it constitutes a model for edematous lungs (130, 144). This proves to be difficult for an *in vivo* model because it is not desirable to drown an animal. Alternatively, we can nebulize the LL-containing solution to coat the alveoli of a living rat, so under these conditions, we can record ATP release in non-edematous lungs (109). To image *in vivo* lungs with our current method, recording of ATP-dependent LL bioluminescence may have to be through an opening of the animal's thoracic cage (intravital microscopy). ATP measurements with pme-LUC, a luciferase probe for living cells, may provide an alternative to our ATP imaging technique (132). Otherwise, simply collecting BALF from live animals and measuring ATP-dependent LL bioluminescence from these samples through a luminometer do remain a feasible option.

Finally, this research contributes to better understanding of the physiological mechanism of ATP release in the lungs. Should the cells release ATP as a result of injury, we can use ATP as a biomarker to assess alveolar damage caused by cell deformation. Already, ATP can be measured in exhaled breath condensate, which may be a sign of lung damage during MV (172). By determining exactly how ATP is released in response to stretch, we may suggest potential targets to modulate both positive and negative impacts, which ATP and its metabolites, namely adenosine, may have in the pathogenesis of lung diseases and respiratory complications, particularly ARDS and VILI. Such therapeutic treatments may minimize or prevent symptoms associated with respiratory distress, which we hope will one day help patients with severe respiratory issues to breathe better.

References

1. Flurkey WH. Yield of ATP molecules per glucose molecule. *Journal of Chemical Education*. 2010;87(3):271-.
2. Liemburg-Apers DC, Imamura H, Forkink M, Nootboom M, Swartz HG, Brock R, et al. Quantitative glucose and ATP sensing in mammalian cells. *Pharm Res*. 2011;28(11):2745-57.
3. Rannels DE. Role of physical forces in compensatory growth of the lung. *Am J Physiol*. 1989;257(4 Pt 1):L179-89.
4. Hyde DM, Hamid Q, Irvin CG. Anatomy, pathology, and physiology of the tracheobronchial tree: emphasis on the distal airways. *J Allergy Clin Immunol*. 2009;124(6 Suppl):S72-7.
5. Adams W. How much air do we breathe. California Environmental Protection Agency, Sacramento. 1994.
6. Ridley C, Thornton DJ. Mucins: the frontline defence of the lung. *Biochem Soc Trans*. 2018;46(5):1099-106.
7. Luxen M, Powell S. *The Theory of Recreational Scuba Diving: Prepare for Your Dive Professional Exam, Be an Informed Recreational Scuba Diver*: Lulu.com; 2017.
8. McGowan SE. The formation of pulmonary alveoli. *The Lung*: Elsevier; 2014. p. 65-84.
9. Hammer GD, McPhee SJ. *Pathophysiology of disease: An Introduction to Clinical Medicine 7/E*: McGraw-Hill Education; 2014.
10. Soleas JP, Paz A, Marcus P, McGuigan A, Waddell TK. Engineering airway epithelium. *J Biomed Biotechnol*. 2012;2012:982971.
11. O'Connell S, Au-Yeung HK, Gregory CJ, Matthews IP. Outdoor and indoor respirable air particulate concentrations in differing urban traffic microenvironments. *J Toxicol Environ Health A*. 2008;71(16):1069-72.
12. Hollenhorst MI, Richter K, Fronius M. Ion transport by pulmonary epithelia. *J Biomed Biotechnol*. 2011;2011:174306.
13. Matthay MA, Robriquet L, Fang X. Alveolar epithelium: role in lung fluid balance and acute lung injury. *Proc Am Thorac Soc*. 2005;2(3):206-13.

14. Roan E, Waters CM. What do we know about mechanical strain in lung alveoli? *American Journal of Physiology-Lung Cellular and Molecular Physiology*. 2011;301(5):L625-L35.
15. Bove PF, Grubb BR, Okada SF, Ribeiro CM, Rogers TD, Randell SH, et al. Human alveolar type II cells secrete and absorb liquid in response to local nucleotide signaling. *J Biol Chem*. 2010;285(45):34939-49.
16. Jain R, Barkauskas CE, Takeda N, Bowie EJ, Aghajanian H, Wang Q, et al. Plasticity of Hox(+)-type I alveolar cells to regenerate type II cells in the lung. *Nat Commun*. 2015;6:6727.
17. Morgenroth K, Ebsen M. Anatomy. In: Papadakos PJ, Lachmann B, Visser-Isles L, editors. *Mechanical Ventilation*. Philadelphia: W.B. Saunders; 2008. p. 69-85.
18. Williams MC. Alveolar type I cells: molecular phenotype and development. *Annu Rev Physiol*. 2003;65(1):669-95.
19. Castranova V, Rabovsky J, Tucker JH, Miles PR. The alveolar type II epithelial cell: a multifunctional pneumocyte. *Toxicol Appl Pharmacol*. 1988;93(3):472-83.
20. Ridge K, Olivera W, Saldias F, Azzam Z, Horowitz S, Rutschman D, et al. Alveolar type 1 cells express the $\alpha 2$ Na, K-ATPase, which contributes to lung liquid clearance. *Circulation research*. 2003;92(4):453-60.
21. Bartoszewski R, Matalon S, Collawn JF. Ion channels of the lung and their role in disease pathogenesis. *American Journal of Physiology-Lung Cellular and Molecular Physiology*. 2017;313(5):L859-L72.
22. Ahmad S, Ahmad A. *Epithelial Regeneration and Lung Stem Cells. Lung Epithelial Biology in the Pathogenesis of Pulmonary Disease*: Elsevier; 2017. p. 91-102.
23. Yang J, Hernandez BJ, Martinez Alanis D, Narvaez del Pilar O, Vila-Ellis L, Akiyama H, et al. The development and plasticity of alveolar type 1 cells. *Development*. 2016;143(1):54-65.
24. Barkauskas CE, Crouse MJ, Rackley CR, Bowie EJ, Keene DR, Stripp BR, et al. Type 2 alveolar cells are stem cells in adult lung. *J Clin Invest*. 2013;123(7):3025-36.
25. Lieber M, Smith B, Szakal A, Nelson-Rees W, Todaro G. A continuous tumor-cell line from a human lung carcinoma with properties of type II alveolar epithelial cells. *Int J Cancer*. 1976;17(1):62-70.

26. Mishra A, Chintagari NR, Guo Y, Weng T, Su L, Liu L. Purinergic P2X7 receptor regulates lung surfactant secretion in a paracrine manner. *J Cell Sci.* 2011;124(Pt 4):657-68.
27. Brochiero E, Dagenais A, Prive A, Berthiaume Y, Grygorczyk R. Evidence of a functional CFTR Cl(-) channel in adult alveolar epithelial cells. *Am J Physiol Lung Cell Mol Physiol.* 2004;287(2):L382-92.
28. Rozycki HJ, Hendricks-Muñoz KD. Structure and development of alveolar epithelial cells. *Fetal and neonatal physiology: Elsevier;* 2017. p. 809-13.
29. Crosby LM, Luellen C, Zhang Z, Tague LL, Sinclair SE, Waters CM. Balance of life and death in alveolar epithelial type II cells: proliferation, apoptosis, and the effects of cyclic stretch on wound healing. *Am J Physiol Lung Cell Mol Physiol.* 2011;301(4):L536-46.
30. Oczypok EA, Perkins TN, Oury TD. Alveolar epithelial cell-derived mediators: potential direct regulators of large airway and vascular responses. *American journal of respiratory cell and molecular biology.* 2017;56(6):694-9.
31. Patel AS, Reigada D, Mitchell CH, Bates SR, Margulies SS, Koval M. Paracrine stimulation of surfactant secretion by extracellular ATP in response to mechanical deformation. *Am J Physiol Lung Cell Mol Physiol.* 2005;289(3):L489-96.
32. Isakson BE, Evans WH, Boitano S. Intercellular Ca²⁺ signaling in alveolar epithelial cells through gap junctions and by extracellular ATP. *American Journal of Physiology-Lung Cellular and Molecular Physiology.* 2001;280(2):L221-L8.
33. Crosby LM, Waters CM. Epithelial repair mechanisms in the lung. *Am J Physiol Lung Cell Mol Physiol.* 2010;298(6):L715-31.
34. Chen L, Deng H, Cui H, Fang J, Zuo Z, Deng J, et al. Inflammatory responses and inflammation-associated diseases in organs. *Oncotarget.* 2018;9(6):7204-18.
35. Moldoveanu B, Otmishi P, Jani P, Walker J, Sarmiento X, Guardiola J, et al. Inflammatory mechanisms in the lung. *J Inflamm Res.* 2009;2:1-11.
36. Driscoll KE, Lindenschmidt RC, Maurer JK, Higgins JM, Ridder G. Pulmonary response to silica or titanium dioxide: inflammatory cells, alveolar macrophage-derived cytokines, and histopathology. *Am J Respir Cell Mol Biol.* 1990;2(4):381-90.

37. Ashbaugh DG, Bigelow DB, Petty TL, Levine BE. Acute respiratory distress in adults. *Lancet*. 1967;2(7511):319-23.
38. Bernard GR, Artigas A, Brigham KL, Carlet J, Falke K, Hudson L, et al. The American-European Consensus Conference on ARDS. Definitions, mechanisms, relevant outcomes, and clinical trial coordination. *American journal of respiratory and critical care medicine*. 1994;149(3):818-24.
39. Force ADT, Ranieri V, Rubenfeld G, Thompson B, Ferguson N, Caldwell E. Acute respiratory distress syndrome. *Jama*. 2012;307(23):2526-33.
40. Thompson BT, Chambers RC, Liu KD. Acute respiratory distress syndrome. *New England Journal of Medicine*. 2017;377(6):562-72.
41. Bein T, Grasso S, Moerer O, Quintel M, Guerin C, Deja M, et al. The standard of care of patients with ARDS: ventilatory settings and rescue therapies for refractory hypoxemia. *Intensive Care Med*. 2016;42(5):699-711.
42. Eckle T, Koeppen M, Eltzschig HK. Role of extracellular adenosine in acute lung injury. *Physiology (Bethesda)*. 2009;24(5):298-306.
43. Zhang K, Wang P, Huang S, Wang X, Li T, Jin Y, et al. Different mechanism of LPS-induced calcium increase in human lung epithelial cell and microvascular endothelial cell: a cell culture study in a model for ARDS. *Mol Biol Rep*. 2014;41(7):4253-9.
44. Bellani G, Laffey JG, Pham T, Fan E, Brochard L, Esteban A, et al. Epidemiology, Patterns of Care, and Mortality for Patients With Acute Respiratory Distress Syndrome in Intensive Care Units in 50 Countries. *JAMA*. 2016;315(8):788-800.
45. Willis MS, Yates CC, Schisler JC. *Fibrosis in Disease: An Organ-Based Guide to Disease Pathophysiology and Therapeutic Considerations*: Springer; 2019.
46. Factor P, Mutlu GM, Chen L, Mohameed J, Akhmedov AT, Meng FJ, et al. Adenosine regulation of alveolar fluid clearance. *Proc Natl Acad Sci U S A*. 2007;104(10):4083-8.
47. Manicone AM. Role of the pulmonary epithelium and inflammatory signals in acute lung injury. *Expert Rev Clin Immunol*. 2009;5(1):63-75.

48. Shah D, Romero F, Stafstrom W, Duong M, Summer R. Extracellular ATP mediates the late phase of neutrophil recruitment to the lung in murine models of acute lung injury. *Am J Physiol Lung Cell Mol Physiol*. 2014;306(2):L152-61.
49. Belete HA, Hubmayr RD, Wang S, Singh RD. The role of purinergic signaling on deformation induced injury and repair responses of alveolar epithelial cells. *PLoS One*. 2011;6(11):e27469.
50. Ye H, Zhan Q, Ren Y, Liu X, Yang C, Wang C. Cyclic deformation-induced injury and differentiation of rat alveolar epithelial type II cells. *Respir Physiol Neurobiol*. 2012;180(2-3):237-46.
51. Pham T, Brochard LJ, Slutsky AS, editors. *Mechanical ventilation: state of the art*. Mayo Clinic Proceedings; 2017: Elsevier.
52. Ito S, Furuya K, Sokabe M, Hasegawa Y. Cellular ATP release in the lung and airway. *AIMS Biophysics*. 2016;3:571-84.
53. Liu M, Tanswell AK, Post M. Mechanical force-induced signal transduction in lung cells. *Am J Physiol*. 1999;277(4):L667-83.
54. Slutsky AS, Ranieri VM. Ventilator-induced lung injury. *N Engl J Med*. 2013;369(22):2126-36.
55. Santos RS, Maia Lda, Oliveira MV, Santos CL, Moraes L, Pinto EF, et al. Biologic impact of mechanical power at high and low tidal volumes in experimental mild acute respiratory distress syndrome. *Anesthesiology: The Journal of the American Society of Anesthesiologists*. 2018;128(6):1193-206.
56. Button B, Boucher RC, University of North Carolina Virtual Lung G. Role of mechanical stress in regulating airway surface hydration and mucus clearance rates. *Respir Physiol Neurobiol*. 2008;163(1-3):189-201.
57. Tschumperlin DJ, Oswari J, Margulies AS. Deformation-induced injury of alveolar epithelial cells. Effect of frequency, duration, and amplitude. *Am J Respir Crit Care Med*. 2000;162(2 Pt 1):357-62.
58. Vlahakis NE, Schroeder MA, Limper AH, Hubmayr RD. Stretch induces cytokine release by alveolar epithelial cells in vitro. *Am J Physiol*. 1999;277(1):L167-73.

59. Li L-F, Ouyang B, Choukroun G, Matyal R, Mascarenhas M, Jafari B, et al. Stretch-induced IL-8 depends on c-Jun NH2-terminal and nuclear factor- κ B-inducing kinases. *American Journal of Physiology-Lung Cellular and Molecular Physiology*. 2003;285(2):L464-L75.
60. Rich PB, Douillet CD, Mahler SA, Husain SA, Boucher RC. Adenosine triphosphate is released during injurious mechanical ventilation and contributes to lung edema. *Journal of Trauma and Acute Care Surgery*. 2003;55(2):290-7.
61. Zimmerman JJ, von Saint André-von Arnim A, McLaughlin J. *Cellular Respiration. Pediatric Critical Care: Elsevier*; 2011. p. 1058-72.
62. Sabirov RZ, Okada Y. ATP release via anion channels. *Purinergic Signal*. 2005;1(4):311-28.
63. Eltzschig HK, Sitkovsky MV, Robson SC. Purinergic signaling during inflammation. *N Engl J Med*. 2012;367(24):2322-33.
64. Frey PA, Arabshahi A. Standard free energy change for the hydrolysis of the alpha, beta-phosphoanhydride bridge in ATP. *Biochemistry*. 1995;34(36):11307-10.
65. Wang C, Huang W, Liao JL. QM/MM investigation of ATP hydrolysis in aqueous solution. *J Phys Chem B*. 2015;119(9):3720-6.
66. Burnstock G, Verkhratsky A. *Mechanisms of ATP release and inactivation. Purinergic signalling and the nervous system: Springer*; 2012. p. 79-118.
67. Zhou J, Alvarez-Elizondo MB, Botvinick E, George SC. Adenosine A1 and prostaglandin e receptor 3 receptors mediate global airway contraction after local epithelial injury. *American journal of respiratory cell and molecular biology*. 2013;48(3):299-305.
68. Ransford GA, Fregien N, Qiu F, Dahl G, Conner GE, Salathe M. Pannexin 1 contributes to ATP release in airway epithelia. *Am J Respir Cell Mol Biol*. 2009;41(5):525-34.
69. Fois G, Winkelmann VE, Bareis L, Staudenmaier L, Hecht E, Ziller C, et al. ATP is stored in lamellar bodies to activate vesicular P2X4 in an autocrine fashion upon exocytosis. *The Journal of general physiology*. 2018;150(2):277-91.
70. Dosch M, Gerber J, Jebbawi F, Beldi G. Mechanisms of ATP Release by Inflammatory Cells. *Int J Mol Sci*. 2018;19(4):1222.
71. Rajagopal S, Ponnusamy M. P2Y Receptor. *Metabotropic GPCRs: TGR5 and P2Y Receptors in Health and Diseases: Springer*; 2018. p. 39-55.

72. Lazarowski ER. Vesicular and conductive mechanisms of nucleotide release. *Purinergic Signal*. 2012;8(3):359-73.
73. Burnstock G, Brouns I, Adriaensen D, Timmermans JP. Purinergic signaling in the airways. *Pharmacol Rev*. 2012;64(4):834-68.
74. Burnstock G. Historical review: ATP as a neurotransmitter. *Trends in pharmacological sciences*. 2006;27(3):166-76.
75. Lazarowski ER, Boucher RC. Purinergic receptors in airway epithelia. *Curr Opin Pharmacol*. 2009;9(3):262-7.
76. Burnstock G, Verkhratsky A. Early history of purinergic signalling. *Purinergic Signalling and the Nervous System*: Springer; 2012. p. 7-66.
77. Burnstock G, Knight GE. Cell culture: complications due to mechanical release of ATP and activation of purinoceptors. *Cell and tissue research*. 2017;370(1):1-11.
78. Yegutkin GG. Nucleotide- and nucleoside-converting ectoenzymes: Important modulators of purinergic signalling cascade. *Biochim Biophys Acta*. 2008;1783(5):673-94.
79. Chambers LA, Rollins BM, Tarran R. Liquid movement across the surface epithelium of large airways. *Respir Physiol Neurobiol*. 2007;159(3):256-70.
80. Picher M, Boucher RC. Human airway ecto-adenylate kinase. A mechanism to propagate ATP signaling on airway surfaces. *J Biol Chem*. 2003;278(13):11256-64.
81. Pelleg A, Polosa R. Adenosine Receptors in the Lungs. *The Adenosine Receptors*: Springer; 2018. p. 461-70.
82. Stefan C, Jansen S, Bollen M. NPP-type ectophosphodiesterases: unity in diversity. *Trends Biochem Sci*. 2005;30(10):542-50.
83. Velasquez S, Eugenin EA. Role of Pannexin-1 hemichannels and purinergic receptors in the pathogenesis of human diseases. *Front Physiol*. 2014;5:96.
84. Tatur S, Kreda S, Lazarowski E, Grygorczyk R. Calcium-dependent release of adenosine and uridine nucleotides from A549 cells. *Purinergic Signal*. 2008;4(2):139-46.
85. Woods PS, Doolittle LM, Hickman-Davis JM, Davis IC. ATP catabolism by tissue nonspecific alkaline phosphatase contributes to development of ARDS in influenza-infected mice. *Am J Physiol Lung Cell Mol Physiol*. 2018;314(1):L83-L92.

86. Ahmad S, Ahmad A, McConville G, Schneider BK, Allen CB, Manzer R, et al. Lung epithelial cells release ATP during ozone exposure: signaling for cell survival. *Free Radic Biol Med.* 2005;39(2):213-26.
87. Akopova I, Tatur S, Grygorczyk M, Luchowski R, Gryczynski I, Gryczynski Z, et al. Imaging exocytosis of ATP-containing vesicles with TIRF microscopy in lung epithelial A549 cells. *Purinergic Signal.* 2012;8(1):59-70.
88. Takahara N, Ito S, Furuya K, Naruse K, Aso H, Kondo M, et al. Real-time imaging of ATP release induced by mechanical stretch in human airway smooth muscle cells. *Am J Respir Cell Mol Biol.* 2014;51(6):772-82.
89. Okada SF, Ribeiro CM, Sesma JI, Seminario-Vidal L, Abdullah LH, van Heusden C, et al. Inflammation promotes airway epithelial ATP release via calcium-dependent vesicular pathways. *Am J Respir Cell Mol Biol.* 2013;49(5):814-20.
90. Button B, Okada SF, Frederick CB, Thelin WR, Boucher RC. Mechanosensitive ATP release maintains proper mucus hydration of airways. *Sci Signal.* 2013;6(279):ra46.
91. Tarran R, Button B, Picher M, Paradiso AM, Ribeiro CM, Lazarowski ER, et al. Normal and cystic fibrosis airway surface liquid homeostasis. The effects of phasic shear stress and viral infections. *J Biol Chem.* 2005;280(42):35751-9.
92. Nagel G, Barbry P, Chabot H, Brochiero E, Hartung K, Grygorczyk R. CFTR fails to inhibit the epithelial sodium channel ENaC expressed in *Xenopus laevis* oocytes. *J Physiol.* 2005;564(Pt 3):671-82.
93. Briel M, Greger R, Kunzelmann K. Cl⁻ transport by cystic fibrosis transmembrane conductance regulator (CFTR) contributes to the inhibition of epithelial Na⁺ channels (ENaCs) in *Xenopus* oocytes co-expressing CFTR and ENaC. *J Physiol.* 1998;508 (Pt 3)(3):825-36.
94. Seminario-Vidal L, Kreda S, Jones L, O'Neal W, Trejo J, Boucher RC, et al. Thrombin promotes release of ATP from lung epithelial cells through coordinated activation of rho- and Ca²⁺-dependent signaling pathways. *Journal of Biological Chemistry.* 2009;284(31):20638-48.
95. Hansen M, Boitano S, Dirksen ER, Sanderson MJ. Intercellular calcium signaling induced by extracellular adenosine 5'-triphosphate and mechanical stimulation in airway epithelial cells. *J Cell Sci.* 1993;106 (Pt 4)(4):995-1004.

96. Tanaka K, Choi J, Cao Y, Stacey G. Extracellular ATP acts as a damage-associated molecular pattern (DAMP) signal in plants. *Frontiers in plant science*. 2014;5:446.
97. Kouzaki H, Iijima K, Kobayashi T, O'Grady SM, Kita H. The danger signal, extracellular ATP, is a sensor for an airborne allergen and triggers IL-33 release and innate Th2-type responses. *The Journal of Immunology*. 2011;186(7):4375-87.
98. Riteau N, Gasse P, Fauconnier L, Gombault A, Couegnat M, Fick L, et al. Extracellular ATP is a danger signal activating P2X7 receptor in lung inflammation and fibrosis. *American journal of respiratory and critical care medicine*. 2010;182(6):774-83.
99. Lopez-Castejon G, Brough D. Understanding the mechanism of IL-1 β secretion. *Cytokine & growth factor reviews*. 2011;22(4):189-95.
100. Leist M, Single B, Castoldi AF, Kühnle S, Nicotera P. Intracellular adenosine triphosphate (ATP) concentration: a switch in the decision between apoptosis and necrosis. *Journal of Experimental Medicine*. 1997;185(8):1481-6.
101. Sikora J, Orlov SN, Furuya K, Grygorczyk R. Hemolysis is a primary ATP-release mechanism in human erythrocytes. *Blood*. 2014;124(13):2150-7.
102. Reddy MM, Quinton PM, Haws C, Wine JJ, Grygorczyk R, Tabcharani JA, et al. Failure of the cystic fibrosis transmembrane conductance regulator to conduct ATP. *Science*. 1996;271(5257):1876-9.
103. Grygorczyk R, Hanrahan JW. CFTR-independent ATP release from epithelial cells triggered by mechanical stimuli. *Am J Physiol*. 1997;272(3 Pt 1):C1058-66.
104. Kang J, Kang N, Lovatt D, Torres A, Zhao Z, Lin J, et al. Connexin 43 hemichannels are permeable to ATP. *J Neurosci*. 2008;28(18):4702-11.
105. Bao L, Sachs F, Dahl G. Connexins are mechanosensitive. *Am J Physiol Cell Physiol*. 2004;287(5):C1389-95.
106. Bao L, Locovei S, Dahl G. Pannexin membrane channels are mechanosensitive conduits for ATP. *FEBS Lett*. 2004;572(1-3):65-8.
107. Qu Y, Misaghi S, Newton K, Gilmour LL, Louie S, Cupp JE, et al. Pannexin-1 is required for ATP release during apoptosis but not for inflammasome activation. *The Journal of Immunology*. 2011;186(11):6553-61.

108. Taruno A. ATP Release Channels. *Int J Mol Sci.* 2018;19(3):808.
109. Grygorczyk R, Boudreault F, Tan JJ, Ponomarchuk O, Sokabe M, Furuya K. Mechanosensitive ATP release in the lungs: New insights from real-time luminescence imaging studies. *Curr Top Membr.* 2019;83:45-76.
110. Sawada K, Echigo N, Juge N, Miyaji T, Otsuka M, Omote H, et al. Identification of a vesicular nucleotide transporter. *Proc Natl Acad Sci U S A.* 2008;105(15):5683-6.
111. Rudnick G. Vesicular ATP transport is a hard (V) NUT to crack. *Proceedings of the National Academy of Sciences.* 2008;105(16):5949-50.
112. Sesma JI, Kreda SM, Okada SF, van Heusden C, Moussa L, Jones LC, et al. Vesicular nucleotide transporter regulates the nucleotide content in airway epithelial mucin granules. *Am J Physiol Cell Physiol.* 2013;304(10):C976-84.
113. Waters CM, Sporn PH, Liu M, Fredberg JJ. Cellular biomechanics in the lung. *Am J Physiol Lung Cell Mol Physiol.* 2002;283(3):L503-9.
114. Suki B, Ito S, Stamenovic D, Lutchen KR, Ingenito EP. Biomechanics of the lung parenchyma: critical roles of collagen and mechanical forces. *J Appl Physiol* (1985). 2005;98(5):1892-9.
115. Schumacker PT. Straining to understand mechanotransduction in the lung. *Am J Physiol Lung Cell Mol Physiol.* 2002;282(5):L881-2.
116. Trepast X, Grabulosa M, Puig F, Maksym GN, Navajas D, Farre R. Viscoelasticity of human alveolar epithelial cells subjected to stretch. *Am J Physiol Lung Cell Mol Physiol.* 2004;287(5):L1025-34.
117. Sanchez-Esteban J, Cicchiello LA, Wang Y, Tsai SW, Williams LK, Torday JS, et al. Mechanical stretch promotes alveolar epithelial type II cell differentiation. *J Appl Physiol* (1985). 2001;91(2):589-95.
118. Boudreault F, Tschumperlin DJ. Stretch-induced mitogen-activated protein kinase activation in lung fibroblasts is independent of receptor tyrosine kinases. *American journal of respiratory cell and molecular biology.* 2010;43(1):64-73.

119. Correa-Meyer E, Pesce L, Guerrero C, Sznajder JI. Cyclic stretch activates ERK1/2 via G proteins and EGFR in alveolar epithelial cells. *Am J Physiol Lung Cell Mol Physiol*. 2002;282(5):L883-91.
120. Hamanaka K, Jian MY, Weber DS, Alvarez DF, Townsley MI, Al-Mehdi AB, et al. TRPV4 initiates the acute calcium-dependent permeability increase during ventilator-induced lung injury in isolated mouse lungs. *Am J Physiol Lung Cell Mol Physiol*. 2007;293(4):L923-32.
121. Seminario-Vidal L, Okada SF, Sesma JI, Kreda SM, van Heusden CA, Zhu Y, et al. Rho signaling regulates pannexin 1-mediated ATP release from airway epithelia. *J Biol Chem*. 2011;286(30):26277-86.
122. Boudreault F, Grygorczyk R. Cell swelling-induced ATP release and gadolinium-sensitive channels. *Am J Physiol Cell Physiol*. 2002;282(1):C219-26.
123. Braunstein GM, Roman RM, Clancy JP, Kudlow BA, Taylor AL, Shylonsky VG, et al. Cystic fibrosis transmembrane conductance regulator facilitates ATP release by stimulating a separate ATP release channel for autocrine control of cell volume regulation. *J Biol Chem*. 2001;276(9):6621-30.
124. Boudreault F, Grygorczyk R. Cell swelling-induced ATP release is tightly dependent on intracellular calcium elevations. *The Journal of physiology*. 2004;561(2):499-513.
125. Groulx N, Boudreault F, Orlov SN, Grygorczyk R. Membrane reserves and hypotonic cell swelling. *J Membr Biol*. 2006;214(1):43-56.
126. Tatur S, Groulx N, Orlov SN, Grygorczyk R. Ca²⁺-dependent ATP release from A549 cells involves synergistic autocrine stimulation by coreleased uridine nucleotides. *J Physiol*. 2007;584(Pt 2):419-35.
127. Ramsingh R, Grygorczyk A, Solecki A, Cherkaoui LS, Berthiaume Y, Grygorczyk R. Cell deformation at the air-liquid interface induces Ca²⁺-dependent ATP release from lung epithelial cells. *American Journal of Physiology-Lung Cellular and Molecular Physiology*. 2011;300(4):L587-L95.
128. Grygorczyk R, Furuya K, Sokabe M. Imaging and characterization of stretch-induced ATP release from alveolar A549 cells. *J Physiol*. 2013;591(5):1195-215.

129. Furuya K, Sokabe M, Grygorczyk R. Real-time luminescence imaging of cellular ATP release. *Methods*. 2014;66(2):330-44.
130. Furuya K, Tan JJ, Boudreault F, Sokabe M, Berthiaume Y, Grygorczyk R. Real-time imaging of inflation-induced ATP release in the ex vivo rat lung. *Am J Physiol Lung Cell Mol Physiol*. 2016;311(5):L956-L69.
131. Mikolajewicz N, Mohammed A, Morris M, Komarova SV. Mechanically stimulated ATP release from mammalian cells: systematic review and meta-analysis. *J Cell Sci*. 2018;131(22):jcs223354.
132. Morciano G, Sarti AC, Marchi S, Missiroli S, Falzoni S, Raffaghello L, et al. Use of luciferase probes to measure ATP in living cells and animals. *Nature protocols*. 2017;12(8):1542.
133. Nakatsu T, Ichiyama S, Hiratake J, Saldanha A, Kobashi N, Sakata K, et al. Structural basis for the spectral difference in luciferase bioluminescence. *Nature*. 2006;440(7082):372-6.
134. Wood KV, Lam YA, McElroy WD. Introduction to beetle luciferases and their applications. *Journal of bioluminescence and chemiluminescence*. 1989;4(1):289-301.
135. Pellegatti P, Falzoni S, Pinton P, Rizzuto R, Di Virgilio F. A novel recombinant plasma membrane-targeted luciferase reveals a new pathway for ATP secretion. *Mol Biol Cell*. 2005;16(8):3659-65.
136. Taylor AL, Kudlow BA, Marrs KL, Gruenert DC, Guggino WB, Schwiebert EM. Bioluminescence detection of ATP release mechanisms in epithelia. *Am J Physiol*. 1998;275(5):C1391-406.
137. Tan JJ, Ponomarchuk O, Grygorczyk R, Boudreault F. Wide field of view quantitative imaging of cellular ATP release. *Am J Physiol Cell Physiol*. 2019;317(3):C566-C75.
138. Sucre JMS, Jetter CS, Loomans H, Williams J, Plosa EJ, Benjamin JT, et al. Successful Establishment of Primary Type II Alveolar Epithelium with 3D Organotypic Coculture. *Am J Respir Cell Mol Biol*. 2018;59(2):158-66.
139. Isakson BE, Seedorf GJ, Lubman RL, Evans WH, Boitano S. Cell-cell communication in heterocellular cultures of alveolar epithelial cells. *American journal of respiratory cell and molecular biology*. 2003;29(5):552-61.

140. Tan JJ, Boudreault F, Adam D, Brochiero E, Grygorczyk R. Type 2 secretory cells are primary source of ATP release in mechanically stretched lung alveolar cells. *Am J Physiol Lung Cell Mol Physiol*. 2020;318(1):L49-L58.
141. Tschumperlin DJ, Margulies SS. Equibiaxial deformation-induced injury of alveolar epithelial cells in vitro. *Am J Physiol*. 1998;275(6):L1173-83.
142. Skotak M, Wang F, Chandra N. An in vitro injury model for SH-SY5Y neuroblastoma cells: effect of strain and strain rate. *J Neurosci Methods*. 2012;205(1):159-68.
143. Chen W, Guidotti G. Soluble apyrases release adp during ATP hydrolysis. *Biochem Biophys Res Commun*. 2001;282(1):90-5.
144. Tan J, Furuya K, Boudreault F, Brochiero E, Grygorczyk R. Mechanisms of Inflation-Induced ATP Release in Ex Vivo Rat Lungs: A Bioluminescence Imaging Study. D108 MECHANISM OF LUNG INJURY: American Thoracic Society; 2019. p. A7245-A.
145. Wikenheiser KA, Vorbroker DK, Rice WR, Clark JC, Bachurski CJ, Oie HK, et al. Production of immortalized distal respiratory epithelial cell lines from surfactant protein C/simian virus 40 large tumor antigen transgenic mice. *Proc Natl Acad Sci U S A*. 1993;90(23):11029-33.
146. Riquelme MA, Cea LA, Vega JL, Boric MP, Monyer H, Bennett MV, et al. The ATP required for potentiation of skeletal muscle contraction is released via pannexin hemichannels. *Neuropharmacology*. 2013;75:594-603.
147. Granot Y, Rubinsky B. Mass Transfer Model for Drug Delivery in Tissue Cells with Reversible Electroporation. *Int J Heat Mass Transf*. 2008;51(23-24):5610-6.
148. Forsyth AM, Braunmuller S, Wan J, Franke T, Stone HA. The effects of membrane cholesterol and simvastatin on red blood cell deformability and ATP release. *Microvasc Res*. 2012;83(3):347-51.
149. Geddes DM, Cargill RS, 2nd, LaPlaca MC. Mechanical stretch to neurons results in a strain rate and magnitude-dependent increase in plasma membrane permeability. *J Neurotrauma*. 2003;20(10):1039-49.

150. Azarashvili T, Odinkova I, Krestinina O, Baburina Y, Grachev D, Teplova V, et al. Role of phosphorylation of porin (VDAC) in regulation of mitochondrial outer membrane under normal conditions and alcohol intoxication. *Biochemistry (Moscow) Supplement Series A: Membrane and Cell Biology*. 2011;5(1):11-20.
151. Edwards YS, Sutherland LM, Power JH, Nicholas TE, Murray AW. Cyclic stretch induces both apoptosis and secretion in rat alveolar type II cells. *FEBS letters*. 1999;448(1):127-30.
152. Hussein O, Walters B, Stroetz R, Valencia P, McCall D, Hubmayr RD. Biophysical determinants of alveolar epithelial plasma membrane wounding associated with mechanical ventilation. *Am J Physiol Lung Cell Mol Physiol*. 2013;305(7):L478-84.
153. Bi G-Q, Alderton JM, Steinhardt RA. Calcium-regulated exocytosis is required for cell membrane resealing. *The Journal of cell biology*. 1995;131(6):1747-58.
154. Cong X, Hubmayr RD, Li C, Zhao X. Plasma membrane wounding and repair in pulmonary diseases. *Am J Physiol Lung Cell Mol Physiol*. 2017;312(3):L371-L91.
155. Gajic O, Lee J, Doerr CH, Berrios JC, Myers JL, Hubmayr RD. Ventilator-induced cell wounding and repair in the intact lung. *Am J Respir Crit Care Med*. 2003;167(8):1057-63.
156. Tang SK, Marshall WF. Self-repairing cells: How single cells heal membrane ruptures and restore lost structures. *Science*. 2017;356(6342):1022-5.
157. Boucher E, Mandato CA. Plasma membrane and cytoskeleton dynamics during single-cell wound healing. *Biochim Biophys Acta*. 2015;1853(10 Pt A):2649-61.
158. Andrews NW, Corrotte M. Plasma membrane repair. *Curr Biol*. 2018;28(8):R392-R7.
159. Farkas O, Lifshitz J, Povlishock JT. Mechanoporation induced by diffuse traumatic brain injury: an irreversible or reversible response to injury? *J Neurosci*. 2006;26(12):3130-40.
160. LaPlaca MC, Lessing MC, Prado GR, Zhou R, Tate CC, Geddes-Klein D, et al. Mechanoporation is a potential indicator of tissue strain and subsequent degeneration following experimental traumatic brain injury. *Clinical Biomechanics*. 2019;64:2-13.
161. Krassowska W, Filev PD. Modeling electroporation in a single cell. *Biophys J*. 2007;92(2):404-17.
162. Hu Y, Wan JM, Yu AC. Membrane perforation and recovery dynamics in microbubble-mediated sonoporation. *Ultrasound Med Biol*. 2013;39(12):2393-405.

163. Helfield B, Chen X, Watkins SC, Villanueva FS. Biophysical insight into mechanisms of sonoporation. *Proceedings of the National Academy of Sciences*. 2016;113(36):9983-8.
164. Matsumoto D, Yamagishi A, Saito M, Sathuluri RR, Silberberg YR, Iwata F, et al. Mechanoporation of living cells for delivery of macromolecules using nanoneedle array. *Journal of bioscience and bioengineering*. 2016;122(6):748-52.
165. Kumar A, Mohan L, Shinde P, Chang H-Y, Nagai M, Santra TS. Mechanoporation: Toward Single Cell Approaches. *Handbook of Single Cell Technologies*. 2018:1-29.
166. Doerr CH, Gajic O, Berrios JC, Caples S, Abdel M, Lymp JF, et al. Hypercapnic acidosis impairs plasma membrane wound resealing in ventilator-injured lungs. *Am J Respir Crit Care Med*. 2005;171(12):1371-7.
167. Kawai Y, Wada F, Sugimura Y, Maki M, Hitomi K. Transglutaminase 2 activity promotes membrane resealing after mechanical damage in the lung cancer cell line A549. *Cell Biol Int*. 2008;32(8):928-34.
168. Godin LM, Vergen J, Prakash YS, Pagano RE, Hubmayr RD. Spatiotemporal dynamics of actin remodeling and endomembrane trafficking in alveolar epithelial type I cell wound healing. *Am J Physiol Lung Cell Mol Physiol*. 2011;300(4):L615-23.
169. Mikolajewicz N, Zimmermann EA, Willie BM, Komarova SV. Mechanically stimulated ATP release from murine bone cells is regulated by a balance of injury and repair. *Elife*. 2018;7:e37812.
170. Gonzalez RF, Allen L, Gonzales L, Ballard PL, Dobbs LG. HTII-280, a biomarker specific to the apical plasma membrane of human lung alveolar type II cells. *J Histochem Cytochem*. 2010;58(10):891-901.
171. Riedl J, Crevenna AH, Kessenbrock K, Yu JH, Neukirchen D, Bista M, et al. Lifeact: a versatile marker to visualize F-actin. *Nat Methods*. 2008;5(7):605-7.
172. van der Zee P, Somhorst P, Molinger J, Hasan D, Gommers D. A feasibility study into adenosine triphosphate measurement in exhaled breath condensate: a potential bedside method to monitor alveolar deformation. *Purinergic signalling*. 2018;14(3):215-21.

Appendices

Appendix A

- **Reference 109** (DOI: 10.1016/bs.ctm.2019.02.001)

Chapter: Chapter Three - Mechanosensitive ATP release in the lungs: New insights from real-time luminescence imaging studies

Book: Current Topics in Membranes (Volume: 83, Pages: 45-76, ISSN: 1063-5823)

Authors: Ryszard Grygorczyk, Francis Boudreault, Ju Jing Tan, Olga Ponomarchuk, Masahiro Sokabe, Kishio Furuya

Publisher: Elsevier

Date: 2019

Reproduced with the permission of Elsevier



Mechanosensitive ATP release in the lungs: New insights from real-time luminescence imaging studies

Ryszard Grygorczyk^{a,b,*}, Francis Boudreault^b, Ju Jing Tan^{a,b},
Olga Ponomarchuk^{b,c}, Masahiro Sokabe^d, Kishio Furuya^d

^aDepartment of Medicine, Université de Montréal, Montréal, QC, Canada

^bCentre de recherche, Centre hospitalier de l'Université de Montréal (CRCHUM), Montréal, QC, Canada

^cFaculty of Biology, M.V. Lomonosov Moscow State University, Moscow, Russia

^dMechanobiology Laboratory, Nagoya University, Graduate School of Medicine, Nagoya, Japan

*Corresponding author: e-mail address: ryszard.grygorczyk@umontreal.ca

Contents

1. Introduction	46
2. Approaches to bioluminescence imaging of cellular ATP release	49
2.1 Real-time luminescence imaging of ATP release	49
2.2 Simplified systems for bioluminescence ATP imaging	52
3. Mechanisms of ATP release	53
3.1 ATP release stimuli	53
3.2 Non-lytic ATP release pathways	53
3.3 ATP release by cell membrane injury and cell lysis	57
4. Mechanosensitive ATP release in lung epithelial cells	58
4.1 Stretch-induced ATP release in A549 alveolar cells	58
4.2 Stretch induces coordinated ATP release in rat primary alveolar type 2 cells	60
4.3 Two components of stretch-induced ATP release in Calu-3 cells	62
4.4 Hypotonic stress-induced ATP release in A549 cells—Contribution of cell lysis	63
5. Inflation-induced ATP release in ex vivo lungs	65
5.1 ATP release in airspaces	65
5.2 ATP release in pulmonary blood vessels	67
6. Conclusions and future directions	68
Reference	70

Abstract

Extracellular ATP and other nucleotides are important autocrine/paracrine mediators that stimulate purinergic receptors and regulate diverse processes in the normal lungs. They are also associated with pathogenesis of a number of respiratory diseases and

clinical complications including acute respiratory distress syndrome and ventilator induced lung injury. Mechanical forces are major stimuli for cellular ATP release but precise mechanisms responsible for this release are still debated. The present review intends to provide the current state of knowledge of the mechanisms of ATP release in the lung. Putative pathways of the release, including the contribution of cell membrane injury and cell lysis are discussed addressing their strength, weaknesses and missing evidence that requires future study. We also provide an overview of the recent technical advances in studying cellular ATP release in vitro and ex vivo. Special attention is given to new insights into lung ATP release obtained with the real-time luminescence ATP imaging. This includes recent data on stretch-induced mechanosensitive ATP release in a model and primary cells of lung alveoli in vitro as well as inflation-induced ATP release in airspaces and pulmonary blood vessels of lungs, ex vivo.



1. Introduction

Intercellular communication initiated by the release of purines as signaling molecules appears to be the most primitive and widespread autocrine and paracrine mechanism in most, if not all, organs and tissues (Burnstock, 2006). The downstream purinergic signaling system consists of a large family of G protein-coupled adenosine (Ado) receptors, P2Y receptors, as well as ionotropic P2X receptors, Fig. 1. Several families of extracellular enzymes contribute to signal diversification by converting/metabolizing one nucleotide species into another, while at the same time, providing a mechanism for the termination of purinergic signals (Abbracchio, Burnstock, Verkhratsky, & Zimmermann, 2009; Lazarowski & Boucher, 2009). With over 50 membrane components or processes involved, it is considered as one of the most versatile signaling system (Novak, 2011). Range of action of the extracellular nucleotides can considerably expand by stimulating the release of other extracellular messengers, which in turn activate additional cellular mechanisms through their own receptors. These include neurotransmitters, hormones, growth factors and other proteins including enzymes, cytokines, lipid mediators, nitric oxide and reactive oxygen species (Zimmermann, 2016). Despite the fundamental importance of purinergic signaling in a variety of physiological and pathophysiological processes in all organs and tissues, the mechanism of the initiating step of this cascade—nucleotide release remains poorly understood (Burnstock, 2008, 2009; Lazarowski, Sesma, Seminario-Vidal, & Kreda, 2011; Praetorius & Leipziger, 2009). This contrasts with enormous progress in molecular and pharmacological characterization of purinergic receptors and purine metabolizing ecto-enzymes (Jacobson & Muller, 2016; Zimmermann, 2000; Zimmermann, Zebisch, & Strater, 2012).

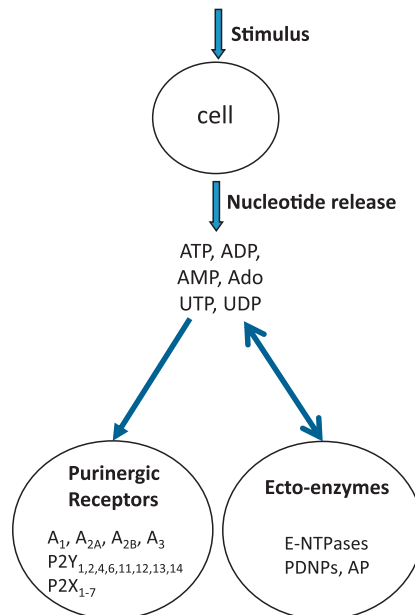


Fig. 1 Purinergic signaling system. Purinergic signaling cascade is initiated by the release of adenosine and uridine nucleotides and their metabolites to the extracellular space. Release pathway may include non-lytic mechanisms (exocytosis, ionic channels) but also plasma membrane injury and cell lysis. Purinergic receptor families include: metabotropic A_1 , A_{2A} , A_{2B} , A_3 —adenosine receptors, $P2Y_{1, 2, 4, 6, 11, 12, 13, 14}$ —receptors, and ionotropic $P2X_{1-7}$ —receptors. Extracellular nucleotides are subjected to hydrolysis and interconversion by secreted and cell surface-attached enzymes that include: ecto-nucleoside triphosphate diphosphohydrolases (E-NTPase), nucleotide pyrophosphatase/phosphodiesterase (PDNP) and alkaline phosphatase (AP).

Purinergic signaling plays important role in vast range of processes in normal and diseased lungs (Burnstock, Brouns, Adriaensen, & Timmermans, 2012; Picher & Boucher, 2011). Extracellular such as ATP, UTP, UDP and Ado modulate multiple components of innate lung defense by controlling ion transport and airway surface liquid homeostasis (Button, Okada, Frederick, Thelin, & Boucher, 2013; Lazarowski et al., 2004; Tarran, 2004), mucus secretion, and ciliary beat (Bucheimer & Linden, 2004; Kreda et al., 2007; Paradiso, Ribeiro, & Boucher, 2001; Ramminger et al., 1999; Stutts, Fitz, Paradiso, & Boucher, 1994). Nucleotides also regulate surfactant secretion by alveolar type 2 (AT2) pneumocytes (Andreeva, Kutuzov, & Voyno-Yasenetskaya, 2007; Patel et al., 2005). Extracellular nucleotide signaling is modified in and contributes to several respiratory pathologies. In clinical settings, significantly elevated levels of extracellular ATP and other purines were found in mechanically ventilated lungs, as

detected in vivo in broncho-alveolar lavage fluids (Verbrugge, de Jong, Keijzer, Vazquez de Anda, & Lachmann, 1999), contributing to altered luminal nucleotide composition and purinoreceptor expression profile as well as promoting IL-6 release and lung edema (Douillet, Robinson, Milano, Boucher, & Rich, 2006; Rich, Douillet, Mahler, Husain, & Boucher, 2003). Accumulating evidence supports major role of extracellular ATP and purinergic signaling in pathophysiology of asthma and chronic obstructive pulmonary diseases (COPD) (Adriaensen & Timmermans, 2004; Aliagas et al., 2018; Idzko et al., 2007; Lommatzsch et al., 2010; Mortaz, Folkerts, Nijkamp, & Henricks, 2010; Pelleg, Schulman, & Barnes, 2016), lung emphysema (Mortaz et al., 2009), and pulmonary fibrosis (Della, Cabiati, Rocchiccioli, Del, & Morales, 2013; Muller et al., 2017). In the airways of cystic fibrosis patients, purinergic control of mucus and pathogen clearance are dysregulated, in part, due to extensive remodeling of purine enzymatic network. The changes involve altered activity, expression, and tissue distribution of NTPDase1 and NTPDase3, the two ectonucleotidases critical for the regulation of ATP on airway surfaces (Fausther, Pelletier, Ribeiro, Sevigny, & Picher, 2010).

Extracellular ATP in the lungs may originate not only from cell-regulated release but also from cell membrane injury and cell lysis. Clinical trials have shown that improperly delivered mechanical ventilation (MV) may worsen or cause lung injury (Dreyfuss, Soler, Basset, & Saumon, 1988; Sugiura, McCulloch, Wren, Dawson, & Froese, 1994). With large tidal volumes, MV produces alveolar overdistension that can be injurious by direct physical disruption of anatomical structures, cell-cell contacts, cell membranes, and stimulate inflammation (Cereda et al., 2013; Uhlig & Uhlig, 2011). The resulting ventilator induced lung injury is characterized by an increased alveolar permeability, pulmonary edema, infiltration of neutrophils, and the release of inflammatory mediators, including ATP (Jaecklin et al., 2011; Nickles et al., 2014; Rich et al., 2003; Tschumperlin, Oswari, & Margulies, 2000). Massive ATP release due to disruption or permeabilization of cell plasma membrane saturates the ATP-hydrolyzing enzyme system (CD39/CD73) (Hasan et al., 2018), leading to its sustained high levels acting as a “danger signal” a component of DAMPs (damage-associated molecular patterns), activating proinflammatory responses via immune cell’s purinergic receptors (Hasan, Blankman, & Nieman, 2017; Mishra, 2013).

To identify ATP release pathways and to map time-dependent distribution of secreted ATP, accurate measurement techniques are required that could provide quantitative spatial and temporal information on extracellular

ATP. Only recently advanced ATP imaging approaches have been developed enabling precise investigation of cellular ATP release in real time and at the single cell level in vitro and ex vivo, capable of providing new insights into the release pathways.



2. Approaches to bioluminescence imaging of cellular ATP release

Several techniques were developed to detect and measure extracellular ATP, including non-imaging approaches such as amperometric ATP electrodes, use of P2X receptor-mediated ion currents as biosensor, as well as fluorescence-based or luciferin-luciferase (LL) bioluminescence methods that may permit ATP imaging, reviewed by [Praetorius and Leipziger \(2009\)](#), [Rajendran, Dane, Conley, and Tantama \(2016\)](#)). The standard approach to study ATP efflux from cells mainly involves collecting aliquots of bulk extracellular solution and subsequent off-line ATP analysis by highly sensitive LL bioluminescence assay. It detects light generated by ATP-dependent luciferase-mediated substrate oxidation, e.g., of D-luciferin, by the commonly used firefly luciferase. The assay could be used for real-time measurements of bulk ATP, e.g., by placing cell cultures covered with LL-containing medium directly in the luminometer measurement chamber. Development of cell surface-attached luciferase allowed monitoring local ATP concentration at the extracellular cell surface in real time ([Beigi, Kobatake, Aizawa, & Dubyak, 1999](#)). However, none of these approaches provides spatial information that would allow not only identification of specific sites or cells releasing ATP but also its quantification and time-dependent spreading toward other cells. Such information is relevant to understand the mechanisms of the release and autocrine/paracrine effects of secreted ATP. In the past decade much effort has been devoted toward direct visualization of extracellular ATP in living systems in real time.

2.1 Real-time luminescence imaging of ATP release

One of the experimental approaches that is compatible with live specimens and provides spatio-temporal insights into the ATP-release process involves real-time visualization of ATP-dependent LL bioluminescence. In this approach, a specimen such as substrate-attached cells is covered with DMEM culture medium containing the LL mixture. After stimulation, e.g., by brief stretching of the flexible substrate, the released ATP reacts with LL, producing photons, [Fig. 2A](#).

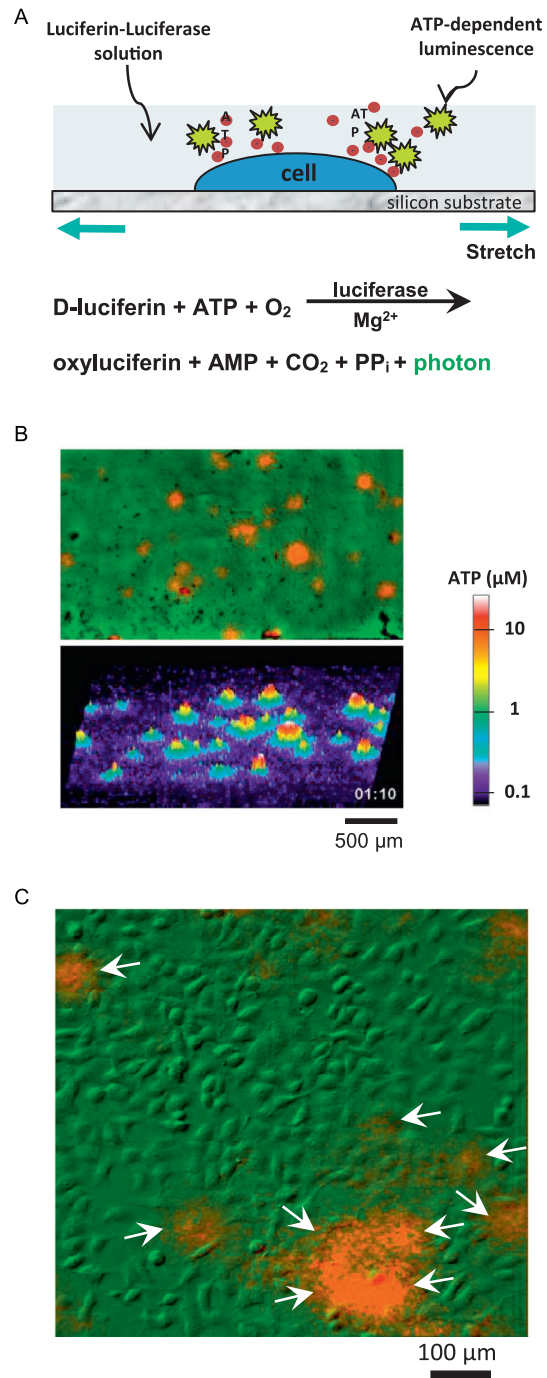


Fig. 2 See figure legend on opposite page.

The major challenge to imaging rapid release of ATP is low-light signal generated by bioluminescence reaction, which imposes substantial constraints on spatial and temporal resolution of ATP detection by this approach. However, continuing improvements in low-light imaging technology allowed high-sensitivity light detection, sufficient for real-time imaging of ATP-dependent luminescence, first reported by [Furuya, Harada, and Sokabe \(2008\)](#) and then used in several subsequent studies ([Grygorczyk, Furuya, & Sokabe, 2013](#); [Murata et al., 2014](#); [Takahara et al., 2014](#); [Yamamoto et al., 2011](#)). Their luminescence imaging microscopy system combines a cooled electron-multiplying charge-coupled device (EMCCD) camera coupled with a water-cooled image intensifier and low-magnification, high numerical aperture (NA) objective. It provides a signal-to-noise ratio sufficient to study ATP release from single cells with ~ 10 nM detection sensitivity and 100 ms temporal resolution ([Furuya, Sokabe, & Grygorczyk, 2014](#)). An example image of stretch-induced ATP release from A549 cells is shown in [Fig. 2B](#) and [C](#). It provides spatio-temporal information on absolute ATP concentration and its diffusion from the release points, that is not possible to obtain with standard luminometry. The system is also equipped with a unique infra-red (IR) differential interference contrast (DIC) imaging, allowing simultaneous identification of ATP-releasing cells and assessing the extent of cell distension during stretch-stimulation. Further instrumental details of the approach could be found in [Furuya et al. \(2014\)](#). The imaging system described here enabled us to investigate ATP release in several cell types and tissues including *ex vivo* lungs ([Furuya et al., 2016](#)), providing new insights into the release mechanisms and purinergic signaling in different biological systems.

Fig. 2 Principles of bioluminescence ATP release imaging. (A) A concept of ATP release imaging via ATP-dependent luciferin-luciferase (LL) luminescence *in vitro*. Cells are covered with DMEM medium containing LL mixture and stimulated by brief (1 s) stretching. Released ATP reacts with LL producing photons. (B) Example image of stretch-induced ATP release from A549 cells. The image is an overlay of DIC IR image of cells grown on silicon substrate (green), and ATP-dependent LL luminescence (red). Image below shows local ATP concentration as pseudo-3D intensity profile where the pseudo-colored luminescence intensity was converted to height. (C) Stretch-induced ATP release from A549 cells recorded at higher magnification with $20\times$ objective reveals that ATP release sites are single cells. The image overlay (green—DIC IR image, red—ATP-dependent luminescence) reveals that ATP is released from single cells (indicated by arrows). *Panel C: The image was taken 3 s after 25% stretch, from Grygorczyk, R., Furuya, K., & Sokabe, M. (2013). Imaging and characterization of stretch-induced ATP release from alveolar A549 cells. The Journal of Physiology, 591, 1195–1215.*

Importantly, the LL is non-toxic for cells and they remain viable for many hours of experimentation. However, similar to the standard LL luminometry, when performing live cell luminescence imaging, attention should be given to potential interference with LL reaction when pharmacological or other interventions (e.g., pH or ion concentration changes) are applied. Bioluminescence signal calibration and verification of its stability over time should be performed for each experimental condition to ensure proper performance of the imaging system.

2.2 Simplified systems for bioluminescence ATP imaging

In the luminescence microscopy system described above, the high sensitivity of light detection was achieved by combining EMCCD camera and specialized low-noise liquid-cooled image intensifier, that results in an overall complexity, precluding its wider use by many laboratories. However, recent improvements in the sensitivity of EMCCD cameras allow observation of stronger ATP release events without image intensifier, albeit with reduced ATP detection sensitivity ($\sim 10 \mu\text{M}$). We have used such simplified system successfully in part of our study of stretch-induced ATP release in primary rat alveolar AT2 cells, described in [Section 4.2](#). Other alternative approaches involve enhancing the light signal captured by the camera. Typical modern microscopes are designed with infinity optics allowing their versatile use with different optical components. However, this comes at the cost of reduced light gathering power, a critical factor for low-light imaging. Therefore, in an alternative approach to avoid these limitations, we used a simple optical system directly mounted on the EMCCD camera, instead of microscope. The system consists of two lenses with a shorter optical path and bigger NA-to-magnification ratio, providing wide field of view (FOV) imaging with significantly boosted light-gathering power, largely exceeding (>50 -fold) those of standard microscopes. This straightforward and cost-affordable approach enabled us to image the whole stretch chamber (approx. $20 \times 20 \text{ mm}$) with cultured rat primary AT2 cells to easily and accurately track the kinetics of stretch-induced secretion of ATP and to map and quantify its time-dependent distribution. Quantitative ATP imaging is required to gain new insights into the mechanisms of cellular ATP release, which are otherwise difficult to assess with a standard microscope that visualizes secreted ATP in spatially restricted regions of interest and lacks the ability of quantifying released ATP in the entire chamber/specimen.



3. Mechanisms of ATP release

3.1 ATP release stimuli

Release of ATP into the extracellular space is a common cellular response to various physical stimuli, which may involve mechanical cell stretch and deformation caused by physical tissue distension (Furuya et al., 2016; Grygorczyk et al., 2013; Sadananda, Kao, Liu, Mansfield, & Burcher, 2012), fluid- or air-flow shear stress (Tarran, Button, & Boucher, 2006; Yamamoto et al., 2011), cell distortion by tension forces at the air-liquid interface (Ramsingh et al., 2011), mechanical stress between motile cilia and mucus layer on airway surfaces (Button et al., 2013), or in vitro hypotonic cell swelling or tilting cell culture plate (Grygorczyk & Hanrahan, 1997a). While mechanical cell stimulation appears by far the most widespread inducer of ATP secretion in all cell types (Mikolajewicz, Mohammed, Morris, & Komarova, 2018), other known stimuli include agonist-dependent receptor-mediated release, where agonists may include thrombin via Ca^{2+} , and Rho-mediated signaling (Seminario-Vidal et al., 2009), and purines themselves (via P2-receptors), resulting in ATP-induced ATP release (Anderson, Bergher, & Swanson, 2004). A spectrum of other nucleotides is co-released with ATP, including adenosine and uridine nucleotides (Kreda et al., 2010; Tatur, Groulx, Orlov, & Grygorczyk, 2007; Tatur, Kreda, Lazarowski, & Grygorczyk, 2008), that can also amplify ATP release by synergistic autocrine/paracrine action on purinergic receptors (Tatur et al., 2007). Interestingly, light-induced ATP release mediated by photoreceptor melanopsin has been recently reported in lens epithelial cells (Pintor, 2018).

3.2 Non-lytic ATP release pathways

ATP release pathways were discussed in previous comprehensive reviews (Lazarowski, Boucher, & Harden, 2003; Praetorius & Leipziger, 2009). There are two major pathways of cellular ATP release: non-lytic (or cell-regulated) and lytic. The non-lytic mode of ATP release is generally divided into conductive (ionic channels) and non-conductive pathways such as exocytosis, with the latter further divided into regulated (Ca^{2+} -dependent) and non-regulated exocytosis (Lazarowski et al., 2011). Cell lysis resulting from plasma membrane rupture allowing the free discharge of cytoplasmic ATP can be induced by physical or chemical stressors; the damage can be transient

or can lead to cell death (Skotak, Wang, & Chandra, 2012). Presently, most research has focused on regulated non-lytic release mechanisms, while release involving plasma membrane injury and/or cell lysis has so far attracted less attention. This mode of release, however, may be taking place not only in pathological conditions, but might be an important contributing factor in certain physiological situations as exemplified by shear stress and hypoxia-induced ATP release from RBCs, as discussed below.

3.2.1 ATP-conducting channels

Historically several ion channels have been implicated in conductive release of cellular ATP, including cystic fibrosis transmembrane conductance regulator (CFTR), P-glycoprotein, connexins hemichannels and pannexins, calcium homeostasis modulator 1 (CALHM1), volume regulated anion channels (VRAC), voltage dependent anion channel (VDAC), and VDAC-like maxi anion channels, reviewed in Taruno (2018). In the case of the CFTR, studies by several independent groups with the patch clamp, lipid bilayer and luminometry techniques, have not revealed any detectable CFTR-mediated or CFTR-regulated ATP release in several epithelial and non-epithelial cells (Grygorczyk & Hanrahan, 1997a, 1997b; Grygorczyk, Tabcharani, & Hanrahan, 1996; Hazama et al., 1999; Li, Ramjeesingh, & Bear, 1996; Reddy et al., 1996; Watt, Lazarowski, & Boucher, 1998).

VRAC and Maxi-Cl channels were implicated in cell volume regulation and ATP release from swollen cells (Okada, Okada, Islam, & Sabirov, 2018; Osei-Owusu, Yang, Vitery, & Qiu, 2018; Sabirov, Merzlyak, Islam, Okada, & Okada, 2016). Both have been recently identified at the molecular level with LRRC8 protein as a main component of VRAC (Qiu et al., 2014; Voss et al., 2014) and organic anion transporter CLCO2A1 (prostaglandin transporter) as a key component of Maxi-Cl channel (Sabirov et al., 2017). Both channels possess a pore, wide enough to pass variety of organic compounds like ATP, glutamate and taurine. It is still debatable whether VRAC is a conduit of ATP release (Okada et al., 2018), but it was suggested that variation of heteromeric subunit structures in LRRC8 hexamer may alter the properties of VRAC allowing for ATP permeation (Osei-Owusu et al., 2018). Activity of both channels is associated with cell proliferation, migration, angiogenesis and apoptosis, and thus the physiological and pathophysiological relevance of these ATP release pathways requires further research.

Pannexins are probably most extensively studied putative ATP channels in the past decade. In particular, Pannex 1-mediated ATP release was

reported in a wide range of cell types, including excitable and non-excitable cells, such as airway epithelial cells and RBCs. The release can be activated by diverse mechanisms including mechanical stimuli, hypotonicity, intracellular Ca^{2+} and receptor-mediated (cAMP) signaling, reviewed in [Chiu, Schappe, Desai and Bayliss \(2018\)](#). However, the role of cAMP signaling pathway in stimulating ATP release (via Pannexin-1 or CFTR) in RBCs was contradicted by recent studies ([Keller et al., 2017](#); [Sikora, Orlov, Furuya, & Grygorczyk, 2014](#)). The unresolved issues concerning the role of Pannex 1 in ATP release include its regulatory mechanisms and basic electrophysiological properties such as ATP permeability and unitary channel conductance, which may depend on the mode of channel activation ([Taruno, 2018](#)).

Calcium homeostasis modulator 1 (CAL HM1) is another example of non-selective channel with large pore similar to that of connexins and pannexins, and implicated in ATP release from type 2 taste receptor cells ([Taruno et al., 2013](#)) and airway epithelial cells ([Workman et al., 2017](#)).

P2X7R is an ATP-gated cation channel found predominantly (but not exclusively) on immune cells but also on AT1 cells ([Chen et al., 2004](#); [Mishra, 2013](#)). P2X7R activation results in a number of downstream events, including the release of pro-inflammatory mediators and cell death. Sustained activation of P2X7R causes permeabilization of plasma membrane due to the formation of cytolytic non-selective pore, which allows fluxes of large molecules (up to 900 Da), leakage of metabolites, ultimately leading to cell death. The nature of such permeability pore is still debated. It may involve a hemichannel protein pannexin-1; but recent reports suggest that it is an intrinsic property of the P2X7R itself ([Di Virgilio, Schmalzing, & Markwardt, 2018](#)). Importantly, it was shown that activation of P2X7R induces release of large amounts of ATP in a model of human embryonic kidney cells via ATP-induced ATP release mechanism ([Pellegatti, Falzoni, Pinton, Rizzuto, & Di Virgilio, 2005](#)).

Regardless of the molecular nature of ATP-conducting channels, they all require pore of large dimensions (0.6–1.1 nm, ([Sabirov & Okada, 2005](#))), resulting in poor selectivity and large conductance (hundreds of pS) for small ions such as K^+ , Na^+ , Cl^- and Ca^{2+} , as exemplified by the well characterized VDAC channel ([Colombini, 2012](#)). Opening of such large ATP permeable pores unavoidably results in massive influx of Ca^{2+} , Na^+ and efflux of K^+ ions downstream their electrochemical gradients, greatly perturbing cell homeostasis. None of the currently known putative plasma membrane ATP channels can allow selective permeation of ATP over small ions,

preserving cell homeostasis. Thus, conductive ATP secretion appears as a crude homeostasis-perturbing approach to “cell-regulated” purinergic signaling. On the other hand, such non-selective conductive release of cytoplasmic ATP can occur without specialized endogenous membrane proteins as a result of injurious mechanical insult or membrane permeabilization by pathogen-derived pore-forming toxins.

3.2.2 Ca^{2+} -dependent exocytosis of ATP-containing vesicles

Vesicular release of ATP is well established mechanism in neuronal and endocrine cells (Praetorius & Leipziger, 2009). Recently accumulated evidence supports such a release pathway also in several epithelial cells of different origin (Feranchak et al., 2010; Kreda et al., 2010; Lazarowski et al., 2011). In particular in lung epithelial cells, our earlier study using flow-through chamber and collecting perfusate aliquots for ATP determination with luminometry demonstrated that hypotonic shock induced transient ATP release from human A549 alveolar and 16HBE14o⁻ bronchial epithelial cells. The release correlated tightly with intracellular Ca^{2+} elevations was significantly diminished in cells loaded with Ca^{2+} chelator BAPTA-AM and was not affected by different inhibitors of putative ATP-conducting channels (NPPB, Gd). Consistent with exocytosis, the release was abolished by temperature reduction to 10 °C (Boudreault & Grygorczyk, 2004). It was subsequently demonstrated that several adenosine and uridine nucleotides are co-released with ATP in a Ca^{2+} -dependent manner (Tatur et al., 2008), and that stress-induced ATP release from alveolar cells is amplified by the synergistic autocrine/paracrine action of co-released uridine (via P2Y₆ receptor) and adenosine nucleotides (Tatur et al., 2007). Similar mechanism of purinergic signal propagation may operate in other cell types as a more general paradigm. Involvement of exocytosis process in hypotonic shock-induced ATP release from A549 cells was most directly demonstrated by observing single exocytotic events of quinacrine-stained, ATP-containing vesicles with total internal reflection fluorescence (TIRF) microscopy in the study by Akopova et al. (2012).

In the lung epithelial cells, similar to neuronal and endocrine cells, ATP often is not the only vesicular cargo but is co-stored, e.g., with surfactant proteins in the lamellar bodies of alveolar type 2 cells (Fois et al., 2018), and co-released upon stimulation. Similarly, ATP and other nucleotides (ADP, AMP) were found as a co-cargo that was released from mucin granules in airway epithelial cells (Kreda et al., 2010). Our recent ATP imaging data with A549 and Calu-3 cells provide further support for such a co-release mechanism.

3.3 ATP release by cell membrane injury and cell lysis

ATP release associated with plasma membrane permeabilization/injury and cell lysis has not been fully appreciated and remains under-investigated. Such a release mechanism is particularly relevant in pathological conditions (e.g., infections) and clinical complications such as ventilator induced lung injury (VILI), where cell overstretch and extensive tissue damage occurs. The plasma membrane integrity is essential for cell survival; therefore, cells possess several evolutionarily conserved mechanisms to rapidly repair the injured membranes and ensure survival. Eukaryotic cells when challenged by mechanical stress or pore forming proteins (native or from invading pathogens), reseal in few seconds and can repair breaches in their plasma membrane of surprisingly large area (Bischofberger, Gonzalez, & van der Goot, 2009). The membrane “holes” may be of different nature, lipidic pores not delimited by protein boundaries typically arise as a result of mechanical stress (Shigematsu, Koshiyama, & Wada, 2015), while membrane damage caused by pore-forming proteins give rise to proteinaceous or proteolipidic pores with well-defined boundaries (Etxaniz, Gonzalez-Bullon, Martin, & Ostolaza, 2018). Depending on the size and nature of the pore the repair mechanisms vary. Patching and clogging processes are involved in the repair of mechanical/physical damage, while shedding (ectocytosis) and endocytosis are implicated in the elimination of pore-forming toxins (Etxaniz et al., 2018; Jimenez & Perez, 2017). Membrane patching is triggered by extracellular Ca^{2+} influx into wounded cells activating lysosomal exocytosis. Clogging involves an accumulation of proteins around the lesion, forming a barrier that prevents the loss of cytoplasmic contents to the extracellular medium and isolates the area of membrane damage. Shedding allows to isolate and expel the toxin pore-damaged membrane area in the form of vesicles called “toxosomes” or “ectosomes.” Endocytosis is an alternative mechanism by which small pores formed by toxins are removed by internalizing the damaged area, including the pore.

Considering the above processes, it is clear that in many situations membrane wounding is transient and could be reversed rapidly by repair mechanisms preventing cell lysis and death. Transient membrane permeabilization during wounding followed by the repair processes will be accompanied by short-lived release of cytoplasmic ATP that may display kinetics and extent similar to that observed with regulated processes (exocytosis, channels). Thus, distinction between the two modes of release (non-lytic and lytic) may be difficult in some situations. Moreover, cells may show transient uptake of lysed/dead cell markers (e.g., propidium iodide), complicating interpretation

of the results. Since short-lived membrane injury can often be encountered during the cell's life, the associated ATP release should be considered as normal and important mechanism contributing to intercellular purinergic signaling in eukaryotic cells. Clearly, such a release is often confronted in ATP release studies and in some cases may represent a legitimate physiologically relevant mechanism. In red blood cells hemolysis was shown to be a primary release mechanism, where it may contribute to local blood flow regulation (Grygorczyk & Orlov, 2017; Sikora et al., 2014; Thomas, 2014). In bone cells regulation of mechanically stimulated ATP release was attributed to a balance of injury and repair (Mikolajewicz, Zimmermann, Willie, & Komarova, 2018).



4. Mechanosensitive ATP release in lung epithelial cells

In Sections 4 and 5, we provide an overview of our recent studies on ATP release performed with real-time bioluminescence ATP imaging. Lung epithelial cells are subjected to several forms of mechanical stresses during the breathing cycle, sneezing and coughing, that includes airflow shear stress, cell stretch, and cell distortion by tension forces at the air-liquid interface, all of which can evoke ATP release. In majority of the following in vitro studies, we used physiologically relevant stretch stimuli or inflation with ex vivo lungs.

4.1 Stretch-induced ATP release in A549 alveolar cells

Stretch is a particularly relevant physiological stimulus in the lungs (Edwards, 2001), where expansion of alveoli during lung inflation leads to significant thinning of the alveolar walls that involves stretch and deformation of the alveolar epithelium. Stretch is also recognized as important physiological stimulus of surfactant secretion by alveolar type 2 cells (Ashino, Ying, Dobbs, & Bhattacharya, 2000; Hildebran, Goerke, & Clements, 1981; Mason & Voelker, 1998; Patel et al., 2005), which may involve synergistic effects of co-released ATP, a potent surfactant secretagogue (Dietl & Haller, 2005; Dietl, Haller, & Frick, 2012). With model human alveolar A549 cells grown on a flexible substrate, we found that 10–30% stretch pulse of 1 s duration induced ATP release in a limited number of discrete sites. Fig. 3A shows an example with cells stimulated by 21% stretch. Each release site was identified on IR images as a single cell. Responses were rapid and some could be noted within 200–300 ms from the start of stretch stimulus. The sequential images clearly show temporal and spatial changes of

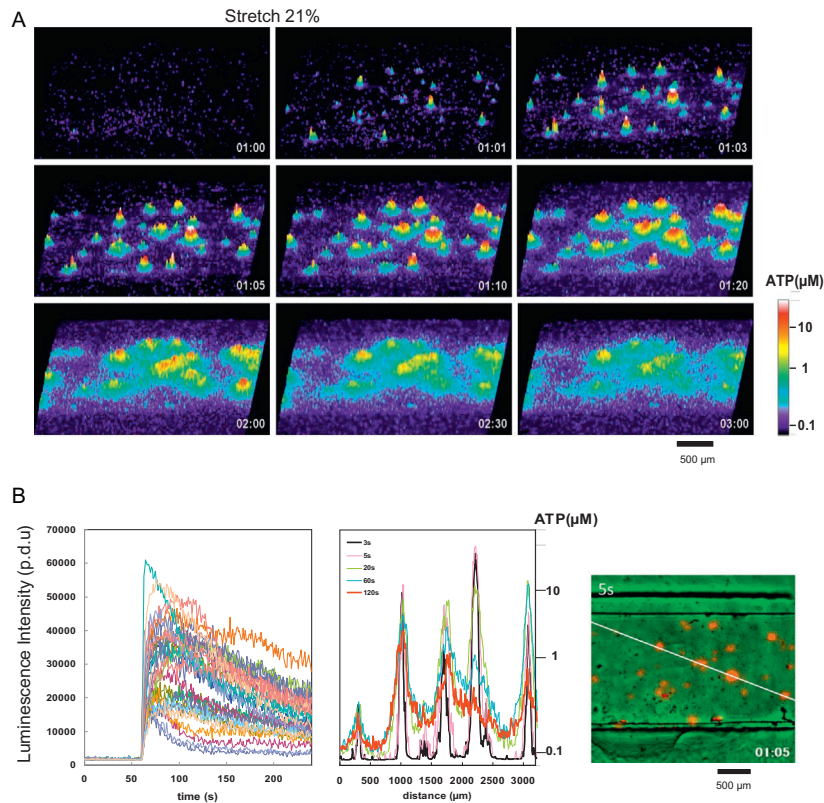


Fig. 3 ATP release from A549 cells after single stretch. (A) Sequence of images showing ATP-dependent luminescence around active cells at different time points after 21% stretch of 1-s duration applied at 1 min. The experiment elapsed time (in min: sec) is indicated in the lower right corner. The release is shown as a pseudo-3D intensity profile where the pseudo-colored luminescence intensity was converted to height. Note the multiple ATP-release sites and high (micromolar) ATP concentration in their vicinity sufficient for autocrine/paracrine stimulation of P2Y receptors on neighboring cells. The images disclose the cell culture area of approximately 3×2 mm. (B) Left graph, time-course of ATP release for all 35 responding cells shown in (A). Middle graph, spreading of released ATP measured along a white line drawn on the image on the right. Color lines represent corresponding ATP concentration profiles observed at 3–120s after the release. Peak ATP concentration reached over $10 \mu\text{M}$ for some cells. At 2 min high sub-micromolar [ATP] is observed at large $>250 \mu\text{m}$ distances from the release sites, sufficient for paracrine purinergic receptors activation. Image on the right, depicts an overlay of luminescence (red) and IR (green) images taken at 5 s after stretching. From Furuya, K., Sokabe, M., & Grygorczyk, R. (2014). Real-time luminescence imaging of cellular ATP release. *Methods*, 66, 330–344.

luminescence intensity, which is calibrated to absolute ATP concentration. Under static conditions (no perfusion), extracellular ATP concentration in the proximity ($\sim 50 \mu\text{m}$ radius) of active cells often reached $10 \mu\text{M}$, sufficient to activate P2 receptors on neighboring cells. The time-course of ATP release from individual cells in this experiment is illustrated on the left graph in Fig. 3B. Kinetic analysis demonstrated that the duration of ATP release was in the range from 10 to 82 s (Grygorczyk et al., 2013). The middle graph in Fig. 3B shows time-dependent changes in released ATP concentration along the line crossing five active release sites, shown in the right image. It is evident from the graph that after the release, extracellular ATP spreads from the release sites up to 1 mm, and its concentration stays at a high sub-micromolar level for several minutes. These spreads are important for ATP actions as local paracrine mediator. For example, our results suggest that ATP release from single alveolar cell may be sufficient to initiate purinergic signaling in the entire human lung alveolus of average $\sim 200 \mu\text{m}$ radius. ATP is a potent surfactant secretagogue and P2 receptor stimulation by high extracellular ATP might be relevant for stimulating exocytosis of surfactant-containing lamellar bodies, which require prolonged elevation of cytoplasmic Ca^{2+} to fully open a fusion pore and proper dispersal of their contents (Dietl et al., 2012). In addition, ATP stored in lamellar bodies themselves may contribute to autocrine stimulation of the surfactant secretion process (Fois et al., 2018).

4.2 Stretch induces coordinated ATP release in rat primary alveolar type 2 cells

Stretch-induced ATP release in rat primary AT2 cells reveals some features not observed in A549 cells. Fig. 4A demonstrates that 1 s stretch of 17% induces release of ATP from individual small clusters of cells, rather than single cells, in a 3-day-old AT2 cell culture. The release is seen as a localized ATP-dependent luminescence signal that peaks at ~ 10 - to 20 -s following the stretch, image (b) in Fig. 4A. However, stronger stretch (44%) induces stronger release from higher number of sites leading to formation of large clouds of released ATP with initially well-defined contour that coincided with substrate areas covered by cells, Fig. 4B, image (b). Defined contour of the released ATP cloud, suggests coordinated ATP release from cells within the active region, which may involve intracellular Ca^{2+} signaling between neighboring cells through gap junctions and by extracellular ATP (Isakson, Evans, & Boitano, 2001). This contrasts with A549 cells, where even at the strongest stretches the release occurred from single cells

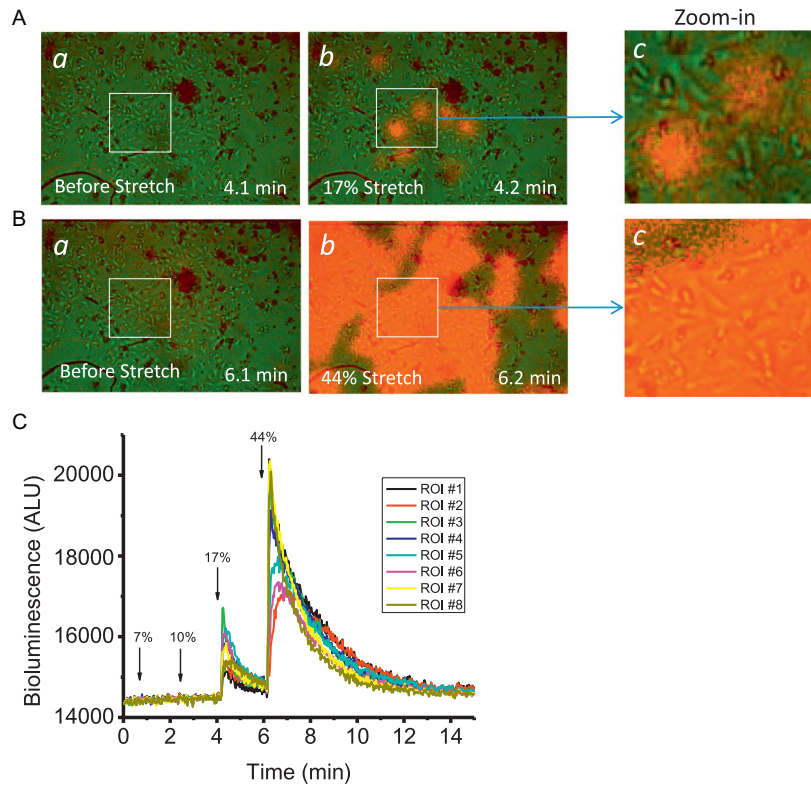


Fig. 4 Stretch-induced ATP release from rat primary AT2 cells. Examples of ATP release-dependent LL luminescence in 3-day-old AT2 cell culture induced by 1 s stretch of 17% and 44%, (A) and (B), respectively. The images show overlay of ATP-dependent luminescence (red), and phase-contrast transmitted light image (green) of AT2 cells grown in the 2×18 mm groove of the silicon stretch chamber. Image (a) was taken before stretch while (b) after the stretch. Images (c) show ATP-release responses in a zoom-in area marked by a rectangle in (b). ATP release was viewed in real-time using simplified imaging system consisting of Zeiss Axio Observer microscope ($5 \times$ lens) and Photometrics® Evolve™ 512 EMCCD camera without image intensifier. Localized small areas of ATP release for 17% stretch (image A, b), correspond to clusters of cells. Clouds of massive ATP release and larger area of active release were observed for stronger 44% stretch, image (B, b) (at 6.2 min, acquired 6 s after the stretch) and zoom-in image (B, c). (C) Time-course of ATP-release responses to a sequence of four stretches of increasing amplitude (from 7% to 44%, arrows) given at 2-min interval. The graph reports bioluminescence changes measured in eight different regions of interest. Data are from the same experiment as in (A) and (B). Only stretches above 10% induced detectable ATP release.

that were scattered randomly amongst inactive cells, which may indicate the absence or deficiency of gap junctional communication in these cells. Following the release, ATP cloud spreads due to diffusion and covers entire FOV of AT2 cell culture within <1 min after stretch (Fig. 4B, c). Full time-course of ATP-dependent luminescence for a sequence of stretches of 7–44% in this experiment is shown on Fig. 4C. While minimal responses were seen at 10% stretch, only stretches of $\geq 17\%$ produced clearly detectable ATP release in this experiment. The release is transient and local concentration of secreted ATP at the release site decreases over time due to consumption by LL reaction and diffusion out of the FOV. Kinetically all release responses were similar displaying a rapid rise followed by exponential decay suggesting a release mechanism that may involve rapid exocytosis of a relatively uniform population of ATP-containing vesicles. This was not the case for ATP release from A549 cells that was stimulated by hypotonic swelling or in submucosal Calu-3 cells stimulated by stretch, where kinetically different components of the release can be observed.

4.3 Two components of stretch-induced ATP release in Calu-3 cells

Calu-3 are mucus secreting cells derived from human airway epithelial submucosal glands. In polarized cell cultures MUC5AC mucin-containing granules could be found subapically in large fraction of these cells. Study by Kreda et al. revealed coordinated release of mucins and nucleotides (ATP, ADP, AMP) in Calu-3 cells involving Ca^{2+} -regulated exocytosis of mucin granules (Kreda et al., 2007, 2010). Direct nucleotide release from mucin-secreting goblet cells provides paracrine purinergic signals for mucin hydration and regulation of airway mucociliary clearance mechanism.

Using real-time luminescence ATP imaging we found that stretch-stimulation of Calu-3 cells induced two types of ATP-release responses, a fast response peaking at 10–15s, similar to that observed in stretch-stimulated A549 cells and a slowly rising response that peaked at 60–90s after the stretch, Fig. 5A (Supplementary Video 1 in the online version at <https://doi.org/10.1016/bs.ctm.2019.02.001>). Fast component may represent rapid vesicular ATP release, while the slow long-lasting component may be consistent with ATP co-release from mucin granules, where delayed discharge of granular ATP is expected due to its slow diffusion through the secreted mucus, Fig. 5B. However, further detailed studies will be required to prove such a mechanism of prolonged ATP secretion.

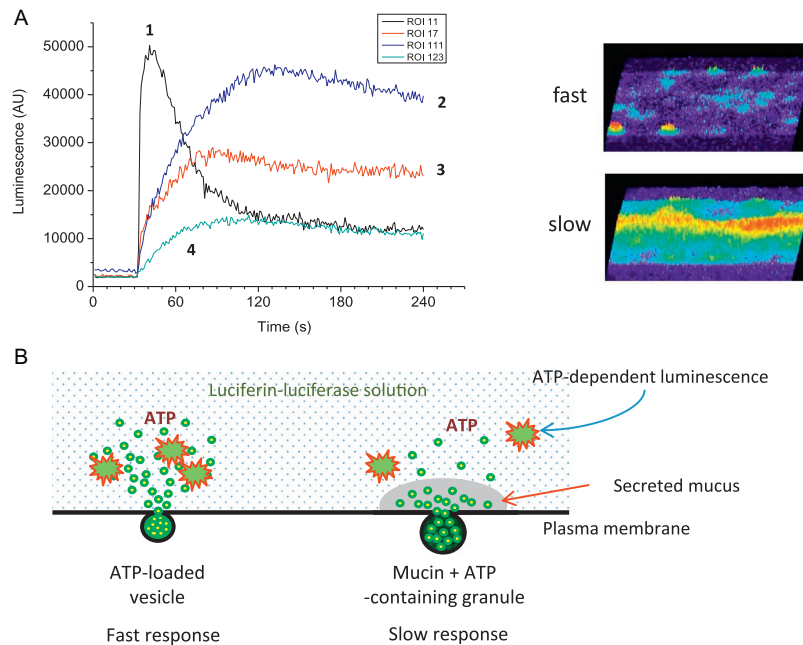


Fig. 5 Stretch-induced ATP release from Calu-3 cells. (A) Example time-course of ATP-release responses in Calu-3 cells stimulated by 1 s stretch of 28%. ATP-dependent LL luminescence is shown in arbitrary light units (ALU). Note the presence of fast (trace 1) and slow responses (traces 2–4). The rising phase of the slow release responses was 16–28-fold slower compared to the fast response. The images on the right show a pseudo-3D intensity profile of ATP-dependent luminescence observed with Calu-3 cell culture in the stretch chamber. Upper image was taken at 10 s and lower image at ~90 s after the stretch, corresponding to peak response of the fast and slow responses, respectively. See Supplementary Video 1 in the online version at <https://doi.org/10.1016/bs.ctm.2019.02.001> for the full time-course of ATP release in this experiment. (B) A cartoon illustrating the concept of delayed ATP release from mucin granules.

4.4 Hypotonic stress-induced ATP release in A549 cells—Contribution of cell lysis

Hypotonic shock is known to evoke ATP release from many cell types and was commonly used as a surrogate of mechanical stimulation in earlier studies by several investigators. In our previous studies we used a flow-through chamber and standard luminometry to investigate kinetics of hypotonic stress-induced ATP release (Boudreault & Grygorczyk, 2004; Tatur et al., 2007). However, no spatial information could be obtained with such approach. Bioluminescence ATP imaging with its superior spatial and temporal resolution can provide new insights into the release process and the underlying mechanisms. In experiment illustrated in Fig. 6, A549 cells were

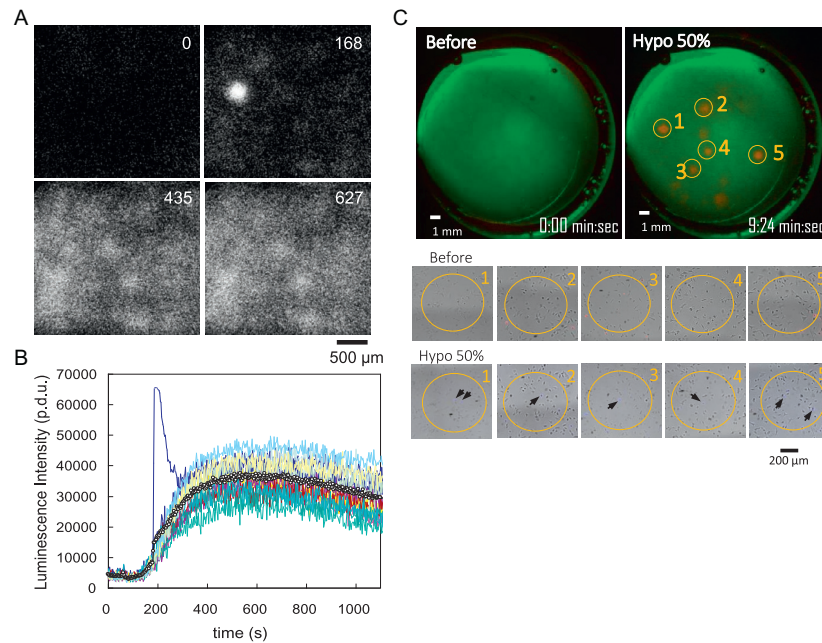


Fig. 6 Hypotonic stress-induced ATP release in A549 cells. (A) 50% Hypotonic shock-induced ATP release in lung alveolar A549 cells. The responses were slow-rising and of diffused appearance, so that ATP-releasing cells could not be clearly identified except for one isolated release spike at 168 s. (B) Time-course of ATP-dependent luminescence observed in several different regions of A549 cell culture in the experiment shown in (A). The slow responses reached maximum at about 600 s. (C) Co-localization of ATP release regions and hypo-induced PI^+ staining of A549 cells. ATP secretion from A549 cells grown in 0.1% FBS for 48 h (fragile cells) on glass coverslip was imaged with LL bioluminescence and a simplified imaging system consisting of large field of view optics and Photometrics[®] Evolve[™] 512 EMCCD camera. Secretion was stimulated by cell swelling in extracellular solution of reduced tonicity (hypo 50%) under static condition (no perfusion). Regions of prominent extracellular ATP level are identified by circles (1–5) on the Hypo 50% image. Plasma membrane permeability to large molecules was assessed prior and post-treatment with propidium iodide (PI) uptake evaluated with an epifluorescence-equipped Zeiss Axio Observer microscope (10 \times objective), lower panel. Images of the entire coverslip were stitched with open-source ImageJ software. A549 cells that were PI^+ before hypo are shown in red, while those that become PI^+ after hypo 50% are shown in blue. All five ATP release regions on image Hypo 50% co-localize with hypo-induced PI^+ cells (arrows) identified on the lower panel images. *Panel B: Images were obtained with 4 \times lens and 500-ms exposure time, from Furuya, K., Sokabe, M., & Grygorczyk, R. (2014). Real-time luminescence imaging of cellular ATP release. Methods, 66, 330–344.*

exposed to hypotonic shock (50%) and bioluminescence imaging was subsequently performed under static condition (no perfusion). We found two types of release events, a slowly rising ATP release response of diffuse appearance in addition to several random but highly localized ATP-release spikes. An example is shown in Fig. 6A and B (Furuya et al., 2014). The extracellular ATP resulting from the slow release reached maximum in 500–700s, but spikes appeared mostly at the beginning of hypotonic stimulation. To further examine the nature of the ATP release spikes, in a subsequent study we used wide FOV ATP imaging system and propidium iodide (PI) fluorescence to detect lysed cells, Fig. 6C. We compared ATP release in cells that were rendered fragile (by culturing them for >24h in low serum medium) and thus prone to cell lysis, and normal control cells cultured in serum-containing medium. While we observed similar slow ATP secretion component in both cell cultures, number of punctuate ATP secretion events was significantly increased in fragile cells (Ponomarchuk, Boudreault, Orlov, & Grygorczyk, 2017). Importantly, all punctuate ATP secretion sites co-localized with PI-positive cells, consistent with cell lysis. Total cell lysis per coverslip caused by acute cell swelling constituted <2% and the amount of normalized ATP release per cell did not differ in control and fragile A549 cells, indicating that contribution of ATP release due to cell lysis is negligible in these experiments. The nature of the slow ATP release remains not fully resolved in this study but likely results from exocytosis of ATP-loaded vesicles (Akopova et al., 2012; Boudreault & Grygorczyk, 2004) and co-release of ATP co-stored with surfactants in lamellar bodies (Fois et al., 2018).



5. Inflation-induced ATP release in ex vivo lungs

While ATP release has been investigated extensively in vitro using isolated lung epithelial cells (Boudreault & Grygorczyk, 2004; Grygorczyk et al., 2013; Kreda et al., 2007; Lazarowski et al., 2011; Okada, Nicholas, Kreda, Lazarowski, & Boucher, 2006), cultured lung cells may inadequately replicate native cell responses because of phenotypic transformations. In the following study to investigate inflation-induced purinergic cell signaling in the native setting in real time, we have applied bioluminescence ATP imaging to lungs of rat, ex vivo.

5.1 ATP release in airspaces

Detection of alveolar ATP release requires instillation into lung airspaces a liquid containing LL reagent, thus limiting study to liquid-filled

“edematous” lungs (Furuya et al., 2016). With this approach, we found that brief inflation (1 s, ~ 20 cm H₂O positive pressure via trachea) induced transient (<30 s) ATP release in a limited number of air-inflated alveolar sacs during their recruitment/opening, Fig. 7A. Released ATP reached

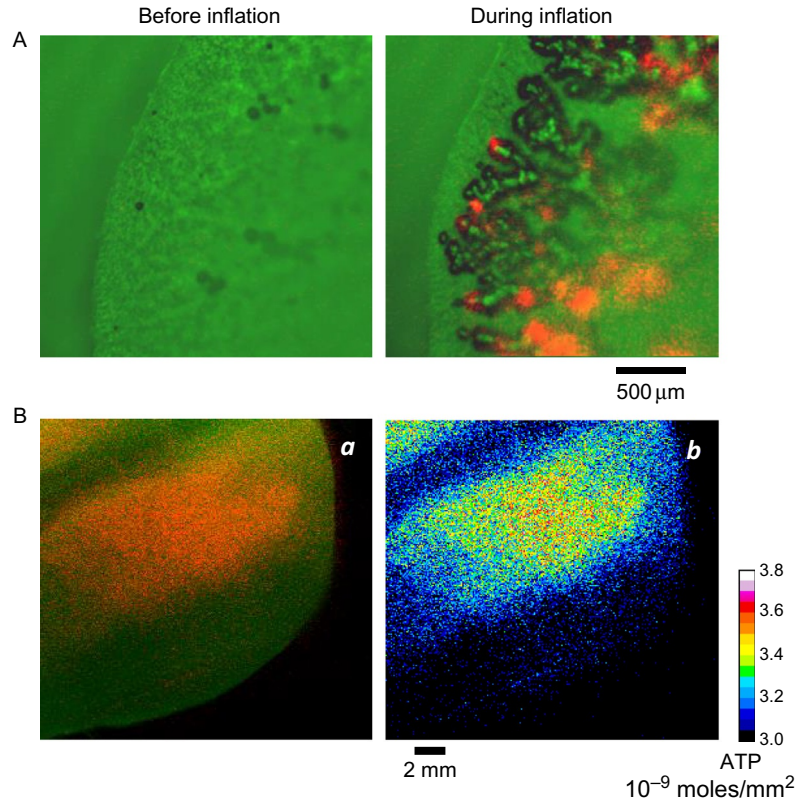


Fig. 7 Inflation-induced ATP release in airspaces of ex vivo rat lung. (A) The overlay images show ATP-dependent luminescence (red) and infra-red (IR) tissue images (green), before and during pressure pulse of ~ 20 cm H₂O. Air-inflated strings of alveolar clusters appear as dark areas on the image. (B) Bioluminescence ATP imaging of “dry” rat lung with LL reagent introduced by nebulization. (a) Overlay image of ATP-LL luminescence (red) and transmitted light image of the lung tissue (green). (b) Tissue distribution of ATP (in femto-moles/mm²) is shown on pseudocolor scale. DMEM containing isotonicity-adjusted LL with 10 mM ATP was introduced into rat lungs via a compressor nebulizer (MedPro AMG 705-470) during five consecutive lung inflations (-20 cm H₂O, 4 s) in artificial thoracic chamber. Bioluminescence was recorded with a simplified wide FOW imaging system, exposure time 10 s. Adapted from Furuya, K., Tan, J. J., Boudreault, F., Sokabe, M., Berthiaume, Y., & Grygorczyk, R. (2016). Real-time imaging of inflation-induced ATP release in the ex vivo rat lung. *American Journal of Physiology. Lung Cellular and Molecular Physiology*, 311, L956–L969.

concentrations in the order of $\sim 10^{-6}$ M, relevant for autocrine/paracrine signaling. Closer analysis revealed that released ATP remained spatially restricted to irregular polygonal shapes the size of alveolar sacs (equivalent diameter of 40–160 μm), suggesting that the elementary unit of ATP responses consist of a single alveolar sacs or their clusters. Only limited ATP diffusion to neighboring alveolar sacs was occasionally observed. ATP release was stimulus-dependent, prolonged (100-s) inflation evoked long-lasting ATP release, which terminated upon alveoli deflation/de-recruitment while cyclic inflation/suction produced cyclic ATP release (Furuya et al., 2016). Several physical stimuli associated with edematous lung inflation such as cell stretch, cell deformation by tension forces at the air-liquid interface and shear stress caused by liquid movement, may contribute to ATP release in lung airspaces observed in this study. The exact role of these different stimuli to ATP release requires future investigations.

In future studies limitations of the edematous lung model could be avoided by delivering LL reagent into lung airspaces with nebulizer. Our preliminary experiments indicate feasibility of such approach, where extra-cellular ATP can be detected in “dry lungs” after nebulization of LL/ATP mixture into airspaces, Fig. 7B.

5.2 ATP release in pulmonary blood vessels

In the lumen of blood vessels ATP contributes to local control of blood flow through interaction with purinergic receptors of vascular endothelial cells and stimulation of nitric oxide synthesis, a powerful relaxant of vascular smooth muscle. Plasma membrane of endothelial cells sense changes in shear stress and stretching and transduce these changes into intracellular biochemical signals (Yamamoto & Ando, 2018), activating multiple signaling pathways including purinergic signaling via the release of ATP.

To visualize ATP release in alveolar blood capillaries of rat lung, LL was introduced into their lumen via pulmonary artery. Inflation induced transient ATP release that displayed a more diffuse pattern, different from that observed in airspaces. Despite diffuse appearance, the responses clearly consisted of several patch-like areas (70–260 μm) corresponding to the size of alveolar sacs or their clusters, Fig. 8. The responses subsided quickly after lung deflation. We have verified that with LL reagent introduced into blood capillaries, ATP-dependent luminescence signal originates exclusively from the lumen of blood vessels without cross-leakage into lung airspaces (Furuya et al., 2016). In the absence of red blood cells in the lung perfusate, released

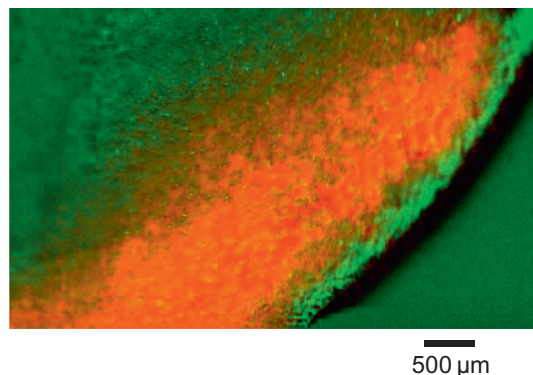


Fig. 8 Inflation-induced ATP release in pulmonary blood capillaries of ex vivo rat. The overlay image shows ATP-dependent luminescence (red) and infra-red (IR) tissue images (green). Patch-like pattern of ATP-dependent luminescence is seen after brief inflation (~ 30 s duration, ~ 10 cm H_2O). Images were acquired with Olympus MVX10 macro-view microscope with $2\times$ objective at $0.63\times$ zoom. From Furuya, K., Tan, J. J., Boudreault, F., Sokabe, M., Berthiaume, Y., & Grygorczyk, R. (2016). Real-time imaging of inflation-induced ATP release in the ex vivo rat lung. *American Journal of Physiology. Lung Cellular and Molecular Physiology*, 311, L956–L969.

ATP originates exclusively from endothelial cells. Fluid shear stress is recognized as important mechanical stimuli acting on vascular endothelial cells augmenting mitochondrial ATP generation and triggering its release (Yamamoto et al., 2011; Yamamoto, Imamura, & Ando, 2018). However, in pulmonary capillaries, significant distension of endothelial cells during lung inflation might be expected, which may also contribute to mechanosensitive release of ATP. Stretch-induced ATP release from human pulmonary microvascular endothelial cells was indeed confirmed in vitro by Ito, Furuya, Sokabe, and Hasegawa (2016). The study demonstrates that inflation induces ATP release in both the compartments—alveoli and the surrounding blood capillary network. The functional units of ATP release consist of alveolar sacs or their clusters. The findings directly confirm that lung inflation initiates purinergic signaling in the intact lung.



6. Conclusions and future directions

Mechanosensitive ATP release appears as a prevailing mode of triggering purinergic signaling cascade in the lungs. Diverse mechanical stimuli and release pathways exist. Exocytosis of ATP-loaded vesicles and several types of intracellular ATP-containing granules is a well-accepted route of

cell-regulated ATP release, supported by wealth of experimental evidence. The physiological and pathophysiological roles and often basic biophysical properties of several putative ATP channels still remain unsettled and require further studies. Recent molecular identification of VRAC and Maxi-Cl channels should allow study of their structure–function relationships, better characterization of their regulation, biophysical/electrophysiological properties and potential role as ATP conduit.

Cell lysis and transient membrane injury emerge as important archaic mechanism of ATP release contributing to intercellular purinergic signaling in the lungs and other organs. Such a release may represent for some cells (e.g., RBCs) a genuine physiologically relevant mechanism that should be considered in clinical and translational studies in the field. Importantly, in some situations it may represent a dominating mode of the release surpassing by far, the contribution of cell-regulated release pathways. Therefore, better understanding of the mechanisms responsible for plasma membrane injury and repair will facilitate development of specific therapeutic approaches promoting resealing of damaged cell membranes (Andrews, Almeida, & Corrotte, 2014), or minimizing injury by increasing cell resilience to injurious stimuli, by, e.g., mechanical priming (Mikolajewicz, Mohammed, et al., 2018; Mikolajewicz, Zimmermann, et al., 2018). This is particularly important in the context of lung injury induced by mechanical ventilation and emphasizes critical role and benefits of using lung protective ventilation protocols to prevent/attenuate injury. It is also worth to consider interventions that will minimize spreading and downstream effects of released ATP in adjacent tissues. Massive release from damaged cells/tissue will result in high sustained levels of extracellular ATP that is required for P2X7 channel activation and formation of lytic pores on neighboring intact cells, consequently inducing secondary P2X7-mediated ATP release. As a protective measure, use of ATP scavengers such as apyrase has been shown to significantly improve survival of ventilated mice (Eckle et al., 2007), while antagonists of P2X7R attenuated the severity of lung injury by inhibiting NLRP3 inflammasome. These are highly promising approaches that should be further explored in future studies.

Recent bioluminescence ATP imaging studies revealed that physiologically relevant stretch induces ATP release from alveolar and endothelial cells, which could spread and exert paracrine effects on other cells at significant distances. In the intact *ex vivo* lung, real-time ATP visualization confirmed directly that inflation induces ATP release in airspaces and in the lumen of pulmonary blood vessels. Future technical improvements of

ATP imaging in lung airspaces should consider use of nebulized LL reagent to avoid the limitations of the LL liquid-instilled edematous lung model. Ultimately, while technically challenging, direct visualization of lung ATP release in live animals using bioluminescence imaging and intravital microscopy should be considered (Rodríguez-Tirado et al., 2016).

Reference

- Abbracchio, M. P., Burnstock, G., Verkhratsky, A., & Zimmermann, H. (2009). Purinergic signalling in the nervous system: An overview. *Trends in Neurosciences*, *32*, 19–29.
- Adriaensen, D., & Timmermans, J. P. (2004). Purinergic signalling in the lung: Important in asthma and COPD? *Current Opinion in Pharmacology*, *4*, 207–214.
- Akopova, I., Tatur, S., Grygorczyk, M., Luchowski, R., Gryczynski, I., Gryczynski, Z., et al. (2012). Imaging exocytosis of ATP-containing vesicles with TIRF microscopy in lung epithelial A549 cells. *Purinergic Signal*, *8*, 59–70.
- Aliagas, E., Munoz-Esquerre, M., Cuevas, E., Careta, O., Huertas, D., Lopez-Sanchez, M., et al. (2018). Is the purinergic pathway involved in the pathology of COPD? Decreased lung CD39 expression at initial stages of COPD. *Respiratory Research*, *19*, 103.
- Anderson, C. M., Bergher, J. P., & Swanson, R. A. (2004). ATP-induced ATP release from astrocytes. *Journal of Neurochemistry*, *88*, 246–256.
- Andreeva, A. V., Kutuzov, M. A., & Voyno-Yasenetskaya, T. A. (2007). Regulation of surfactant secretion in alveolar type II cells. *American Journal of Physiology. Lung Cellular and Molecular Physiology*, *293*, L259–L271.
- Andrews, N. W., Almeida, P. E., & Corrotte, M. (2014). Damage control: Cellular mechanisms of plasma membrane repair. *Trends in Cell Biology*, *24*, 734–742.
- Ashino, Y., Ying, X., Dobbs, L. G., & Bhattacharya, J. (2000). $[Ca^{2+}]_i$ oscillations regulate type II cell exocytosis in the pulmonary alveolus. *American Journal of Physiology. Lung Cellular and Molecular Physiology*, *279*, L5–L13.
- Beigi, R., Kobatake, E., Aizawa, M., & Dubyak, G. R. (1999). Detection of local ATP release from activated platelets using cell surface-attached firefly luciferase. *The American Journal of Physiology*, *276*, C267–C278.
- Bischofberger, M., Gonzalez, M. R., & van der Goot, F. G. (2009). Membrane injury by pore-forming proteins. *Current Opinion in Cell Biology*, *21*, 589–595.
- Boudreault, F., & Grygorczyk, R. (2004). Cell swelling-induced ATP release is tightly dependent on intracellular calcium elevations. *The Journal of Physiology*, *561*, 499–513.
- Bucheimer, R. E., & Linden, J. (2004). Purinergic regulation of epithelial transport. *The Journal of Physiology*, *555*, 311–321.
- Burnstock, G. (2006). Purinergic signalling. *British Journal of Pharmacology*, *147*(Suppl. 1), S172–S181.
- Burnstock, G. (2008). Unresolved issues and controversies in purinergic signalling. *The Journal of Physiology*, *586*, 3307–3312.
- Burnstock, G. (2009). Purinergic signalling: Past, present and future. *Brazilian Journal of Medical and Biological Research*, *42*, 3–8.
- Burnstock, G., Brouns, I., Adriaensen, D., & Timmermans, J. P. (2012). Purinergic signaling in the airways. *Pharmacological Reviews*, *64*, 834–868.
- Button, B., Okada, S. F., Frederick, C. B., Thelin, W. R., & Boucher, R. C. (2013). Mechanosensitive ATP release maintains proper mucus hydration of airways. *Science Signaling*, *6*, ra46.
- Cereda, M., Emami, K., Xin, Y., Kadlecsek, S., Kuzma, N. N., Mongkolwisetwara, P., et al. (2013). Imaging the interaction of atelectasis and overdistension in surfactant-depleted lungs. *Critical Care Medicine*, *41*, 527–535.

- Chen, Z., Jin, N., Narasraju, T., Chen, J., McFarland, L. R., Scott, M., et al. (2004). Identification of two novel markers for alveolar epithelial type I and II cells. *Biochemical and Biophysical Research Communications*, *319*, 774–780.
- Chiu, Y. H., Schappe, M. S., Desai, B. N., & Bayliss, D. A. (2018). Revisiting multimodal activation and channel properties of Pannexin 1. *The Journal of General Physiology*, *150*, 19–39.
- Colombini, M. (2012). VDAC structure, selectivity, and dynamics. *Biochimica et Biophysica Acta*, *1818*, 1457–1465.
- Della, L. V., Cabiati, M., Rocchiccioli, S., Del, R. S., & Morales, M. A. (2013). The role of the adenosinergic system in lung fibrosis. *Pharmacological Research*, *76*, 182–189.
- Di Virgilio, F., Schmalzing, G., & Markwardt, F. (2018). The elusive P2X7 macropore. *Trends in Cell Biology*, *28*, 392–404.
- Dietl, P., & Haller, T. (2005). Exocytosis of lung surfactant: From the secretory vesicle to the air-liquid interface. *Annual Review of Physiology*, *67*, 595–621.
- Dietl, P., Haller, T., & Frick, M. (2012). Spatio-temporal aspects, pathways and actions of Ca(2+) in surfactant secreting pulmonary alveolar type II pneumocytes. *Cell Calcium*, *52*, 296–302.
- Douillet, C. D., Robinson, W. P., III, Milano, P. M., Boucher, R. C., & Rich, P. B. (2006). Nucleotides induce IL-6 release from human airway epithelia via P2Y2 and p38 MAPK-dependent pathways. *American Journal of Physiology. Lung Cellular and Molecular Physiology*, *291*, L734–L746.
- Dreyfuss, D., Soler, P., Basset, G., & Saumon, G. (1988). High inflation pressure pulmonary edema. Respective effects of high airway pressure, high tidal volume, and positive end-expiratory pressure. *The American Review of Respiratory Disease*, *137*, 1159–1164.
- Eckle, T., Fullbier, L., Wehrmann, M., Khoury, J., Mittelbronn, M., Ibla, J., et al. (2007). Identification of ectonucleotidases CD39 and CD73 in innate protection during acute lung injury. *Journal of Immunology*, *178*, 8127–8137.
- Edwards, Y. S. (2001). Stretch stimulation: Its effects on alveolar type II cell function in the lung. *Comparative Biochemistry and Physiology. Part A, Molecular & Integrative Physiology*, *129*, 245–260.
- Etxaniz, A., Gonzalez-Bullon, D., Martin, C., & Ostolaza, H. (2018). Membrane repair mechanisms against permeabilization by pore-forming toxins. *Toxins (Basel)*, *10*(6), 234. <https://doi.org/10.3390/toxins10060234>.
- Fausther, M., Pelletier, J., Ribeiro, C. M., Sevigny, J., & Picher, M. (2010). Cystic fibrosis remodels the regulation of purinergic signaling by NTPDase1 (CD39) and NTPDase3. *American Journal of Physiology. Lung Cellular and Molecular Physiology*, *298*, L804–L818.
- Feranchak, A. P., Lewis, M. A., Kresge, C., Sathe, M., Bugde, A., Luby-Phelps, K., et al. (2010). Initiation of purinergic signaling by exocytosis of ATP-containing vesicles in liver epithelium. *The Journal of Biological Chemistry*, *285*, 8138–8147.
- Fois, G., Winkelmann, V. E., Bareis, L., Staudenmaier, L., Hecht, E., Ziller, C., et al. (2018). ATP is stored in lamellar bodies to activate vesicular P2X4 in an autocrine fashion upon exocytosis. *The Journal of General Physiology*, *150*, 277–291.
- Furuya, K., Harada, K., & Sokabe, M. (2008). Three types of ATP-release in mammary epithelial cells revealed by ATP imaging. *Purinergic Signalling*, *4*(Suppl. 5), S91.
- Furuya, K., Sokabe, M., & Grygorczyk, R. (2014). Real-time luminescence imaging of cellular ATP release. *Methods*, *66*, 330–344.
- Furuya, K., Tan, J. J., Boudreault, F., Sokabe, M., Berthiaume, Y., & Grygorczyk, R. (2016). Real-time imaging of inflation-induced ATP release in the ex vivo rat lung. *American Journal of Physiology. Lung Cellular and Molecular Physiology*, *311*, L956–L969.
- Grygorczyk, R., Furuya, K., & Sokabe, M. (2013). Imaging and characterization of stretch-induced ATP release from alveolar A549 cells. *The Journal of Physiology*, *591*, 1195–1215.

- Grygorczyk, R., & Hanrahan, J. W. (1997a). CFTR-independent ATP release from epithelial cells triggered by mechanical stimuli. *The American Journal of Physiology*, *272*, C1058–C1066.
- Grygorczyk, R., & Hanrahan, J. W. (1997b). Cystic fibrosis transmembrane conductance regulator and adenosine triphosphate [response]. *Science*, *275*, 1325–1326.
- Grygorczyk, R., & Orlov, S. N. (2017). Effects of hypoxia on erythrocyte membrane properties—implications for intravascular hemolysis and purinergic control of blood flow. *Frontiers in Physiology*, *8*, 1110.
- Grygorczyk, R., Tabcharani, J. A., & Hanrahan, J. W. (1996). CFTR channels expressed in CHO cells do not have detectable ATP conductance. *The Journal of Membrane Biology*, *151*, 139–148.
- Hasan, D., Blankman, P., & Nieman, G. F. (2017). Purinergic signalling links mechanical breath profile and alveolar mechanics with the pro-inflammatory innate immune response causing ventilation-induced lung injury. *Purinergic Signal*, *13*, 363–386.
- Hasan, D., Satalin, J., van der Zee, P., Kollisch-Singule, M., Blankman, P., Shono, A., et al. (2018). Excessive extracellular ATP desensitizes P2Y2 and P2X4 ATP receptors provoking surfactant impairment ending in ventilation-induced lung injury. *International Journal of Molecular Sciences*, *19*.
- Hazama, A., Shimizu, T., Ando-Akatsuka, Y., Hayashi, S., Tanaka, S., Maeno, E., et al. (1999). Swelling-induced, CFTR-independent ATP release from a human epithelial cell line: Lack of correlation with volume-sensitive $Cl(-)$ channels. *The Journal of General Physiology*, *114*, 525–533.
- Hildebran, J. N., Goerke, J., & Clements, J. A. (1981). Surfactant release in excised rat lung is stimulated by air inflation. *Journal of Applied Physiology: Respiratory, Environmental and Exercise Physiology*, *51*, 905–910.
- Idzko, M., Hammad, H., van Nimwegen, M., Kool, M., Willart, M. A., Muskens, F., et al. (2007). Extracellular ATP triggers and maintains asthmatic airway inflammation by activating dendritic cells. *Nature Medicine*, *13*, 913–919.
- Isakson, B. E., Evans, W. H., & Boitano, S. (2001). Interacellular Ca^{2+} signaling in alveolar epithelial cells through gap junctions and by extracellular ATP. *American Journal of Physiology. Lung Cellular and Molecular Physiology*, *280*, L221–L228.
- Ito, S., Furuya, K., Sokabe, M., & Hasegawa, Y. (2016). Cellular ATP release in the lung and airway. *AIMS Biophysics*, *3*, 571–584.
- Jacobson, K. A., & Muller, C. E. (2016). Medicinal chemistry of adenosine, P2Y and P2X receptors. *Neuropharmacology*, *104*, 31–49.
- Jaecklin, T., Engelberts, D., Otulakowski, G., O’Brodivich, H., Post, M., & Kavanagh, B. P. (2011). Lung-derived soluble mediators are pathogenic in ventilator-induced lung injury. *American Journal of Physiology Lung Cellular and Molecular Physiology*, *300*, L648–L658.
- Jimenez, A. J., & Perez, F. (2017). Plasma membrane repair: The adaptable cell life-insurance. *Current Opinion in Cell Biology*, *47*, 99–107.
- Keller, A. S., Diederich, L., Panknin, C., DeLalio, L. J., Drake, J. C., Sherman, R., et al. (2017). Possible roles for ATP release from RBCs exclude the cAMP-mediated *Panx1* pathway. *American Journal of Physiology. Cell Physiology*, *313*, C593–C603.
- Kreda, S. M., Okada, S. F., Van Heusden, C. A., O’neal, W., Gabriel, S., Abdullah, L., et al. (2007). Coordinated release of nucleotides and mucin from human airway epithelial Calu-3 cells. *Journal of Physiology (London)*, *584*, 245–259.
- Kreda, S. M., Seminario-Vidal, L., Van Heusden, C. A., O’neal, W., Jones, L., Boucher, R. C., et al. (2010). Receptor-promoted exocytosis of airway epithelial mucin granules containing a spectrum of adenine nucleotides. *The Journal of Physiology*, *588*, 2255–2267.

- Lazarowski, E. R., & Boucher, R. C. (2009). Purinergic receptors in airway epithelia. *Current Opinion in Pharmacology*, 9, 262–267.
- Lazarowski, E. R., Boucher, R. C., & Harden, T. K. (2003). Mechanisms of release of nucleotides and integration of their action as P2X- and P2Y-receptor activating molecules. *Molecular Pharmacology*, 64, 785–795.
- Lazarowski, E. R., Sesma, J. I., Seminario-Vidal, L., & Kreda, S. M. (2011). Molecular mechanisms of purine and pyrimidine nucleotide release. *Advances in Pharmacology*, 61, 221–261.
- Lazarowski, E. R., Tarran, R., Grubb, B. R., Van Heusden, C. A., Okada, S., & Boucher, R. C. (2004). Nucleotide release provides a mechanism for airway surface liquid homeostasis. *The Journal of Biological Chemistry*, 279, 36855–36864.
- Li, C., Ramjeeasingh, M., & Bear, C. E. (1996). Purified cystic fibrosis transmembrane conductance regulator (CFTR) does not function as an ATP channel. *The Journal of Biological Chemistry*, 271, 11623–11626.
- Lommatzsch, M., Cicko, S., Muller, T., Lucattelli, M., Bratke, K., Stoll, P., et al. (2010). Extracellular adenosine triphosphate and chronic obstructive pulmonary disease. *American Journal of Respiratory and Critical Care Medicine*, 181, 928–934.
- Mason, R. J., & Voelker, D. R. (1998). Regulatory mechanisms of surfactant secretion. *Biochimica et Biophysica Acta*, 1408, 226–240.
- Mikolajewicz, N., Mohammed, A., Morris, M., & Komarova, S. V. (2018). Mechanically stimulated ATP release from mammalian cells: Systematic review and meta-analysis. *Journal of Cell Science*, 131.
- Mikolajewicz, N., Zimmermann, E. A., Willie, B. M., & Komarova, S. V. (2018). Mechanically stimulated ATP release from murine bone cells is regulated by a balance of injury and repair. *eLife*, 7, 1–23.
- Mishra, A. (2013). New insights of P2X7 receptor signaling pathway in alveolar functions. *Journal of Biomedical Science*, 20, 26.
- Mortaz, E., Braber, S., Nazary, M., Givi, M. E., Nijkamp, F. P., & Folkerts, G. (2009). ATP in the pathogenesis of lung emphysema. *European Journal of Pharmacology*, 619, 92–96.
- Mortaz, E., Folkerts, G., Nijkamp, F. P., & Henricks, P. A. (2010). ATP and the pathogenesis of COPD. *European Journal of Pharmacology*, 638, 1–4.
- Muller, T., Fay, S., Vieira, R. P., Karmouty-Quintana, H., Cicko, S., Ayata, C. K., et al. (2017). P2Y6 receptor activation promotes inflammation and tissue remodeling in pulmonary fibrosis. *Frontiers in Immunology*, 8, 1028.
- Murata, N., Ito, S., Furuya, K., Takahara, N., Naruse, K., Aso, H., et al. (2014). Ca²⁺ influx and ATP release mediated by mechanical stretch in human lung fibroblasts. *Biochemical and Biophysical Research Communications*, 453, 101–105.
- Nickles, H. T., Sumkauskaitė, M., Wang, X., Wegner, I., Puderbach, M., & Kuebler, W. M. (2014). Mechanical ventilation causes airway distension with proinflammatory sequelae in mice. *American Journal of Physiology. Lung Cellular and Molecular Physiology*, 307, L27–L37.
- Novak, I. (2011). Purinergic signalling in epithelial ion transport: Regulation of secretion and absorption. *Acta Physiologica (Oxford, England)*, 202, 501–522.
- Okada, S. F., Nicholas, R. A., Kreda, S. M., Lazarowski, E. R., & Boucher, R. C. (2006). Physiological regulation of ATP release at the apical surface of human airway epithelia. *The Journal of Biological Chemistry*, 281, 22992–23002.
- Okada, Y., Okada, T., Islam, M. R., & Sabirov, R. Z. (2018). Molecular identities and ATP release activities of two types of volume-regulatory anion channels, VSOR and Maxi-Cl. *Current Topics in Membranes*, 81, 125–176.
- Osei-Owusu, J., Yang, J., Vitery, M. D. C., & Qiu, Z. (2018). Molecular biology and physiology of volume-regulated anion channel (VRAC). *Current Topics in Membranes*, 81, 177–203.

- Paradiso, A. M., Ribeiro, C. M., & Boucher, R. C. (2001). Polarized signaling via purinoceptors in normal and cystic fibrosis airway epithelia. *The Journal of General Physiology*, *117*, 53–67.
- Patel, A. S., Reigada, D., Mitchell, C. H., Bates, S. R., Margulies, S. S., & Koval, M. (2005). Paracrine stimulation of surfactant secretion by extracellular ATP in response to mechanical deformation. *American Journal of Physiology. Lung Cellular and Molecular Physiology*, *289*, L489–L496.
- Pelleg, A., Schulman, E. S., & Barnes, P. J. (2016). Extracellular adenosine 5'-triphosphate in obstructive airway diseases. *Chest*, *150*, 908–915.
- Pellegatti, P., Falzoni, S., Pinton, P., Rizzuto, R., & Di Virgilio, F. (2005). A novel recombinant plasma membrane-targeted luciferase reveals a new pathway for ATP secretion. *Molecular Biology of the Cell*, *16*, 3659–3665.
- Picher, M., & Boucher, R. C. (2011). *Purinergic regulation of respiratory diseases*. Springer Netherlands.
- Pintor, J. (2018). Light-induced ATP release from the lens. *Purinergic Signal*, *14*, 499–504.
- Ponomarchuk, O., Boudreault, F., Orlov, S. N., & Grygorczyk, R. (2017). Mechanosensitive ATP release involves a non-conductive pathway: Evidence from large field of view real-time imaging. *Biophysical Journal*, *112*(Suppl. 1), 311A.
- Praetorius, H. A., & Leipziger, J. (2009). ATP release from non-excitable cells. *Purinergic Signal*, *5*, 433–446.
- Qiu, Z., Dubin, A. E., Mathur, J., Tu, B., Reddy, K., Miraglia, L. J., et al. (2014). SWELL1, a plasma membrane protein, is an essential component of volume-regulated anion channel. *Cell*, *157*, 447–458.
- Rajendran, M., Dane, E., Conley, J., & Tantama, M. (2016). Imaging adenosine triphosphate (ATP). *The Biological Bulletin*, *231*, 73–84.
- Ramminger, S. J., Collett, A., Baines, D. L., Murphie, H., McAlroy, H. L., Olver, R. E., et al. (1999). P2Y2 receptor-mediated inhibition of ion transport in distal lung epithelial cells. *British Journal of Pharmacology*, *128*, 293–300.
- Ramsingh, R., Grygorczyk, A., Solecki, A., Cherkaoui, L. S., Berthiaume, Y., & Grygorczyk, R. (2011). Cell deformation at the air-liquid interface induces Ca²⁺-dependent ATP release from lung epithelial cells. *American Journal of Physiology. Lung Cellular and Molecular Physiology*, *300*, L587–L595.
- Reddy, M. M., Quinton, P. M., Haws, C., Wine, J. J., Grygorczyk, R., Tabcharani, J. A., et al. (1996). Failure of the cystic fibrosis transmembrane conductance regulator to conduct ATP. *Science*, *271*, 1876–1879.
- Rich, P. B., Douillet, C. D., Mahler, S. A., Husain, S. A., & Boucher, R. C. (2003). Adenosine triphosphate is released during injurious mechanical ventilation and contributes to lung edema. *The Journal of Trauma*, *55*, 290–297.
- Rodriguez-Tirado, C., Kitamura, T., Kato, Y., Pollard, J. W., Condeelis, J. S., & Entenberg, D. (2016). Long-term high-resolution intravital microscopy in the lung with a vacuum stabilized imaging window. *Journal of Visualized Experiments*, 1–13.
- Sabirov, R. Z., Merzlyak, P. G., Islam, M. R., Okada, T., & Okada, Y. (2016). The properties, functions, and pathophysiology of maxi-anion channels. *Pflügers Archiv*, *468*, 405–420.
- Sabirov, R. Z., Merzlyak, P. G., Okada, T., Islam, M. R., Uramoto, H., Mori, T., et al. (2017). The organic anion transporter SLCO2A1 constitutes the core component of the Maxi-Cl channel. *The EMBO Journal*, *36*, 3309–3324.
- Sabirov, R. Z., & Okada, Y. (2005). ATP release via anion channels. *Purinergic Signal*, *1*, 311–328.
- Sadananda, P., Kao, F. C., Liu, L., Mansfield, K. J., & Burcher, E. (2012). Acid and stretch, but not capsaicin, are effective stimuli for ATP release in the porcine bladder mucosa: Are ASIC and TRPV1 receptors involved? *European Journal of Pharmacology*, *683*, 252–259.

- Seminario-Vidal, L., Kreda, S., Jones, L., O'neal, W., Trejo, J., Boucher, R. C., et al. (2009). Thrombin promotes release of ATP from lung epithelial cells through coordinated activation of rho- and Ca²⁺-dependent signaling pathways. *The Journal of Biological Chemistry*, *284*, 20638–20648.
- Shigematsu, T., Koshiyama, K., & Wada, S. (2015). Effects of stretching speed on mechanical rupture of phospholipid/cholesterol bilayers: Molecular dynamics simulation. *Scientific Reports*, *5*, 15369.
- Sikora, J., Orlov, S. N., Furuya, K., & Grygorczyk, R. (2014). Hemolysis is a primary ATP-release mechanism in human erythrocytes. *Blood*, *124*, 2150–2157.
- Skotak, M., Wang, F., & Chandra, N. (2012). An in vitro injury model for SH-SY5Y neuroblastoma cells: Effect of strain and strain rate. *Journal of Neuroscience Methods*, *205*, 159–168.
- Stutts, M. J., Fitz, J. G., Paradiso, A. M., & Boucher, R. C. (1994). Multiple modes of regulation of airway epithelial chloride secretion by extracellular ATP. *The American Journal of Physiology*, *267*, C1442–C1451.
- Sugiura, M., McCulloch, P. R., Wren, S., Dawson, R. H., & Froese, A. B. (1994). Ventilator pattern influences neutrophil influx and activation in atelectasis-prone rabbit lung. *Journal of Applied Physiology (Bethesda, MD: 1985)*, *77*, 1355–1365.
- Takahara, N., Ito, S., Furuya, K., Naruse, K., Aso, H., Kondo, M., et al. (2014). Real-time imaging of ATP release induced by mechanical stretch in human airway smooth muscle cells. *American Journal of Respiratory Cell and Molecular Biology*, *51*, 772–782.
- Tarran, R. (2004). Regulation of airway surface liquid volume and mucus transport by active ion transport. *Proceedings of the American Thoracic Society*, *1*, 42–46.
- Tarran, R., Button, B., & Boucher, R. C. (2006). Regulation of normal and cystic fibrosis airway surface liquid volume by phasic shear stress. *Annual Review of Physiology*, *68*, 543–561.
- Taruno, A. (2018). ATP release channels. *International Journal of Molecular Sciences*, *19*.
- Taruno, A., Vingtdoux, V., Ohmoto, M., Ma, Z., Dvoryanchikov, G., Li, A., et al. (2013). CALHM1 ion channel mediates purinergic neurotransmission of sweet, bitter and umami tastes. *Nature*, *495*, 223–226.
- Tatur, S., Groulx, N., Orlov, S. N., & Grygorczyk, R. (2007). Ca²⁺-dependent ATP release from A549 cells involves synergistic autocrine stimulation by coreleased uridine nucleotides. *The Journal of Physiology*, *584*, 419–435.
- Tatur, S., Kreda, S., Lazarowski, E., & Grygorczyk, R. (2008). Calcium-dependent release of adenosine and uridine nucleotides from A549 cells. *Purinergic Signal*, *4*, 139–146.
- Thomas, S. L. (2014). Intravascular hemolysis: The sacrifice of few.... *Blood*, *124*, 2011–2012.
- Tschumperlin, D. J., Oswari, J., & Margulies, A. S. (2000). Deformation-induced injury of alveolar epithelial cells. Effect of frequency, duration, and amplitude. *American Journal of Respiratory and Critical Care Medicine*, *162*, 357–362.
- Uhlig, U., & Uhlig, S. (2011). Ventilation-induced lung injury. *Comprehensive Physiology*, *1*, 635–661.
- Verbrugge, S. J., de Jong, J. W., Keijzer, E., Vazquez de Anda, G., & Lachmann, B. (1999). Purine in bronchoalveolar lavage fluid as a marker of ventilation-induced lung injury. *Critical Care Medicine*, *27*, 779–783.
- Voss, F. K., Ullrich, F., Munch, J., Lazarow, K., Lutter, D., Mah, N., et al. (2014). Identification of LRRC8 heteromers as an essential component of the volume-regulated anion channel VRAC. *Science*, *344*, 634–638.
- Watt, W. C., Lazarowski, E. R., & Boucher, R. C. (1998). Cystic fibrosis transmembrane regulator-independent release of ATP. Its implications for the regulation of P2Y2 receptors in airway epithelia. *The Journal of Biological Chemistry*, *273*, 14053–14058.

- Workman, A. D., Carey, R. M., Chen, B., Saunders, C. J., Marambaud, P., Mitchell, C. H., et al. (2017). CALHM1-mediated ATP release and ciliary beat frequency modulation in nasal epithelial cells. *Scientific Reports*, 7, 6687.
- Yamamoto, K., & Ando, J. (2018). Emerging role of plasma membranes in vascular endothelial mechanosensing. *Circulation Journal*, 82, 2691–2698.
- Yamamoto, K., Furuya, K., Nakamura, M., Kobatake, E., Sokabe, M., & Ando, J. (2011). Visualization of flow-induced ATP release and triggering of Ca^{2+} waves at caveolae in vascular endothelial cells. *Journal of Cell Science*, 124, 3477–3483.
- Yamamoto, K., Imamura, H., & Ando, J. (2018). Shear stress augments mitochondrial ATP generation that triggers ATP release and Ca^{2+} signaling in vascular endothelial cells. *American Journal of Physiology. Heart and Circulatory Physiology*, 315, H1477–H1485.
- Zimmermann, H. (2000). Extracellular metabolism of ATP and other nucleotides. *Naunyn-Schmiedeberg's Archives of Pharmacology*, 362, 299–309.
- Zimmermann, H. (2016). Extracellular ATP and other nucleotides-ubiquitous triggers of intercellular messenger release. *Purinergic Signal*, 12, 25–57.
- Zimmermann, H., Zebisch, M., & Sträter, N. (2012). Cellular function and molecular structure of ecto-nucleotidases. *Purinergic Signal*, 8, 437–502.

Appendix B

- **Reference 130** (DOI: 10.1152/ajplung.00425.2015)

Real-time imaging of inflation-induced ATP release in the ex vivo rat lung

Kishio Furuya, Ju Jing Tan, Francis Boudreault, Masahiro Sokabe, Yves Berthiaume, and Ryszard Grygorczyk

American Journal of Physiology-Lung Cellular and Molecular Physiology 2016 311:5, L956-L969

Reproduced with the permission of American Physiological Society

CALL FOR PAPERS | *Real-time Visualization of Lung Function: from Micro to Macro*

Real-time imaging of inflation-induced ATP release in the ex vivo rat lung

Kishio Furuya,¹ Ju Jing Tan,² Francis Boudreault,² Masahiro Sokabe,¹ Yves Berthiaume,^{3,4}
and Ryszard Grygorczyk^{2,3}

¹Mechanobiology Laboratory, Graduate School of Medicine, Nagoya University, Nagoya, Japan; ²Centre de recherche, Centre hospitalier de l'Université de Montréal (CRCHUM), Montreal, Quebec, Canada; ³Department of Medicine, Université de Montréal, Montreal, Quebec, Canada; and ⁴Institut de recherches cliniques de Montréal (IRCM), Quebec, Canada

Submitted 11 December 2015; accepted in final form 13 September 2016

Furuya K, Tan JJ, Boudreault F, Sokabe M, Berthiaume Y, Grygorczyk R. Real-time imaging of inflation-induced ATP release in the ex vivo rat lung. *Am J Physiol Lung Cell Mol Physiol* 311: L956–L969, 2016. First published September 16, 2016; doi:10.1152/ajplung.00425.2015.—Extracellular ATP and other nucleotides are important autocrine/paracrine mediators that regulate diverse processes critical for lung function, including mucociliary clearance, surfactant secretion, and local blood flow. Cellular ATP release is mechanosensitive; however, the impact of physical stimuli on ATP release during breathing has never been tested in intact lungs in real time and remains elusive. In this pilot study, we investigated inflation-induced ATP release in rat lungs ex vivo by real-time luciferin-luciferase (LL) bioluminescence imaging coupled with simultaneous infrared tissue imaging to identify ATP-releasing sites. With LL solution introduced into air spaces, brief inflation of such edematous lung (1 s, ~20 cmH₂O) induced transient (<30 s) ATP release in a limited number of air-inflated alveolar sacs during their recruitment/opening. Released ATP reached concentrations of ~10⁻⁶ M, relevant for autocrine/paracrine signaling, but it remained spatially restricted to single alveolar sacs or their clusters. ATP release was stimulus dependent: prolonged (100 s) inflation evoked long-lasting ATP release that terminated upon alveoli deflation/derecruitment while cyclic inflation/suction produced cyclic ATP release. With LL introduced into blood vessels, inflation induced transient ATP release in many small patchlike areas the size of alveolar sacs. Findings suggest that inflation induces ATP release in both alveoli and the surrounding blood capillary network; the functional units of ATP release presumably consist of alveolar sacs or their clusters. Our study demonstrates the feasibility of real-time ATP release imaging in ex vivo lungs and provides the first direct evidence of inflation-induced ATP release in lung air spaces and in pulmonary blood capillaries, highlighting the importance of purinergic signaling in lung function.

lung ATP release; luminescence microscopy; mechanical stimulation; infrared imaging; lung inflation

EXTRACELLULAR ATP AND OTHER purines are ubiquitous mediators of local intercellular signaling within the body that involves P1 (Ado), P2Y, and P2X purinergic receptor families as well as diverse system of ectoenzymes for purine breakdown and conversion (6). In the lungs, purines regulate a variety of processes critical for lung function, including mucociliary clearance in the airways, surfactant secretion in alveoli, neutrophil chemotaxis, and local blood flow (7, 8, 45). Extracellular nucleotides and purinergic signaling have also been im-

plicated in the pathogenesis of a wide range of respiratory diseases and associated clinical complications, such as ventilator-induced lung injury, acute respiratory distress syndrome, asthma, and chronic obstructive pulmonary disease (1, 14, 20, 23, 33). Despite the physiological and pathophysiological importance of extracellular nucleotides, their sources in the lung, efflux mechanisms, and regulatory pathways remain poorly defined. In recent years, it has become clear that, under normal physiological and many pathological conditions, intact cells release ATP into the extracellular environment, and frequently this release is mechanosensitive (19, 29, 39). Lung epithelial cells are subjected to several forms of mechanical stresses during the breathing cycle and coughing, including airflow shear stress, cell stretch, and cell distortion by tension forces at the air-liquid interface, all of which can evoke nonlytic ATP release. Indeed, in vitro studies have disclosed that regulated nucleotide release from epithelial cells is exquisitely sensitive to mechanical perturbations, including cell culture plate tilting (19, 29), fluid flow-induced shear stress (48, 52), mechanical stress between motile cilia and mucus layer (10), cell distortion by tension forces at the air-liquid interface (41), and cell stretch (16, 18, 35, 42, 47). Cell stretch is a particularly relevant physiological stimulus in the lungs (15), where expansion of alveoli during the breathing cycle leads to significant thinning of the alveolar walls that involves stretch and deformation of the alveolar epithelium. Stretch is also recognized as an important physiological stimulus of surfactant secretion by alveolar type II (ATII) cells (3, 22, 32, 37), which may comprise synergistic effects of coreleased ATP, a potent surfactant secretagogue, but the exact mechanisms of this process are not fully understood (12, 13). Beside stretch, airflow shear stress and cell deformation by tension forces at the air-liquid interface may also contribute to mechanosensitive ATP release in the lung. In pulmonary edema where a significant amount of liquid can accumulate in the air spaces, inflation induced liquid movement may generate shear stress while thinning of the liquid layer in expanding air spaces may expose the epithelium to tension forces at the air liquid interface.

ATP in the lumen of blood vessels contributes to local control of blood flow via activation of purinergic receptors of vascular endothelial cells, resulting in synthesis of nitric oxide and other powerful relaxation factors of smooth muscle vasculature (9, 40). Shear stress and hypoxia are known stimuli of intravascular ATP release from endothelial cells (4) and red blood cells (46) in many organs including lungs; however, the inflation-induced ATP release in the lumen of pulmonary blood

Address for reprint requests and other correspondence: R. Grygorczyk, CRCHUM-Pavillon R, 900, rue St-Denis, Montréal, Québec, Canada H2X 0A9 (e-mail: ryszard.grygorczyk@umontreal.ca).

capillaries of intact lungs has never been investigated in real time.

Previous studies of ATP secretion in the lung were based on bulk measurements such as lung lavage that do not provide insights into cellular processes and may by themselves induce mechanosensitive release (14). While ATP release has been investigated extensively in vitro using isolated lung epithelial cells (5, 18, 25, 30, 36), cultured lung cells may inadequately replicate native cell responses because of phenotypic transformations. Real-time lung microscopy could allow the investigation of cell signaling in the native setting (24, 26, 27, 31, 34). Here, we describe a pilot study on the effect of lung inflation on ATP release in isolated rat lungs using real-time luciferin-luciferase (LL) bioluminescence imaging coupled with simultaneous infrared (IR) differential interference contrast (IR-DIC) imaging to identify ATP-releasing sites. To the best of our knowledge, ours is the first study to demonstrate the feasibility of real-time ATP release imaging in lungs *ex vivo*.

MATERIALS AND METHODS

Microscopy setups and data analysis. To visualize ATP release in real time and identify ATP-releasing sites, we deployed an imaging system that simultaneously combines high-sensitivity bioluminescence detection of ATP and IR-DIC tissue images (16, 17). Briefly, we used an upright BX51WI Olympus microscope (lens $\times 4$, $\times 10$, or $\times 20$) equipped with two electron multiplying charge-coupled device (EMCCD) cameras (for luminescence and IR imaging), as well as an image intensifier. The luminescence produced by ATP-dependent luciferin oxidation reaction was detected with a cooled EMCCD camera (Cascade 512F, Photometrics, Tucson, AZ) equipped with a water-cooled image intensifier (C8600-04, Hamamatsu Photonics, Hamamatsu, Japan). IR-DIC images were captured by a second EMCCD camera (Cascade 512F). We also employed a MacroView microscope system for low-magnification ATP imaging. We used a MacroZoom Microscope (MV10, Olympus, zooming range $\times 0.63$ – 6.3) equipped with $\times 2$ objective (MV PLAPO), double-port magnification change unit (WI-DPMC) for IR optics, and IR/visible illumination system via glass fiber. The luminescence was detected with a cooled EMCCD camera (ImagEM, Hamamatsu Photonics) and the IR image was detected by a cooled CCD camera (CoolSnap HQ, Photometrics). This MacroView microscope system does not utilize an image intensifier; therefore, despite lower magnification compared with the upright microscope system (BX51WI Olympus), it provides images of higher resolution. All ATP-imaging experiments were performed at $32 \pm 3^\circ\text{C}$.

Data acquisition was performed with MetaMorph (version 7.5 or 7.8, Molecular Devices, Downingtown, PA) installed on separate computers for luminescence and IR imaging. The data were acquired with 100- or 500-ms intervals and during offline analysis (MetaMorph) the data were typically averaged using a 10- or 6-plane jumping average routine. Both systems were equipped with a fluorescence attachment allowing acquisition of fluorescence images immediately before or after the luminescence imaging. For higher resolution fluorescence imaging, we used an upright laser scanning confocal microscope (LSM510-Axioskop2, Zeiss) equipped with $\times 10$ (Achromplan, Zeiss) and $\times 20$ (XLUMPlanFL, Olympus) objectives, or Leica TCS-SP5 with $\times 20$ objective. 3D reconstruction of optically sliced sample was done by Zen software with a transparent mode (Zeiss). To enhance the contrast of IR and fluorescence images, we applied a shading correction that involved dividing the acquired image by the background image (MetaMorph). The background images were obtained by low-pass filtering of each original image with filter width of 30–40 pixels. The size distribution of the ATP luminescence was determined by a morphometry analysis using

equivalent diameter mode (MetaMorph), which calculated an equivalent diameter from the area of ATP responses.

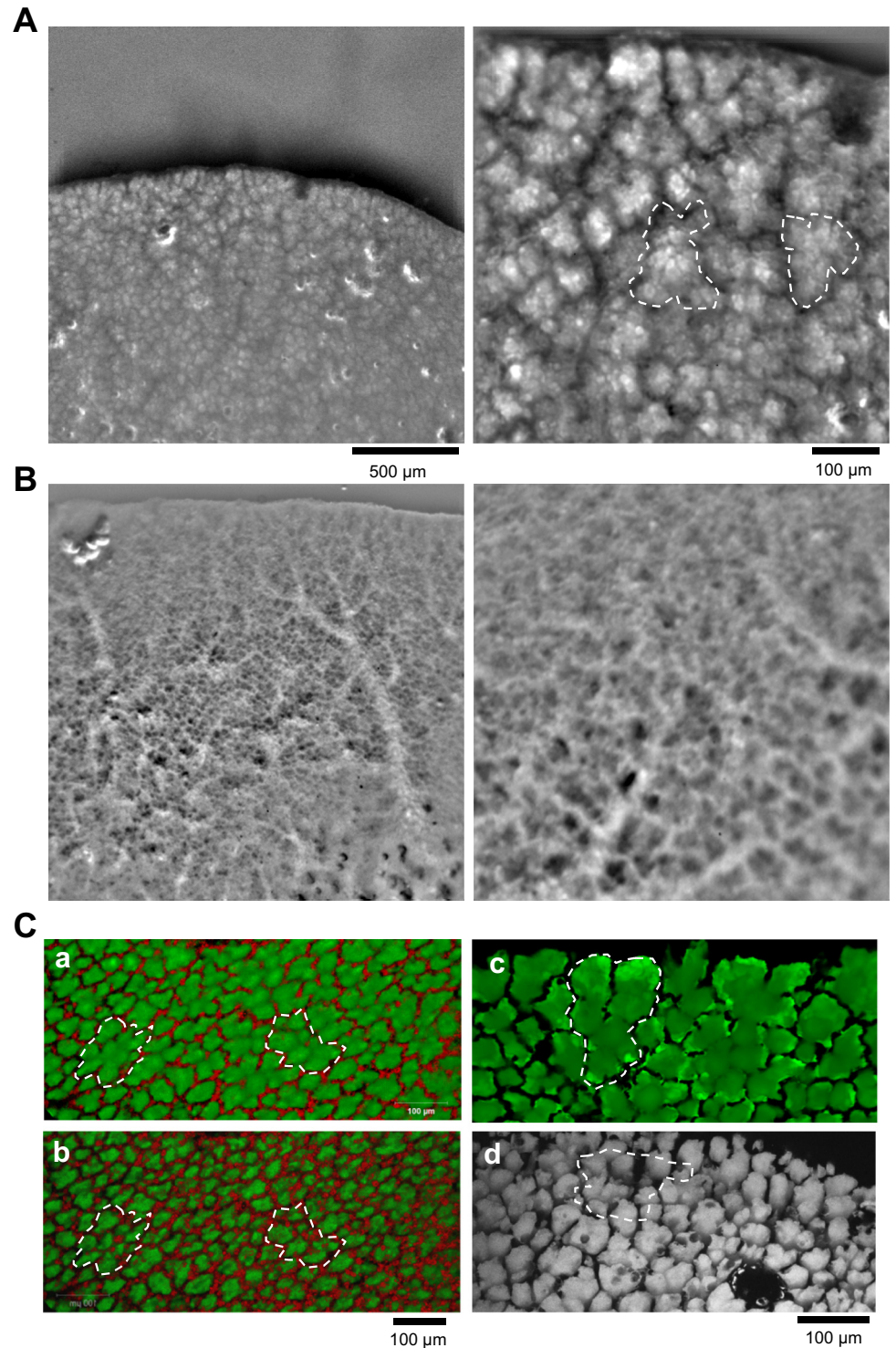
Lung isolation and preparation for *ex vivo* luminescence ATP imaging. Animal care and all experimental procedures used in the study were approved by the Animal Experiment Review Committee, Graduate School of Medicine, Nagoya University (approval nos. 26377 and 27219). Two- to 3-wk-old male Wistar rats (Japan SLC, Hamamatsu, Japan), weighing 100–120 g were studied. Their lungs were excised via a midline sternotomy after induction of pentobarbital sodium anesthesia (50 mg/kg ip) and systemic heparinization (1,000 IU/kg iv), as described in Ref. 21. After chest opening, the lower portions of the right and left ventricles were cut away, the gavage needle tip was inserted into the pulmonary artery, and perfusion was started immediately, with returning perfusate dripping from the left ventricle onto a pad. The perfusate consisted of HEPES-buffered RPMI 1640 medium supplemented with 4% BSA to equilibrate oncotic pressure. The excised lungs were placed in an open wet imaging chamber and air spaces were slowly instilled via trachea with 1 ml of HEPES-buffered DMEM containing LL (Lucifer HS, Kikkoman, Tokyo, Japan) and methylene blue (0.05%). The latter helped to localize those lung areas that were reached by the LL reagent. Subsequently, a few air pressure pulses (10–20 cmH₂O) were applied to ventilate the lung and promote liquid redistribution in the tissues. In some experiments a cell membrane-impermeant form of a fluorescent dye calcein (10 μM , Dojindo, Kumamoto, Japan) or FITC-dextran (20 kDa) conjugate (Sigma Aldrich) was included in the LL reagent to investigate its distribution in the lung by fluorescence microscopy. To investigate ATP release in the lumen of pulmonary blood capillaries the LL-containing solution was introduced via the pulmonary artery into lung blood vessels. For a double-staining experiment, LL/calcein was introduced via trachea, while Rhodamine B (10 μM , TCI, Tokyo, Japan) containing HEPES-buffered DMEM was perfused via pulmonary artery. It should be noted that our ATP imaging approach relies on the bioluminescence reaction in the extracellular space, where luciferase catalyzes oxidation of the substrate luciferin and requires the presence of ATP. If LL reagent is uniformly and abundantly distributed within the lung air spaces or blood vessels, luminescence can only be generated when, e.g., cellular ATP is released into the extracellular space. Furthermore, lack of the signal in the resting lung serves as a negative control, demonstrating absence of extracellular ATP prior to stimulation.

In this study, the lungs were inflated by positive (intra-alveolar) pressure, which simulates mechanical ventilation. Inflation was produced manually with a 1-ml syringe connected via polyethylene tubing to the trachea and pressure was monitored with a digital differential pressure manometer (HD700, Exttech Instruments, Nashua, NH). Perfusion was stopped during luminescence imaging, but lung viability was well preserved due to relatively short experiment duration (30 to 60 min), as judged by the maintained ATP release responsiveness to stimuli.

RESULTS

Distribution of LL reagent in the lung. Because visualization of ATP release required instillation of LL-containing solution into the lung prior to the experiment, we investigated its distribution by fluorescence microscopy with fluorescent dye calcein that was included in the LL solution. Figure 1A shows epifluorescence images of lung tissue with LL/calcein solution instilled into air spaces. Images were taken using a fluorescence channel on the same microscopy setup that was used for luminescence ATP imaging (Olympus MV10). A widespread and uniform fluorescence staining of all air spaces is seen in the entire portion of the lung reached by the LL/calcein solution. Due to different volume/thickness of individual calcein-filled alveolar sacs, they show variable fluorescence intensities, es-

Fig. 1. Widespread and uniform distribution of LL reagent instilled into the lung. **A:** fluorescence images of rat lung tissue instilled via trachea with LL solution containing the fluorescent dye calcein. Images were obtained with an Olympus MV10 microscope with $\times 2$ and $\times 6.3$ zoom (*left* and *right* images, respectively). A widespread distribution of the dye throughout all air spaces in the portion of lung tissue that was reached by the LL solution could be seen. It also shows clustering of several alveolar sacs (dotted line). Shading correction using averaging filter (see MATERIALS AND METHODS) was applied to enhance the contrast of images. **B:** fluorescence images of rat lung with LL/calcein solution instilled into the lumen of pulmonary blood vessels obtained with $\times 2$ and $\times 6.3$ zoom (*left* and *right* images, respectively). Bright fluorescence clearly delineates vessels of different caliber, while air spaces remain dark and nonfluorescent, indicating no leakage of the dye from the blood compartment. **C:** double-label confocal images with rhodamine solution (red) introduced into pulmonary vessels and LL/calcein (green) into the air spaces (*a* and *b*). Stack of confocal images were 3D reconstructed with a transparent mode. Image *a* shows a view from inside the lung and image *b* shows a view of the same area from the outside with mirror image conversion for easy comparison. Note a widespread and uniform distribution of LL/calcein throughout the tissue air spaces and clear separation from the blood capillaries surrounding the alveolar sacs. Several alveolar sacs (dotted lines) form clusters with a common lumen seen in *a*, while *b* shows their view from the outer lung surface (see Supplemental Movies S1 and S2). Image *c* shows enlarged view from the lumen side, clearly demonstrating uniform distribution of LL/calcein. A large cluster of alveolar sac (dotted line) is seen in the most distal lung region. Similar uniform fluid distribution in the lumen of alveolar sacs was obtained with FITC-dextran staining taken with Leica TCS-SP5 confocal microscope and $\times 20$ lens (image *d*).



pecially apparent at higher magnification. With LL/calcein introduced into pulmonary blood vessels quite different distribution of fluorescence staining was observed (Fig. 1B). Bright fluorescence clearly delineates vessels of different caliber including capillaries surrounding individual alveolar sacs. However, air spaces remain nonfluorescent and appear dark indicating absence of dye leakage from blood compartment. This is confirmed on double-label confocal lung images *a* and *b* in Fig. 1C, where solution containing rhodamine (red) was introduced

into pulmonary vessels while LL/calcein (green) was introduced into air spaces. Both are 3D reconstructed images with a transparent mode, where *a* shows the view from the lumen side and *b* from outside of the lung (see also Supplemental Movies S1 and S2; Supplemental Material for this article is available online at the Journal website). LL/calcein appears to be present in all air spaces throughout the visible portion of the tissue with clear separation from the blood compartment, consistent with no detectable cross leakage of the dyes. Image

c on Fig. 1C shows another 3D-reconstructed view of lung air spaces from the lumen side but at the most distal area of the lung. It also clearly shows uniform distribution of calcein fluorescence in all alveolar sacs in the loaded lung area. Similar widespread and uniform fluid distribution was observed with dextran-FITC labeling (Fig. 1C, image *d*). The data demonstrate that under our experimental conditions the LL reagent is uniformly and abundantly available for detecting cellular ATP release in lung air spaces. Furthermore, with LL solution introduced via pulmonary artery ATP release could be visualized separately in the lumen of pulmonary blood vessels.

Impact of fluid instillation on alveolar inflation micromechanics. Because instillation of LL-containing fluid into the air spaces may affect lung responses to air inflation, Fig. 2A compares IR-DIC images of control lung and a lung that was instilled with 1 ml of LL solution 30 min prior to the experiment (images *a* and *b*, respectively). The lungs were inflated with 1-s positive pressure pulse of ~ 20 cmH₂O from a resting pressure level of 0–2 cmH₂O. Applied pressure pulse caused sequential inflation/opening of multiple alveolar sacs, visible on IR images as dark-edged strings because of light refraction at the air-liquid interface in air-filled alveoli. The striking difference was significantly larger expansion (by $\sim 92\%$) of air inflated alveolar spaces in the liquid-instilled compared with the control lung (Fig. 2B). This may have resulted from prestretch and overdistension of air-filled alveoli juxtaposed with multiple fluid-filled alveoli, as reported previously by Perlman et al. (38). The data are consistent with the notion that under our experimental conditions LL-containing lungs are in a state resembling pulmonary edema and exhibit an altered micromechanics of alveolar inflation.

Single inflation-induced ATP release. Imaging the thin distal regions of lung tissue, at the edges of the lung lobes, allows clear visualization of both ATP release via ATP-dependent luminescence and individual alveolar sacs on IR images. With this approach spatial localization of ATP release sites can be achieved with reasonably high resolution, even with low-power lenses, e.g., $\times 4$ (NA 0.28). Figure 3A (see also Supplemental Movie S3 in Supplemental Material) is an example of ATP release time course in a rat lung instilled with LL-containing medium via the trachea and stimulated by brief air inflation with 1-s positive pressure pulse of ~ 20 cmH₂O from resting pressure level of 0–2 cmH₂O. It initiated sequential opening of multiple alveolar sacs in the form of branching strings followed by their gradual retraction after pressure was released. Lung expansion also produced flashes of luminescence due to ATP release (shown in red), which occurred at the leading tips of air-filled strings of alveolar sacs during their inflation. ATP release sites appeared as highly localized small spots in distal lung areas that were in focus, e.g., two sites marked by white circles on frame 137. Other ATP release sites presented more diffuse luminescence, likely due to out-of-focus localization and the presence of overlaid tissue in a three-dimensional tissue sample, e.g., in proximal lung areas seen in the center-lower part of the images. ATP release typically lasted 4–30 s (Fig. 3B). Shorter release events were usually observed in distal lung regions while proximal regions showed longer release times. Release events occurred in a limited number of sites, e.g., in Fig. 3A, up to ~ 40 sites of ATP release can be recognized in the visible portion of lung tissue. Local ATP-dependent luminescence in this example reached

over 22,000 arbitrary units (AU) which for the same gain settings used in our earlier in vitro study (17, 18) might be expected for ATP concentrations in the micromolar ($\sim 10^{-6}$ M) range. However, the actual calibration of ATP/luminescence in lung tissue is more challenging and was not performed in this study.

Alveolar derecruitment terminates ATP release. In experiments such as illustrated in Fig. 3, ATP release durations were widespread ranging from 4 to 30 s. Closer analysis of IR-DIC images revealed that the two shortest ATP release responses (shown in Fig. 3A at 137 s) occurred in distal alveoli at the tips of inflated sacs that closed rapidly after pressure release. This can be seen by comparing IR-DIC tissue images, e.g., an image at 137 s, i.e., 2 s after stimulation and at the peak of ATP release, with an image 8 s later (at 145 s elapsed time), when ATP release terminated completely at these two sites (Fig. 4Ab). Retraction of air-filled alveolar sacs due to alveoli deflation precisely at ATP release sites coincided with ATP release termination, suggesting that early termination of ATP release might be related to declining mechanical strain, or relief of cell deformation by tension forces at the air-liquid interface in edematous lung during relaxation and alveolar derecruitment. This is also consistent with the observation that shorter spikes of ATP release were observed in distal lung regions, which also showed faster tissue relaxation compared with proximal parts of lung tissue where longer ATP release responses occurred (see Fig. 3B). It suggests that preventing alveolar derecruitment, e.g., by applying longer pressure pulse, should produce long-lasting ATP release events, which was indeed confirmed in an experiment illustrated in Fig. 4B, where lung inflation by 15 cmH₂O pressure was held for 100 s. During such prolonged stimulation, the tissue showed little relaxation with long-lasting ATP release in at least seven different sites in the field of view. Average ATP release duration (τ) almost doubled and presented less variation ($\tau = 39 \pm 4.4$ s) (Fig. 4, C and D), compared with the experiment illustrated in Fig. 3B where short 1-s stimuli produced ATP release events of shorter average duration and larger variation $\tau = 21.5 \pm 8.3$ s.

ATP release responses to repeated stimulation. Figure 5A shows sites of ATP-dependent luminescence in lung tissue subjected to two sequential inflations (5-s pulses of ~ 20 cmH₂O) separated by 30-min recovery (images *a* and *b*, respectively). Images were acquired with stereoscopic Macro-Zoom microscope (Olympus MV10). In contrast to transmitted light tissue images shown in Fig. 3, here reflected IR light is collected and air-inflated alveoli show up as a bright areas. The first stimulation caused inflation-induced ATP release in two nonadjacent areas, whereas during the second stimulation ATP release occurred only in newly inflated/recruited regions but not in the ones that were inflated and responded during the first inflation (delineated by broken lines in *b*). The data suggest that ATP release occurs predominantly in a newly recruited lung area during opening of alveolar sacs. Figure 5B shows similar two-pulse experiment (images *a* and *b*, respectively) at higher magnification ($\times 4$ lens) with transmitted IR light tissue images, demonstrating that sparks of luminescence representing ATP release occurred almost exclusively at the leading tips of air-filled strings of alveolar sacs. These ATP release sites for the first and second stimulation are overlaid in image *a* of Fig. 5C and displayed in red and green, respectively, showing no

overlap for the two stimuli. With the first inflation ATP release occurred mainly in the middle portion of the tissue image, whereas during the second stimulation it was outside this area but always at the tips of newly formed air-filled sacs that did

not overlap with those formed during the first pulse. This can be seen in image *b* of Fig. 5C, which represents overlaid IR-DIC images of lung tissue at maximal expansion during the two inflations. The dark-edged air-filled strings of alveolar sacs formed by the first and second inflation appear in red and green, respectively. In contrast to ATP release sites, they overlapped significantly in proximal but not in distal regions where their tips often extended to different parts of tissue for the two pressure pulses. The data suggest that ATP release is induced exclusively during opening/recruitment of new air-filled alveolar sacs and occurs only in a limited number of sacs.

Effect of cyclic inflation/deflation on ATP release. To test effect of cyclic stimulation we imaged a thick central portion of the lung focusing on deeper tissue section. A brief (1 to 3 s) positive and negative pressure pulses (approximately $+20/-10$ cmH₂O) at ~ 15 -s interval were applied to rapidly inflate and deflate the lung. With this approach individual alveolar sacs and ATP release sites can't be well resolved, especially in deeper tissue regions, because of tissue movements during stimulation and more diffuse IR and luminescence images. However, the average luminescence signal could still be measured, originating from many ATP release sites within a tissue interrogation volume (determined by depth of focus) and may include alveoli and airways. In the experiment reported in Fig. 6, the lung was subjected to cyclic pressure/suction pulses, which resulted in cyclic ATP release-dependent luminescence changes that closely followed lung inflation and showed rapid decay during forced lung exhalation/deflation. Release was stronger for the first pulse of 3-s duration, compared with subsequent shorter 1-s pulses, demonstrating that ATP release is stimulus dependent and varies with stimulus duration and frequency. Termination of ATP release during alveolar derecruitment described above likely contributes to the decaying phase of ATP release during forced lung deflations illustrated in Fig. 6. After correcting tissue movements, averaging of the residual ATP-dependent luminescence clearly shows a localized dotlike pattern of the responses (Fig. 6, bottom right corner image).

ATP release sites are clusters of alveolar sacs. Highly localized ATP release is also apparent in experiments when larger portion of the lung was imaged with MacroView microscope (Fig. 7A; see Supplemental Movie S4). In this experiment, a large number of inflation-induced ATP release events coincidentally occurred right in the focal plane and are well in focus. Closer inspection of ATP-dependent luminescence (Fig. 7B) shows that ATP responses were contained within small areas and did not spread outside these spots as might be expected for free diffusion (see Supplemental Movie S5). Size distribution of luminescence responses is shown in Fig. 7C.

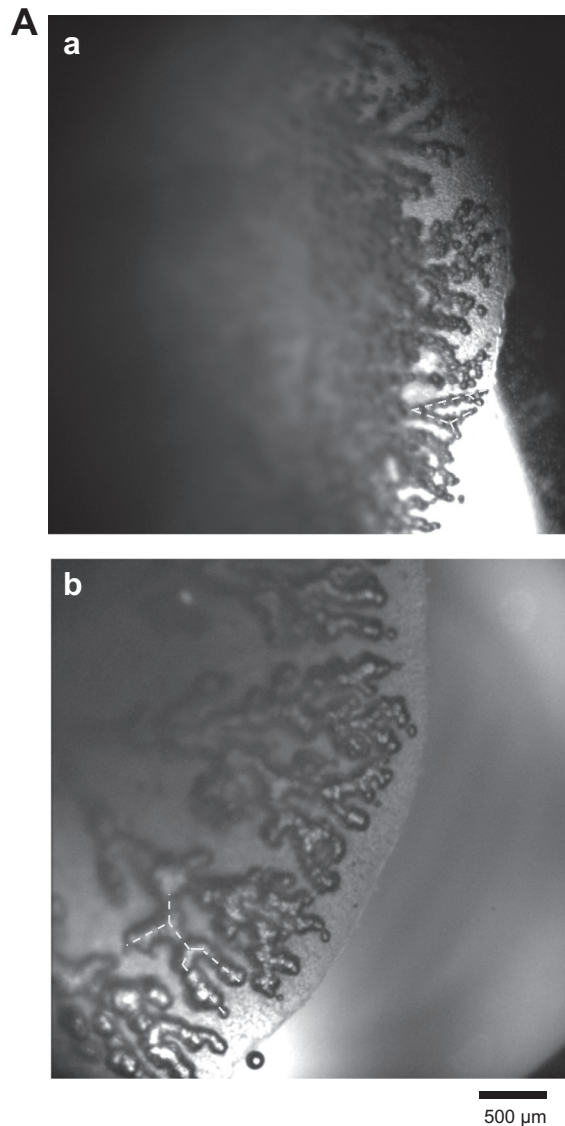


Fig. 2. Air inflation of normal and edematous lung. *A*: IR-DIC images of air-inflated control lung (*a*) and lung instilled with 1 ml of LL-containing solution 30 min prior to the experiment (*b*). The lungs were inflated with 1-s positive pressure pulse of ~ 20 cmH₂O from the resting level of 0–2 cmH₂O. The entire field of view is $\sim 3.3 \times 3.3$ mm. The data representative of $n = 6$ (control) and $n = 6$ (edematous) lungs. *B*: average width (\pm SE) of air-inflated strings of alveolar sacs was significantly (92%) larger in fluid-instilled edematous lungs compared with the control ($P < 0.05$). The data were calculated from cross-sectional area of all visible air-filled alveolar sacs divided by their length (broken lines in *A*, shown as an example).

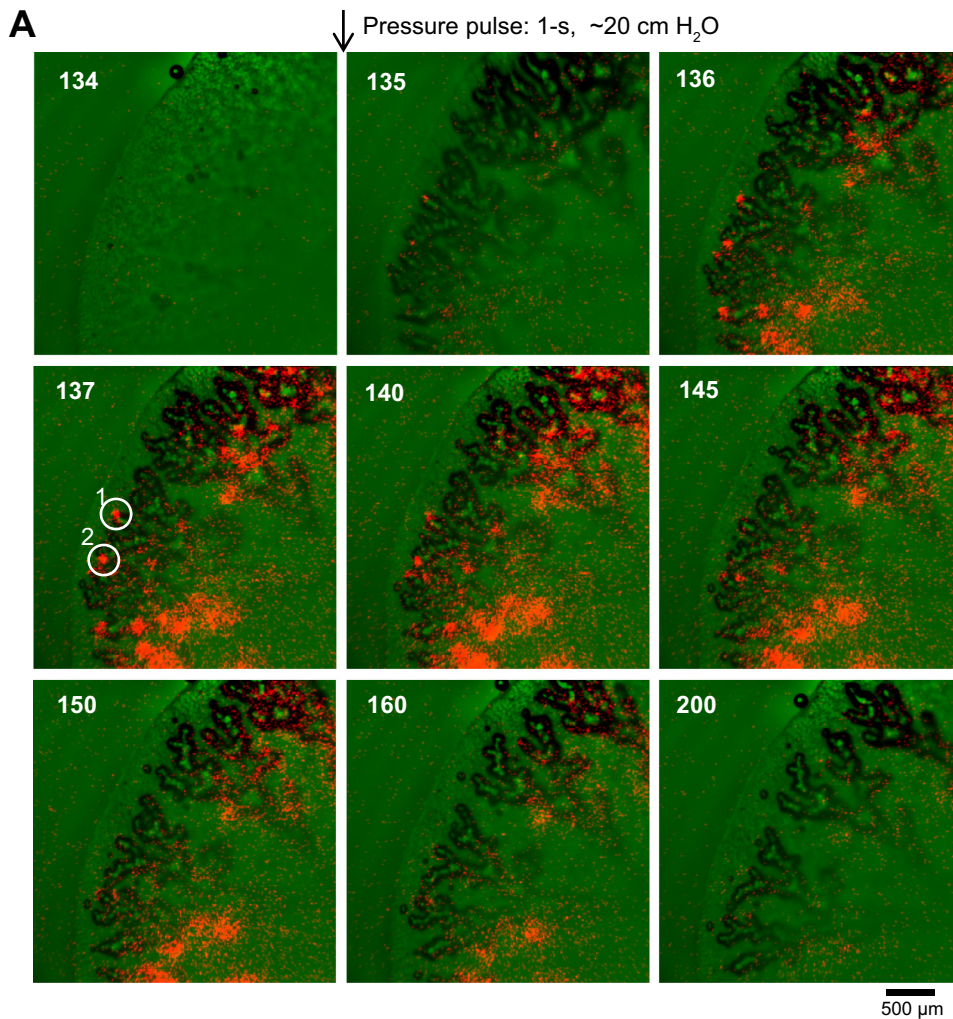
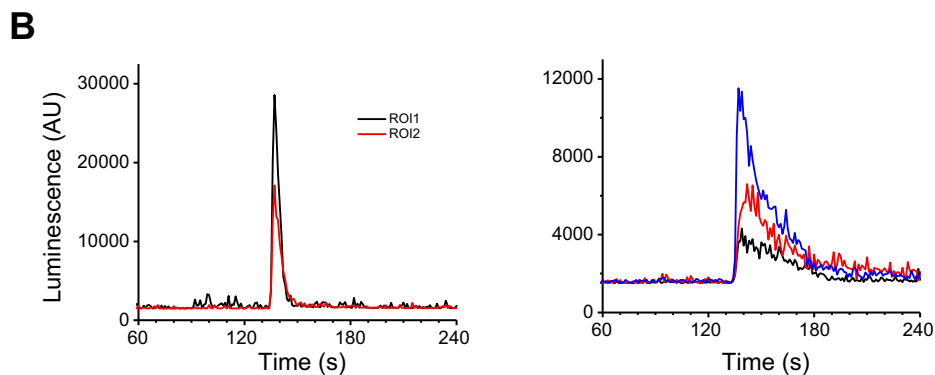


Fig. 3. ATP release in alveolar spaces in rat lung induced by single inflation *ex vivo*. **A:** sequence of overlay images illustrating localization of ATP-dependent luminescence (red) and IR-DIC tissue images (green). Elapsed time (in seconds) is given in the top left corners. At 135 s a pressure pulse (1 s, ~20 cmH₂O) was applied via the trachea to inflate the lungs. Inflated, air-filled alveolar sacs appear as dark-edged areas on IR images. Note inflation-caused tissue shift. Localized luminescence “sparks” due to ATP release occur at leading tips of some air-filled alveolar sacs, e.g., regions of interest (ROI) 1 and 2, marked by white circles on image acquired at 137 s (see Supplemental Movie S3). LL-containing medium was introduced into the air spaces ~20 min before experiment. Images were acquired with a $\times 4$ objective. The experiment was replicated with 6 separate lung preparations. **B:** time course of intra-alveolar ATP release in distal regions marked as ROI 1 and 2, *left*, and proximal regions (center lower image area), *right*. The latter illustrates examples of longer-lasting (up to 30 s) ATP release responses seen in more proximal lung areas of the same experiment. For clarity, only 3 responses of ~40 in the field of view are shown.

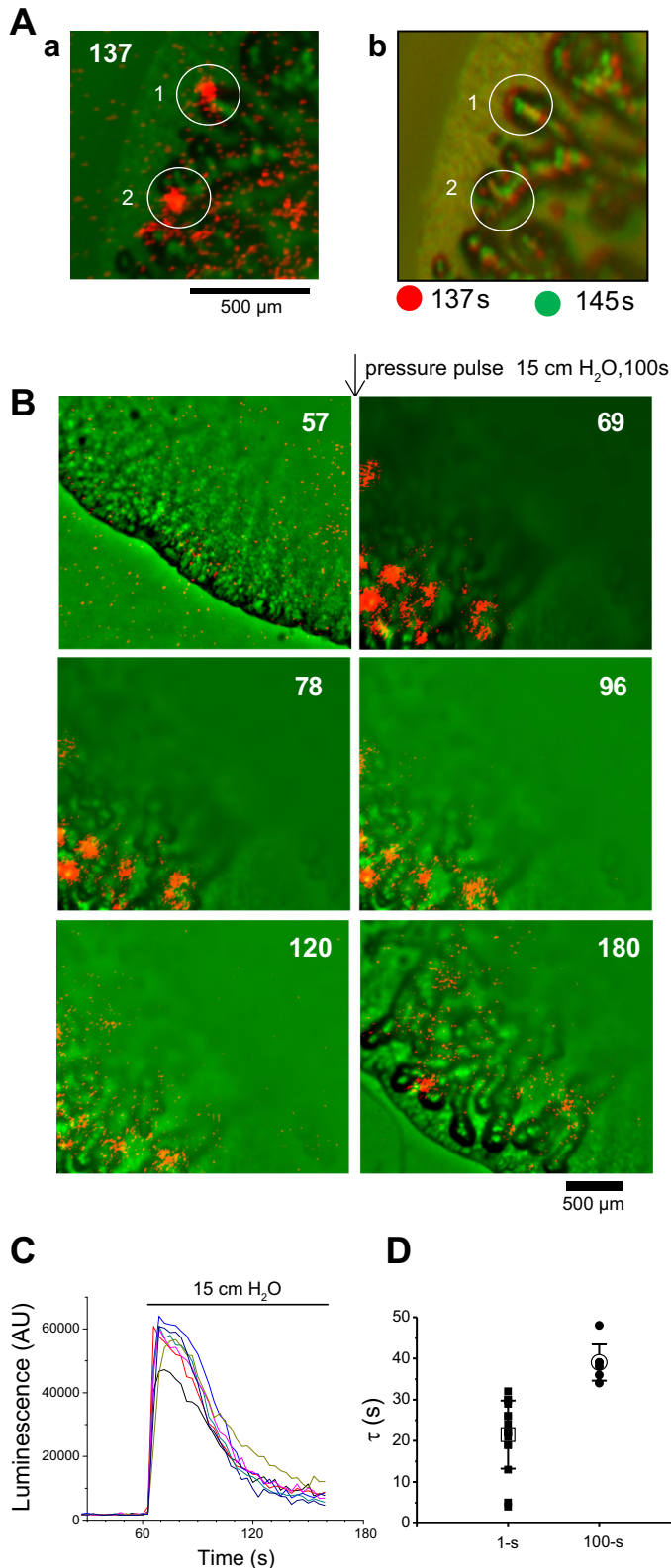


Several high-intensity responses of large and medium size (equivalent diameter over 160 μm and around 120 μm , respectively) could be seen in Fig. 7B. In addition, a large number of small-size responses (dots of 40–80 μm in diameter) could be resolved in the background (e.g., image at 13.0 s in *B*), displaying weak intensity with a frequent fluctuation (see Supplemental Movie S5). The shape and size of large luminescence responses correspond well with irregular polygonal shape and size of alveolar sacs, suggesting that the elementary unit of ATP responses consist of single alveolar sacs or their clusters as shown in Fig. 1 (areas delineated by broken

lines). Interestingly, a few weak luminescence protrusions could be observed (arrows in Fig. 7B), indicating that limited ATP diffusion to neighboring alveolar sacs may occasionally occur.

To demonstrate reproducibility of inflation-induced ATP release responses observed in different experiments and/or evoked by repeated stimulation of the same lung preparation, we have analyzed number of responses and their peak intensities in 10 regions where almost all responses were in focus, such as those delineated in Fig. 5A. Data in Table 1 show that the average number of responses per square millimeter of

inflated lung region (5.56 ± 0.26 , range 4.5 to 7.1) and average peak response intensity ($22,069 \pm 1,489$ AU) are remarkably similar in all analyzed regions, which demonstrates high reliability of our experimental system, allowing for a quantitative data analysis.



Inflation-induced ATP release in pulmonary blood capillaries. Luminescence imaging can also visualize ATP release in alveolar capillary network when LL-containing solution is perfused into pulmonary blood vessels via pulmonary artery. When the lung was inflated by air injection through the trachea, the luminescence was observed in restricted lung regions resembling those seen with inflation-induced ATP release in air spaces. Figure 8A shows ATP release responses in the pulmonary capillary network induced by two brief inflations (image *a*). They displayed a widespread diffuse pattern distinctly different from that observed in alveoli. The responses subsided quickly after deflation or during weak inflations (image *b*) and did not spread outside the active area. While the responses appear diffuse, they consisted of many small patchlike responding areas (arrows in Fig. 8A, see also Supplemental Movie S6). The same patchlike responses of ATP-dependent luminescence is more clearly seen in image *c* that was obtained in another experiment where ATP release was induced by inflation at 30 s. The size of these patches was ~ 70 to $260 \mu\text{m}$, corresponding to the size of alveolar sacs or their clusters. In experiment reported in Fig. 8B lung was stimulated with three air pressure pulses applied via trachea to induce ATP release and promote its distribution in blood capillaries. Several minutes later after the peak response subsided, the residual faint luminescence was recorded for several minutes and averaged. A ring-shaped honeycomb-like luminescence pattern is apparent as expected for staining the lumen of blood capillaries surrounding air-filled alveolar spaces. Consistent with this notion, linescans of luminescence intensity show peaks of luminescence at the edges of air-filled alveolar sacs and lower signal in their lumens.

Experiments demonstrate that alveolar inflation induces transient ATP release in the lumen of the pulmonary blood capillary network. The release occurs in several small patchlike regions, likely capillary network surrounding clusters of alveolar sacs and, in the absence of perfusion, it is followed by

Fig. 4. Effect of alveolar derecruitment on intra-alveolar ATP release duration. *A, a*: zoomed-in image of lung tissue where brief ATP release events occurred, as shown on Fig. 3A at 137 s. Red represents ATP release-dependent luminescence and green IR-DIC lung tissue. *b*: Overlay of 2 IR-DIC tissue images acquired at 137 and 145 s, i.e., at the peak of ATP release at maximal inflation, and after ATP release at these sites ceased completely because of tissue relaxation. The image reveals changes in tissue position at the 2 time points, where the overlapping areas that did not change their position are seen in black, while those that had shifted show up in colors. This occurred at some edges of air-filled sacs, where red represents position at 137 s and green at 145 s. Note that sites of brief ATP release events (shown in *a*) match well with sites where tissue had retracted rapidly after pressure release (red/green edges in image *b*). *B*: effect of prolonged inflation on ATP release. Sequential overlay images display ATP-dependent luminescence (red) and IR-DIC tissue images (green). Time (in seconds) is indicated in the top right corners. At 60 s, a pressure pulse (~ 15 cm H_2O) was applied via the trachea to inflate the lung and was held for 100 s. Localized luminescence due to ATP release occur at the leading tips of some air-filled alveolar sacs in the distal lung region. *C*: time course of intra-alveolar ATP release in response to prolonged inflation at 7 sites shown in *B*. In this experiment camera exposure time was 500 ms. With this setting luminescence intensity of 60,000 AU corresponds to 23,000 AU measured with 100-ms exposure time typically used in other experiments. *D*: ATP release decay time (τ), to $1/e$ of the peak for responses induced by 1-s inflation in Fig. 3A experiment (■), or 100-s inflation in experiment shown in *B* above (●), respectively. Means \pm SD are indicated by open symbols, $n = 16$ or 7 for the 2 corresponding experiments. The means are significantly different $P < 0.05$, 1-way ANOVA test.

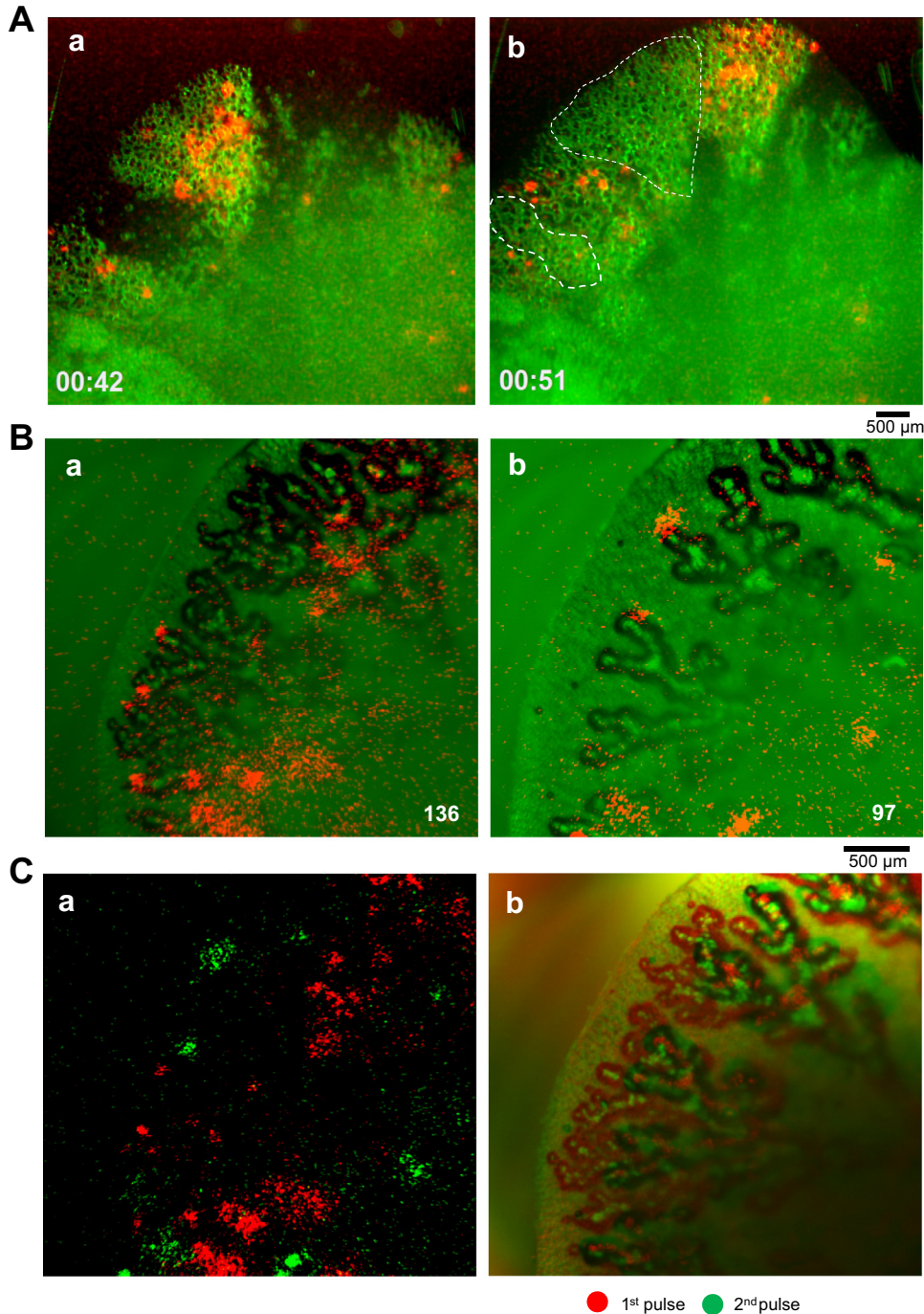


Fig. 5. Intra-alveolar ATP release responses to repeated stimulation. *A*: overlay of IR tissue images (green) and peak ATP-dependent luminescence (red) in response to 2 consecutive pressure pulses (5 s, ~ 20 cmH₂O) separated by 30-min recovery period at 0–2 cmH₂O (images *a* and *b*, respectively). Note that during 2nd inflation (image *b*), ATP release occurred only in newly recruited/inflated areas with no release in the regions that were inflated and responded during the 1st stimulus (marked by broken lines). Elapsed time (in min:s) of each experiment is indicated in the lower left corner. Solution containing LL and calcein was introduced into the air spaces ~ 20 min before the first inflation; images were acquired with MacroView Olympus MV10 microscope with $\times 2$ objective, $\times 0.63$ zoom. *B*: overlay of IR-DIC (transmitted light) tissue images (green) and peak ATP-dependent luminescence (red) in response to 2 consecutive inflations (1 s, ~ 20 cmH₂O) separated by 30-min recovery period at 0–2 cmH₂O (images *a* and *b*, respectively). Note that for both stimuli ATP release occurred at the tips of newly recruited alveolar sacs. Elapsed time (in seconds) of each experiment is indicated in the bottom right corner. LL-containing medium was introduced into the air spaces ~ 20 min before the first inflation; images were acquired with upright BX51WI Olympus microscope with $\times 4$ objective. *C*, *a*: overlaid luminescence images showing ATP release sites for the 1st and 2nd stimulation (red and green, respectively) shown in *Ba* and *Bb*. Note that there is no overlap of ATP release sites for the 2 stimuli. *b*: Overlaid IR-DIC images present air-filled alveolar sacs with red edges corresponding to 1st stimulation, and with green edges to 2nd stimulation shown in *Ba* and *Bb*. They overlap significantly in proximal but not in distal regions where their tips extend to different tissue areas.

relatively slow diffusional ATP spreading within capillary lumens.

DISCUSSION

In this work, we applied simultaneous real-time luminescence ATP imaging and IR tissue imaging to investigate inflation-induced ATP release in rat lungs *ex vivo*. To the best of our knowledge, ours is the first study to demonstrate the feasibility of imaging ATP release in real time in intact lung tissue. To visualize ATP release in lung air spaces via ATP-dependent luminescence, up to 1 ml of LL-containing DMEM was instilled in the lung 20–30 min before the experiment

started. Although some liquid could be reabsorbed rapidly, most alveoli will remain fluid-filled during subsequent imaging experiments due to relatively large volume of instilled fluid. In microinjected rat alveoli liquid clearance was attributed, in part, to rapid fluid ejection to adjacent air-filled alveoli (51). In our study, such a clearance mechanism could result in more uniform redistribution of LL reagent in a larger number of adjacent alveoli during its instillation. Indeed, fluorescence microscopy with calcein or FITC-dextran included in the LL solution confirmed its widespread and uniform distribution in essentially all air spaces throughout the tissue region reached by the dye, with no cross-leakage to the blood compartment.

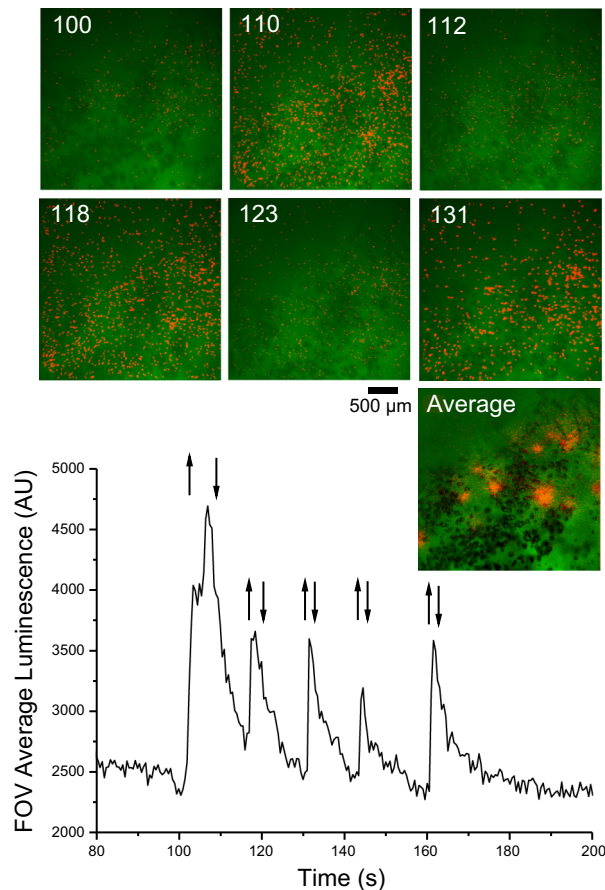


Fig. 6. Effect of cyclic inflation-deflation on ATP release in alveolar spaces. A series of brief positive and negative pressure pulses (approximately $+20/-10$ cmH₂O) was applied at ~ 15 -s intervals to rapidly inflate and deflate the lung. The first pulse was of ~ 3 -s duration and subsequent pulses were of 1 s. Images show examples of overlaid IR-DIC tissue images (green) and ATP-dependent luminescence images (red) at time points indicated in the top left corners, corresponding to the first 3 peaks on the graph below. Due to large tissue thickness and its movement during inflation/deflation only diffused images of inflated alveolar sacs and spread luminescence signal can be observed in these images. After the peak response and tissue movement subsided, images of weak residual luminescence were recorded (for 57 s), realigned to correct brief tissue shifts and averaged. The image (Average) shows a clear dotlike pattern of cumulative ATP-dependent luminescence. The graph below shows changes in average luminescence in the field of view (FOV) of the lung imaged in the center part of the tissue, arrows indicate pressure/suction pulses. LL-containing medium was introduced into the air spaces ~ 30 min before the first inflation; images were acquired with upright BX51WI Olympus microscope and $\times 4$ objective.

Thus, in the edematous lung model used in this study, LL reagent should be uniformly and abundantly available for the bioluminescence reaction with ATP released from cells. Because all alveoli are uniformly filled with LL fluid, it might be also expected that during air inflation and opening/recruiting of an alveolus most liquid will remain within alveolar space, lining the alveolar walls. Therefore, there should be comparable amount of LL reagent retained in the fluid lining walls of an air-inflated alveolus as in a fully liquid-filled alveolus prior to its recruitment.

One consequence of such widespread liquid distribution is altered alveolar mechanics, where liquid-filled alveolus adjacent to an air-filled alveolus will shrink, imposing mechanical stress on air-filled alveolus via septum deformation, resulting

in its preexpansion and reduced alveolar compliance (38). This could explain the exaggerated size of inflated alveolar sacs in LL-filled edematous lungs compared with controls despite similar applied pressure pulse. Enhanced alveolar cell stretch in overdistended alveoli could also be an important factor contributing to the observed inflation-induced ATP release. Flat alveolar type I (ATI) cells, owing to their large surface area, might be more predisposed for sensing stretch during alveolar inflation consistent with their proposed role as alveolar mechanotransducers (3). However, preliminary tests indicate that alveolar inflation/expansion by fluid injection induces fewer and weaker ATP release responses compared with inflation by air (not shown). This suggests that while cell stretch alone is capable of inducing ATP release in fluid-filled alveoli, other forces dominate the responses in the presence of air. These may include shear stress due to fluid/air movement and cell deformation by tension forces at the air/liquid interface. Cuboidal ATII cells are particularly predisposed to detect increased surface tension at the air-liquid interface that may result from, e.g., reduced surfactant level, causing cell deformation and Ca^{2+} -dependent ATP release, as observed in *in vitro* studies with A549 cells (18, 41). Thus several stimuli (cell stretch, deformation by tension forces at the air-liquid interface, and shear stress caused by liquid movement) all may have contributed to inflation-induced ATP release observed in our study. The exact role of these different mechanisms in air inflation-induced ATP release requires future investigations.

In this study we observed that ATP release sites remain spatially restricted to small elementary units. Their size and fluctuating polygonal-like shapes suggest that they are single alveolar sacs or their clusters that share a common wide lumen, as shown in Fig. 1C (areas delineated by broken lines). While there seems to be no barrier for ATP spreading within a lumen of such elementary unit, it does not propagate outside that area. We also found that lung inflation induces ATP release in a limited number of sites, i.e., alveolar sacs or their clusters, during their opening/recruitment. Experiments with the MacroView microscopy system showed that, in addition to a limited number of stronger large-size ($120-160$ μm) responses, occasionally a large number of weak fluctuating responses of smaller size ($40-80$ μm) were observed (Fig. 7B). Distribution of large responses may correspond to clusters of alveolar sacs, while the small and weak responses may occur in single alveolar sacs. Indeed, data in Table 1 show that density of stronger responses of 5.56 ± 0.26 per square millimeter is comparable to the density of alveolar sacs clusters illustrated in Fig. 1C. Nevertheless, further experiments will be required to address these possibilities in more detail. ATP-dependent LL luminescence responses in this study were in the range of 5,000 to 42,000 AU (average 22,000 AU). Although not calibrated directly in lung tissue, our earlier *in vitro* work suggests that such luminescence responses observed with the same imaging system would be consistent with released ATP concentrations on the order of $\sim 10^{-6}$ M (17, 18), sufficient for autocrine/paracrine signaling and stimulation of, e.g., surfactant secretion by ATII pneumocytes.

The responding regions were not uniformly distributed in the lung sample and repeated stimulation of rat lung induced ATP release in different nonoverlapping release sites, often involving different lung segments. This may result from heterogeneity of edematous tissue, especially when stimulated by non-

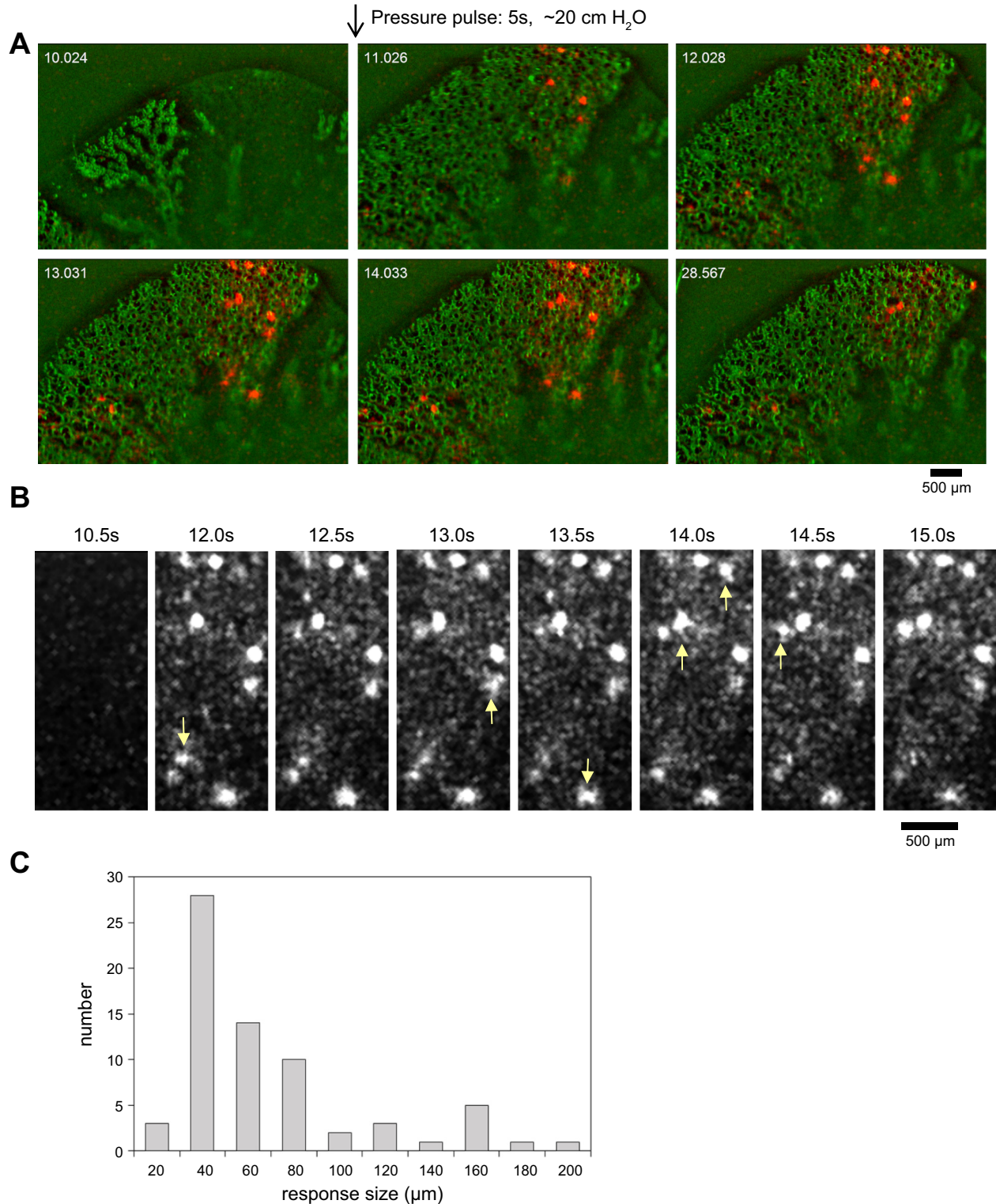


Fig. 7. ATP release sites in air spaces are single alveolar sacs or their clusters. *A*: time sequence of overlaid IR-DIC tissue images (green) and ATP-dependent luminescence (red). ATP release was induced by a pressure pulse (5 s, ~20 cmH₂O) via trachea. A large number of inflation-induced ATP release events could be seen in focus. Luminescence responses were contained almost exclusively within dotlike small areas (Supplemental Movie S4). Images were acquired with MacroView Olympus MV10 microscope with $\times 2$ objective (at $\times 0.63$ zoom) and no time averaging was performed. *B*: time sequence of magnified luminescence images acquired at 500-ms interval shows that ATP-dependent luminescence is contained within irregularly shaped areas that change their shape over time. Occasionally protrusions could be observed (arrows), which may indicate some ATP diffusion to neighboring alveolar sacs (Supplemental Movie S5). *C*: size distribution of luminescence responses such as those shown in *B*. Equivalent diameters were calculated from the area of each response. Note that large ATP responses have a diameter over 160 μm and a medium one is around 120 μm .

Table 1. Number and peak intensity of inflation-induced intra-alveolar ATP-release responses in active lung regions

Region	Number of Responses	Region Area, mm ²	Number/mm ²	Average Peak Intensity	Standard Error
1	18	3.66	4.9	22,466	±1,800
2	8	1.43	5.6	15,487	±712
3	17	3.01	5.6	27,963	±1,912
4	14	2.51	5.6	18,773	±1,131
5	10	2.22	4.5	20,572	±936
6	13	2.01	6.5	27,154	±262
7	8	1.45	5.5	20,120	±4,128
8	15	2.61	5.7	21,697	±2,021
9	18	2.53	7.1	17,079	±1,046
10	14	3.12	4.5	29,380	±1,872
Average			5.56	22,069	
Standard Error			±0.26	±1,489	

Ten regions (from 5 experiments performed with 4 different lung preparations) were manually delineated with MetaMorph, and the number of large-size (>100 μm) and stronger responses (peak intensity >7 000 AU), peak intensity, and region area were analyzed. For each region, density of responses (number/mm²) and average peak response \pm SE are shown in the 3 righthand columns, respectively. ATP release was stimulated by 1- to 100-s pressure pulse of 15 to 20 cmH₂O. The average density of the responses and their average peak intensity (\pm SE) for the 10 analyzed regions are very similar (bottom rows).

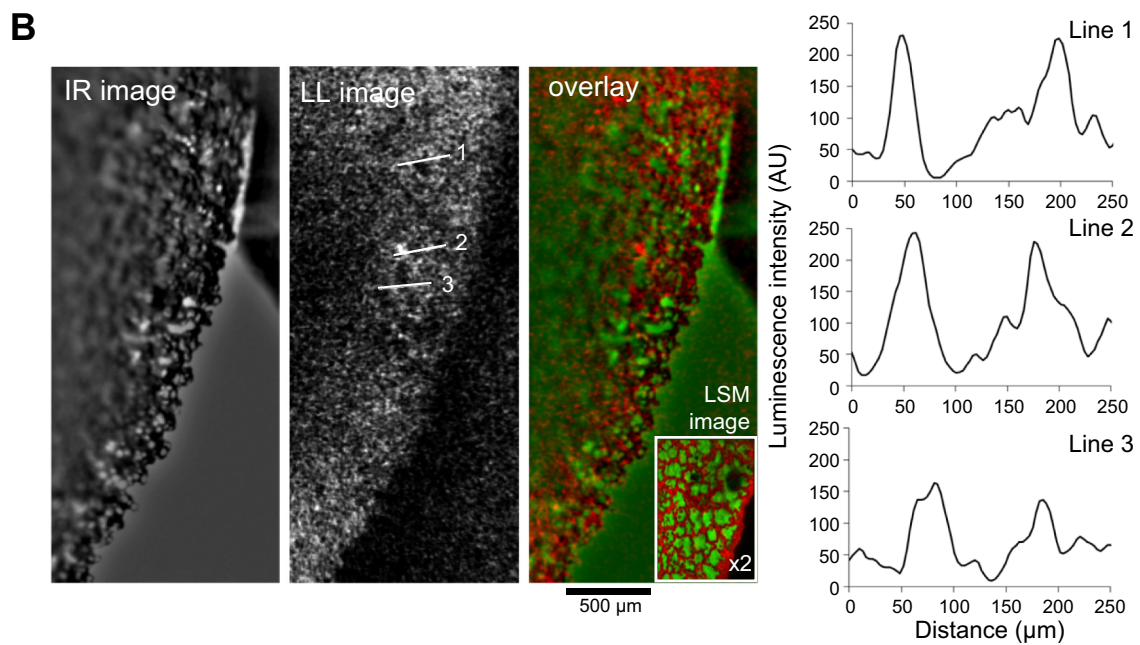
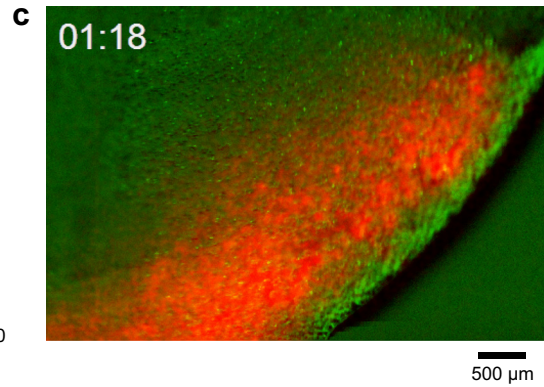
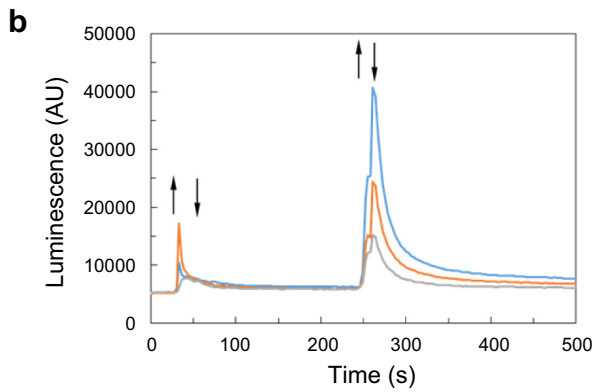
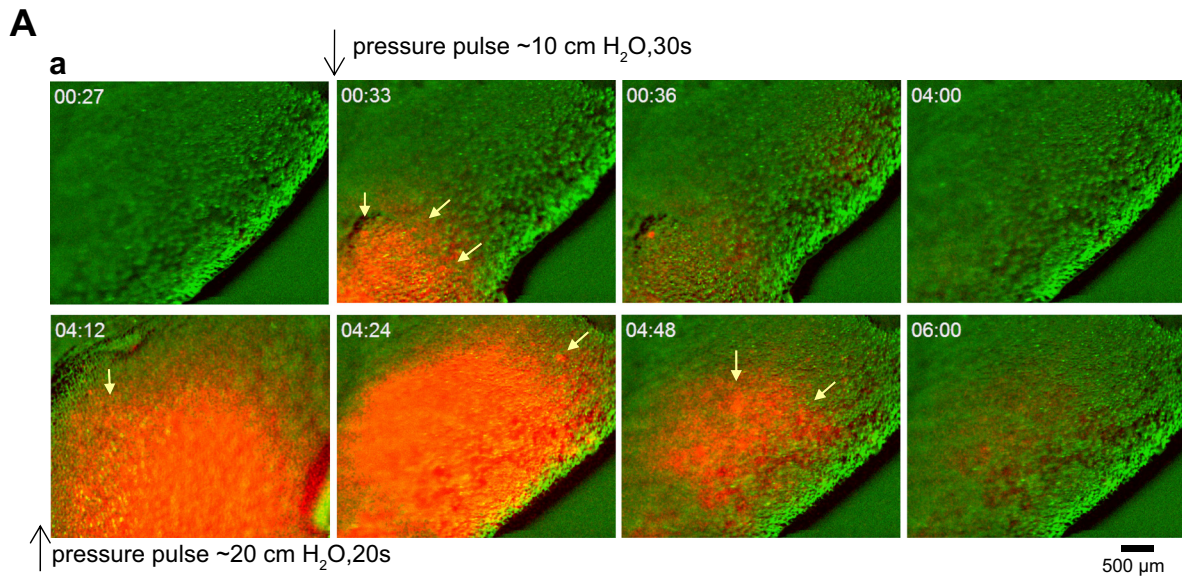
physiological positive-pressure air injection via delicate network of liquid-occluded air ducts. In a lavage lung injury model, alveolar recruitment was shown to be time and pressure dependent (2); the same phenomenon likely applies also to edematous lung model of our study. Consistent with this model recruitment of different alveolar segments by 2 successive pressure pulses, as illustrated in Fig. 5A, likely corresponds to the opening of larger airways that supply these segments. Regarding nonoverlapping release sites in the recruited lung segment, there might be at least two reasons for such effect. First, as Fig. 5 suggests, ATP release occurs only in newly opened/recruited alveoli within strings of alveolar sacs; those tips extend to different portions of the tissue during repeated inflation. Secondly, previous study with A549 cells showed that, when the cells are subjected to repeated stimulation by stretch, ATP release responses occurred in different nonoverlapping sets of cells, suggesting that not all cells are in a release-ready state at all times. This might be expected, e.g., due exocytotic depletion of ATP-containing vesicles by first stimulus and the fact that ATP release is controlled by several well-established time-dependent factors including cell metabolism and activation of different

signaling pathways, such as Ca²⁺ (49, 50) and Rho/Rho kinases (43, 44).

The present study showed that inflation-induced ATP release in alveolar spaces is stimulus dependent, with time course and intensity closely depending on inflation pressure, duration, and frequency. Prolonged (100 s) stimulation evoked long-lasting ATP release. This observation may suggest that the beneficial effects of positive end-expiratory pressure used to mitigate end-expiratory alveolar collapse during mechanical ventilation may result, in part, from promoting sustained ATP release and ATP-dependent surfactant secretion. We also observed that duration of release was contingent on the distal vs. proximal alveoli location. Distal lung regions, which showed faster tissue relaxation and alveoli closing, also presented shorter spikes of ATP release compared with proximal areas of lung tissue. Early termination of ATP release in distal regions might be related to the rapid relief of physical forces acting on alveolar cells, such as stretch or tension forces at the air/liquid interface, during alveoli deflation/derecruitment in relaxing lung. Interestingly, the relatively long ATP release responses seen in proximal lung areas, or during prolonged inflations (Fig. 4), decay faster compared with those detected in *in vitro* studies with several other cell types, including A549 cells (18). Possible factors of such phenomena besides relief of physical strain may include fast reuptake or degradation of extracellular ATP in alveolar lumen. Furthermore, the small volume of alveolar sacs (~1 nl) may limit available LL reagent for prolonged reaction especially in the air-inflated alveolar sacs, where diffusion barrier may prevent supply from the surrounding areas. At present we cannot define all the mechanisms that determine the characteristic time of ATP release in alveolar sacs and further studies are required.

We report here that inflation of alveoli also induced intravascular ATP release in pulmonary blood capillary network. In the absence of red blood cells in the lung perfusate, released ATP originates exclusively from endothelial cells. Fluid shear stress is recognized as an important mechanical stimulus acting on vascular endothelial cells causing ATP release (52). However, in pulmonary capillaries, significant distension of endothelial cells during lung inflation might be expected, which may also contribute to mechanosensitive release of ATP. The lung regions where ATP release responses in pulmonary capillaries took place were spatially restricted and may correspond to the same regions where intra-alveolar ATP release occurred. The responses consisted of many small patchlike areas, and

Fig. 8. Imaging ATP release in pulmonary blood vessels. A, *a*: time sequence of overlaid IR-DIC images of the lung tissue (green) and ATP-dependent luminescence images (red). LL-containing medium was introduced into the pulmonary blood vessels and perfusion was halted for the rest of the experiment. ATP release in the pulmonary capillary network was stimulated by brief inflation at 30 s (~30 s duration, ~10 cmH₂O), followed by a second inflation at 4 min (~20 s, ~20 cmH₂O), *top* and *bottom* rows of images, respectively (Supplemental Movie S6). The responses displayed a patchlike but diffuse luminescence pattern in the entire active area. This is distinctly different from highly localized ATP release responses observed in alveoli. *b*: Time course of the luminescence responses measured in 3 arbitrary ROIs in the active area. A patchlike pattern of ATP-dependent luminescence in pulmonary capillaries is clearly seen in another experiment shown on image *c*, where ATP release was induced by inflation at 30 s. Images were acquired with Olympus MV10 MacroView microscope with $\times 2$ objective at $\times 0.63$ zoom. The experiment was replicated with 3 separate lung preparations. *B*: cumulative luminescence image of pulmonary blood capillaries. The 3 panels are IR-DIC tissue image, ATP-dependent luminescence (LL image) and their overlay (shown in green and red, respectively). Images were acquired with upright BX51WI Olympus microscope and $\times 4$ objective. Lung was stimulated with 3 air pressure pulses (1 s, ~20 cmH₂O) applied via the trachea. After the peak response subsided, the residual luminescence was recorded for several minutes and averaged. Network of ring-shaped luminescence consistent with widespread staining the lumen of blood capillaries surrounding air-filled alveolar sacs could be seen. For comparison, *inset* shows a laser scanning confocal microscope (LSM) image of rhodamine-stained pulmonary capillaries (such as shown in Fig. 1C), clearly demonstrating similar pattern of pulmonary capillary network. *Inset* is $\times 2$ magnified compared with the luminescence image. Graphs at *right* show examples of luminescence intensity along lines (1–3, indicated in the *middle* panel), revealing higher luminescence around inflated alveolar sacs compared with their lumen.



their size (70–260 μm) suggests that the capillary network surrounding alveolar sacs, or their clusters, constitutes an elementary response unit. This is similar to the responses in the air spaces; however, an important difference is that in air spaces the ATP responses remain enclosed within such elementary units, while in the capillary network they show slow diffusive spreading. The ATP response could disperse rapidly if normal blood circulation were present contributing to purinergic control of pulmonary vessels caliber and local blood flow.

The present work also has important limitations. We employed an open imaging chamber and positive intra-alveolar pressure to inflate the lungs, which narrowed our study to conditions resembling lung mechanical ventilation. Due to the instillation of ~ 1 ml saline (containing LL reagent), lung conditions resemble pulmonary edema, while prolonged periods of near-zero intra-alveolar pressure during lung isolation may cause significant atelectasis (11, 28). Further simplifications/limitations include lack of lung perfusion during image acquisition and manual inflation, which provided limited control of stimuli parameters (rate, amplitude, frequency). Despite these shortcomings, our real-time ATP imaging study establishes a good starting point for future investigations with better controlled stimuli, continuous lung perfusion, and use of an artificial thorax chamber with negative pressure to inflate the lung, resembling physiological conditions.

In summary, the present work provides the first evidence of inflation-induced ATP release in air spaces and in the lumen of pulmonary capillaries in lungs *ex vivo*, highlighting the importance of purinergic signaling in lung function. In both cases, the functional units of ATP release presumably consist of alveolar sacs or their clusters. Within our experimental confines, it demonstrates direct association of ATP release in edematous lungs with alveolar recruitment and early termination by derecruitment. The described approaches should enable further studies of the underlying ATP release mechanism(s) and their regulation and role under different experimental settings resembling physiological and pathophysiological conditions, such as mechanical ventilation.

GRANTS

This work was supported in part by the Canadian Institutes of Health Research (MOP64364 to R. Grygorczyk), by the Japan Society for the Promotion of Science (JSPS) (R. Grygorczyk), and by JSPS KAKENHI Grants nos. 24590274 and 15K08174 (K. Furuya).

DISCLOSURES

No conflicts of interest, financial or otherwise, are declared by the author(s).

AUTHOR CONTRIBUTIONS

K.F. and R.G. conception and design of research; K.F. and R.G. performed experiments; K.F., J.J.T., and R.G. analyzed data; K.F., F.B., M.S., Y.B., and R.G. interpreted results of experiments; K.F., J.J.T., and R.G. prepared figures; K.F., J.J.T., F.B., Y.B., and R.G. edited and revised manuscript; K.F., J.J.T., F.B., M.S., Y.B., and R.G. approved final version of manuscript; R.G. drafted manuscript.

REFERENCES

1. **Adriaensen D, Timmermans JP.** Purinergic signalling in the lung: important in asthma and COPD? *Curr Opin Pharmacol* 4: 207–214, 2004.
2. **Albert SP, DiRocco J, Allen GB, Bates JH, Lafollette R, Kubiak BD, Fischer J, Maroney S, Nieman GF.** The role of time and pressure on alveolar recruitment. *J Appl Physiol* 106: 757–765, 2009.
3. **Ashino Y, Ying X, Dobbs LG, Bhattacharya J.** $[\text{Ca}^{2+}]_i$ oscillations regulate type II cell exocytosis in the pulmonary alveolus. *Am J Physiol Lung Cell Mol Physiol* 279: L5–L13, 2000.
4. **Bodin P, Burnstock G.** Synergistic effect of acute hypoxia on flow-induced release of ATP from cultured endothelial cells. *Experientia* 51: 256–259, 1995.
5. **Boudreault F, Grygorczyk R.** Cell swelling-induced ATP release is tightly dependent on intracellular calcium elevations. *J Physiol* 561: 499–513, 2004.
6. **Burnstock G.** Purinergic signalling: past, present and future. *Braz J Med Biol Res* 42: 3–8, 2009.
7. **Burnstock G.** Blood cells: an historical account of the roles of purinergic signalling. *Purinergic Signal* 11: 411–434, 2015.
8. **Burnstock G, Brouns I, Adriaensen D, Timmermans JP.** Purinergic signaling in the airways. *Pharmacol Rev* 64: 834–868, 2012.
9. **Burnstock G, Ralevic V.** Purinergic signaling and blood vessels in health and disease. *Pharmacol Rev* 66: 102–192, 2014.
10. **Button B, Okada SF, Frederick CB, Thelin WR, Boucher RC.** Mechanosensitive ATP release maintains proper mucus hydration of airways. *Sci Signal* 6: ra46, 2013.
11. **Cereda M, Emami K, Xin Y, Kadlecik S, Kuzma NN, Mongkolwisetwara P, Profka H, Pickup S, Ishii M, Kavanagh BP, Deutschman CS, Rizi RR.** Imaging the interaction of atelectasis and overdistension in surfactant-depleted lungs. *Crit Care Med* 41: 527–535, 2013.
12. **Dietl P, Haller T.** Exocytosis of lung surfactant: from the secretory vesicle to the air-liquid interface. *Annu Rev Physiol* 67: 595–621, 2005.
13. **Dietl P, Haller T, Frick M.** Spatio-temporal aspects, pathways and actions of Ca^{2+} in surfactant secreting pulmonary alveolar type II pneumocytes. *Cell Calcium* 52: 296–302, 2012.
14. **Douillet CD, Robinson WP III, Zarzaur BL, Lazarowski ER, Boucher RC, Rich PB.** Mechanical ventilation alters airway nucleotides and purinoceptors in lung and extrapulmonary organs. *Am J Respir Cell Mol Biol* 32: 52–58, 2005.
15. **Edwards YS.** Stretch stimulation: its effects on alveolar type II cell function in the lung. *Comp Biochem Physiol A Mol Integr Physiol* 129: 245–260, 2001.
16. **Furuya K, Harada K, Sokabe M.** Three types of ATP-release in mammary epithelial cells revealed by ATP imaging. *Purinergic Signal Suppl* 5: S91, 2008.
17. **Furuya K, Sokabe M, Grygorczyk R.** Real-time luminescence imaging of cellular ATP release. *Methods* 66: 330–344, 2014.
18. **Grygorczyk R, Furuya K, Sokabe M.** Imaging and characterization of stretch-induced ATP release from alveolar A549 cells. *J Physiol* 591: 1195–1215, 2013.
19. **Grygorczyk R, Hanrahan JW.** CFTR-independent ATP release from epithelial cells triggered by mechanical stimuli. *Am J Physiol Cell Physiol* 272: C1058–C1066, 1997.
20. **Hallman M, Glumoff V, Ramet M.** Surfactant in respiratory distress syndrome and lung injury. *Comp Biochem Physiol A Mol Integr Physiol* 129: 287–294, 2001.
21. **Hayashi T, Kawakami M, Sasaki S, Katsumata T, Mori H, Yoshida H, Nakahari T.** ATP regulation of ciliary beat frequency in rat tracheal and distal airway epithelium. *Exp Physiol* 90: 535–544, 2005.
22. **Hildebran JN, Goerke J, Clements JA.** Surfactant release in excised rat lung is stimulated by air inflation. *J Appl Physiol* 51: 905–910, 1981.
23. **Idzko M, Hammad H, van Nimwegen M, Kool M, Willart MA, Muskens F, Hoogsteden HC, Luttmann W, Ferrari D, Di Virgilio F, Virchow JC Jr, Lambrecht BN.** Extracellular ATP triggers and maintains asthmatic airway inflammation by activating dendritic cells. *Nat Med* 13: 913–919, 2007.
24. **Kiefmann R, Islam MN, Lindert J, Parthasarathi K, Bhattacharya J.** Paracrine purinergic signaling determines lung endothelial nitric oxide production. *Am J Physiol Lung Cell Mol Physiol* 296: L901–L910, 2009.
25. **Kreda SM, Okada SF, Van Heusden CA, O'Neal W, Gabriel S, Abdullah L, Davis CW, Boucher RC, Lazarowski ER.** Coordinated release of nucleotides and mucin from human airway epithelial Calu-3 cells. *J Physiol* 584: 245–259, 2007.
26. **Kuebler WM, Parthasarathi K, Lindert J, Bhattacharya J.** Real-time lung microscopy. *J Appl Physiol* 102: 1255–1264, 2007.

27. **Kuebler WM, Parthasarathi K, Wang PM, Bhattacharya J.** A novel signaling mechanism between gas and blood compartments of the lung. *J Clin Invest* 105: 905–913, 2000.
28. **Lachmann B, Robertson B, Vogel J.** In vivo lung lavage as an experimental model of the respiratory distress syndrome. *Acta Anaesthesiol Scand* 24: 231–236, 1980.
29. **Lazarowski ER, Homolya L, Boucher RC, Harden TK.** Direct demonstration of mechanically induced release of cellular UTP and its implication for uridine nucleotide receptor activation. *J Biol Chem* 272: 24348–24354, 1997.
30. **Lazarowski ER, Sesma JI, Seminario-Vidal L, Kreda SM.** Molecular mechanisms of purine and pyrimidine nucleotide release. *Adv Pharmacol* 61: 221–261, 2011.
31. **Looney MR, Bhattacharya J.** Live imaging of the lung. *Annu Rev Physiol* 76: 431–445, 2014.
32. **Mason RJ, Voelker DR.** Regulatory mechanisms of surfactant secretion. *Biochim Biophys Acta* 1408: 226–240, 1998.
33. **Mortaz E, Folkerts G, Nijkamp FP, Henricks PA.** ATP and the pathogenesis of COPD. *Eur J Pharmacol* 638: 1–4, 2010.
34. **Morty RE, Matalon S.** “Real-time visualization of lung function: from micro to macro.” *Am J Physiol Lung Cell Mol Physiol* 304: L1–L3, 2013.
35. **Murata N, Ito S, Furuya K, Takahara N, Naruse K, Aso H, Kondo M, Sokabe M, Hasegawa Y.** Ca²⁺ influx and ATP release mediated by mechanical stretch in human lung fibroblasts. *Biochem Biophys Res Commun* 453: 101–105, 2014.
36. **Okada SF, Nicholas RA, Kreda SM, Lazarowski ER, Boucher RC.** Physiological regulation of ATP release at the apical surface of human airway epithelia. *J Biol Chem* 281: 22992–23002, 2006.
37. **Patel AS, Reigada D, Mitchell CH, Bates SR, Margulies SS, Koval M.** Paracrine stimulation of surfactant secretion by extracellular ATP in response to mechanical deformation. *Am J Physiol Lung Cell Mol Physiol* 289: L489–L496, 2005.
38. **Perlman CE, Lederer DJ, Bhattacharya J.** Micromechanics of alveolar edema. *Am J Respir Cell Mol Biol* 44: 34–39, 2011.
39. **Praetorius HA, Leipziger J.** ATP release from non-excitabile cells. *Purinergic Signal* 5: 433–446, 2009.
40. **Ralevic V, Dunn WR.** Purinergic transmission in blood vessels. *Auton Neurosci* 191: 48–66, 2015.
41. **Ramsingh R, Grygorczyk A, Solecki A, Cherkaoui LS, Berthiaume Y, Grygorczyk R.** Cell deformation at the air-liquid interface induces Ca²⁺-dependent ATP release from lung epithelial cells. *Am J Physiol Lung Cell Mol Physiol* 300: L587–L595, 2011.
42. **Sadananda P, Kao FC, Liu L, Mansfield KJ, Burcher E.** Acid and stretch, but not capsaicin, are effective stimuli for ATP release in the porcine bladder mucosa: are ASIC and TRPV1 receptors involved? *Eur J Pharmacol* 683: 252–259, 2012.
43. **Seminario-Vidal L, Kreda S, Jones L, O’Neal W, Trejo J, Boucher RC, Lazarowski ER.** Thrombin promotes release of ATP from lung epithelial cells through coordinated activation of rho- and Ca²⁺-dependent signaling pathways. *J Biol Chem* 284: 20638–20648, 2009.
44. **Seminario-Vidal L, Okada SF, Sesma JI, Kreda SM, Van Heusden CA, Zhu Y, Jones LC, O’Neal WK, Penuela S, Laird DW, Boucher RC, Lazarowski ER.** Rho signaling regulates pannexin 1-mediated ATP release from airway epithelia. *J Biol Chem* 286: 26277–26286, 2011.
45. **Sikora J, Orlov SN, Furuya K, Grygorczyk R.** Hemolysis is a primary ATP-release mechanism in human erythrocytes. *Blood* 124: 2150–2157, 2014.
46. **Sprague RS, Ellsworth ML, Stephenson AH, Lonigro AJ.** ATP: the red blood cell link to NO and local control of the pulmonary circulation. *Am J Physiol Heart Circ Physiol* 271: H2717–H2722, 1996.
47. **Takahara N, Ito S, Furuya K, Naruse K, Aso H, Kondo M, Sokabe M, Hasegawa Y.** Real-time imaging of ATP release induced by mechanical stretch in human airway smooth muscle cells. *Am J Respir Cell Mol Biol* 51: 772–782, 2014.
48. **Tarran R, Button B, Boucher RC.** Regulation of normal and cystic fibrosis airway surface liquid volume by phasic shear stress. *Annu Rev Physiol* 68: 543–561, 2006.
49. **Tatur S, Groulx N, Orlov SN, Grygorczyk R.** Ca²⁺-dependent ATP release from A549 cells involves synergistic autocrine stimulation by coreleased uridine nucleotides. *J Physiol* 584: 419–435, 2007.
50. **Tatur S, Kreda S, Lazarowski E, Grygorczyk R.** Calcium-dependent release of adenosine and uridine nucleotides from A549 cells. *Purinergic Signal* 4: 139–146, 2008.
51. **Wang PM, Ashino Y, Ichimura H, Bhattacharya J.** Rapid alveolar liquid removal by a novel convective mechanism. *Am J Physiol Lung Cell Mol Physiol* 281: L1327–L1334, 2001.
52. **Yamamoto K, Furuya K, Nakamura M, Kobatake E, Sokabe M, Ando J.** Visualization of flow-induced ATP release and triggering of Ca²⁺ waves at caveolae in vascular endothelial cells. *J Cell Sci* 124: 3477–3483, 2011.

Appendix C

- **Reference 137** (DOI: 10.1152/ajpcell.00096.2019)

Wide field of view quantitative imaging of cellular ATP release

Ju Jing Tan, Olga Ponomarchuk, Ryszard Grygorczyk, and Francis Boudreault

American Journal of Physiology-Cell Physiology 2019 317:3, C566-C575

Reproduced with the permission of American Physiological Society

METHODS IN CELL PHYSIOLOGY

Wide field of view quantitative imaging of cellular ATP release

Ju Jing Tan,^{1,2} Olga Ponomarchuk,¹ Ryszard Grygorczyk,^{1,2} and Francis Boudreault¹

¹Centre de Recherche du Centre Hospitalier de l'Université de Montréal, Montreal, Quebec, Canada; and ²Department of Medicine, Université de Montréal, Montreal, Quebec, Canada

Submitted 21 March 2019; accepted in final form 17 June 2019

Tan JJ, Ponomarchuk O, Grygorczyk R, Boudreault F. Wide field of view quantitative imaging of cellular ATP release. *Am J Physiol Cell Physiol* 317: C566–C575, 2019. First published June 19, 2019; doi:10.1152/ajpcell.00096.2019.—Although several mechanical stressors promote ATP secretion from eukaryotic cells, few mechanosensitive pathways for ATP release have been precisely characterized and none have been clearly identified. To facilitate progress, we report here a wide field of view ($\sim 20 \times 20$ mm sample area) imaging technique paired with a quantitative image analysis to accurately map the dynamics of ATP release from a cell population. The approach has been tested on A549 cells stretched at high initial strain rate ($2\text{--}5\text{ s}^{-1}$) or swelled by hypotonic shock. The amount of ATP secreted in response to a series of five graded stretch pulses (5–37% linear deformation, 1-s duration at 25°C) changed nonmonotonically with respect to strain amplitude and was inhomogeneous across the cell monolayer. In a typical experiment, extracellular ATP density averaged 250 fmol/mm², but the area of detectable signal covered only $\sim 40\%$ of the cells. In some areas, ATP accumulation peaked around 900 fmol/mm², which corresponded to an estimated concentration of 4.5 μM . The total amount of ATP released from the combined stretch pulses reached 384 ± 224 pmol/million cells ($n = 4$). Compared with stretch, hypotonic shock (50%, 30°C) elicited a more homogeneous ATP secretion from the entire cell population but at a lower yield totaling 28 ± 12 pmol/million cells ($n = 4$). The quantitative extracellular ATP mapping of several thousand cells at once, with this wide field of view imaging system, will help identify ATP release pathways by providing unique insights on the dynamics and inhomogeneities of the cellular ATP secretion that are otherwise difficult to assess within the smaller field of view of a microscope.

ATP release; bioluminescence; imaging; mechanical stress

INTRODUCTION

Extracellular adenosine 5'-triphosphate was recognized as a signaling molecule several decades ago, and many of its target purinergic receptors of the P2X₁₋₇ and P2Y_{1,2,4,6,11-14} families have since been sequenced and pharmacologically characterized (3). Yet several aspects regarding the modes of signaling of this nucleotide remain perplexing. In particular, while mechanical deformations of all kinds have been found to stimulate ATP release, no mechanosensitive pathways permitting ATP secretion have been unambiguously characterized as of today (9, 10, 18). There are currently two major acknowledged modes of cellular ATP release: lytic and nonlytic. Cell lysis resulting from plasma membrane rupture allowing the free passage of cytosolic ATP can be induced by physical or

chemical stressors; the damages can be transient or lead to cell death (16). The nonlytic mode of ATP release is generally divided into conductive (ionic channels) and nonconductive pathways, with the latter further splitting up into regulated and nonregulated exocytosis (9).

Regardless of the stimulus under investigation, an accurate measurement technique for ATP is necessary to identify the transmembrane pathways used by this nucleotide. The most widely used technique to detect and quantify ATP is the luciferase-luciferin (LL) assay, a photon-producing enzymatic reaction whose light intensity serves as an indicator of ATP content in the solution. An alternative to the soluble luciferase is the pmeLUC cell expression system, featuring a plasma membrane-bound and extracellular-facing luciferase enzyme. It is a versatile tool suitable for *in vitro* as well as *in vivo* applications (12). However, in most cell-based experimental assays, the quantity of released ATP is tiny, and either soluble or membrane-bound luciferase approaches yield a very faint bioluminescent signal that is barely detectable with a conventional microscopy imaging system. Therefore, the standard procedure to quantify cellular ATP release generally involves collecting bulk extracellular solution for subsequent offline determination of ATP content using a luminometer or a plate reader. Although such approaches constitute a highly sensitive biochemical assay for ATP detection, it cannot provide information on the spatial kinetics of ATP release, a prerequisite to fully characterize and solve the identity of ATP release pathways.

To accurately map cellular ATP release, it is essential to combine a microscopy setup that has a strong light-gathering power with a very sensitive light detection apparatus. Currently available digital cameras with maximal light sensitivity, such as an electron-multiplying charge-coupled device (EMCCD), although well suited for low-light applications in fluorescence microscopy, are not yet adequate for such extremely low bioluminescent signal. A simple technique to circumvent this weak source of luminescence is to capture light for longer periods of time (8, 11). With this approach, however, the advantages of an imaging system mostly vanish as the spatial kinetics of ATP efflux (light emission) is lost. Image intensifier has been used with success for ATP imaging (6, 17), but it is an expensive and not widely available solution.

The brightness of an image acquired with a microscope increases with the objective's numerical aperture (NA) but decreases with the lateral magnification (M) (*Eq. 1*). Since in general the NA of microscope objectives changes in proportion to their magnification, very little brightness can be gained by choosing an objective with the highest NA available. Besides, in most modern microscopes, the need to fit complex optical

Address for reprint requests and other correspondence: F. Boudreault, Centre de Recherche du CHUM 900, rue Saint-Denis, Pavillon R Montreal, QC H2X 0A9, Canada (e-mail: francis.boudreault@umontreal.ca).

components within the main optical path results in longer lens-to-lens distance and thereby substantial loss of peripheral and off-axis image-forming rays.

$$\text{Image brightness} \propto \left(\frac{\text{NA}}{M}\right)^2 \quad (1)$$

Thus, to boost the light intensity signal, we chose a macroscopic imaging approach similar to the one described by Feranchak et al. (5), but instead of a 1:1 object-to-image magnification, we chose a threefold reduction ($M = 0.33$) with an objective lens of $\text{NA} = 0.15$. Based on Eq. 1, the theoretical increase in brightness from those optical parameters alone compared with, for example, a $\times 5/0.25$ objective is $[(0.15/0.33)/(0.25/5)]^2 = 83$ -fold. The true increase in captured luminescence with our imaging system can surpass this ratio, however, due to its shorter optical path compared with nowadays microscope. While this higher light-gathering power came at the cost of reducing the image resolution, our imaging system with its wide field of view (FOV) that spans the whole of our experimental chambers ($\sim 20 \times 20$ mm), coupled with our approach to map and quantify over time the distribution and rate of secreted ATP in our experimental chambers, provided new insights on the overall nature and dynamics of the cellular ATP secretion otherwise difficult to assess with standard microscopes and their small FOV.

MATERIALS AND METHODS

Cells. Human lung carcinoma A549 cells were grown on cell culture dishes (Cellstar; Greiner Bio-One, Frickenhausen, Germany) in HyClone High Glucose Dulbecco's modified Eagle's medium (GE Healthcare Life Sciences, HyClone Laboratories, Logan, UT) supplemented with 10% fetal bovine serum, 2 mM L-glutamine, 50 U/mL penicillin-G, and 50 $\mu\text{g}/\text{mL}$ streptomycin sulfate (antibiotics were only included in media of cells grown for hypo experiments) at 37°C and 5% CO_2 . For stretch experiments, trypsinized A549 cells were seeded at ~ 700 cells/ mm^2 ($\sim 25,000$ cells/ 36 mm^2) with culture media on a bottom-stretchable chamber (see below) and kept at 37°C and 5% CO_2 until the time of the experiment. For hypotonic shock, A549 cells after trypsinization were seeded with culture media on 15-mm-diameter glass coverslips and used after they reached 90% confluence (~ 400 – 500 cells/ mm^2 ; 24–72 h after plating). All added media constituents were from Gibco/ThermoFisher Scientific (Burlington, ON, Canada).

Stretch experiments. Stretch chambers were made with a Sylgard 184 silicone elastomer base and curing agent (Dow Corning, Midland, MI) as described previously (6, 7). The elastomer base and curing agent were poured into the stretch chamber's mold and then baked for 1 h at 60°C . To facilitate the attachment of cells onto silicone, the 2-mm-wide stretchable groove was coated with 20% collagen type I from rat tail diluted in distilled H_2O (Sigma-Aldrich, St. Louis, MO). During all stretch experiments, cells were bathed in 200 μL of Gibco's phenol red-free DMEM (Invitrogen Canada, Burlington, ON, Canada) containing the ATP detection reagents prepared as follows: one vial of ATP assay mix-lyophilized powder (Sigma-Aldrich) was reconstituted with 5 mL of sterile double-distilled water and isotonicity adjusted with $5\times$ physiological solution (LL). For ATP imaging, 100 μL of the isotonicity adjusted LL was added to 100 μL of Gibco's phenol red-free DMEM (LL-DMEM).

The stretch chamber mounted on the stage of our custom-designed ATP imaging system (see below) was clamped to the STREX NS-600W Cell Stretching System (STREX, Osaka, Japan). The stretching apparatus applied a horizontal stretch onto the silicone chamber for 1 s. All stretch experiments consisted of five consecutive stretch pulses of increasing amplitude at 5-min intervals. Effective applied strains,

along the main axis of load application, were measured on images acquired after the experiments with a repetition of the stretch sequence.

Hypotonic challenge. A549 cells on glass coverslips were placed in a glass-bottomed (25-mm diameter coverslip no. 1) chamber (RC-40LP; Warner Instruments, Hamden, CT), bathed in LL-DMEM solution (500 μL), and warmed at 30°C with a DH-35 Culture Dish Heater (Warner) wired to a TC-324B Automatic Heater Controller (Warner) until hypotonic challenge. To keep the ATP detection reaction reagents at prehypotonic levels, the added hypotonic LL solution (hypoLL) contained the same level of LL reagent as LL-DMEM (for details see *Stretch experiments*). The luciferase reaction is well known for its sensitivity to ionic content, however (1). For instance, if the ionic concentration of an isotonic medium is lowered by 50%, it will result in approximate doubling of the luciferase reaction speed. As a result, before converting the pixel values into ATP (see ATP calibration and quantification), we divided by 2 the rate of light units (LU) per second. In addition, to keep divalent cation concentration constant during the course of the experiments, the hypoLL also contained (in mM) 1 MgCl_2 and 1 CaCl_2 (Fisher Scientific, Pittsburgh, PA). ATP release was stimulated by adding 500 μL of hypoLL solution to the chamber ($\sim 50\%$ hypo final).

ATP release imaging. We chose an inverted configuration for the imaging system, with the EMCCD camera Evolve 512 (Photometrics, Tucson, AZ) placed underneath the experimental stage (see Fig. 1A). To position the stretch or hypotonic shock chamber, we used a standard manual mechanical XY translational stage. Focus was provided by moving vertically the camera positioned on a pinion-and-rack system. We selected a parallel path (sometimes referred to as infinity space) in our optical design, but instead of a distance between the two main lenses in excess of 200 mm, as typically used in infinity-corrected microscopes, we shortened it to 40 mm. This shorter distance means that more of the off-axis peripheral rays are captured, hence resulting in enhanced brightness. For the objective, we chose a standard bi-convex lens with $f_{\text{obj}} = 75$ mm ($D_{\text{obj}} = 25$ mm, $\text{NA} = 0.15$), and we fixed to the EMCCD camera a standard c-mount convex-type camera lens with $f_{\text{cam}} = 25$ mm ($D_{\text{cam}} = 20$ mm) that resulted in $\times 0.33$ ($f_{\text{cam}}/f_{\text{obj}}$) magnification (3-fold reduction). It should be noted that this particular optical configuration with large-diameter lenses and magnification at or below $\times 1$ is similar to macrophotography. Given the size of the camera chip per the manufacturer's specifications of 6.7×6.7 mm (512×512 , 13 μm pixel size), the resulting FOV was $\sim 20 \times 20$ mm. With such a wide FOV, large-diameter lenses are essential to minimize optical aberrations. Our imaging system is not entirely devoid of optical aberrations, however. In particular, coma aberrations from intense punctual light sources, e.g., from isolated cells suddenly ruptured by lysis, have been observed at the periphery of the field of view during hypotonic assay. Those image distortions are minor and not expected to diminish appreciably the exactness of the ATP quantification but will be addressed in the future.

To further amplify the signal, we set the on-chip camera binning at 2×2 , achieving a final resolution of ~ 78 $\mu\text{m}/\text{pixel}$. Control of the EMCCD and data acquisition were done via AxioVision software (AxioVs40 V 4.8.2.0; Carl Zeiss MicroImaging, Jena, Germany). Images were acquired at 0.5-Hz frequency and 1-s exposure time for stretch and for hypo at 0.2 Hz and 5-s exposure and gain settings at the lowest readout speed at 5 MHz. Stacks of 900 images were captured and stored for offline analyses with Metamorph (Meta Series Software 7.7.9; Molecular Devices, Downingtown, PA) or ImageJ open-source software (15).

To acquire brightfield images of the stretch or hypotonic chamber (Fig. 1B), we installed an external variable illumination source (incandescent bulb, 15 W, T6/collector lens $f_{\text{coll}} = 25$ mm, $D_{\text{coll}} = 40$ mm) in-line with a standard condenser ($f_{\text{cond}} = 60$ mm, $D_{\text{cond}} = 40$ mm, $\text{NA} = 0.3$). We also placed a diaphragm in the parallel optical path for additional light intensity control and fine-tuning for the

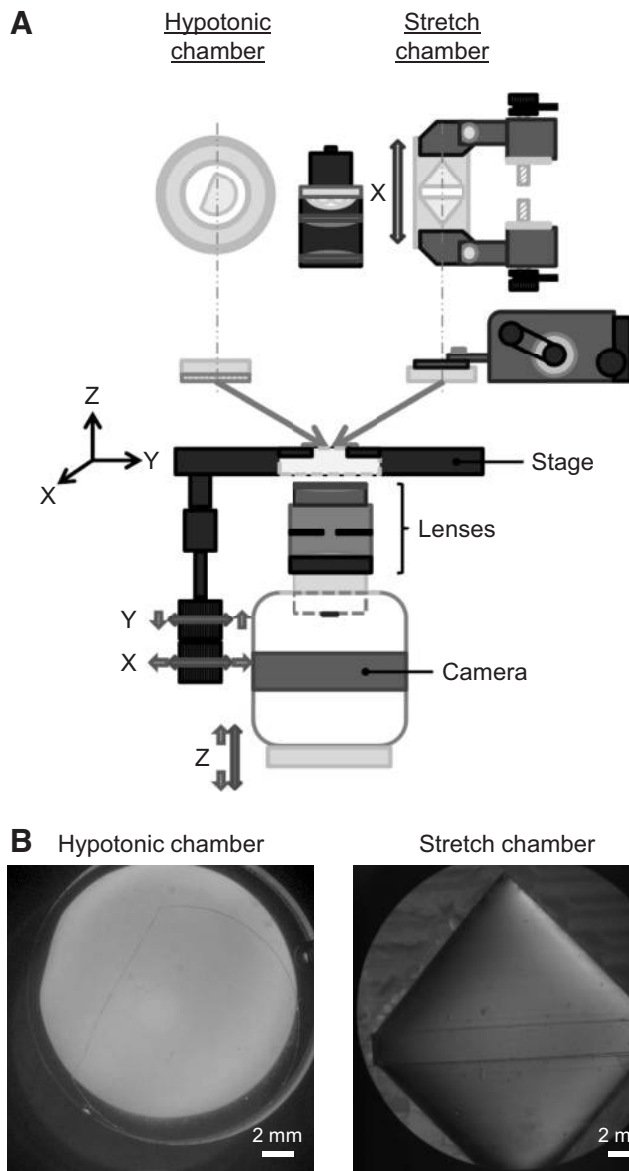
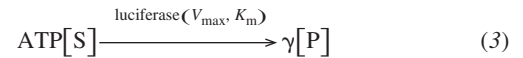
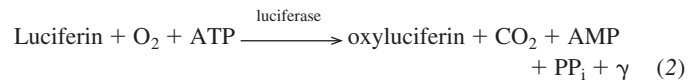


Fig. 1. Experimental setup for imaging ATP release from cultured cells. **A:** a Photometrics Evolve 512 electron-multiplying charge-coupled device (EMCCD) camera is mounted on a pinion-and-rack device for z-axis focus and installed under a translational (x-y-axis) mechanical stage. A pair of lenses with a 3:1 object-to-image ratio and a working distance of ~ 70 mm are attached on the camera. Cells are seeded onto either a 2×18 mm collagen-coated groove of a flexible silicon chamber for stretch experiments or a 15-mm-diameter glass coverslip for hypotonic shock challenge. During the experiments, cells are covered with DMEM containing LL reagent. The stretch chamber is attached to a stretching apparatus fixed on the movable stage. The hypotonic chamber is fixed directly on the stage and kept warm with an incubator (not shown). An incandescent lamp installed above the stage and centered in the system's optical axis is turned on only during pre- and postexperiment brightfield image acquisition. **B:** the coverslip placed in hypotonic chamber and the rectangular stretchable groove area can be visualized in brightfield acquisition mode.

brightfield-acquired images. Finally, to minimize light background, the entire imaging system was installed inside an opaque box and was accessible through a front door panel.

ATP calibration and quantification. Extracellular luminescence, in contrast to intracellular fluorescence, is not enclosed within the boundary of cellular membranes; the spatial distribution of the light-

emitting reaction is governed by time-dependent diffusion processes and is dispersed throughout the fluid covering the cells. Since the light intensity captured in the image is proportional not only to $[\text{ATP}]_0$ but also to the depth (in the object space) of the in situ generated luminescence, an ATP calibration technique independent of the dimensions of the light-generating reaction is required. This is achieved by calibrating the rate of light generation with respect to the quantity of ATP_0 molecules rather than its local concentration.



Although ATP is only a cofactor in the LL reaction and light (γ) a by-product of it (see chemical reaction 2, PP_i : inorganic pyrophosphate), when using this reaction for ATP determination with $[\text{luciferin}] \gg [\text{ATP}]$, we can posit ATP as the sole reactant and light as the main product as described in the simplified chemical reaction 3 (the rate of production of oxyluciferin can be directly inferred from the rate of light generation). By using the Michaelis-Menten equation $\Delta[\text{P}]/\Delta t = (V_{\max} \times [\text{S}] / (K_m + [\text{S}]))$ and assuming $K_m \sim 200 \mu\text{M}$ (4) $> [\text{S}] = [\text{ATP}]$, we obtain this simplified relation: $(\Delta\gamma/\Delta t)/V = (V_{\max}/K_m) \times [\text{ATP}]$ (V : volume of reaction), where the rate of photon production ($\Delta\gamma/\Delta t$) per unit of volume is linearly proportional to the concentration of ATP. Multiplying both sides of the equation by V yields the volume-independent relationship: $\Delta\gamma/\Delta t = (V_{\max}/K_m) \times \text{ATP}$, which directly relates the rate of photon emission to the quantity of ATP molecules. We rearranged this equation and combined the enzymatic reaction constants and other parameters pertaining to the specifics of our imaging system into a single calibration factor (see Eq. 4). An example of parameters intrinsically included in this factor is the numerical aperture. The imaging system collects only a fraction of all the photons generated by the reaction. The capture ratio of those photons is determined by the NA, but it remains constant for the entire FOV and is unaffected by the signal intensity. In Eq. 4, the rate of photon generation ($\Delta\gamma/\Delta t$) is replaced by the pixel intensity value [identified as light unit (LU)] divided by the exposure time (Δt) of the image. The quantity of ATP_0 for a region of interest (ROI) in the recorded image covering the whole chamber or a subarea within and containing n pixels can then be obtained from the sum of individual pixel values divided by exposure time and multiplied by the calibration factor:

$$\text{ATP}_{\text{ROI}}(\text{moles}) = \text{calibration_factor} \left(\frac{\text{moles} \cdot \text{s}}{\text{LU}} \right) \times \frac{1}{\Delta t(\text{s})} \sum_{i=1}^{n \text{ pixels}} \text{pixel_value}_i(\text{LU}) \quad (4)$$

To determine the value of the calibration factor, we first recorded the light intensity generated by known concentrations of ATP (5 nM to 50 μM , in 10-fold increments) within the stretch chamber for three volumes (18, 36, and 54 μL) of solution. The volumes were chosen to achieve heights of liquid of 1, 1.5, and 2 mm. Those height increments serve to validate that a large proportion of the luminescence is captured longitudinally along the optical axis of our imaging system, a property dependent on optical characteristics such as the depth of field. This validation requires that while keeping the ATP concentration unchanged, a step increase in solution height will augment the light signal in proportion. The ATP-Mg_2 dissolved in DMEM was pre-mixed 1:1 with LL-DMEM (2 \times) and then immediately transferred within the stretch chamber and images acquired as described above (see *ATP release imaging*) during 1 min. The slowly declining rate of LU per second (minus background level) for the whole chamber was then averaged over the first 10 s. We reported the results

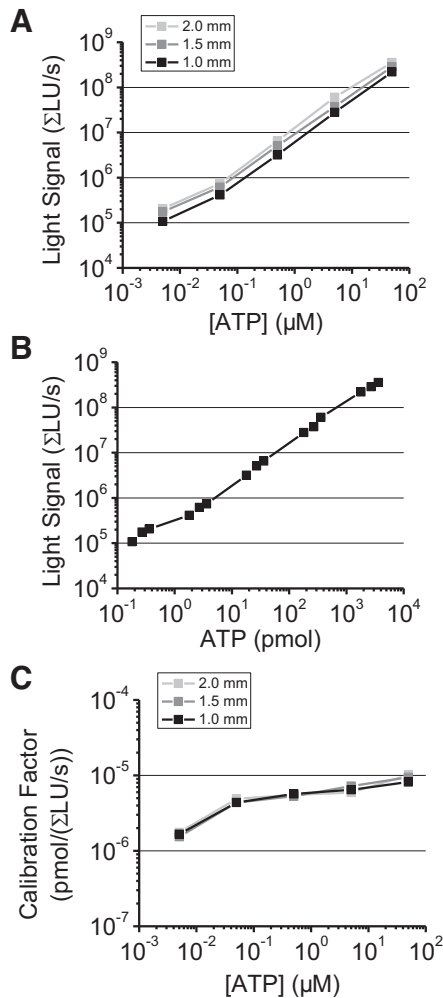


Fig. 2. Calibration factor determination. *A*: light signal in Σ LU/s (background corrected) against a series of [ATP] for 3 different heights of solution within the stretchable groove. Note that for a given Σ LU/s value, the [ATP] is undetermined without knowing the height of the reaction. Also, for a given [ATP], the light signal increases proportionally with the height of the reaction: with 1 mm signal as reference, the increases in light signal for all [ATP] are 1.5 ± 0.15 (1.5:1 mm) and 1.9 ± 0.22 (2:1 mm). *B*: light signal (Σ LU/s) against total ATP. In contrast to *A*, there is only one corresponding quantity of ATP for a given light signal value. *C*: calibration factor varies slightly with [ATP]. The average of the measured calibration factor was used to calibrate all ATP experiments (stretch and hypo). LU, light unit.

for the three series of volume (corresponding height) and [ATP] in Fig. 2*A* and the calculated quantity of ATP for the 15 combinations of volume and [ATP] in Fig. 2*B*.

Note that while there are three possible rates of light generation (1 for each height) for a given [ATP] (Fig. 2*A*), only a unique value exists for a given quantity of ATP (Fig. 2*B*). Note also how the ATP-light signal relationship on Fig. 2*B* displays a strong linear proportionality over several orders of magnitude of ATP molecule content. Another important observation from those calibration measurements is the additive property of the relationship, whereby the rate of light generation from a 2-mm layer of a given concentration of ATP is approximately twice the value of a 1-mm layer at the same concentration (light signal at 2 mm/1 mm = 1.9 ± 0.22). Thus, the 2-mm layer can otherwise be regarded as two stacked layers of 1 mm each. We believe this additive property to remain valid even with two hypothetically immiscible layers containing different ATP concentrations. We further reason that it can be extended to a gradient of ATP

concentration, whereby a series of layers of infinitesimal height can be integrated over the entire depth to obtain the quantity of ATP molecules. In short, the rate of light production is a direct measure of the current quantity of ATP molecules independent of the spatial distribution of ATP. The calibration factor calculated from the average of individual ratio of ATP (moles) over light signal (LU/s) for each data point ($n = 15$) in Fig. 2*B* is $5 \pm 2.6 \times 10^{-18}$ moles·s⁻¹·LU⁻¹ (mean \pm SD). In other words, 1 LU/s corresponds approximately to 5 amol or 3×10^6 molecules of ATP. Although the calibration factor is not influenced by the height of the reaction (Fig. 2*C*), there is a small deviation from linearity with respect of [ATP] (Fig. 2*C*). As a result, using the average of the calibration factor ratio comes with the caveat that as the light signal gets bigger, ATP underestimation grows. Even though this small deviation from linearity is not believed to significantly impact the accuracy of the measurements, a complete 3D modeling of diffusion processes and enzymatic kinetics could be implemented to minimize the anticipated underestimation and further improve ATP quantification.

Based on our pseudo-first-order reaction assumption, we have calculated the half-life of the calibration signal decay at two submicromolar concentration for the three volumes of solution and obtained: $t_{1/2} = 6.6 \pm 0.2$ min, $R^2 > 0.90$ at 0.05 μ M ($n = 3$) and $t_{1/2} = 6.8 \pm 0.2$ min, $R^2 > 0.95$ at 0.5 μ M ($n = 3$). The magnitude of this parameter indicates that the detectable luminescence takes considerable time to decay. At higher ATP concentration ($>5 \mu$ M), however, the measured half-life from our calibration assay shortens: $t_{1/2} = 5.6 \pm 0.1$ min, $R^2 > 0.95$ at 5 μ M ($n = 3$) and $t_{1/2} = 4.2 \pm 0.9$ min, $R^2 > 0.99$ at 50 μ M ($n = 3$). The reason for this deviation is well known and is a consequence of the typical “flash kinetics” of the LL reaction at elevated reactant concentration that had been explained mainly by the generation of the autoinhibitory product dehydroluciferyl-adenylate (L-AMP) (14). In the context of experimental stretching of cells this is not a concern, since L-AMP diffuses away from the main sites of reaction and has a negligible impact on the speed of the reaction. To demonstrate this, we simulated the ATP efflux originating from several cells as a large punctual source by injecting (PLI-100A Picoliter Microinjector; Warner) a small volume of ATP solution ($<10 \mu$ L) at high concentrations (100 μ M) in a RC-40LP glass-bottomed cell-free chamber filled with LL solution (~ 1 mL) and measured the half-life from the signal coming from the initially small but bright source and then continuously expanding but fading luminescence to obtain $t_{1/2} = 7.6 \pm 1.0$ min, $R^2 > 0.90$ ($n = 3$). Thus, even though we used a high level of ATP concentration (100 μ M), there was no diminution in half-life compared with our calibration assay at submicromolar values of 0.05 μ M and 0.5 μ M (unpaired *t*-test, two-tailed, $P = 0.24$ and $P = 0.29$, respectively).

The image noise distribution of the EMCCD camera at baseline (dark current; no illumination) was Gaussian (Kolmogorov-Smirnov test: $P = 0.134$ H₀: distribution is normal), and its standard deviation (σ_{noise}) tended toward 5 LU/pixel (e.g., for 1-s exposure this yields a rate of 5 LU/s/pixel equivalent to 25 amol ATP/pixel). At pixel level per 1-s exposure image, we suppose that this reading noise limits ATP detection to $3\sigma_{\text{noise}} = 75$ amol or 0.075 fmol (per pixel). Note that the signal noise from the LL reaction may exceed this value.

The individual LU values per pixel for the 1-s acquisition time for stretch (or 5 s for hypo) were converted into ATP, with the calibration factor and linear fitting on ImageJ. The total amount of detectable extracellular ATP (ATP_o) within the chamber or a smaller specific ROI can be calculated and monitored over the entire course of the experiment. The quantity of secreted ATP for each stretch impulse is calculated by subtracting the prestretch ATP_o level from the stretch-generated peak value. The rate of ATP release, expressed in fmol/s or pmol/s, is the first derivative of ATP_o within any ROI over time. Color-coded images reporting ATP_o density in fmol/mm² (1 pixel image = 6×10^{-3} mm²) with respect to the surface substrate or rate of ATP release density in (fmol/s)/mm² were generated with ImageJ.

RESULTS

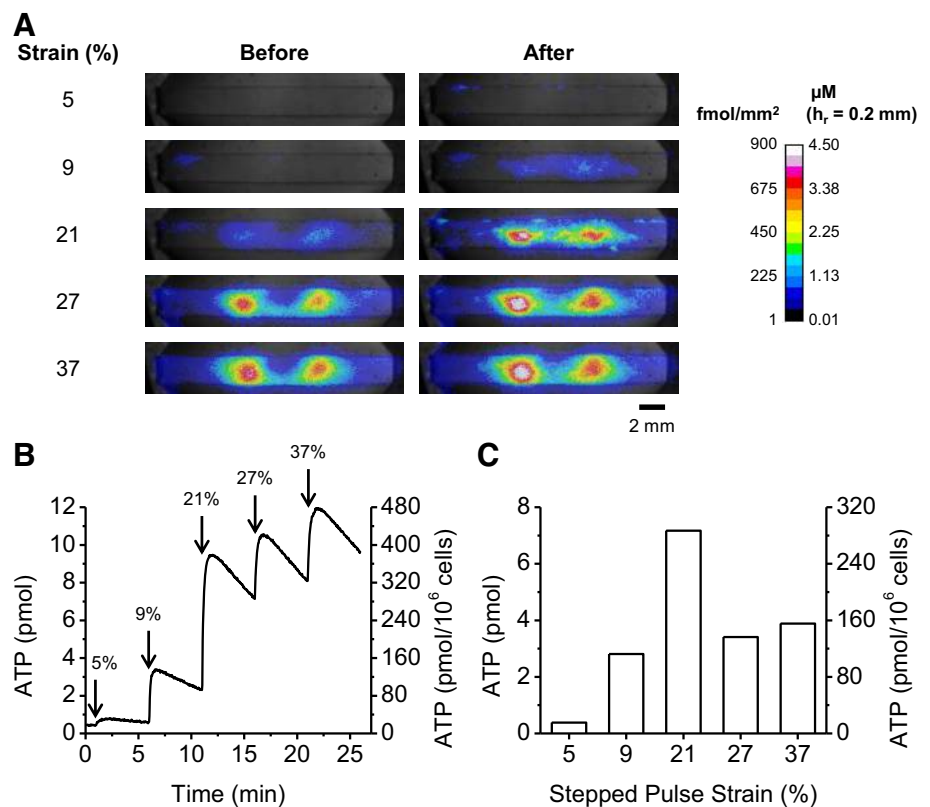
Cell stretch and amount of ATP secretion. To test the sensitivity and resolution of our wide FOV quantitative ATP imaging approach, we first uniaxially stretched silicone substrate-adherent A549 cells. Application of a stretch pulse at high initial speed ($2\text{--}5\text{ s}^{-1}$) is known to result in rapid ATP secretion (7) and, as such, is well suited to assess the temporal resolution of our imaging system. All five graded stepped pulses, applied every five minutes, generated a detectable and quantifiable signal.

The ATP_o density images pre- and poststretch of a typical experiment are presented in Fig. 3A. Local increases in extracellular ATP can be detected as early as 5% strain, but ATP_o level rose mostly near the edge of the chamber, perhaps as a result of localized stress concentration. Some isolated areas reached an ATP density of $\sim 180\text{ fmol/mm}^2$ (Fig. 3A, *top right*), although their contribution to the overall ATP secretion level was minimal (Fig. 3B). Whereas the detectable signal from the following pulse (9%) was more widespread, it remained concentrated mostly in the middle region of the stretched area, with a range covering ($\sim 14\text{ mm}^2$ or 40% of the stretchable groove) and a maximal ATP_o density of $\sim 250\text{ fmol/mm}^2$. The 5-min interval between stretch pulses is too short for the complete breakdown of ATP_o by ectoATPases and LL reaction below the theoretical detection level of $12.5\text{ fmol ATP/mm}^2$ ($0.075\text{ fmol/pixel} \div 6 \times 10^{-3}\text{ mm}^2/\text{pixel}$). In consequence, ATP signal remnants from the previous stretch were still present before application of the 21% extension load, but the addition of newly released ATP can be measured by subtracting pre- from poststretch level (Fig. 3C). The 21% deformation created a markedly inhomogeneous distribution of

extracellular ATP, with two distinct regions where ATP_o density triples to $>750\text{ fmol/mm}^2$ (Fig. 3A). While ATP_o density continued to rise with the subsequent 27 and 37% strain, it was due mostly to additional ATP release in the vicinity of already existing high accumulation ATP, not as a result of higher ATP efflux. The stretch-induced ATP response was not monotonic. The 21% strain produced the highest response with $\sim 7\text{ pmol}$ of secreted ATP for the whole chamber, a magnitude more than twice the previous stretches, and declined thereafter for the subsequent loads. This threshold level at 21% strain had been identified for all four independent chambers tested and is comparable with that occurring during lung inflation. It has been estimated that at total lung capacity inflation, the distension of alveolar space measured from fixed rat lungs reaches a maximum of $\sim 37\%$ surface strain (19), which corresponds to 17% linear strain, assuming an equibiaxial field of deformation.

For autocrine/paracrine purinergic studies with ATP as an effector, it is essential to estimate the concentration of extracellular ATP. We can derive an average value for [ATP]_o in the vicinity of the cell monolayer from the map of ATP_o density level and the estimated extent of the LL reaction. The upper limit of the LL reaction (emitting a detectable signal) is not known, but assuming the reaction initially grows into a hemispherical shape, it should correspond to the lateral diffusion radius of small isolated ATP sources on the acquired images. The height of the reaction was varying and was not uniformly distributed throughout the chamber, but we found that a 200- μm limit was a good approximation for the experiment shown in Fig. 3A. We reported the average [ATP]_o on the alternate calibration bar for this estimated reaction height (h_r).

Fig. 3. Quantitative imaging of extracellular ATP for an entire stretchable area (*sample no. 1*). **A**: overlay color-coded images of ATP density or average [ATP]_o (reaction height, $h_r = 200\text{ }\mu\text{m}$) over transmitted light (static) image of the stretch chamber (gray) with A549 cells ($\sim 25,000$). Images have been cropped to show only the stretchable groove. ATP release is shown in response to a sequence of 5 uniaxial 1-s duration stretch pulses of increasing amplitude (from 5 to 37% strain) given at 5-min intervals (25°C). Extracellular ATP density recorded seconds before (*left*) and after stretch (*right*). Note that with the stimulation protocol used in this experiment, the ATP-dependent luminescence in those images does not fully return to the background level between the consecutive stretches. **B**: the quantity of released ATP (in pmol) in function of time during the experiment illustrated in A. The timing of stretch stimuli is indicated by arrows. **C**: bar graph indicating ATP released (pmol) at each given stretch. The quantity of ATP secreted by cells was calculated from B by subtracting prestretch from after stretch peak value.



Since the concentration is derived from ATP_o accumulation in the chamber, the largest area with the highest [ATP]_o at 4.5 μM for this experiment was seen after the last stretch (37% strain) took place. The [ATP]_o in vicinity of the cell surface ought to be higher, however, due to the existence of a gradient of ATP_o concentration near the cell surface and upward.

While a complete 3D modeling will be required to fully characterize the vertical distribution of ATP in the medium, we attempted nonetheless at estimating the [ATP]_o near the cell surface by hypothesizing a linear distribution of ATP_o. Our rationale is based on the ATP breakdown activity of endogenous cell-attached ecto-ATPases coupled with the consumption from LL reaction being proportional to the concentration of ATP. We expect those processes to lessen the concentration gradient and thereby “linearize” the vertical distribution of ATP. We assumed the [ATP]_o upward and away from the monolayer surface to be low: [ATP]_{away} ~1 nM. The formula for the [ATP]_o near the monolayer at the location of highest [ATP]_o can be expressed as: [ATP]_{average} = ([ATP]_{near} - [ATP]_{away})/2 = 4.5 μM. Solving for the unknown gives [ATP]_{near} = 9 μM.

Cell stretch and rate of ATP secretion. While the amount of secreted ATP and ATP_o density map reveal the extent of the bulk release of ATP per chamber and per normalized surface as well as the nature of the inhomogeneous secretion pattern, the true dynamics of ATP secretion are best revealed with the time derivative of the ATP accumulation response. The highly transient nature of ATP secretion by stretch is depicted in Fig. 4 and can be seen for all five incremental loads. As opposed to the accumulated ATP, the rate of release already went back to

prestretch level before the subsequent stretch as depicted on the color-coded images (Fig. 4A). But similarly to the amount of ATP secreted, a threshold was also crossed at 21% strain (Fig. 4B) with a peak rate of 1.2 pmol/s. Whether a small lingering ATP efflux persisted poststretch and/or that ATP-induced ATP release took place between load pulses could not be resolved. This ATP efflux, if it existed, ought to have been small since it failed to override the feeble but continuous degradation of ATP from LL reaction and ecto-ATPases, as shown on Fig. 4B, with the return to pre-stretch baseline level in less than ~1 min for all applied deformations.

In addition, half-life analysis of the decay signal past the culminating ATP accumulation suggested that very little, if any, additional ATP had been released. The average half-life from all interpulse decay signals from the four stretch chambers we analyzed in this report was $t_{1/2} = 9.3 \pm 2.2$ min, $R^2 > 0.90$ ($n = 20$). This average half-life value is slightly higher than the ones from our cell-free experiments ($t_{1/2} \sim 7$ min) described in MATERIALS AND METHODS. If additional ATP had been released after the stretch pulse, it would have supplemented the level of ATP and accordingly increased the half-life to a value higher than the one we measured in the absence of cells. The amplitude of this increase, however, is extremely small. For instance, in Fig. 3B, the half-life from the decaying signal following the 21% deformation load was $t_{1/2} = 9.8$ min. In the same graph at ~16 min, corresponding to ~4 min past the 21% strain peak of cumulated ATP and just before the next incoming stretch, there was a total of ~7.4 pmol in the chamber. Had the half-life been 7 min instead of the measured 9.8 min, the remaining ATP would have been 6.7 pmol (-0.7

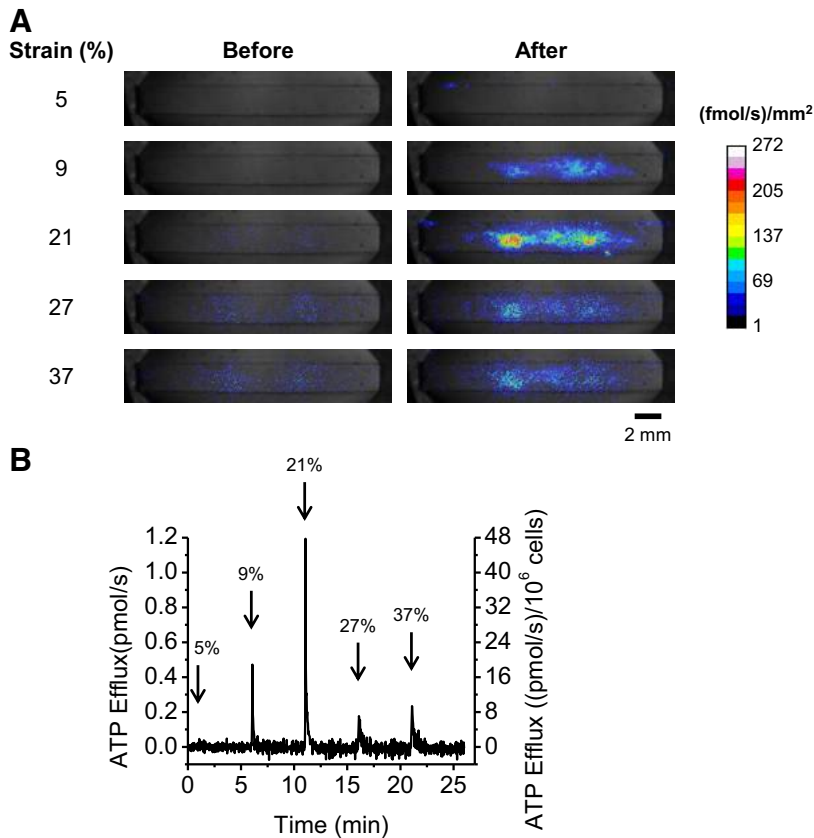


Fig. 4. Quantitative imaging of ATP efflux for whole stretchable groove (*sample no. 1*). **A**: overlay images of time derivative of total ATP signal (described in Fig. 3) over brightfield image of the A549 cell-adherent stretchable groove. *Left* and *right* columns show density images of ATP recorded seconds before and after stretch, respectively. Note that, as opposed to the prestretch images in Fig. 3A, the rate of ATP-dependent luminescence in those images returns to near background levels before the following stretch. **B**: ATP efflux in function of time during the experiments illustrated in A. The timing of stretch stimuli is indicated by arrows.

pmol) and the difference in rate of ATP release during this period would have amounted to only $+0.003$ pmol/s, a tiny value when compared with reported efflux at Fig. 4B. Thus, the luminescent signal between stretch pulses is almost entirely remnants from the previous stretch and a consequence of the slow degradation of ATP but unlikely a result of substantial ATP secretion.

Regional analysis of ATP secretion. The ability to monitor extracellular ATP fluctuation, not only for the whole chamber but also for any region of interest (ROI), is another interesting feature of our integrative ATP quantification technique. The total production rate of photons in any region in the chamber, represented by the sum of LU in this region on the image,

corresponds to the quantity of ATP_o present in this location from the surface of cells and above. To illustrate this, we tracked the variation in ATP_o content for five different ROIs of 0.4 mm^2 from another stretch assay (Fig. 5). The quantity of ATP detected in the extracellular medium in response to stretching this chamber and the ATP efflux (Figs. 5, B–C) was less than that described in Fig. 3 and had a different distribution (Fig. 5A) but presented the same strain threshold. The cumulated ATP_o for all five regions and their corresponding efflux is shown in Fig. 5, D and E. As expected, the values are much lower than the whole chamber (see Fig. 5B), with <10 fmol per pulse stretches for most ROIs, with the exception of ROI no. 3 reaching ~ 40 fmol at 21% strain pulse. While the

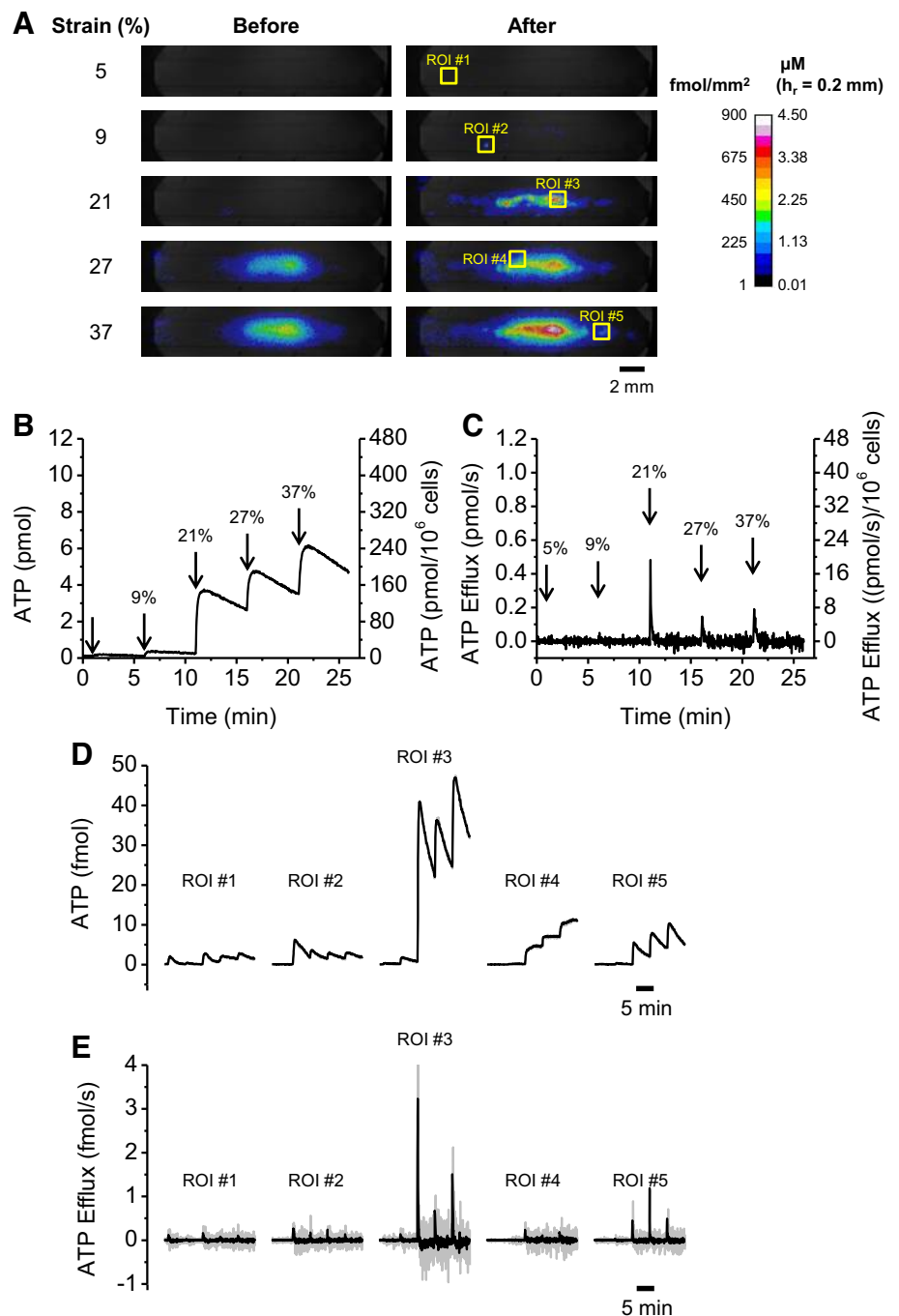


Fig. 5. Quantitative imaging of regional ATP release by stretch (*sample no. 2*). **A**: ATP density and average $[\text{ATP}]_o$ (reaction height, $h_r = 200 \mu\text{m}$) overlaid on transmitted light image of the stretch chamber are shown in response to a sequence of 5 uniaxial 1-s duration stretch pulses of increasing amplitude (from 5 to 37% strain) given at 5-min intervals at 25°C . Extracellular ATP density images for each pulse recorded immediately before or after stretch are shown. Note that similarly to the experiment presented in Fig. 3A, the major ATP secretion activity is localized in the middle portion of the stretchable zone. **B**: quantity of released ATP (in pmol) by A549 cells in function of time for the whole chamber. Stretch stimuli occurrences are indicated by arrows. **C**: ATP efflux in function of time for whole chamber derived from **B**. **D**: ATP accumulation response from the 5 regions outlined in **A**. For clarity, the positions of the regions of interest (ROI) are shown on a single image, but analysis was performed over the complete experimental time course. **E**: rate of ATP release for the 5 regions indicated in **A**. Data were smoothed with a running average ($n = 5$) before the derivative calculation to reduce the signal noise from the luciferase-luciferin reaction and better highlight the peak values. Gray area is $\pm\text{SD}$.

ATP efflux kinetics of the individual regions ROI no. 3–5 located near or within the main response area (see Fig. 5A) resembled, albeit at lower magnitude, the ones observed for the whole chamber, the isolated regions (ROI nos. 1 and 2) presented a contrasting response with near-maximal ATP response at lower strain values (5 and 9%).

Mean normalized ATP secretion. Figure 6A summarizes the stretch-induced ATP accumulation in extracellular medium over time for four independent experiments. The nearly continuous accumulation of ATP in the extracellular medium masks the very dynamic response of A549 cells under mechanical stretch. The ATP secretion activity occurred immediately after the onset of stretch and dissipated in <5 s. The average amount of secreted ATP after each pulse and the peak efflux

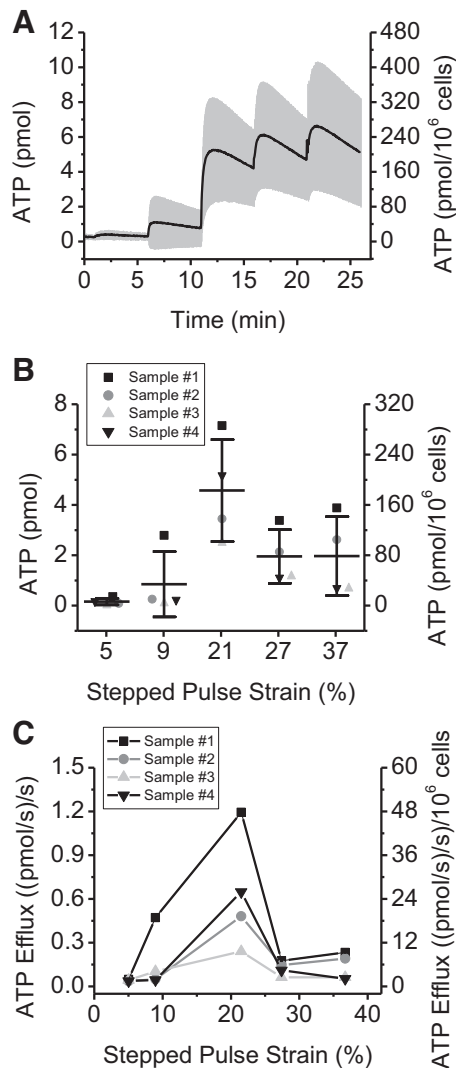


Fig. 6. Summary of accumulated ATP release per chamber/pulse and rate per pulse. ATP secretion and max efflux per pulse of increasing strain are not monotonic. A: average total ATP secreted per chamber and normalized per million cells in response to pulse stretch of increasing strain ($n = 4$ chambers). Gray area is \pm SD. B: ATP secreted per pulse. C: maximal ATP efflux per pulse of increasing strain. Data come from the same set of experiments analyzed in A. Note the similar pattern of response for total ATP secreted (in B) and ATP efflux per pulse. Mean \pm SD (strain): 1.7 ± 0.2 (5%), 6.7 ± 8.2 (9%), 25.6 ± 16.2 (21%), 5.0 ± 1.9 (27%), and 5.4 ± 3.6 (37%) $\text{pmol} \cdot \text{s}^{-1} \cdot \text{million}$ of cells $^{-1}$ ($n = 4$).

during the burst of ATP release are reported on Fig. 6, B and C. Maximal responses were observed at 21% deformation, with ATP release reaching 184 ± 81 pmol/million cells (or 184 ± 81 amol/cell) and ATP efflux climbing to 26 ± 16 (pmol/s)/million cells (or 26 ± 16 (amol/s)/cell).

Given that an adherent A549 cell has a volume of ~ 5 – 10 pL (2), and assuming the cytosolic fraction occupies the whole cell, with an estimated cytosolic ATP concentration of 1–5 mM, the total cytosolic ATP content would reach 5–50 fmol/cell. Thus, in response to a 21% strain, ~ 0.4 – 4% of cytosolic ATP content has been expelled extracellularly. Our imaging system clearly showed that not all cells were responsive, however, and that higher values for a single stretch can be anticipated in high release areas. For example, in the experiment shown in Fig. 3A at 21% deformation, the level of ATP attained 280 pmol/million cells (280 amol/cell) for the whole chamber, but the density map revealed a peak region reaching ~ 900 fmol/ mm^2 from a prestretch value of ~ 200 fmol/ mm^2 . With a relative ATP density gain of ~ 700 fmol/ mm^2 and the seeding cell density of 700 cells/ mm^2 (see MATERIALS AND METHODS), we computed ~ 1 fmol/cell or 2–20% of total cytosolic ATP content in this high-release zone from a single stretch. The rate of ATP release also showed considerable spatial heterogeneity. On Fig. 4A, for instance, the same region presented the highest ATP efflux, reaching ~ 270 (fmol/s)/ mm^2 and normalizing this rate with cell density yields ~ 386 (amol/s)/cell.

Hypotonic shock and ATP secretion. A sudden decrease in medium tonicity is another well-studied stimulus known to provoke ATP secretion (2). We tested A549 cells, which were seeded on glass coverslips and mounted on the stand of our real-time imaging system, for swelling-induced extracellular ATP elevation. To prevent cells from being acutely exposed to the remotely controlled addition of hypotonic solution, a small piece of the coverslip underneath the tip of the fluid dispenser was removed before testing, and hypotonic solution was added slowly (~ 3 – 5 s) to minimize mechanical perturbation while achieving a steady mixing.

Compared with stretch experiments, the secretion dynamics progressed at a slower pace and was more homogeneous. In the experiment shown in Fig. 7A, the distribution of secreted ATP was evenly spread over the cell population during the initial phase of the response ($t < 15$ min; Fig. 7B) within 10 min after the addition of hypotonic fluid and ~ 3 min after the rise of detectable ATP above background level (Fig. 7B). Afterward, a hot spot of ATP release gradually expanded near the edge of the coverslip. The ATP_o density, ranging between 20 and 30 fmol/ mm^2 for most of the coverslip during the rising phase of the response (Fig. 7A), climbed in excess of 100 fmol/ mm^2 in this hot spot region but remained far from the density level observed during stretch loads (see Fig. 3A and 5A). This heterogeneous luminescence intensity, markedly distinct at $t = 37.5$ min (Fig. 7A), is likely a consequence of spatial differences in ATP efflux arising from regional variation in cell density. This may not be the sole explanation, however, since the heterogeneity of ATP accumulation was augmented even further after ATP secretion had ceased ($t > 37.5$ min). This nonhomogeneous spatial distribution in bioluminescence appears related in part to the chemistry of the ongoing enzymatic reaction with the spatial segregation and establishment of gradients of either reagents or ATP throughout the volume of

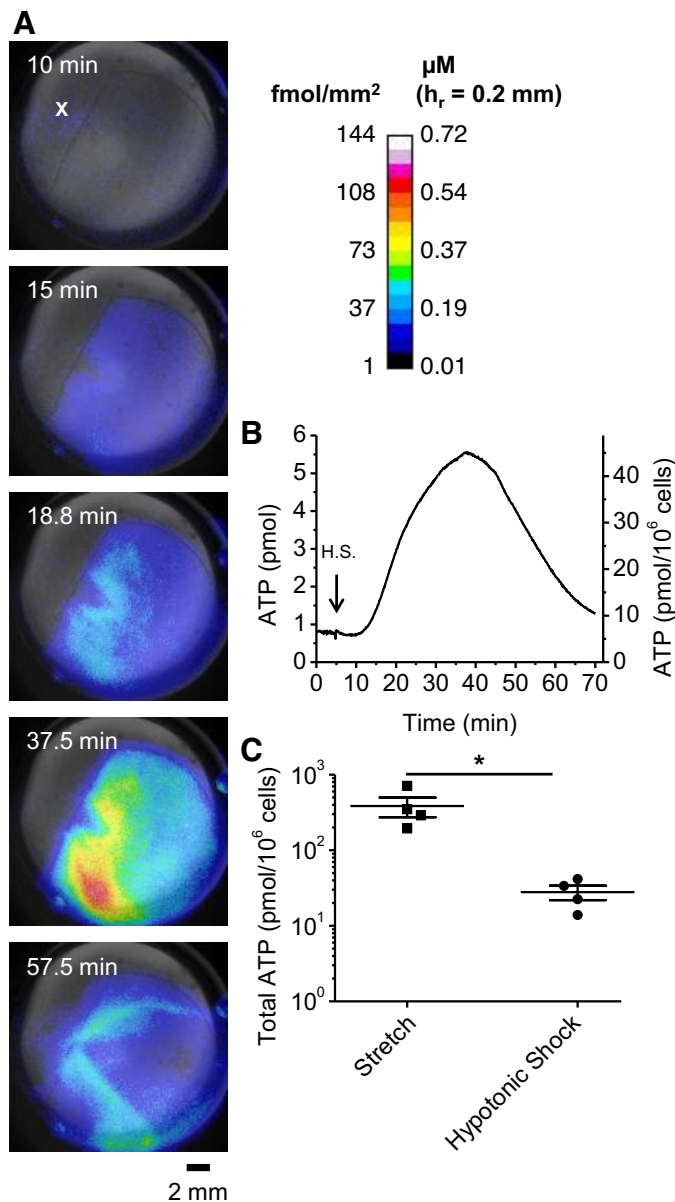


Fig. 7. Quantitative imaging of ATP efflux induced by hypotonic shock. A549 cell swelling results in initially more homogeneous ATP secretion but slower efflux than stretch. **A**: color-coded images of ATP density or average [ATP]_o (reaction height, $h_r = 200 \mu\text{m}$) overlaid on brightfield-acquired (static) image of the hypotonic chamber (gray) are shown in response to an acute diminution of extracellular fluid tonicity (50%) at 30°C. HypoLL solution was added at a location marked with an X at $t = 5 \text{ min}$. Note that the addition of the hypotonic solution to the medium containing protein-rich LL solution created 2 air bubbles located at the periphery of the chamber wall. They did not interfere with the reaction but reflected some of the luminescence, and were especially visible at $t = 37.5 \text{ min}$. **B**: cumulated ATP in the chamber over time has been calculated similarly as stretch experiments and is presented for the whole experiment until luminescence level went back to initial level. The detectable ATP efflux lasted for several minutes and ceased $\sim 33 \text{ min}$ after the onset of hypotonic shock. **C**: total ATP secretion from stretch load (sum of all 5 consecutive stretch pulses; $n = 4$) and hypotonic challenge per million of A549 cells ($n = 4$). Secretion levels were different ($*P < 0.05$) by Mann-Whitney test (R, version 3.4.1 Open-source software <http://www.R-project.org/>).

the reaction rather than exclusively linked to cellular ATP efflux, although this cannot be answered firmly unless a more detailed three-dimensional diffusion analysis and enzymatic kinetics of the reaction is undertaken.

Contrary to stretch, the hypotonically induced secretion lasted several minutes after the initiation of cell swelling (Fig. 7B). This sluggish response has been observed on three other independently tested coverslips. In a previous report from our laboratory, using an offline analysis and a perfusion chamber, the measured swelling-induced ATP efflux peaked around 1.5 min after the medium tonicity was lowered and reached a mean rate of $5 \pm 1.1 \text{ pmol}\cdot\text{s}^{-1}\cdot\text{million cells}^{-1}$ ($n = 9$) or $5 \pm 1.1 \text{ amol}\cdot\text{s}^{-1}\cdot\text{cell}^{-1}$ (2), but here, the efflux halted at 0.03 ± 0.01 (pmol/s)/million cells or 30 ± 10 (zmol/s)/cell and at a much later time: $\sim 15 \text{ min}$ on average after medium dilution ($n = 4$). While this lower ATP secretion is mostly a consequence of diminished release, a prolonged but feeble ATP efflux tends toward underestimation. Indeed, when the ATP efflux is strong, it largely exceeds the ATP breakdown from the LL-reaction and ectoATPases, but a weak ATP efflux struggles to accumulate ATP_o in the chamber against that constant degradation. Several reasons, in addition to the ATP breakdown activity of the ecto-ATPases and LL reaction, could explain those differences. The first and foremost is the lack of perfusion resulting in a slower change in bulk medium tonicity, a critical factor determining the rate of cell swelling (13). Other factors include the lower experimental temperature, 30°C instead of 37°C in (2), and the absence of tonic fluid shear mixing the cell boundary layer in the present configuration. In addition to efflux, the total hypo-induced ATP release ($n = 4$) was similarly smaller at $28 \pm 12 \text{ pmol/million cells}$ (Fig. 7C) when compared with the former study from our lab (2) with $1,002 \pm 154 \text{ pmol/million A549 cells}$ ($n = 9$). Notice that the total amount of ATP secreted from the sum of the five stretch pulses reached $384 \pm 224 \text{ pmol/million A549 cells}$ (Fig. 7C).

DISCUSSION

The real-time ATP imaging technique described herein produces images with superior brightness when compared with a standard microscope, thanks to its threefold object-to-image reduction. It also expands considerably the field of view to encompass the whole of typical experimental chambers used for ATP release investigation and permits to exclusively visualize the heterogeneous nature of mechanosensitive ATP release from a cell monolayer. It is also a compact free-standing imaging system easy to enclose in a light-tight box for benchtop assays and a less expensive solution than other microscopy-based techniques. Other advantages of macroscopic imaging include a very long working distance ($\sim 70 \text{ mm}$ with the lenses described in this study) to accommodate a variety of experimental chambers and the option to change the magnification level with additional lenses.

A large proportion of earlier ATP release studies had reported dimensionless LU in lieu of quantity of ATP, making it difficult to compare the cellular responses between independent studies and further impeding the progress in search of the nature and identities of ATP release pathways. The quantification of ATP from recorded images as detailed in the present report will help eliminate this difficulty and facilitate interstudies comparisons. In addition, our ability to identify areas of

higher rate of ATP secretion and accumulation despite the limited resolution of our imaging system enabled us to estimate peak ATP secretion at the cellular level, an important characteristic to help identify the mechanisms of ATP release. Furthermore, by estimating the extent of ATP diffusion, we could produce a fair approximation of the local concentration of ATP in the vicinity of the cell, an essential measure for purinergic signaling studies. Finally, we are also looking forward to improving the ATP mapping accuracy by estimating the ATP distribution in the extracellular fluid using a 3D model incorporating enzymatic kinetics and diffusion processes.

In conclusion, our macroscopic wide FOV quantitative ATP imaging approach, despite its lower imaging resolution when compared with that of a microscope, has nonetheless a very high level of ATP_o mapping resolution and quantification. Further, by revealing the big picture, this novel approach will enrich our understanding of the inhomogeneities and subtle dynamics of mechanically triggered ATP secretion from a cell monolayer.

GRANTS

This study was supported by Canadian Institutes of Health Research (MOP64364) and Natural Sciences and Engineering Research Council of Canada (R. Grygorczyk).

DISCLOSURES

No conflicts of interest, financial or otherwise, are declared by the authors.

AUTHOR CONTRIBUTIONS

J.J.T., O.P., R.G., and F.B. conceived and designed research; J.J.T. and O.P. performed experiments; J.J.T., O.P., and F.B. analyzed data; J.J.T., O.P., R.G., and F.B. interpreted results of experiments; J.J.T. prepared figures; J.J.T., R.G., and F.B. drafted manuscript; J.J.T., O.P., R.G., and F.B. edited and revised manuscript; J.J.T., O.P., R.G., and F.B. approved final version of manuscript.

REFERENCES

- Boudreault F, Grygorczyk R. Cell swelling-induced ATP release and gadolinium-sensitive channels. *Am J Physiol Cell Physiol* 282: C219–C226, 2002. doi:10.1152/ajpcell.00317.2001.
- Boudreault F, Grygorczyk R. Cell swelling-induced ATP release is tightly dependent on intracellular calcium elevations. *J Physiol* 561: 499–513, 2004. doi:10.1113/jphysiol.2004.072306.
- Burnstock G. Purine and pyrimidine receptors. *Cell Mol Life Sci* 64: 1471–1483, 2007. doi:10.1007/s00018-007-6497-0.
- DeLuca M, McElroy WD. Two kinetically distinguishable ATP sites in firefly luciferase. *Biochem Biophys Res Commun* 123: 764–770, 1984. doi:10.1016/0006-291X(84)90295-X.
- Feranchak AP, Lewis MA, Kresge C, Sathe M, Bugde A, Luby-Phelps K, Antich PP, Fitz JG. Initiation of purinergic signaling by exocytosis of ATP-containing vesicles in liver epithelium. *J Biol Chem* 285: 8138–8147, 2010. doi:10.1074/jbc.M109.065482.
- Furuya K, Sokabe M, Grygorczyk R. Real-time luminescence imaging of cellular ATP release. *Methods* 66: 330–344, 2014. doi:10.1016/j.ymeth.2013.08.007.
- Grygorczyk R, Furuya K, Sokabe M. Imaging and characterization of stretch-induced ATP release from alveolar A549 cells. *J Physiol* 591: 1195–1215, 2013. doi:10.1113/jphysiol.2012.244145.
- Koizumi S, Fujishita K, Inoue K, Shigemoto-Mogami Y, Tsuda M, Inoue K. Ca²⁺ waves in keratinocytes are transmitted to sensory neurons: the involvement of extracellular ATP and P2Y2 receptor activation. *Biochem J* 380: 329–338, 2004. doi:10.1042/bj20031089.
- Lazarowski ER. Vesicular and conductive mechanisms of nucleotide release. *Purinergic Signal* 8: 359–373, 2012. doi:10.1007/s11302-012-9304-9.
- Lohman AW, Billaud M, Isakson BE. Mechanisms of ATP release and signalling in the blood vessel wall. *Cardiovasc Res* 95: 269–280, 2012. doi:10.1093/cvr/cvs187.
- Mochizuki T, Sokabe T, Araki I, Fujishita K, Shibasaki K, Uchida K, Naruse K, Koizumi S, Takeda M, Tominaga M. The TRPV4 cation channel mediates stretch-evoked Ca²⁺ influx and ATP release in primary urothelial cell cultures. *J Biol Chem* 284: 21257–21264, 2009. doi:10.1074/jbc.M109.020206.
- Pellegatti P, Falzoni S, Pinton P, Rizzuto R, Di Virgilio F. A novel recombinant plasma membrane-targeted luciferase reveals a new pathway for ATP secretion. *Mol Biol Cell* 16: 3659–3665, 2005. doi:10.1091/mbc.e05-03-0222.
- Ponomarchuk O, Boudreault F, Orlov SN, Grygorczyk R. Calcium is not required for triggering volume restoration in hypotonically challenged A549 epithelial cells. *Pflugers Arch* 468: 2075–2085, 2016. doi:10.1007/s00424-016-1896-4.
- Ribeiro C, Esteves da Silva JC. Kinetics of inhibition of firefly luciferase by oxyluciferin and dehydroluciferin-adenylate. *Photochem Photobiol Sci* 7: 1085–1090, 2008. doi:10.1039/b809935a.
- Schindelin J, Arganda-Carreras I, Frise E, Kaynig V, Longair M, Pietzsch T, Preibisch S, Rueden C, Saalfeld S, Schmid B, Tinevez JY, White DJ, Hartenstein V, Eliceiri K, Tomancak P, Cardona A. Fiji: an open-source platform for biological-image analysis. *Nat Methods* 9: 676–682, 2012. doi:10.1038/nmeth.2019.
- Skotak M, Wang F, Chandra N. An in vitro injury model for SH-SY5Y neuroblastoma cells: effect of strain and strain rate. *J Neurosci Methods* 205: 159–168, 2012. doi:10.1016/j.jneumeth.2012.01.001.
- Takada H, Yonekawa J, Matsumoto M, Furuya K, Sokabe M. Hyperforin/HP-β-cyclodextrin enhances mechanosensitive Ca²⁺ signaling in HaCaT keratinocytes and in atopic skin ex vivo which accelerates wound healing. *BioMed Res Int* 2017: 1–9, 2017. doi:10.1155/2017/8701801.
- Taruno A. ATP release channels. *Int J Mol Sci* 19: 808, 2018. doi:10.3390/ijms19030808.
- Tschumperlin DJ, Margulies SS. Equibiaxial deformation-induced injury of alveolar epithelial cells in vitro. *Am J Physiol Lung Cell Mol Physiol* 275: L1173–L1183, 1998. doi:10.1152/ajplung.1998.275.6.L1173.

Appendix D

- **Reference 140** (DOI: 10.1152/ajplung.00321.2019)

Type 2 secretory cells are primary source of ATP release in mechanically stretched lung alveolar cells

Ju Jing Tan, Francis Boudreault, Damien Adam, Emmanuelle Brochiero, and Ryszard Grygorczyk

American Journal of Physiology-Lung Cellular and Molecular Physiology 2020 318:1, L49-L58

Reproduced with the permission of American Physiological Society

RESEARCH ARTICLE

Type 2 secretory cells are primary source of ATP release in mechanically stretched lung alveolar cells

Ju Jing Tan,^{1,2} Francis Boudreault,¹ Damien Adam,^{1,2} Emmanuelle Brochiero,^{1,2} and Ryszard Grygorczyk^{1,2}

¹Centre de recherche du Centre hospitalier de l'Université de Montréal, Montreal, Quebec, Canada; and ²Department of Medicine, Université de Montréal, Montreal, Quebec, Canada

Submitted 8 August 2019; accepted in final form 3 October 2019

Tan JJ, Boudreault F, Adam D, Brochiero E, Grygorczyk R. Type 2 secretory cells are primary source of ATP release in mechanically stretched lung alveolar cells. *Am J Physiol Lung Cell Mol Physiol* 318: L49–L58, 2020. First published October 9, 2019; doi: 10.1152/ajplung.00321.2019.—Extracellular ATP and its metabolites are potent paracrine modulators of lung alveolar cell function, including surfactant secretion and fluid transport, but the sources and mechanism of intra-alveolar ATP release remain unclear. To determine the contribution of gas-exchanging alveolar type 1 (AT1) and surfactant-secreting type 2 (AT2) cells to stretch-induced ATP release, we used quantitative real-time luminescence ATP imaging and rat primary alveolar cells cultured on silicon substrate for 2–7 days. When cultured on solid support, primary AT2 cells progressively transdifferentiated into AT1-like cells with ~20% of cells showing AT1 phenotype by day 2–3 (AT2:AT1 ≈ 4:1), while on day 7, the AT2:AT1 cell ratio was reversed with up to 80% of the cells displaying characteristics of AT1 cells. Stretch (1 s, 5–35%) induced ATP release from AT2/AT1 cell cultures, and it was highest on days 2 and 3 but declined in older cultures. ATP release tightly correlated with the number of remaining AT2 cells in culture, consistent with ~10-fold lower ATP release by AT1 than AT2 cells. ATP release was unaffected by inhibitors of putative ATP channels carbenoxolone and probenecid but was significantly diminished in cells loaded with calcium chelator BAPTA. These pharmacological modulators had similar effects on stretch-induced intracellular Ca²⁺ responses measured by Fura2 fluorescence. The study revealed that AT2 cells are the primary source of stretch-induced ATP release in heterocellular AT2/AT1 cell cultures, suggesting similar contribution in intact alveoli. Our results support a role for calcium-regulated mechanism but not ATP-conducting channels in ATP release by alveolar epithelial cells. lung ATP release; mechanosensitivity; purinergic signaling

INTRODUCTION

The mammalian lung alveolar epithelium comprises two main cell types, gas-exchanging squamous alveolar type 1 (AT1) and cuboidal surfactant-secreting alveolar type 2 (AT2) cells. AT2 cells synthesize and secrete surfactants, regulate depth of alveolar lining fluid, initiate the innate immune response, and act as progenitors for AT1 and AT2 cells during natural regeneration and epithelial repair after injury (7, 26). Even though in human alveolus the number of AT2 cells is higher than AT1 cells, the thin and large surface area of AT1

cells covers >95% of the alveolus surface. Pulmonary epithelial cells are constantly subjected to physical forces as a result of the cyclic breathing, coughing, and sneezing. These forces include air flow shear stress in the airways, cell stretch during alveoli inflation, and cell distortion by tension forces at the air-liquid interface in the alveoli and airways. Under clinically relevant pathological conditions, such as lung edema and mechanical ventilation, considerable fluid shear stress may also occur. Moreover, edematous lungs show inhomogeneous inflation in which some air-filled alveoli adjacent to the liquid-filled ones are subjected to significant overdistensions during breathing (29), which may lead to ventilator-induced lung injury (VILI). It is characterized by mechanical rupture of pulmonary structures, inflammation, and edema and constitutes a major clinical complication in ventilated patients in the intensive care unit (8, 43).

Mechanical forces, particularly stretch, play important roles in regulating lung function, development, alveolar cell differentiation and regeneration after injury (12, 33, 36). This requires translation of mechanical stimuli into biochemical signals, which often involves stress-sensitive release of ATP and activation of purinergic signaling events (19, 24, 32). Extracellular ATP and other nucleotides can bind to nucleotide-specific cell-surface purinergic receptors, which are categorized into ionotropic P2X_{1–7} receptors and G-protein-coupled P2Y_{1,2,4,6,11,12,13,14} receptors. The potential of extracellular nucleotide signaling is further diversified by the presence of nucleotidases, which sequentially hydrolyze ATP to ADP, AMP, and finally adenosine (45). Adenosine in turn may activate another family of G-protein-coupled receptors consisting of A₁, A_{2A}, A_{2B}, and A₃ subtypes (38). In the lungs, purinergic receptors are expressed on epithelial cells lining the lung surfaces, including AT2/AT1 cells, and often many receptor subtypes may be present on the same cell (4, 23). Purinergic signaling regulates surfactant release and all three components of the mucociliary clearance system: cilia beat frequency, fluid, and mucus secretion (6, 37). It also plays an important role in a number of lung diseases and associated clinical complications, including asthma, chronic obstructive pulmonary disease, acute respiratory distress syndrome, and VILI (6, 20). In experimental animal models, considerable amounts of ATP and other purines were found in the alveolar space of mechanically ventilated rat lungs as detected in vivo in bronchoalveolar lavage fluids (10, 35, 44). Excessively high levels of extracellular ATP act as a danger-associated signal and contribute to the pathogenesis of VILI by triggering the

Address for reprint requests and other correspondence: R. Grygorczyk, Centre de recherche du CHUM, 900, rue Saint-Denis, Pavillon R, Montréal, QC H2X 0A9, Canada (e-mail: ryszard.grygorczyk@umontreal.ca).

release of multiple proinflammatory mediators, lung inflammation, edema, and tissue damage (20). Given the critical responses that extracellular nucleotides can evoke in the lungs under physiological and pathophysiological conditions, it is of importance to understand the mechanism of cellular ATP release: the first step of purinergic signaling cascade. Besides cell injury-induced release, several pathways have been implicated in nonlytic release of ATP, including channels and/or Ca^{2+} -regulated exocytosis of ATP-loaded vesicles, but the exact mechanisms are still debated (17, 25, 31).

Release of cellular nucleotides is stress sensitive, as demonstrated by several groups (19, 24). Physical forces, such as mechanical stretch, cell deformation by tension forces at the air-liquid interface, and hypotonic shock induce increases in intracellular calcium levels ($[\text{Ca}^{2+}]_i$) and $[\text{Ca}^{2+}]_i$ -dependent release of ATP out of the cell (3, 40, 41). In carcinoma A549 cell line, a model of human alveolar cells, single stretch stimulus of more than 10% was sufficient to induce $[\text{Ca}^{2+}]_i$ -dependent ATP release with local ATP concentrations exceeding 10 μM (18). A recent real-time bioluminescence ATP imaging study with ex vivo rat lungs provided the first direct evidence that inflation induces ATP release in lung airspaces. The functional units where ATP release occurred consisted of alveolar sacs or their clusters (15). However, the contribution of AT1/AT2 cells lining the alveoli could not be determined in these experiments. Ex vivo confocal microscopy study has determined that the bulk of the alveolar distension during lung expansion occurs in AT1 and not AT2 cells (28), suggesting that AT1 cells act as a mechanosensor where transient intracellular Ca^{2+} signaling is initiated during lung inflation (2). However, conflicting data exist regarding the sources of intra-alveolar ATP release. In vitro studies with rat primary alveolar cells by Isakson et al. (21, 22) indicate that AT2 cells act as the primary source of extracellular ATP, while a study by Patel et al. (27) suggested that AT1 cells release significantly more ATP than AT2 cells and thus have a principal role in paracrine stimulation of surfactant secretion by AT2 cells. These early studies used bulk luminometry for ATP determinations, which lack spatial information on ATP release sites and have limited sensitivity and temporal resolution. These limitations could be overcome with the use of recently established real-time, high-sensitivity ATP release imaging technique (14) or a simplified low-cost version of that system based on wide-field-of-view (WFOV) imaging (39). Therefore, the objective of this study was to address the question of cellular source and mechanism of ATP release in mechanically distended AT2 and AT1 cell cultures using a quantitative WFOV ATP imaging approach. Clarifying release mechanisms and sources of intra-alveolar ATP is important for better understanding intercellular communication that coordinates alveoli responses to mechanical stimuli under physiological and pathological conditions, such as mechanical ventilation.

METHODS

Cell culture. Primary alveolar epithelial cells were isolated from lungs of adult male Sprague-Dawley rats (175–200 g, Charles River Laboratories, Senneville, QC, Canada), according to a well-established protocol as previously described (5, 16). In brief, the lungs were first washed to remove red blood cells and most of the alveolar macrophages before digestion with elastase (Worthington, Lakewood, NJ). They were then minced, and the resulting suspension was filtered.

A differential adherence technique (9, 16) was then used to discard the remaining macrophages bound on IgG and to purify alveolar epithelial cells. The freshly isolated alveolar cells were seeded onto custom-designed silicon chambers in MEM (Thermo Fisher Scientific Ltd., Saint-Laurent, QC, Canada) containing 10% fetal bovine serum (FBS, Wisent, Saint-Bruno, QC, Canada), 0.08 mg/L gentamicin, Septra (3 $\mu\text{g}/\text{mL}$ trimethoprim + 17 $\mu\text{g}/\text{mL}$ sulfamethoxazole, Glaxo Smith Kline Biologicals, Laval, QC, Canada), 0.2% NaHCO_3 (Sigma-Aldrich, Oakville, ON, Canada), 10 mM HEPES, and 2 mM L-glutamine (Thermo Fisher Scientific Ltd.). After seeding, alveolar cells were cultured for up to 7 days in MEM-FBS medium without Septra. All procedures pertaining to the use of animals were approved by the Comité Institutionnel de protection des animaux of the Centre de recherche du Centre hospitalier de l'Université de Montréal in compliance with guidelines of the Canadian Council of Animal Care.

Alkaline phosphatase histochemical staining. High alkaline phosphatase (AP) activity of AT2 cells is particularly useful to discriminate between AT2 and AT1 cells. AP staining was performed in cultures of freshly isolated alveolar cells seeded on silicone chamber or on 35×10 mm Petri dishes (Sarstedt Inc., Montreal, QC, Canada). On day 2, 3, 4, and 7 after seeding, cells were fixed, stained with 0.05% Fast Blue BB, and counterstained with 0.1% neutral red solution, as described in Ref. 42. Blue staining identified cells with high alkaline phosphatase activity present in AT2 cells, whereas those that counterstained in red only were AT1 cells (5, 11).

Immunofluorescence staining. For immunofluorescence staining, alveolar cells were seeded on an 8-well Laboratory-Tek (Nunc, Thermo Fisher Scientific, Rochester, NY). At 3 or 7 days after seeding, cells were fixed with 4% paraformaldehyde, permeabilized with Triton 0.1%, blocked, and then incubated overnight (4°C) with primary antibodies, anti-pro-surfactant protein C (1:100, EMD Millipore Corporation, Billerica, MA) or anti-aquaporin 5 (1:100, Alomone Laboratories Ltd., Jerusalem, Israel). After blocking, a secondary antibody [donkey anti-rabbit IgG conjugated with Alexa Fluor 633 (1:200, Life Technologies, Thermo Fisher Scientific, Rockford, IL)] was then applied for 1 h at room temperature. Following a wash with PBS, a 4',6-diamidino-2-phenylindole, dihydrochloride (DAPI, 1:1,000, Life Technologies, Thermo Fisher Scientific, Burlington, ON, Canada) was added for 15 min and then washed (3 \times) with PBS. Slides were mounted with Prolong Gold (Invitrogen, Thermo Fisher Scientific) and preserved in darkness at 4°C. Pictures were taken with a fluorescence microscope (Olympus, BY53; magnification $\times 20$ or $\times 40$) and images were analyzed with Icy software (Institut Pasteur, France). For analysis, typically 800 cells/condition/experiment were used, $n = 8$ from 4 different cell preparations (animals).

Stretch chamber and stretching device. Stretch chambers were made with Sylgard 184 silicone (Dow Corning Corporation, Midland, MI) as described previously (14, 18). Briefly, silicone elastomer base and curing agent mixture were poured into a mold and baked for 1 h at 60°C. The mold-made flexible silicone block constituted our stretch chamber with a 2-mm wide groove in the center where cells could be seeded. To facilitate attachment of cells to the silicone surface, the groove was coated with 20% collagen type 1 (Sigma) diluted in H_2O . For experiments, the chamber was attached to a stretching device (STREX, Cell Stretching System STB-150-W, B-Bridge International, Inc., Cupertino, CA) mounted on a stage above our custom-designed ATP imaging system (39). The stretching apparatus applied a horizontal distension onto the silicon chamber. In a typical experiment, five consecutive stretches of 1-s duration were applied at 5-min intervals with increasing nominal amplitudes. The real stretch amplitudes reported in the figures were measured after each experiment using the acquired images of the stretch chamber.

Real-time, wide-field-of-view bioluminescence ATP imaging. We used a WFOV luminescence ATP imaging as described in Ref. 39. Briefly, this approach uses a low-power objective ($\times 0.33$) mounted directly on an electron multiplying charge-coupled device (EMCCD) camera allowing a real-time two-dimensional (2D) visualization and

quantification of ATP contained in the entire stretch chamber following its release from cells. During image analysis, the individual light unit values per pixel for the 1-s acquisition time were converted into ATP quantity with the calibration factor and linear fitting using ImageJ. The total amount of detectable extracellular ATP (ATP_o) within the chamber could be calculated and monitored over the entire course of the experiment. The quantity of secreted ATP for each stretch pulse was calculated by subtracting the prestretch ATP_o level from the stretch-generated peak value. The rate of ATP release, expressed in fmol/s or pmol/s, is the first time derivative of ATP_o . Color-coded images reporting ATP_o density in fmol/mm² (one pixel image = 6×10^{-3} mm²) with respect to the substrate surface or rate of ATP release density in (fmol/s)/mm² were generated with ImageJ. On some images estimates of ATP_o concentration (in μ M) is given as an average value along the z-axis assuming 200 μ m height of a liquid layer above the cells where ATP-dependent LL reaction generates luminescence signal (39).

For imaging of cellular ATP release, stock of LL solution was prepared as follows. One vial of LL (Sigma-Aldrich Corporation, St. Louis, MO) was reconstituted with 5 mL of sterile double-distilled water and isotonicity adjusted with $5\times$ physiological solution. One milliliter aliquots of the stock solution were stored in a freezer and

used within 1 mo. Once thawed, the LL aliquot was used only during the day of experimentation, and its activity was checked using ATP standard TD 20/20 luminometer (Turner BioSystems, Sunnyvale, CA). Before the ATP imaging experiment, cells in the stretch chamber were covered with 200 μ L solution mixture containing 100 μ L of LL stock solution and 100 μ L of Gibco's phenol red-free Dulbecco's modified Eagle's medium (DMEM, Invitrogen Canada Inc., Burlington, ON, Canada). Following stretch stimulation, luminescence produced by ATP-dependent LL reaction was captured by the EMCCD camera Evolve 512 (Photometrics, Tucson, AZ) in our custom-designed wide field of view system. Control of the EMCCD and data acquisition were done via AxioVision software (AxioVs40 V 4.8.2.0, Carl Zeiss MicroImaging GmbH, Jena, Germany). Images were acquired at 0.5 Hz frequency with 1-s exposure time, with gain settings at the lowest, readout speed at 5 MHz, and 2×2 binning. Stacks of 900 images were captured and stored for offline analyses with Meta-morph (Meta Series Software 7.7.9, Molecular Devices, Downingtown, PA) or ImageJ open-source software.

Intracellular calcium measurements. Calcium imaging experiments were performed as described in Ref. 30. Briefly, AT2 cells were loaded with a ratiometric fluorescent probe Fura2-AM (10 μ M, Molecular Probes, Thermo Fisher Scientific) in MEM + FBS cell

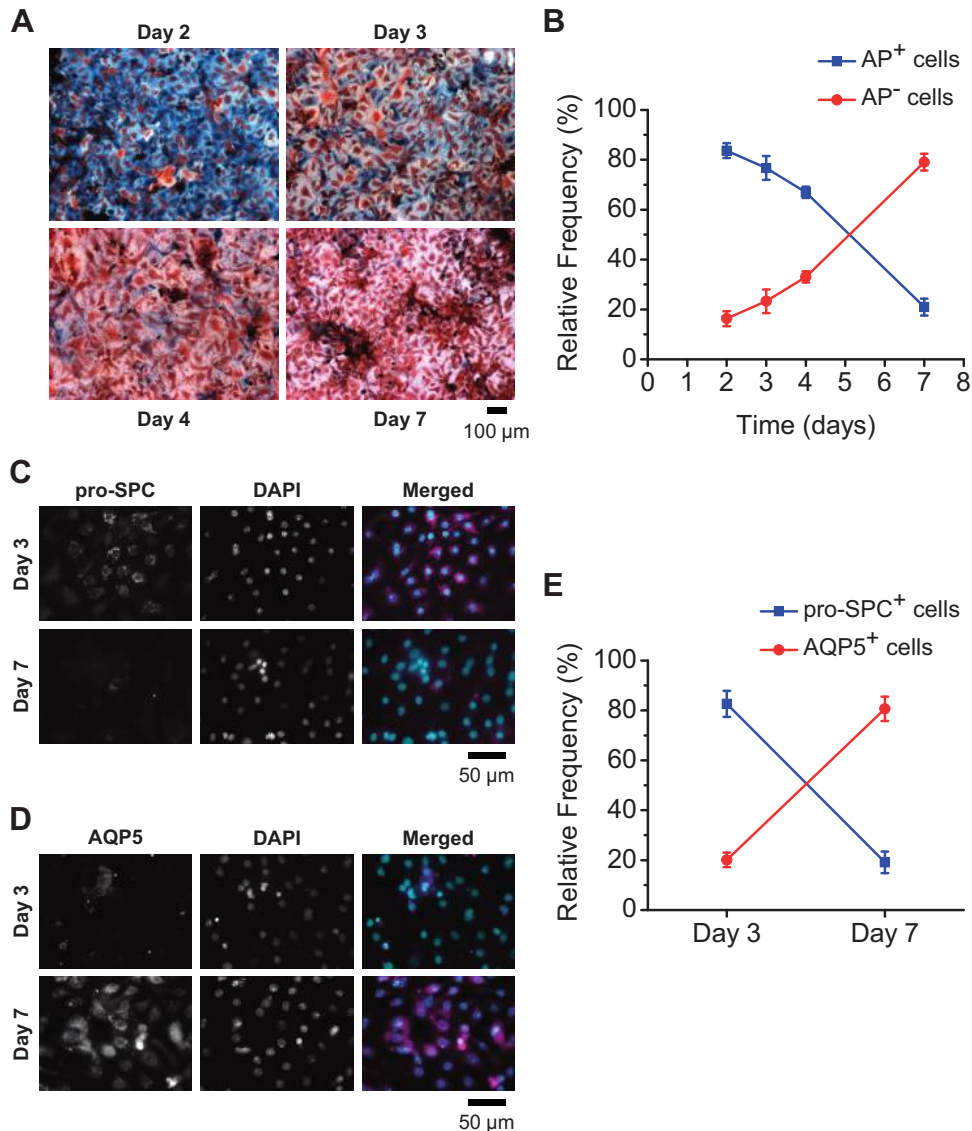


Fig. 1. Phenotypic changes of rat primary alveolar epithelial cells in culture. **A:** changes in alkaline phosphatase (AP) staining of alveolar type 2 (AT2) and alveolar type 1 (AT1) cell cultures grown on flexible silicone stretch chamber as a function of time (days 2–7). Blue staining indicates AP activity, which is characteristic of AT2 cells, while those counterstained in red only correspond to AT1 cells. Images are representative of three independent cell preparations. **B:** relative number (in %) of AT2 and AT1 cells (blue and red lines, respectively) as a function of time in culture. Data are mean \pm SD of three independent experiments. For analysis, cells with AP activity (AP⁺, blue/red) and without AP activity (AP⁻, red only), corresponding to AT2 or AT1-like phenotypes, respectively, were manually counted. Note a time-dependent gradual loss of AT2 phenotype and increase of AT1-like phenotype. The pictures were taken with $\times 20$ phase-contrast objective and the Eclipse TE200 (Nikon) microscope equipped with an Axiocam ICc 1 (Zeiss) camera. **C** and **D:** immunostaining of 3- and 7-day-old alveolar epithelial cell cultures with anti-pro-surfactant protein C (pro-SPC) (marker of AT2 cells) or anti-aquaporin (AQP)-5 (marker of AT1 cells) and secondary antibody conjugated to Alexa Fluor 633 (magenta on merged images). Nuclei were then counterstained with DAPI (cyan on merged images). Images are representative of eight independent experiments from four different cell preparations (four animals). **E:** quantification of the number of pro-SPC (pro-SPC⁺, blue line) and AQP5 (AQP5⁺, red line) positive cells in 3- and 7-day-old alveolar epithelial cell cultures, presented as percentage of total cells (DAPI staining); $n = 8$.

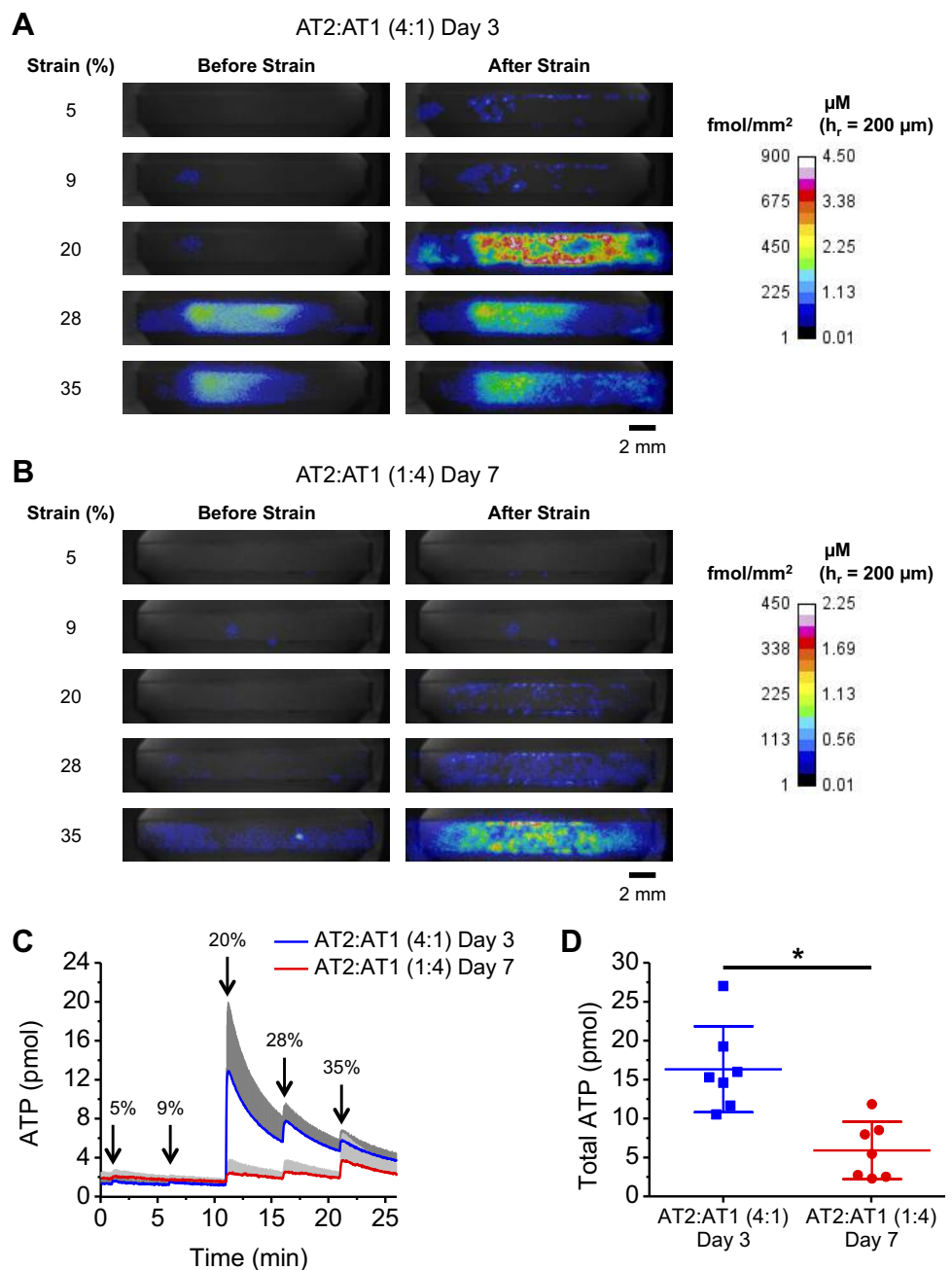
culture medium for 1 h (37°C, 5% CO₂). Cells were then washed in MEM + FBS, and the medium was changed to phenol-free DMEM. During the experiment, cells were exposed to alternate (100 ms) 340/380 nm illumination from a high-pressure mercury short arc lamp (100 W/2, Osram GmbH, Augsburg, Germany) via interference filters (Chroma Technology, Brattleboro, VT) mounted on a filter wheel (Sutter Lambda 10-C, Sutter Instrument, Novato, CA). Fluorescence images were recorded at 1- to 3-s intervals with a MicroMAX digital camera (Princeton Instruments Inc., Trenton, NJ) and stored for later analysis. As a positive control for Ca²⁺ detection, 30 μL of 100 μM ATP was applied to the cells (13 μM final concentration) at the end of each experiment. Changes of [Ca²⁺]_i are shown as Fura2 fluorescence F₃₄₀/F₃₈₀ ratio normalized to initial baseline level.

Pharmacological modulators of ATP release and Ca²⁺ signaling. To study the physiological mechanisms for ATP release, ATP and Ca²⁺ imaging experiments were carried out in the presence of 100

μM carbenoxolone (CBX) or 2.5 mM probenecid (PRO) from Sigma-Aldrich, Inc. (St. Louis, MO) in phenol-free DMEM. To study the role of [Ca²⁺]_i, AT2 cells were pretreated with 25 μM BAPTA (Life Technologies, Burlington, ON, Canada) and reconstituted in DMSO (Sigma-Aldrich Canada Co., Oakville, ON, Canada) in MEM + FBS. Controls were also pretreated with MEM + FBS with the same amount of DMSO but without BAPTA.

Statistics. Results are expressed as mean ± SD. Statistical analyses were performed with R (3.6.0) to compare averages of samples between their conditions. When comparing the average between two groups, an *F* test was first performed to determine whether the variance of both groups was equal to perform the adequate *t* test. For smaller samples (*n* = 3–4), Wilcoxon–Mann–Whitney and Kruskal–Wallis *H* tests were performed to compare with the average of two or more groups, respectively. Pearson product-moment correlation was

Fig. 2. Quantification of stretch-induced ATP release in alveolar type 2 (AT2) and alveolar type 1 (AT1) cell cultures. **A:** example images of two-dimensional (2D) ATP density map (fmol/mm²; see pseudocolor scale) in 3-day-old cell culture containing predominantly AT2 cells (AT2:AT1 ratio of 4:1) at the peak of response to a sequence of 1-s stretches of 5–35% applied at 5-min intervals. Left and right columns show ATP density map before and after stretch stimulus, respectively. Residual ATP released by preceding stretches is clearly visible on images in the Before Strain column, particularly after the 20% and 28% stretch. Estimated ATP concentrations (in μM) are also indicated on the pseudocolor scale bar that represents the average value for the 200-μm-high reaction layer (*h_r*) of fluid covering the cells (see METHODS). **B:** example images of 2D ATP density map in 7-day-old cell culture containing predominantly AT1 cells (AT2:AT1 ratio of 1:4) at the peak of response to a sequence of stretches described in A. Note different pseudocolor scale and significantly lower ATP release responses compared with those shown in A. **C:** the graph shows a full time course of ATP released from cells in the entire chamber in response to a sequence of five 1-s stretches of increasing amplitude (see labels on each trace) as described in A. The blue and red traces represent mean ± SD (gray shadow, *n* = 7) for 3- and 7-day-old cell cultures, respectively. For clarity only positive direction of SD is shown. **D:** cumulative ATP released in response to a sequence of stretches (5–35%) for 3- and 7-day-old cell cultures in the experiment shown in C. The quantity of secreted ATP for each stretch pulse is calculated by subtracting the pre-stretch extracellular ATP (ATP_o) level from the stretch-generated peak value (see METHODS). Data are shown as a scatterplot with mean ± SD for seven independent experiments. Student's *t* test shows statistical difference between both groups (*P* < 0.05). The 3-day-old cultures (AT2:AT1 ratio of 4:1) release almost three times more ATP than 7-day-old cultures (AT2:AT1 ratio of 1:4). **P* < 0.05.



used for evaluating linear association between two variables. Differences between groups were considered to be significant at $P < 0.05$.

RESULTS

Phenotypic changes of cultured rat primary alveolar epithelial cells. Freshly isolated rat primary alveolar cells were grown on collagen-coated silicon stretch chambers for up to 7 days. AT2 phenotype was identified by alkaline phosphatase staining (blue color, Fig. 1A). AT2 was highest on day 2, but it was gradually lost on days 3–7 when cells progressively acquired AT1-like phenotype, indicated by red counterstain. Figure 1B shows the relative number of AT2 and AT1-like cells on different days in culture as determined by alkaline phosphatase staining. It demonstrates that on days 2 and 3, ~80% of cells still showed AT2 phenotype, corresponding to AT2/AT1 ratio of 4:1, while on day 7, the ratio was reversed to 1:4, with ~80% of cells showing AT1-like phenotype. Gradual transdifferentiation of cultured AT2 to AT1-like cells was further supported by time-dependent reduction of specific immunostaining with

pro-surfactant protein C (pro-SPC, marker of AT2 cells) and increased expression of aquaporin-5 (characteristic of AT1 cells) on day 7 compared with day 3 in culture (Fig. 1, C and D, respectively). Quantitative analysis of cell immunostaining (Fig. 1E) demonstrated high consistency with AP staining presented in Fig. 1B. Subsequently, we examined stretch-induced ATP release in such heterocellular 2- to 7-day-old cultures of different AT2 and AT1 cell content.

Stretch-induced ATP release is diminished in cell cultures of low AT2 cell content. Using a quantitative WFOV luminescence imaging approach, we first compared stretch-induced ATP release in 3- and 7-day-old alveolar cell cultures containing predominantly (~80%) AT2 or AT1-like cells, respectively. To quantitate ATP release, luminescence images were converted to two-dimensional (2D) ATP density maps (in fmol/mm²), or expressed as concentration (in μ M, as described in METHODS). Figure 2A shows an example of an ATP density map (see pseudocolor scale) of a 3-day-old cell culture containing predominantly AT2 cells (AT2:AT1 ratio of 4:1) before the

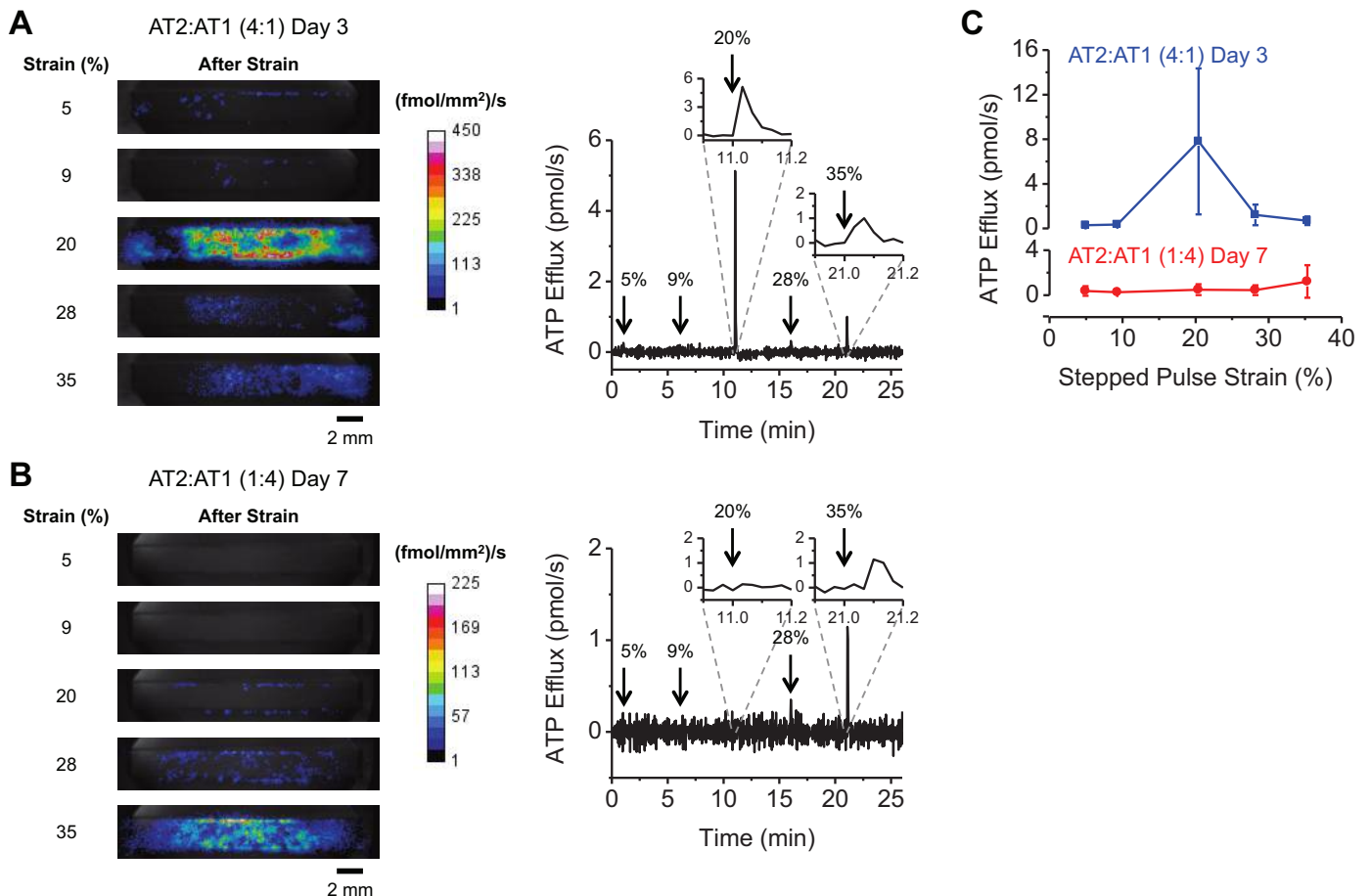


Fig. 3. Quantification of the rate of ATP release. **A**: examples of two-dimensional (2D) maps of ATP release rate (in fmol/mm²/s) at the peak response in 3-day-old cell culture induced by a sequence of 1-s stretches of 5–35% applied at 5-min intervals in an experiment similar to that shown in Fig. 2A. The highest rate of ATP release was observed at 20% stretch. The graph on the right shows the time course of ATP release rate averaged for the entire area of the stretch chamber. Note very short duration (<5–10 s) of ATP release following stretch stimulation. The insets show spikes of ATP efflux at expanded time scale during 20% stretch (at 11 min) and 35% stretch (at 21 min). **B**: example of 2D maps of ATP release rate (fmol/mm²/s) at the peak response in 7-day-old cells induced by a sequence of stretches in an experiment similar to that shown in A. Only at the highest stretch of 35% was significant ATP efflux observed. The graph on the right shows the time course of ATP efflux averaged for the entire area of the stretch chamber. The insets show the time course of ATP efflux at expanded time scale during 20% stretch (at 11 min) and 35% stretch (at 21 min). **C**: comparison of the peak of ATP efflux (rate of ATP) release for stepped pulse stretches of increasing amplitude in 3- and 7-day-old cell cultures (blue and red traces, respectively). Data are mean \pm SD of seven independent experiments. AT1, alveolar type 1; AT2, alveolar type 2.

stretch stimulation and at the peak of response to 1-s stretches of 5–35% applied at 5-min intervals. Small ATP release that was localized to a limited number of release sites was seen for low stretches of 5% and 9% but increased significantly for stronger stretches, with a maximum response observed at 20% stretch. It involved the release from almost all cells in the stretch chamber, reaching, in some areas, up to 900 fmol/mm², corresponding to local ATP concentration of ~4.5 μM. Figure 2B presents similar ATP density maps for 7-day-old alveolar cell culture and shows that ATP release responses were significantly diminished in these cells. Only at the highest stretch of 35% was significant ATP release of 300–400 fmol/mm² observed. The graph in Fig. 2C compares the full time course of ATP released in the entire chamber containing 3-day or 7-day-old cell cultures induced by a sequence of stretches (5–35%) delivered at 5-min intervals. For 3-day-old cells, it peaked at 20% stretch and was significantly higher (>6-fold at the peak) when compared with the peak release in 7-day-old cells observed at 35% stretch. Figure 2D compares cumulative ATP released in response to all delivered stretches during the experiment and demonstrates an average of ~3-fold higher release in 3-day-old cells compared with 7-day-old cell cultures.

Next, we analyzed the rate of ATP release. Figure 3A illustrates an example of 2D maps of ATP release rate (ATP efflux, in fmol·mm⁻²·s⁻¹) at the peak of response after five consecutive stretches of 5% to 35%. It was calculated from a sequence of ATP density maps such as those illustrated in Fig. 2A. Low stretches of 5–10% produced small but detectable ATP efflux. The peak response was observed at 20% stretch with the efflux of ATP reaching ~450 fmol/mm²/s in some spots. The graph on the right shows the full time course of ATP release rate averaged for the entire area of the stretch chamber. Note the very short duration (spikes) of ATP release following stretch stimulation and the absence of the release between the stretches. The insets show the spikes of ATP efflux at expanded time scale during 20% stretch (at 11 min) and 35% stretch (at 21 min), demonstrating their duration of <5 s and their peaks of ~5 pmol/s and ~1 pmol/s, respectively. By contrast, 7-day-old cell cultures showed no response or very low responses for stretches of up to 28%, and only at the highest stretch of 35% was considerable ATP efflux (reaching 200 fmol/mm²/s) observed, as shown in 2D maps in Fig. 3B. The corresponding full time course of ATP efflux in the entire chamber is shown on the right, with the spike of ATP release of ~1 pmol/s in response to 35% extension (at 21 min). Figure 3C compares the average rate of ATP release (*n* = 5) in response to stretches of increasing amplitude for 3-day-old and 7-day-old cell cultures with AT2:AT1 of 4:1 and AT2:AT1 of 1:4, respectively. It shows that, in AT2-rich cell cultures, ATP efflux peaked at ~20% stretch but declined for stronger stretches of >25%, while in AT1-rich cultures, significant efflux was observed only at the maximal stretches of 28–35%. The data demonstrated that in cultures containing predominantly AT2 cells the maximal rate of ATP release was observed at lower stretches, and it was ~5-fold higher when compared with older cell cultures containing mostly AT1 cells.

The relative contribution of AT2 and AT1 cells to ATP release was quantified by comparing total ATP release with relative AT2 cell content remaining on each day of culture from 2 to 7 days (Fig. 4). The stretch-induced release of ATP

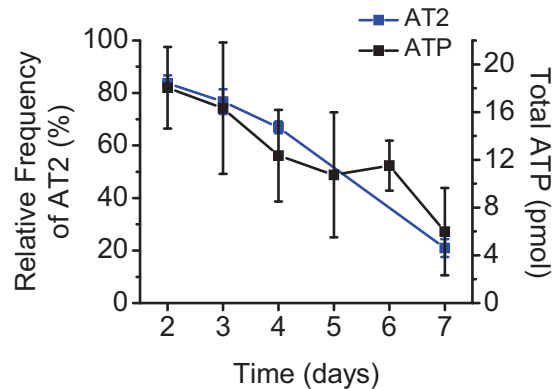


Fig. 4. Stretch-induced ATP release closely correlates with alveolar type 2 (AT2) cell content in AT2 and alveolar type 1 (AT1) cell cultures. ATP release (pmol, black line, scale on the right) in alveolar cells decreases with the time in culture (from day 2 to 7). Total cumulative ATP release after sequence of stretches was calculated as described in Fig. 2D. Data are mean \pm SD of *n* = 3–7 independent experiments. The graph is superimposed on AT2 cell content data of Fig. 1B (blue line) to directly compare with relative AT2 cell content (in %, left scale). Note a close correlation between the decreasing ATP release and number of remaining AT2 cells. Statistical analysis (Pearson's product-moment correlation) reveals a strong correlation between ATP release and AT2 cell number (correlation coefficient $r = 0.94$, $P = 0.0053$).

was found to be the highest in early cell cultures (days 2 and 3) but declined progressively for older cultures, showing a tight correlation between decreasing ATP release and the number of remaining AT2 cells (Pearson's correlation coefficient $r = 0.94$, $P = 0.0053$). The data strongly suggest that AT2 cells are the major contributors of stretch-induced ATP release.

Effects of ATP release modulators. To determine the mechanism of stretch-induced ATP release in 3-day-old alveolar epithelial cells, we tested the effects of two commonly used inhibitors of putative ATP channels, carbenoxolone (CBX) and probenecid (PRO). Figure 5A shows the time course of ATP release induced by 9% and 20% stretch under control conditions and in the presence of CBX or PRO. Although the time course of release was not affected, CBX showed a tendency to reduce the peak ATP release and total released ATP (Fig. 5A), but the effects remained not statistically significant. Interestingly, PRO produced a noticeable increase of the peak and total ATP release, but the effect was not statistically significant either. Thus, the results do not support involvement of putative ATP channels, such as pannexin 1, in stretch-induced ATP release in alveolar cells.

To explore the possible involvement of intracellular Ca²⁺ signaling in ATP release via regulated exocytosis of ATP-containing vesicles (1, 40), cells were loaded with BAPTA-AM to chelate free intracellular Ca²⁺. Figure 5B shows significant (~40%) inhibition of the peak of stretch-induced ATP release and total released ATP in BAPTA-loaded cells. Data demonstrate the importance of intracellular Ca²⁺ signaling in regulating stretch-induced ATP release. Therefore, we subsequently explored stretch-induced intracellular Ca²⁺ responses in more detail in AT2/AT1 cells using Fura2 fluorescence microscopy.

Stretch-induced intracellular Ca²⁺ responses in AT2 cells. Fig. 6A shows pseudocolor images of Fura2 F₃₄₀/F₃₈₀ fluorescence ratio in 3-day-old AT2 cell culture subjected to stretch stimulation. At lower stretches (~5%) rapid [Ca²⁺]_i responses were observed in very few single cells. The number of re-

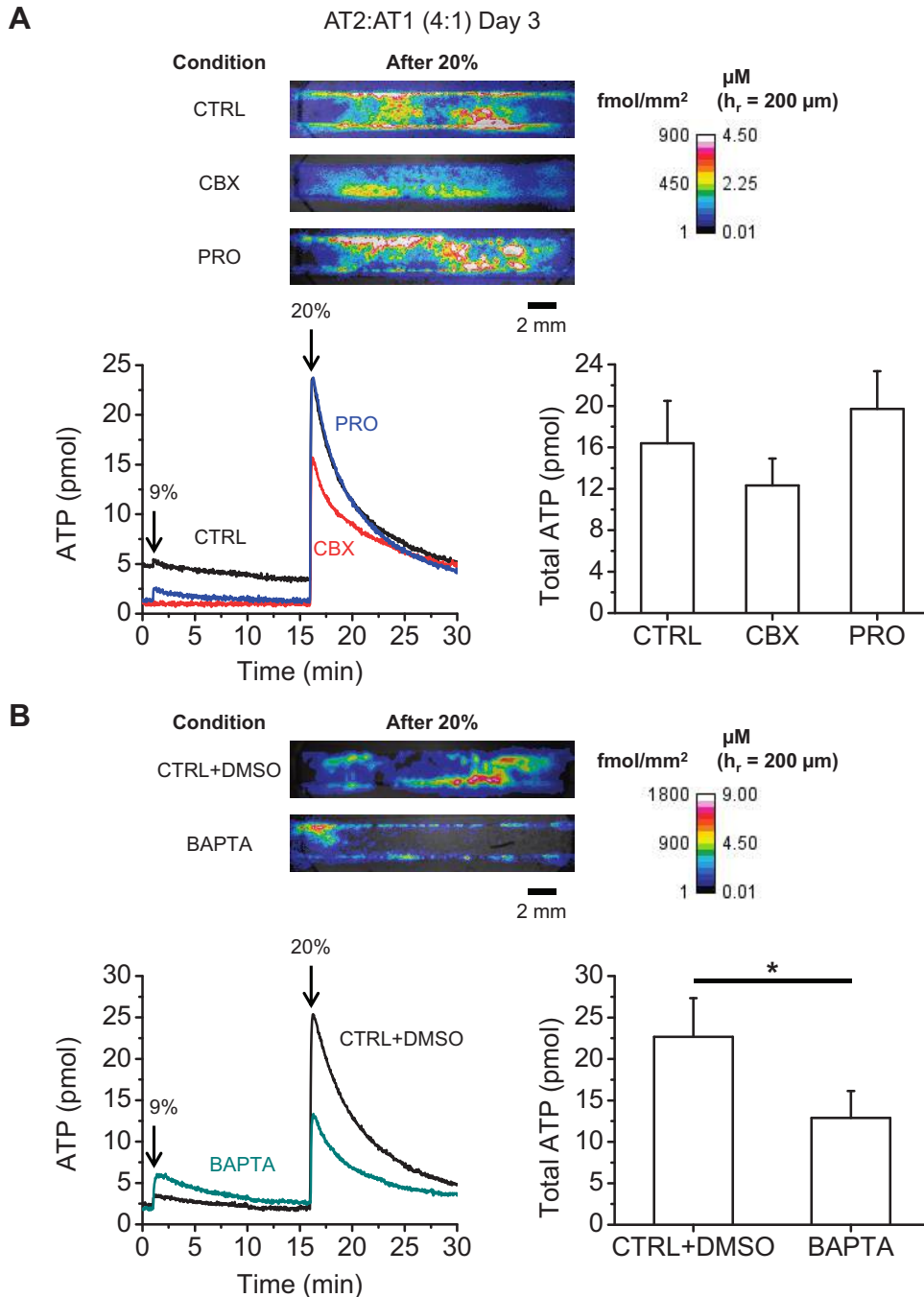


Fig. 5. Effect of ATP release modulators. *A*: time course of ATP release in response to two stretches (9% and 20%) in 3-day-old cultures of control alveolar type 2 (AT2) cells (CTRL, representative of $n = 3$), and cells treated with 100 μ M carbenoxolone (CBX) or 2.5 mM probenecid (PRO, $n = 3$). ATP imaging and stretch stimulations were performed with inhibitors included in the LL + DMEM covering the cells. Images above show representative ATP density maps (fmol/mm²; see pseudocolor scale) at the peak response to 20% stretch for the three conditions (CTRL, CBX and PRO). Bar graph on the right shows the corresponding total quantity of secreted ATP (mean \pm SD, $n = 3$) for each condition. There was no significant difference between all three groups [CTRL (16.4 ± 4.1 pmol), CBX (12.3 ± 2.6 pmol), and PRO (19.7 ± 3.6 pmol), $P = 0.11$]. *B*: effect of Ca²⁺ chelator BAPTA on ATP release in 3-day-old cultures of AT2 cells. Time course of ATP release (pmol) in response to two stretches (9% and 20%) in control AT2 cells treated with vehicle (DMSO, 30 min) and in cells loaded with 25 μ M BAPTA-AM for 30 min (representative of $n = 3$). Prior to ATP imaging, cells in the stretch chamber were washed with PBS solution and bathed in DMEM containing isotonic LL. Images above show examples of ATP density maps (fmol/mm²; see pseudocolor scale) at the peak response to 20% stretch for the two conditions (CTRL and BAPTA). Estimated ATP concentration (in μ M) is also indicated on the pseudocolor scale bar. Bar graph on the right shows total ATP released (mean \pm SD) during the entire experiment. Cells loaded with BAPTA showed statistically significant reduction of ATP release (12.9 ± 3.3 pmol) compared with the controls (22.7 ± 4.7 pmol), $*P < 0.05$.

sponding cells increased with rising stretch amplitude and involved mostly clusters of adjacent cells. Interestingly, CBX inhibited and PRO stimulated stretch-induced [Ca²⁺]_i responses, which were almost completely abolished in BAPTA-loaded cells (Fig. 6B). These effects on [Ca²⁺]_i are similar to those observed for ATP release, suggesting that the slight inhibition of ATP release by CBX and stimulation by PRO may be an indirect result of their effects on [Ca²⁺]_i signaling rather than on ATP conductive pathway.

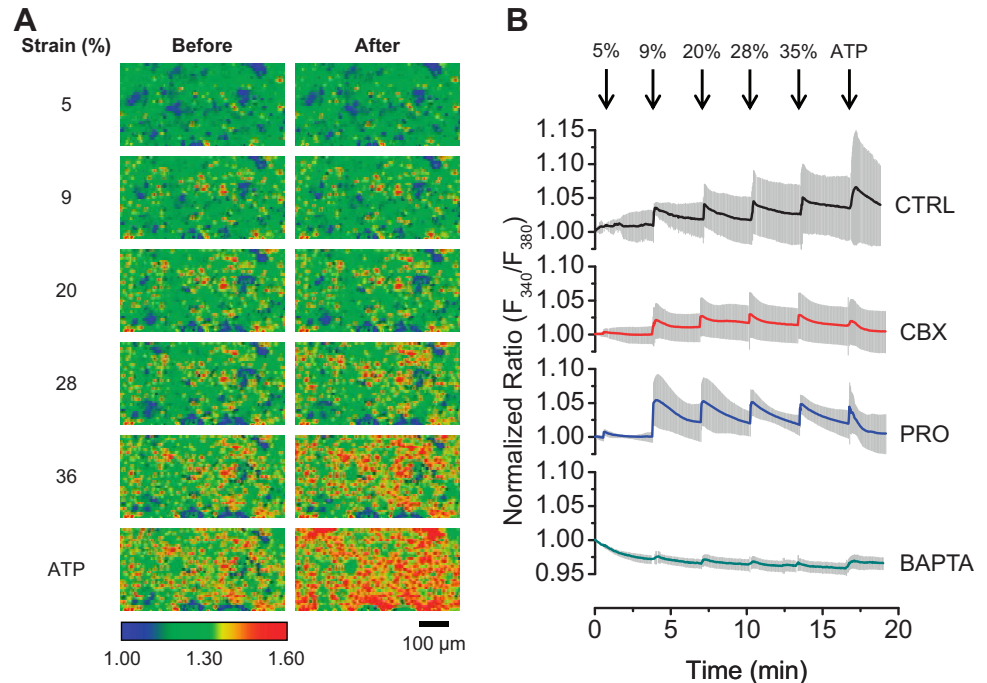
DISCUSSION

The goal of this study was to investigate the cellular source (AT2 vs. AT1 cells) and the mechanism of stretch-induced ATP

release in primary AT2 and AT1 cell cultures of rat lungs. We found that AT2 cells, when grown in a 2D culture on collagen-coated silicon stretch chambers, transdifferentiate over time into AT1 cells. This agrees with previous reports where cells were cultured on various substrates, including fibronectin-coated silicon and glass coverslips, or tissue culture treated plastic (21, 22). Using such heterocellular AT2 and AT1 cultures on different days after cell seeding, we have 1) characterized the quantity and rate of stretch-induced ATP release and 2) determined the relationship between the release and AT2/AT1 cell ratio that varied approximately from 4:1 to 1:4.

ATP release kinetics and quantity. Data of ATP release rate demonstrated that 1-s stretch induced very transient efflux of

Fig. 6. Stretch-induced intracellular Ca^{2+} responses in alveolar type 2 (AT2) cells. **A**: examples of a typical stretch-induced $[\text{Ca}^{2+}]_i$ responses in control (CTRL) 3-day-old AT2 cell cultures. *Left and right* columns display example images of Fura2 fluorescence ratio (F_{340}/F_{380}) in cells before and after stretch, respectively. Pseudocolor scale bar was normalized to initial F_{340}/F_{380} baseline value. Color turning from blue or green to yellow or red indicates increase in $[\text{Ca}^{2+}]_i$. Note the increased number of responding cells for stronger stretches. ATP (13 μM final concentration) was added at the end of each experiment and served as a positive control. Images are representative of four independent experiments. **B**: time course of $[\text{Ca}^{2+}]_i$ responses evoked by a sequence of five stretches of increasing amplitude (5–35%) given at 5-min intervals (arrows) in control cells and cells treated with carbenoxolone (CBX), probenecid (PRO), or BAPTA. Traces represent mean \pm SD from four experiments. Note that CBX inhibits and PRO stimulates stretch-induced $[\text{Ca}^{2+}]_i$ responses in AT2 cells, while BAPTA reduced the baseline level of $[\text{Ca}^{2+}]_i$ and almost completely abolished the responses to stretch stimulation.



cellular ATP immediately after the onset of stretch that dissipated in less than 5–10 s. Such kinetics were similar in AT2-rich (day 2 and 3) and AT1-rich (day 7) cell cultures. It was also comparable with the responses observed in our earlier study with A549 cells, a model of human AT2 cells, in which ATP release was examined with the same WFOV approach and the duration of the release was also found to be <10 s (39). The 2–3-day-old cell cultures were significantly more susceptible to stretch stimulation, responding at 5–10% distension and reaching maximum response at 20%, while 7-day old cells were essentially nonresponsive to lower deformations and released noticeable ATP only at the highest strain of 35%. In that respect, the 2- to 3-day-old rat primary AT2 cells appear to be comparable with A549 cells, which showed a similar threshold for ATP release responses of $\sim 10\%$ strain (18).

Transient release resulted in accumulation of significant amounts of extracellular ATP_o that persisted for 5- to 15-min before returning to the prestretch level due to its relatively slow consumption by LL reaction and breakdown by ectoATPases, as discussed before (39). From the data of Fig. 2D, we have determined that the average amount of secreted ATP was 0.72 ± 0.14 fmol/cell and 0.24 ± 0.15 fmol/cell on day 3 and 7, respectively. For comparison, in A549 cells the cumulative ATP released in response to a similar sequence of 5 stretches of increasing amplitude was 0.18 ± 0.08 fmol/cell (39), i.e., comparable with 7-day-old alveolar cell cultures. Importantly, with an estimated cytosolic ATP concentration of 1–5 mM, it could be calculated that for a single stretch of 20%, the total quantity of released ATP in 3-day-old alveolar cells was 0.47 fmol/cell, which represents only ~ 0.9 –9% of cytosolic ATP content. In A549 cells, in response to a 21% strain, ~ 0.4 –4% of cytosolic ATP content has been expelled extracellularly (39).

Based on the total amounts of released ATP in a typical experiment, such as those illustrated in Fig. 2 (5 sequential stretches of 5–35%), and the relative AT2 to AT1 cell content on day 3 and day 7, one can estimate relative contribution of

AT2 and AT1 cells to the release. We found that, on average, AT2 cells release at least 11-fold more ATP than AT1 cells, i.e., ~ 880 pmol versus 80 pmol per 10^6 cells, respectively. This estimate is based on the assumption that the phenotype-specific capability of releasing ATP by AT2 and AT1 cells does not change with cell number/density and days in culture. This model also does not consider the effect of cell-to-cell communication that could modulate/synchronize cellular Ca^{2+} and ATP responses (see below). However, with the precise determinations of ATP release and cell number, this model does not exclude the possibility that AT1 cells do not secrete ATP at all and AT2 cells are the sole contributors. At the present, we have no direct proof that in 7-day-old cell cultures only the remaining AT2 cells are contributors to ATP release. It would require identifying individual ATP-releasing cells, which is technically challenging with the current version of WFOV approach due to limited spatial resolution (39).

Our findings that AT2 cells are the major contributor to ATP release differs from that reported by Patel et al. (27). They found that at lower stretches (21% change in surface area = 10% linear), AT1 cells released 5 times more ATP than AT2 cells, but at higher distension of 30% area change (14% linear), the release was similar in both cell types. The cause of this discrepancy is not clear but could be due to several important methodological differences between the two studies. Patel et al. used continuous stretch for 10 min, and all experiments were conducted in the presence of 100 μM ARL-67156 to inhibit ATP degradation by ecto-ATPases and improve detection of released ATP. Moreover, ATP was evaluated at one time point after the stretch by sampling the cell media that represented bulk ATP concentration with no information on its temporal and spatial distribution. Therefore, it is difficult to compare their data with that obtained using recently improved technology for quantitative ATP measurements in which cellular ATP efflux was investigated in 2D in real time, and cells were stimulated by physiologically more relevant 1-s stretching in

the absence of ecto-ATPase inhibitors. Results of this study are consistent with Isakson et al. (21, 22), who found that in heterocellular AT2/AT1 cultures, stimulation of single AT2 cells with micropipette touching generated intracellular Ca^{2+} signals that propagated to neighboring cells via two routes, one involving gap junctions and the other via the release of ATP. The latter was inhibited by degradation of extracellular ATP with apyrase. Conversely, when single AT1 cells were mechanically stimulated, propagation of Ca^{2+} signals was inhibited only by gap junction blockers but not by apyrase, suggesting that only AT2 cells are capable of ATP release.

It is interesting to note that AT2 cells, as primary releasers of ATP, also show high alkaline phosphatase activity, an ecto-ATPase and marker of AT2 cells. Coexpression of high ecto-ATPase activity at the ATP release sites may have functional significance, serving to terminate/diverge the ATP-mediated purinergic signaling.

Mechanism of ATP release. Failure of ATP channel inhibitors to significantly affect stretch-induced ATP release in AT2 cells indicates that the release mechanism does not involve pannexin/connexin channels (34). By contrast, significant reduction of the release in BAPTA-loaded cells is consistent with $[\text{Ca}^{2+}]_i$ -dependent mechanisms, such as exocytosis of ATP-containing vesicles. It has been shown previously that ATP is stored in intracellular vesicles in A549 cells (1) and in lamellar bodies of AT2 cells (13). Moreover, exocytotic release of ATP has been directly demonstrated by total internal reflection fluorescence microscopy in A549 alveolar cells (1), making it a plausible mechanism also contributing to the release in primary AT2 cells. On the other hand, residual ~50% ATP release in BATA-loaded cells could represent a Ca^{2+} -independent nonexocytotic mechanism of the release. The nature of such pathway is currently under investigation.

Some differences in stretch-induced ATP release between A549 and AT2 cells can be noted. In A549 cells, ATP is released mostly from isolated cells with no evidence for coordinated release from adjacent cells (18). This contrasts with our recent study with rat primary AT2 cells, in which, using luminescence microscopy of higher spatial resolution compared with the WFOV approach used herein, we have found that the release occurs from clusters of cells producing dense clouds of released ATP for stronger stimuli (17). Such ability of AT2 cells to coordinately release ATP from cell clusters likely involves cell-to-cell communication and synchronization of the release by intracellular Ca^{2+} signals via gap junctions. This notion is consistent with stretch-induced Ca^{2+} responses observed in clusters of adjacent cells in our Fura2 experiments and in the study of Isakson et al. (21, 22).

Conclusion. In summary, our results demonstrate that AT2 cells are major, perhaps sole, contributors to mechanosensitive ATP release in primary cultures of rat AT2/AT1 cells and strongly suggest that they may have a similar role in intact alveoli in vivo. Because the bulk of the alveolar distension during lung expansion occurs in AT1 cells (28), they may act as principal mechanosensors in which transient increase of $[\text{Ca}^{2+}]_i$ occurs during lung inflation, initiating a Ca^{2+} signal that is communicated via gap junction to adjacent AT1 and AT2 cells (2). Although both cell types have the capability to generate Ca^{2+} signals in response to stretch, the Ca^{2+} -regulated release of ATP occurs primarily from the secretory AT2 cells. By paracrine stimulation of purinergic receptors on

neighboring cells, it contributes to $[\text{Ca}^{2+}]_i$ wave propagation and triggering purinergic signaling-regulated responses such as surfactant secretion. Further studies should aim to employ whole lung ATP imaging (15) combined with fluorescence cell imaging and molecular biology approaches to elucidate the role of ATP release and specific purinergic receptors in alveoli functions under physiological and pathological conditions. Better understanding of alveolar ATP release pathways and sources will facilitate translation to new therapies and optimization of ventilation strategies to improve survival of critically ill patients.

ACKNOWLEDGMENTS

We give special thanks to members of E. Brochiero's laboratory (Anik Privé, Jasmine Chebli, Mélissa Aubin Vega, and Caroline Landry) for the isolation and primary culture of alveolar cells.

GRANTS

This work was supported by Canadian Institutes of Health Research Grants MOP64364 (to R. Grygorczyk) and PJT15340 (to E. Brochiero) and the Natural Sciences and Engineering Research Council of Canada Grant RGPIN-2016-04378 (to E. Brochiero).

DISCLOSURES

No conflicts of interest, financial or otherwise, are declared by the authors.

AUTHOR CONTRIBUTIONS

F.B. and R.G. conceived and designed research; J.J.T., D.A., and F.B. performed experiments; J.J.T., F.B., D.A., and R.G. analyzed data; J.J.T., F.B., D.A., E.B., and R.G. interpreted results of experiments; J.J.T., D.A., and F.B. prepared figures; J.J.T., E.B., and R.G. drafted manuscript; J.J.T., F.B., D.A., E.B., and R.G. edited and revised manuscript; J.J.T., F.B., D.A., E.B., and R.G. approved final version of manuscript.

REFERENCES

1. Akopova I, Tatur S, Grygorczyk M, Luchowski R, Gryczynski I, Gryczynski Z, Borejdo J, Grygorczyk R. Imaging exocytosis of ATP-containing vesicles with TIRF microscopy in lung epithelial A549 cells. *Purinergic Signal* 8: 59–70, 2012. doi:10.1007/s11302-011-9259-2.
2. Ashino Y, Ying X, Dobbs LG, Bhattacharya J. $[\text{Ca}^{2+}]_i$ oscillations regulate type II cell exocytosis in the pulmonary alveolus. *Am J Physiol Lung Cell Mol Physiol* 279: L5–L13, 2000. doi:10.1152/ajplung.2000.279.1.L5.
3. Boudreault F, Grygorczyk R. Cell swelling-induced ATP release is tightly dependent on intracellular calcium elevations. *J Physiol* 561: 499–513, 2004. doi:10.1113/jphysiol.2004.072306.
4. Bove PF, Grubb BR, Okada SF, Ribeiro CM, Rogers TD, Randell SH, O'Neal WK, Boucher RC. Human alveolar type II cells secrete and absorb liquid in response to local nucleotide signaling. *J Biol Chem* 285: 34939–34949, 2010. doi:10.1074/jbc.M110.162933.
5. Brochiero E, Dagenais A, Privé A, Berthiaume Y, Grygorczyk R. Evidence of a functional CFTR Cl^- channel in adult alveolar epithelial cells. *Am J Physiol Lung Cell Mol Physiol* 287: L382–L392, 2004. doi:10.1152/ajplung.00320.2002.
6. Burnstock G, Brouns I, Adriaensen D, Timmermans JP. Purinergic signaling in the airways. *Pharmacol Rev* 64: 834–868, 2012. doi:10.1124/pr.111.005389.
7. Castranova V, Rabovsky J, Tucker JH, Miles PR. The alveolar type II epithelial cell: a multifunctional pneumocyte. *Toxicol Appl Pharmacol* 93: 472–483, 1988. doi:10.1016/0041-008X(88)90051-8.
8. Cereda M, Emami K, Xin Y, Kadlecsek S, Kuzma NN, Mongkolwisetwara P, Profka H, Pickup S, Ishii M, Kavanagh BP, Deutschman CS, Rizi RR. Imaging the interaction of atelectasis and overdistension in surfactant-depleted lungs. *Crit Care Med* 41: 527–535, 2013. doi:10.1097/CCM.0b013e31826ab1f2.
9. Dobbs LG, Gonzalez R, Williams MC. An improved method for isolating type II cells in high yield and purity. *Am Rev Respir Dis* 134: 141–145, 1986. doi:10.1164/arrd.1986.134.1.141.

10. Douillet CD, Robinson WP III, Milano PM, Boucher RC, Rich PB. Nucleotides induce IL-6 release from human airway epithelia via P2Y2 and p38 MAPK-dependent pathways. *Am J Physiol Lung Cell Mol Physiol* 291: L734–L746, 2006. doi:10.1152/ajplung.00389.2005.
11. Edelson JD, Shannon JM, Mason RJ. Alkaline phosphatase: a marker of alveolar type II cell differentiation. *Am Rev Respir Dis* 138: 1268–1275, 1988. doi:10.1164/ajrcm/138.5.1268.
12. Edwards YS. Stretch stimulation: its effects on alveolar type II cell function in the lung. *Comp Biochem Physiol A Mol Integr Physiol* 129: 245–260, 2001. doi:10.1016/S1095-6433(01)00321-X.
13. Fois G, Winkelmann VE, Bareis L, Staudenmaier L, Hecht E, Ziller C, Ehinger K, Schymeinsky J, Kranz C, Frick M. ATP is stored in lamellar bodies to activate vesicular P2X₄ in an autocrine fashion upon exocytosis. *J Gen Physiol* 150: 277–291, 2018. doi:10.1085/jgp.2017111870.
14. Furuya K, Sokabe M, Grygorczyk R. Real-time luminescence imaging of cellular ATP release. *Methods* 66: 330–344, 2014. doi:10.1016/j.ymeth.2013.08.007.
15. Furuya K, Tan JJ, Boudreault F, Sokabe M, Berthiaume Y, Grygorczyk R. Real-time imaging of inflation-induced ATP release in the ex vivo rat lung. *Am J Physiol Lung Cell Mol Physiol* 311: L956–L969, 2016. doi:10.1152/ajplung.00425.2015.
16. Girault A, Chebli J, Privé A, Trinh NT, Maillé E, Grygorczyk R, Brochiero E. Complementary roles of KCa3.1 channels and β 1-integrin during alveolar epithelial repair. *Respir Res* 16: 100, 2015. doi:10.1186/s12931-015-0263-x.
17. Grygorczyk R, Boudreault F, Tan JJ, Ponomarchuk O, Sokabe M, Furuya K. Mechanosensitive ATP release in the lungs: new insights from real-time luminescence imaging studies. *Curr Top Membr* 83: 45–76, 2019. doi:10.1016/bs.ctm.2019.02.001.
18. Grygorczyk R, Furuya K, Sokabe M. Imaging and characterization of stretch-induced ATP release from alveolar A549 cells. *J Physiol* 591: 1195–1215, 2013. doi:10.1113/jphysiol.2012.244145.
19. Grygorczyk R, Hanrahan JW. CFTR-independent ATP release from epithelial cells triggered by mechanical stimuli. *Am J Physiol* 272: C1058–C1066, 1997. doi:10.1152/ajpcell.1997.272.3.C1058.
20. Hasan D, Blankman P, Nieman GF. Purinergic signalling links mechanical breath profile and alveolar mechanics with the pro-inflammatory innate immune response causing ventilation-induced lung injury. *Purinergic Signal* 13: 363–386, 2017. doi:10.1007/s11302-017-9564-5.
21. Isakson BE, Evans WH, Boitano S. Intercellular Ca²⁺ signaling in alveolar epithelial cells through gap junctions and by extracellular ATP. *Am J Physiol Lung Cell Mol Physiol* 280: L221–L228, 2001. doi:10.1152/ajplung.2001.280.2.L221.
22. Isakson BE, Seedorf GJ, Lubman RL, Evans WH, Boitano S. Cell-cell communication in heterocellular cultures of alveolar epithelial cells. *Am J Respir Cell Mol Biol* 29: 552–561, 2003. doi:10.1165/rcmb.2002-0281OC.
23. Lazarowski ER, Boucher RC. Purinergic receptors in airway epithelia. *Curr Opin Pharmacol* 9: 262–267, 2009. doi:10.1016/j.coph.2009.02.004.
24. Lazarowski ER, Homolya L, Boucher RC, Harden TK. Direct demonstration of mechanically induced release of cellular UTP and its implication for uridine nucleotide receptor activation. *J Biol Chem* 272: 24348–24354, 1997. doi:10.1074/jbc.272.39.24348.
25. Lazarowski ER, Sesma JI, Seminario-Vidal L, Kreda SM. Molecular mechanisms of purine and pyrimidine nucleotide release. *Adv Pharmacol* 61: 221–261, 2011. doi:10.1016/B978-0-12-385526-8.00008-4.
26. Olajuyin AM, Zhang X, Ji HL. Alveolar type 2 progenitor cells for lung injury repair. *Cell Death Discov* 5: 63, 2019. doi:10.1038/s41420-019-0147-9.
27. Patel AS, Reigada D, Mitchell CH, Bates SR, Margulies SS, Koval M. Paracrine stimulation of surfactant secretion by extracellular ATP in response to mechanical deformation. *Am J Physiol Lung Cell Mol Physiol* 289: L489–L496, 2005. doi:10.1152/ajplung.00074.2005.
28. Perlman CE, Bhattacharya J. Alveolar expansion imaged by optical sectioning microscopy. *J Appl Physiol* (1985) 103: 1037–1044, 2007. doi:10.1152/japplphysiol.00160.2007.
29. Perlman CE, Lederer DJ, Bhattacharya J. Micromechanics of alveolar edema. *Am J Respir Cell Mol Biol* 44: 34–39, 2011. doi:10.1165/rcmb.2009-0005OC.
30. Ponomarchuk O, Boudreault F, Orlov SN, Grygorczyk R. Calcium is not required for triggering volume restoration in hypotonically challenged A549 epithelial cells. *Pflugers Arch* 468: 2075–2085, 2016. doi:10.1007/s00424-016-1896-4.
31. Praetorius HA, Leipziger J. ATP release from non-excitabile cells. *Purinergic Signal* 5: 433–446, 2009. doi:10.1007/s11302-009-9146-2.
32. Ramsingh R, Grygorczyk A, Solecki A, Cherkaoui LS, Berthiaume Y, Grygorczyk R. Cell deformation at the air-liquid interface induces Ca²⁺-dependent ATP release from lung epithelial cells. *Am J Physiol Lung Cell Mol Physiol* 300: L587–L595, 2011. doi:10.1152/ajplung.00345.2010.
33. Rannels DE. Role of physical forces in compensatory growth of the lung. *Am J Physiol Lung Cell Mol Physiol* 257: L179–L189, 1989. doi:10.1152/ajplung.1989.257.4.L179.
34. Ransford GA, Fregien N, Qiu F, Dahl G, Conner GE, Salathe M. Pannexin 1 contributes to ATP release in airway epithelia. *Am J Respir Cell Mol Biol* 41: 525–534, 2009. doi:10.1165/rcmb.2008-0367OC.
35. Rich PB, Douillet CD, Mahler SA, Husain SA, Boucher RC. Adenosine triphosphate is released during injurious mechanical ventilation and contributes to lung edema. *J Trauma* 55: 290–297, 2003. doi:10.1097/01.TA.0000078882.11919.AF.
36. Sanchez-Esteban J, Cicchiello LA, Wang Y, Tsai SW, Williams LK, Torday JS, Rubin LP. Mechanical stretch promotes alveolar epithelial type II cell differentiation. *J Appl Physiol* (1985) 91: 589–595, 2001. doi:10.1152/jappl.2001.91.2.589.
37. Schmid A, Clunes LA, Salathe M, Verdugo P, Dietl P, Davis CW, Tarran R. Nucleotide-mediated airway clearance. *Subcell Biochem* 55: 95–138, 2011. doi:10.1007/978-94-007-1217-1_5.
38. Sheth S, Brito R, Mukherjee D, Rybak LP, Ramkumar V. Adenosine receptors: expression, function and regulation. *Int J Mol Sci* 15: 2024–2052, 2014. doi:10.3390/ijms15022024.
39. Tan JJ, Ponomarchuk O, Grygorczyk R, Boudreault F. Wide field of view quantitative imaging of cellular ATP release. *Am J Physiol Cell Physiol* 317: C566–C575, 2019. doi:10.1152/ajpcell.00096.2019.
40. Tatur S, Groulx N, Orlov SN, Grygorczyk R. Ca²⁺-dependent ATP release from A549 cells involves synergistic autocrine stimulation by coreleased uridine nucleotides. *J Physiol* 584: 419–435, 2007. doi:10.1113/jphysiol.2007.133314.
41. Tatur S, Kreda S, Lazarowski E, Grygorczyk R. Calcium-dependent release of adenosine and uridine nucleotides from A549 cells. *Purinergic Signal* 4: 139–146, 2008. doi:10.1007/s11302-007-9059-x.
42. Trinh NT, Privé A, Kheir L, Bourret JC, Hijazi T, Amraei MG, Noël J, Brochiero E. Involvement of K_{ATP} and KvLQT1 K⁺ channels in EGF-stimulated alveolar epithelial cell repair processes. *Am J Physiol Lung Cell Mol Physiol* 293: L870–L882, 2007. doi:10.1152/ajplung.00362.2006.
43. Uhlig U, Uhlig S. Ventilation-induced lung injury. *Compr Physiol* 1: 635–661, 2011. doi:10.1002/cphy.c100004.
44. Verbrugge SJ, de Jong JW, Keijzer E, Vazquez de Anda G, Lachmann B. Purine in bronchoalveolar lavage fluid as a marker of ventilation-induced lung injury. *Crit Care Med* 27: 779–783, 1999. doi:10.1097/00003246-199904000-00035.
45. Yegutkin GG. Nucleotide- and nucleoside-converting ectoenzymes: Important modulators of purinergic signalling cascade. *Biochim Biophys Acta* 1783: 673–694, 2008. doi:10.1016/j.bbamcr.2008.01.024.